The effect of forest conversion from coniferous to broadleaved forests on deep seepage rates in North-west Germany

Von der Fakultät für Mathematik und Naturwissenschaften der Carl von Ossietzky Universität Oldenburg zur Erlangung des Grades und Titels eines

Doktor rerum naturalium (Dr. rer. nat.)

angenommene Dissertation

von Herrn Kilian Loesch

geboren am 10.07.1991 in Braunschweig

Gutachterin:	Prof. Dr. Gudrun Massmann
	Institut für Biologie und Umweltwissenschaften, Carl von Ossietzky Universität Oldenburg, Ammerländer Heerstraße 114-118, 26129 Oldenburg
Zweitgutachter:	Prof. Dr. Karl-Heinz Feger
	Institut für Bodenkunde und Standortslehre, Technische Universität Dresden, Pienner Straße 19, 01737 Tharandt
Tag der Disputation:	Mittwoch, den 1. März 2023

Preface

This thesis is part of the research project “Wasserwald Versickerungs Monitoring” (WasMon) conducted by the Chamber of Agriculture Lower Saxony (LWK Niedersachsen) under the supervision of Dr. Karsten Mohr. The project (Grant-Nr.: 22WA401331) was funded by the Forest Climate Fund (FNR), which is part of the special Climate and Transformation Fund and is established under the joint leadership of the Federal Ministry of the Environment, Nature Conservation and Nuclear Safety (BMUV) and the Federal Ministry of Food and Agriculture (BMEL). Further project sponsors were the municipal utilities of Hannover (enercity) and Oldenburg (VWG) as well as the Chamber of Agriculture Lower Saxony. The project duration was from January 2018 to January 2022.

The study sites are located in private forests in the Northwest German lowlands and were selected by the Chamber of Agriculture Lower Saxony and enercity. The technical equipment for soil moisture, stand precipitation and meteorological measurements was provided and installed by Umwelt-Geräte-Technik GmbH in Müncheberg, enercity, Dr. Karsten Mohr and Kilian Loesch. The technical equipment and support for soil analyses in the laboratory were provided by the University of Oldenburg (Elke Ahrensfeld, Ulrike Kücks).

The project design as well as methods and results were vividly discussed with inter-disciplinary experts from the University of Oldenburg (Prof. Dr. Gudrun Massmann, Dr. Janek Greskowiak), Thünen Institute for Forest Ecosystem Research in Eberswalde (Prof. Dr. Jürgen Müller) and Northwest German Forest Research Institute (NW-FVA) in Göttingen (Dr. Henning Meesenburg).

Abstract

Forests have a major impact on the water balance at landscape level. Compared to other ecosystems, they evaporate large amounts of water and only a small proportion seeps into deep soil layers below the root zone. Deep percolation is higher under deciduous forests than under coniferous forests. The effect of mixed forests on deep percolation has received little attention so far. The conversion of coniferous to deciduous forests and potentially also to mixed forests can be used as an effective tool to increase groundwater recharge rates, which benefits drinking water production, agriculture, forestry, and ecosystems in water scarce areas.

In Northwest Germany, Scots pine (*Pinus sylvestris*) stands grow on sandy, groundwater-distant sites and are suitable for forest conversion with e. g. European beech (*Fagus sylvatica*). At three sites in western (Sandkrug), central (Elze) and eastern (Wibbese) Lower Saxony, the effect of forest conversion on seepage rates was investigated in pure and mixed stands of pine, beech and Douglas fir. In the period between January 2019 and October 2020, intensive investigations of site characteristics as well as continuous meteorological, stand precipitation and soil moisture measurements were carried out on the experimental plots. Based on these data, the water balance model LWF-Brook90 was adjusted individually in a multi-step calibration process. Based on the successfully calibrated model, the water balance terms interception, transpiration and deep seepage could then be estimated.

The measured and modelled water flux data reveal a clear effect of forest conversion on the water balance. In the study period (January 2019 – October 2020), gross precipitation (P) sums ranged from 1079 mm (Wibbese) to 1467 mm (Sandkrug). The interception was 14 % of P in the pure beech forest (Elze) and between 18 % and 32 % of P in the pure pine forests (Sandkrug, Elze, Wibbese) in the study period. In the studied mixed pine-beech stands, interception was mostly at the level of pure pine stands. In mixed pine-beech stands, where pine still grows very densely, the interception was even at a higher level than in pure pine stands. Deep seepage rates vary between 25 % of P and 44 % of P in pure pine stands. In the pure beech stand, deep seepage is significantly higher at 58 % of P. In mixed pine-beech stands, deep seepage is in the range of pure pine stands. The comparison of two mixed pine forests with 5 years old beech and Douglas fir show no difference in deep seepage, which implies that evergreen (Douglas fir) and deciduous (beech) trees do not yet have a great effect on deep seepage at this conversion stage. Thinning of the pine tree layer in Wibbese reduced interception by about one-third, and deep seepage increased by 8% to 24%.

In this study, only a positive effect after conversion to a pure deciduous stand is evident. For mixed stands, the study doesn't show a positive effect. In mixed forests, a higher degree of thinning can raise seepage rates above those found in pure pine stands. A higher degree of thinning may also be applied to pure pine stands. Absolute deep seepage rates are thereby strongly weather dependent and thus only specifically valid for the study period. To further increase the validity of the numbers, the study period should be significantly extended to include wet weather periods in addition to the intermittently very dry years of 2019 and 2020. In addition, the influence of the ground vegetation should be explicitly considered in the model and the parameterization of rooting depth and density should be further developed.

The results can serve as a basis for an economic evaluation of the ecosystem service groundwater recharge, which is necessary to promote groundwater-emphasized forest conversion. Considering climate change, it will be all the more important to convert forests site-specifically so that they can keep pace with changing climate conditions. Even though beech may not be suitable for all forest sites, tree species selection should take into account the water-promoting properties of broadleaved trees.

Zusammenfassung

Wälder haben einen entscheidenden Einfluss auf den Landschaftswasserhaushalt. Im Vergleich zu anderen Ökosystemen verdunsten sie große Mengen des über den Niederschlag eingetragenen Wassers, so dass nur ein verhältnismäßig kleiner Anteil in tiefe Bodenschichten unterhalb des Wurzelraums versickert. Die Tiefensickerung ist dabei unter Laubwald höher als unter Nadelwald. Der Effekt von Mischwäldern auf die Tiefensickerung ist bisher nur wenig erforscht. In dieser Studie wird untersucht, wie sich der Umbau von reinen Kiefernwäldern in Kiefern-Buche-Mischwälder und reine Buchenwälder auf die Tiefensickerung unter den standörtlichen Gegebenheiten Nordwestdeutschlands auswirken. Aufgrund bisheriger Erkenntnisse wird von einer Erhöhung der Tiefensickerung mit dem Waldumbau hin zu Misch- und reinen Laubwäldern ausgegangen.

In Nordwestdeutschland stocken auf grundwasserfernen und sandigen Standorten überwiegend Waldkieferbestände (*Pinus sylvestris*), die sich für den Umbau u. a. mit der Rotbuche (*Fagus sylvatica*) eignen. An drei Standorten im westlichen (Sandkrug), mittleren (Elze) und östlichen (Wibbese) Niedersachsen wurde auf insgesamt neun Waldflächen der Effekt des Waldumbaus auf die Sickerwasserraten ermittelt. Dabei wurden drei Kiefernreinbestände, vier Kiefernbestände mit Buchen-Voranbau, ein Kiefernbestand mit Douglasien-Voranbau und ein Buchenreinbestand berücksichtigt. Auf den Versuchsflächen wurden im Untersuchungszeitraum zwischen Januar 2019 und Oktober 2020 intensive Untersuchungen der Standorteigenschaften zusammen mit kontinuierlichen Messungen von Meteorologie, Bestandsniederschlag und Bodenfeuchte vorgenommen. Auf dieser Datengrundlage wurde das Wasserhaushaltsmodell *LWF-Brook90* in einem mehrschrittigen Kalibrierprozess für die jeweiligen Versuchsstandorte angepasst. Mit Hilfe des erfolgreich kalibrierten Modells konnten die Wasserbilanzterme Interzeption, Transpiration und Tiefensickerung valide abgeschätzt werden.

Aus den Mess- und Modelldaten geht ein deutlicher Effekt des Waldumbaus auf den Standortwasserhaushalt hervor. Im Untersuchungszeitraum fielen zwischen 1079 mm (Wibbese) und 1467 mm (Sandkrug) Niederschlag. Die Interzeption betrug im gesamten Untersuchungszeitraum 14 % des Freilandniederschlags (P) im reinen Buchenwald (Elze) und zwischen 18 % und 32 % des Freilandniederschlags in den reinen Kiefernbeständen (Sandkrug, Elze, Wibbese). In den untersuchten Kiefern-Buchen-Mischbeständen lag die Interzeption meist auf dem Niveau der reinen Kiefernbestände. In Kiefern-Buchen-Mischbeständen, in denen der Kiefernschirm noch sehr dicht wächst, lag die Interzeption sogar auf einem höheren Niveau als im Kiefernreinbestand. Die berechneten Sickerwasserraten variieren in reinen Kiefernbeständen zwischen 25 % und 44 % des Freilandniederschlags. Im reinen Buchenbestand ist die Tiefensickerung mit 58 % des Freilandniederschlags deutlich erhöht. In den Kiefern-Buchen-Mischbeständen liegt die Tiefensickerung im Bereich der reinen Kiefernbestände. In der frühen Umbauphase konnte dabei am Standort Wibbese noch kein Unterschied zwischen einem Kiefern-Buche und Kiefer-Douglasie Mischbestand festgestellt werden. Eine Auflichtung des Kiefernschirms am Standort Wibbese reduzierte die Interzeption etwa um ein Drittel, die Tiefensickerung stieg um 8 % bis 24 % an.

Auch wenn die absoluten Zahlen stark witterungsabhängig und somit nur spezifisch für den Untersuchungszeitraum gültig sind, so zeigt sich ein deutlich positiver Einfluss des Waldumbaus, spätestens bei der Überführung in einen reinen Laubholzbestand. Im Mischwald-

stadium kann ein höherer Durchforstungsgrad und ein gezieltes Waldmanagement die Sickerwasserraten über das Niveau des Kiefernreinbestands anheben. Das zusätzlich generierte Wasser könnte insbesondere in Wassermangelphasen der Trinkwassergewinnung, der Land- und Forstwirtschaft sowie den Ökosystemen zu Gute kommen. Um die Aussagekraft der Zahlen weiter zu steigern, sollte der Untersuchungszeitraum deutlich verlängert werden, so dass neben der zeitweilig sehr trockenen Jahre 2019 und 2020 auch nasse Witterungsperioden berücksichtigt werden. In der Modellierung sollte zudem der Einfluss der Bodenvegetation explizit berücksichtigt sowie die Parametrisierung der Durchwurzelungstiefe und –dichte weiterentwickelt werden.

Die Ergebnisse können als Grundlage für eine ökonomische Bewertung der Ökosystemdienstleistung Grundwasserneubildung dienen, welche notwendig ist, um grundwasserbetonten Waldumbau zu fördern. Mit Blick auf den Klimawandel wird es umso wichtiger sein, die Wälder standortgerecht so umzubauen, dass sie mit den Klimaveränderungen Schritt halten können. Auch wenn die Buche dabei nicht für alle Standorte geeignet sein wird, so sollten bei der Baumartenwahl die wasserfördernden Eigenschaften anderer Laubbäume berücksichtigt werden.

Table of Contents

Preface I
Abstract III
Zusammenfassung V
Table of Contents VII
List of Figures XI
List of Tables XV
List of Abbreviations XIX
1 Introduction 1
2 Theory and current state of research 4
2.1 Forest conversion from Scots pine to European beech 4
2.2 The water cycle in forest ecosystems 6
2.3 Methods to determine the water cycle in forest ecosystems 9
2.3.1 Measuring the hydrological cycle in forest ecosystems 10
2.3.2 Modelling the hydrological cycle in forest ecosystems 12
2.4 Measuring the effect of forest type on the water cycle 18
2.4.1 Species-specific vegetation data 18
2.4.2 Interception and stemflow of tree vegetation 18
2.4.3 Transpiration of tree vegetation 21
2.4.4 Evapotranspiration of forest ground vegetation 22
2.4.5 Deep seepage and groundwater recharge rates below forests 23
3 Methods 27
3.1 Study sites 27
3.1.1 Sandkrug 28
3.1.2 Elze 30
3.1.3 Wibbese 33
3.2 In situ measurements 36
3.2.1 Meteorological parameters 36
3.2.2 Stand precipitation and soil moisture 37
3.2.3 Phenology and Leaf Area Index 39
3.2.4 Soil 42
3.3 Modelling 44
3.3.1 Modelling strategy 44
3.3.2 Model setup 44
3.3.3 Sensitivity analysis 48
3.3.4 Manual calibration of interception parameters 51
3.3.5 Automatic calibration of soil and evapotranspiration parameters 51

3.3.6 Model validation 53
3.3.7 Resulting water balance components 53
4 Results 54
4.1 Sandkrug 54
4.1.1 Precipitation measurements 54
4.1.2 Soil measurements 55
4.1.3 Phenology & Plant Area Index measurements 56
4.1.4 Stand precipitation measurements 57
4.1.5 Soil moisture measurements 57
4.1.6 Sensitivity analysis 59
4.1.7 Calibration and validation of interception evaporation parameters 62
4.1.8 Calibration and validation of soil and evapotranspiration parameters 64
4.1.9 Modelled water balance and deep seepage rates 68
4.2 Elze 70
4.2.1 Precipitation measurements 70
4.2.2 Soil measurements 71
4.2.3 Phenology & Plant Area Index measurements 72
4.2.4 Stand precipitation measurements 73
4.2.5 Soil moisture measurements 75
4.2.6 Sensitivity analysis 78
4.2.7 Calibration and validation of interception evaporation parameters 79
4.2.8 Calibration and validation of soil and evapotranspiration parameters 82
4.2.9 Modelled water balance and deep seepage rates 87
4.3 Wibbese 91
4.3.1 Precipitation measurements 91
4.3.2 Soil measurements 92
4.3.3 Phenology & Plant Area Index measurements 93
4.3.4 Stand precipitation measurements 94
4.3.5 Soil moisture measurements 94
4.3.6 Sensitivity analysis 97
4.3.7 Calibration and validation of interception evaporation parameters 98
4.3.8 Calibration and validation of soil and evapotranspiration parameters 101
4.3.9 Modelled water balance and deep seepage rates 106
5. Discussion 111
5.1 Discussion of measurement results 111
5.1.1 Discussion of vegetation parameter measurements 111
5.1.2 Discussion of stand precipitation measurements 112

5.1.3 Discussion of soil moisture measurements ... 114
5.2 Discussion of modelled deep seepage and evapotranspiration ... 115
5.2.1 Calibration of model parameters ... 115
5.2.2 Modelled transpiration and soil evaporation ... 117
5.2.3 Modelled deep seepage ... 117
5.3 Suitability of the methods applied ... 119
5.3.1 Methods to measure LAI, stand precipitation and soil moisture ... 119
5.3.2 Methods to model the water balance ... 121
5.4 Limitations of the study ... 123
5.4.1 Suitability of the tree species selected for forest conversion ... 123
5.4.2 Suitability of the study sites ... 123
5.4.3 Representativeness and length of study period ... 124
5.4.4 The role of ground vegetation ... 125
5.5 Implications for the temporal development of deep seepage during forest conversion ... 126
5.6 Recommendations to increase deep seepage during forest conversion ... 128
6. Conclusion & Outlook ... 129
Literature ... 131
Appendix ... XXI
Vegetation measurements ... XXI
Precipitation measurements ... XXV
Soil measurements ... XXVI
Interception measurements ... XXXII
Soil moisture measurements ... XXXV
LWF-Brook90 ... XL
Declaration of originality and confirmation of conformance ... XLIX
Acknowledgements ... LI
Curriculum Vitae ... LII

List of Figures

Figure 1: Components of the water cycle in a forest ecosystem 7
Figure 2: Schematic illustration of a forest lysimeter 11
Figure 3: Modelled water fluxes in LWF-Brook90 14
Figure 4: The LWFBrook90R workflow 15
Figure 5: Stand precipitation in pine, beech and mixed pine and beech forests 21
Figure 6: Deep seepage rates in pine, beech and mixed pine and beech forests 24
Figure 7: Location of the study sites Sandkrug, Elze and Wibbese 27
Figure 8: Forest observations plots in Sandkrug 29
Figure 9: Dominating ground cover in SREF and SB20 30
Figure 10: Forest observation plots in Elze 31
Figure 11: Dominating ground cover in EREF, EB5, EB15 and EB25 32
Figure 12: Forest observation plots in Wibbese 34
Figure 13: Dominating ground cover in WREF, WB5 and WD5 35
Figure 14: Meteorological observation site in Wibbese 36
Figure 15: Illustration of stand precipitation and soil moisture measurements 37
Figure 16: Measurement of stand precipitation 38
Figure 17: Measurement of soil moisture 38
Figure 18: Location of soil moisture sensors and stand precipitation gutters 39
Figure 19: Example of DHP 40
Figure 20: Scanned litter fall sample 41
Figure 21: The modelling workflow used for water balance modelling 44
Figure 22: Seasonal LAI construction methods in LWF-Brook90R 46
Figure 23: Relative root depth distribution construction in LWF-Brook90 47
Figure 24: Abbreviations used for the investigated forest plots in Sandkrug 54
Figure 25: Measured monthly precipitation in Sandkrug 54
Figure 26: Soil profiles in Sandkrug 55
Figure 27: Total Plant Area Index in SREF (pine) and SB20 (pine, beech) 56
Figure 28: Mean interception rates in SREF and SB20 57
Figure 29: Soil moisture observations in Sandkrug 58
Figure 30: Results of the sensitivity analysis in Sandkrug 60
Figure 31: Course of the PAI in the model after calibration 62

Figure 32: Modelled and observed stand precipitation in SREF and SB20 63
Figure 33: The effect of calibrating the empirical MvG parameters 64
Figure 34: Observed and calibrated modelled soil moisture (50 cm), Sandkrug 66
Figure 35: Observed and calibrated modelled soil moisture (200 cm), Sandkrug 67
Figure 36: Monthly water budgets in SREF and SB20 68
Figure 37: Total modelled water fluxes in SREF and SB20 69
Figure 38: Abbreviations used for the investigated forest plots in Elze 70
Figure 39: Measured monthly precipitation in Elze 70
Figure 40: Soil profiles in E REF, E B5, E B15, E B25 71
Figure 41: Total PAI in EREF, EB5, EB15 and EB25 73
Figure 42: Mean interception rates in EREF, EB15 and EB25 74
Figure 43: Mean interception rates in EREF, EB5, EB15 and EB25 75
Figure 44: Soil moisture observations in Elze 76
Figure 45: Results of the sensitivity analysis in Elze 78
Figure 46: Course of the PAI in the model after calibration in Elze 80
Figure 47: Modelled and observed stand precipitation in Elze 81
Figure 48: The effect of calibrating the empirical MvG parameters 83
Figure 49: Observed and calibrated modelled soil moisture (50 cm), Elze 85
Figure 50: Observed and calibrated modelled soil moisture (200 cm), Elze 87
Figure 51: Monthly water budgets in EREF, EB5, EB15 and EB25 89
Figure 52: Total modelled water fluxes in EREF, EB5, EB15 and EB25 90
Figure 53: Abbreviations used for the investigated forest plots in Wibbese 91
Figure 54: Measured monthly precipitation in Wibbese 91
Figure 55: Soil profiles in Wibbese 92
Figure 56: Total PAI in WREF, WB5 and WD5 93
Figure 57: Mean interception rates in WREF, WB5 and WD5 94
Figure 58: Soil moisture observations in Wibbese 96
Figure 59: Results of the sensitivity analysis in Wibbese 97
Figure 60: Course of the PAI in the model after calibration in Wibbese 99
Figure 61: Modelled and observed stand precipitation in WREF, WB5 and WD5 101
Figure 62: The effect of calibrating the empirical MvG parameters in Wibbese 102
Figure 63: Observed and calibrated modelled soil moisture (50 cm), Wibbese 105

Figure 64: Observed and calibrated modelled soil moisture (200 cm), Wibbese 106
Figure 65: Monthly water budgets in WREF, WB5 and WD5 107
Figure 66: Total modelled water fluxes in WREF, WB5 and WD5 108
Figure 67: Modelled water fluxes in WREF, WB5, WD5 before and after thinning 109
Figure 68: Measured daily precipitation sums in Sandkrug, Elze and Wibbese XXV
Figure 69: Grain size distribution measurements in Sandkrug, Elze and Wibbese XXVIII
Figure 70: Soil moisture courses in 50 cm and 200 cm depth for every forest plot XXXIX

List of Tables

Table 1: Throughfall, Interception and Stem Flow for pine and beech 20
Table 2: Selected ground vegetation evapotranspiration rates from literature 23
Table 3: Selected litter interception values from literature 23
Table 4: Modelled deep seepage in converted forests in Northeast Lower Saxony 26
Table 5: Study site details 28
Table 6: Detailed information about stand parameters 28
Table 7: Stand parameters in Sandkrug 29
Table 8: Stand parameters in Elze 32
Table 9: Stand parameters in Wibbese 33
Table 10: Technical details of the meteorological sensors . 37
Table 11: Summary of methods used to derive LAI at the forest plots 42
Table 12: Meteorological input data required as input for LWF-Brook90 45
Table 13: Soil input data required as input for LWF-Brook90 45
Table 14: Initial plot-specific model parameterization 48
Table 15: Parameters selected for sensitivity analysis 49
Table 16: Ranges for the parameters maxlai and sai in the sensitivity analysis 50
Table 17: Precipitation sums in Sandkrug 54
Table 18: Depth-specific soil texture in Sandkrug 55
Table 19: Assessment of phenology in Sandkrug 56
Table 20: Statistical measures of daily soil moisture in Sandkrug 59
Table 21: NSE separating behavioural / non-behavioural model runs in Sandkrug 59
Table 22: Fixed model parameter values in Sandkrug 61
Table 23: Calibrated interception parameters in Sandkrug 62
Table 24: Observed and modelled stand precipitation in Sandkrug 63
Table 25: Original values of the MvG parameters in Sandkrug 64
Table 26: Depth-specific soil hydraulic parameters in Sandkrug 65
Table 27: Calibrated evapotranspiration and infiltration parameters in Sandkrug 65
Table 28: Precipitation sums in Elze 70
Table 29: Depth-specific soil textures in Elze 71
Table 30: Assessment of phenology in Elze 72
Table 31: Interception measurement dates in Elze 74

Table 32: Statistical measures of daily soil moisture in Elze 77
Table 33: NSE separating behavioural / non-behavioural model runs in Elze 78
Table 34: Fixed model parameter values in Elze 79
Table 35: Calibrated interception parameters in Elze 80
Table 36: Observed and modelled stand precipitation in Elze 82
Table 37: Original values of the MvG parameters in Elze 82
Table 38: Depth-specific soil hydraulic parameters in Elze 83
Table 39: Calibrated evapotranspiration and infiltration parameters in Elze 84
Table 40: Precipitation sums in Wibbese 91
Table 41: Depth-specific soil textures in Wibbese 92
Table 42: Interception measurement dates in Wibbese 94
Table 43: Statistical measures of daily soil moisture in Wibbese 97
Table 44: NSE separating behavioural / non-behavioural model runs in Wibbese 97
Table 45: Fixed model parameter values in Wibbese 98
Table 46: Calibrated interception parameter values in Wibbese 99
Table 47: Observed and modelled stand precipitation in Wibbese 100
Table 48: Original values of the empirical MvG parameters in Wibbese 101
Table 49: Depth-specific soil hydraulic parameters in Wibbese 102
Table 50: Calibrated evapotranspiration and infiltration parameters in Wibbese 103
Table 51: The effect of thinning on modelled water fluxes in WB5 and WD5 110
Table 52: Stand parameters assessed for Sandkrug, Elze and Wibbese XXI
Table 53: Dominating ground vegetation species at the forest plots XXII
Table 54: The classification of tree canopy XXII
Table 55: LAI of European beech in SB20, EB15 and EB25 XXIII
Table 56: LAI of Scots pine and European beech in Sandkrug, Elze and Wibbese XXIII
Table 57: LAI construction based on DHP and litter fall XXIV
Table 58: Measured depth-specific gravel content [%] at the forest plots XXIX
Table 59: Measured bulk density [g/cm3] at the forest plots XXIX
Table 60: Measured organic carbon content [%] at the forest plots XXIX
Table 61: Aggregated soil properties in Sandkrug XXX
Table 62: Aggregated soil properties in Elze XXXI
Table 63: Aggregated soil properties in Wibbese XXXI

Table 64: Stand precipitation and interception in Sandkrug XXXII
Table 65: Stand precipitation and interception in Elze XXXII
Table 66: Stand precipitation and interception in Wibbese XXXV
Table 67: Details about model parameters in LWF-Brook90R XL
Table 68: Model Soil File for Sandkrug XLV
Table 69: Model Soil File for Elze XLVI
Table 70: Model Soil File for Wibbese XLVII

List of Abbreviations

Model parameters of LWF-Brook90

All model parameters are described in Table 67 in the appendix.

Frequently occurring abbreviations

alpha	Mualem van Genuchten Parameter Alpha
BA	Basal Area
C_{Org}	Soil Organic Carbon Content [Mass-%]
CI5	5% Confidence Interval
CI95	95 % Confidence Interval
CR	Capillary Rise
DBH	Diameter at Breast Height
DHP	Digital Hemispherical Photography
DOY	Day of Year
DWD	German Weather Service (Deutscher Wetterdienst)
E_S	Soil Evaporation
EREF	Forest Plot Elze (Scots Pine 80a)
EB5	Forest Plot Elze (Scots Pine 80a, European Beech 5a)
EB15	Forest Plot Elze (Scots Pine 80a, European Beech 15a)
EB25	Forest Plot Elze (European Beech 25a)
FDR	Frequency-Domain-Reflectometry
GR	Groundwater Recharge
I_T	Tree Interception Evaporation
I_G	Ground Vegetation Interception Evaporation
IF	Interflow / Lateral Flow
Int_{Mod}	Mean Modelled Interception
Int_{Obs}	Mean Observed Interception
Int_{summer}	Modelled Interception in Summer
Int_{winter}	Modelled Interception in Winter
INTR	Rain Interception Storage in LWF-Brook90
INTS	Snow Interception Storage in LWF-Brook90
INF	Infiltration
IQR90	90 % Interquartile Range between CI5 and CI95
ksat	Saturated hydraulic conductivity
LAI	Leaf Area Index
LWF	State Institue of Bavaria for Forestry and Silviculture
LWF-Brook90R	Hydrological Model LWF-Brook90 implemented in R
M	Median
MAE	Mean Absolute Error
Max	Maximum
MCMC	Monte Carlo Markov Chain
MF	Macropore Flow / Preferential Flow
Min	Minimum
mpar	Mualem van Genuchten Parameter m
MvG	Mualem van Genuchten

npar	Mualem van Genuchten Parameter n
NSE	Nash Sutcliffe Efficiency
OF	Overland Flow / Surface Flow
P	Gross Precipitation
PAI	Plant Area Index
PTF	Pedotransfer Function
RWU	Root Water Uptake
S	Seepage Flow
S_D	Deep Seepage Flow
SAI	Stem Area Index
SB20	Forest Plot Sandkrug (Scots Pine 70a, European Beech 20a)
SD	Stand Density
SDEV	Standard Deviation
SF	Stem Flow
SMT-100	Soil Moisture Sensor SMT-100
SREF	Forest Plot Sandkrug (Scots Pine 70a)
Sum_{Mod}	Total Modelled Stand Precipitation Sum
Sum_{Obs}	Total Observed Stand Precipitation Sum
SWS	Soil Water Storage
T	Air Temperature
T_T	Tree Transpiration
T_G	Ground Vegetation Transpiration
thr	Residual Water Content
ths	Saturated Water Content
TF	Throughfall
TDR	Time-Domain-Reflectometry
tort	Tortuosity Factor
VC	Coefficient of Variation
WB5	Forest Plot Wibbese (Scots Pine 70a, European Beech 5a)
WD5	Forest Plot Wibbese (Scots Pine 70a, Douglas Fir 5a)
WREF	Forest Plot Wibbese (Scots Pine 70a)

2.3.2. Modelling the hydrological cycle in forest ecosystems

D	Observation Data (Bayes Theorem)
DREAM	Differential Evolution Adaptive Metropolis
$p(\theta\|D)$	Posterior Distribution (Bayes Theorem)
$p(\theta)$	Prior Distribution of Model Parameters (Bayes Theorem)
$p(D\|\theta)$	Likelihood Function (Bayes Theorem)
SCEM	Shuffled Complex Evolution Metropolis
Z	Marginal Likelihood (Bayes Theorem)
Θ	Vector of Model Data (Bayes Theorem)

3.2.3. Phenology and Leaf Area Index

A_m	Leaf Area of Main Sample (Litter Fall Sampling)
A_t	Total Leaf Area of Sample (Litter Fall Sampling)

A_{traps}	Total Sampling Area (Litter Fall Sampling)
A_s	Leaf Area of Litter Sub Sample (Litter Fall Sampling)
BA_b	Beech Basal Area
BA_p	Pine Basal Area
ICP Forests	International Co-operative Programme on Assessment and Monitoring of Air Pollution Effects on Forests
LAI_c	Coniferous Share of LAI
LAI_d	Deciduous Share of LAI
$LAI_{EB25, max}$	Maximum summer LAI in EB25
LAI_{max}	Maximum LAI of the Year (Litter Fall Sampling)
$LAI_{max, mixed}$	Maximum LAI of the Year for the Mixed Forest
$LAI_{min, mixed}$	Minimum LAI of the Year for the Mixed Forest
LAI_{sample}	Leaf Area Index of Sample (Litter Fall Sampling)
LFS	Litter Fall Sampling
m_m	Dry Mass of Main Sample (Litter Fall Sampling)
m_s	Dry Mass of Sub Sample (Litter Fall Sampling)
$PAI_{EB25, winter}$	PAI of EB25 in winter
SAI_{EB25}	SAI of EB25
SAI_m	SAI of Mixed Forest
SLA_s	Specific Leaf Area of the Sub Sample
α	Woody to Total Plant Area Ratio (LAI Calculation)
α_m	Woody to Total Plant Area Ratio for the Mixed Forest (LAI Calculation)
α_p	Woody to Total Plant Area Ratio for Pine(LAI Calculation)
γ	Needle-to-Shoot Area Ratio (LAI Calculation)
γ_p	Needle-to-Shoot Area Ratio for Pine (LAI Calculation)

3.2.4. Soil

d_b	Bulk Density of the Soil [g/cm³]
H_2O_2	Hydrogen Peroxide
IL	Ignition Loss [Mass-%]
m_{ad}	Mass of Absolute Dry Soil Material [g]
m_b	Mass of Soil Sample after Ignition in the Furnace [g]
m_d	Dry Mass of Soil Sample [g]
m_{pc}	Mass of Porcelain Crucible [g]

3.3.2. Model setup

d	Soil depth (Betamodel)
$densef_{WB5}$	Model Parameter *densef* for WB5 to simulate Thinning
$densef_{WD5}$	Model Parameter *densef* for WD5 to simulate Thinning
e	Vapor Pressure [kPa]
e_s	Saturated Vapor Pressure [Pa]
globrad	Global Radiation Sum
$LAI_{WB5, obs}$	Observed Leaf Area Index in WB5
$LAI_{WB5, mod, after\ thinning}$	Modelled Leaf Area Index in WB5 after Thinning

$LAI_{WB5,\ mod,\ before\ thinning}$	Modelled Leaf Area Index in WB5 before Thinning
$LAI_{WD5,\ obs}$	Observed Leaf Area Index in WD5
$LAI_{WD5,\ mod,\ after\ thinning}$	Modelled Leaf Area Index in WD5 after Thinning
$LAI_{WD5,\ mod,\ before\ thinning}$	Modelled Leaf Area Index in WD5 before Thinning
$LAI_{WREF,\ obs}$	Observed Leaf Area Index in WREF
$LAI_{WREF,\ mod}$	Modelled Leaf Area Index in WREF
prec	Precipitation
RH	Relative Humidity of Air [%]
tmax	Maximum temperature
tmean	Mean Temperature
tmin	Minimum Temperature
vappres	Vapour Pressure
wind	Mean Wind Speed
y	Cumulative Root Fraction (Betamodel)
β	Depth Coefficient (Betamodel)

3.3.3. Sensitivity analysis

D_{max}	Maximum Distance between behavioural and non-behavioral empirical cumulative distribution function (Kolmogorov-Smirnov-Test)
Q_{sim}^{t}	Modelled Value at time t (NSE Calculation)
Q_{obs}^{t}	Observed Value at time t (NSE Calculation)
$\bar{Q}_{obs}$	Mean observed Value (NSE Calculation)
t	Number of Time Steps (NSE & MAE Calculation)

3.3.5. Automatic calibration

logp	Gaussian Likelihood of a Model Simulation for a given State Variable
$logp_{mod}$	Overall Gaussian Likelihood Value of a Model Simulation
$logp_{sp}$	Gaussian Likelihood Value for Stand Precipitation
$logp_{th50}$	Gaussian Likelihood Value for Soil Moisture (50 cm)
$logp_{th200}$	Gaussian Likelihood Value for Soil Moisture (200 cm)
len_{sp}	Number of Stand Precipitation Observations
len_{th50}	Number of Soil Moisture Observations
mod_i	Modelled State Variable at a given Time Step
n	Number of Parameters / Observations
obs_i	Observed State Variable at a given Time Step
$\overline{obs}$	Mean Value of all Observed State Variable Values
prior	Prior Probability for the Parameters
x_i	Parameter Value
μ_i	Initial Parameter Value
σ	Standard Deviation

1 Introduction

In the past, water was always available in Northwest Germany (Lower Saxony) in sufficient quantity and high quality for water-dependent and terrestrial ecosystems, drinking water and industrial water supply. The main drinking water resources for private and industrial water supply in Lower Saxony are groundwater and artificial water reservoirs in the Harz mountains (NLWKN 2022). Thereby, the majority of drinking water (86 %) is obtained from groundwater (Landesamt für Bergbau 2022). Groundwater is thus essential for a reliable water supply with drinking water for private households and industry. Groundwater also serves as the main source for irrigation of arable land in Northeast Lower Saxony (Ostermann 2020).

Groundwater is an important part of the water cycle: From precipitation input, which is usually abundant in Northwest Germany, a substantial share either evaporates from vegetation surfaces, flows at the soil surface to a stream or infiltrates into the soil. In the soil, water is stored and can be extracted by plants (transpiration). If more water infiltrates the soil than can be consumed by vegetation or stored in the soil, the water seeps into deeper soil layers (deep seepage). On sandy and permeable sites, the majority of this excess water seeps into the groundwater as groundwater recharge (Bartsch & Röhrig 2016).

Apart from climate conditions, land cover and its management strongly affect the water cycle and thus groundwater recharge at the landscape level. In Lower Saxony, farmland (55 %) and forests (25 %) account for a major share of the total land area (Landesamt für Statistik Niedersachsen 2020, Niedersächsisches Ministerium für Ernährung Landwirtschaft und Verbraucherschutz 2022). Silvicultural and agricultural management practices therefore strongly affect landscape hydrology. Considering previous estimations, mean annual groundwater recharge rates in Lower Saxony are considerably lower in forests (260 mm a^{-1}) compared to grassland (320 mm a^{-1}) or farmland (380 mm a^{-1}). Forests thus consume more water than grassland or cropland (Ahrends et al. 2018). Climate change projections indicate that these deep seepage rates will decrease due to altered precipitation patterns, rising temperatures and increasing evapotranspiration rates in Lower Saxony within the next decades (Ahrends et al. 2018, Sutmöller 2014).

The specific water consumption of a forest depends on tree species composition and forest management and can vary significantly (Müller 2005, Sutmöller 2014). Comparing deciduous and evergreen forests, deciduous forests consume less water and increase deep seepage: Deciduous trees lose their leaves in winter, which reduces evapotranspiration and increases deep seepage. Evergreen trees, on the other hand, consume water all year round. Furthermore, the flat leaves of deciduous trees store smaller water amounts than the often cylindrically arranged needles of evergreen trees. Thus, deciduous trees evaporate less water from their surface than evergreen trees. In addition, stem flow of deciduous trees is often higher than of evergreen trees and substantially increases soil infiltration and deep seepage. In mixed evergreen and deciduous forests, characteristics of both evergreen and deciduous trees interact in a complex manner and resulting water fluxes depend on the mixing ratio of the tree species and is challenging to quantify (Müller 2011, 2012).

Deep seepage in forests can be investigated by means of direct measurements (lysimeters, tracer hydrology) or indirectly by using hydrological models (Golden et al. 2015, Hendriksson et al. 2013, Müller 2011). Comprehensive investigations of deep seepage rates in various evergreen, deciduous and mixed forests in Northeast Germany have been carried

out by Müller (2012) by using lysimeters. Deep seepage depends on the amount and temporal distribution of annual rainfall and thus varies from year to year. In the longer term, deep seepage ranges between 20 % and 40 % of mean annual precipitation sum in beech (*Fagus sylvatica*) forests in various ages. In comparable Scots pine (*Pinus sylvestris*) forests, deep seepage varies between 0 % and 30 %, being lower than in beech forests at any time. Deep seepage rates in mixed pine and beech forests are generally lower than in pure beech forests and higher than in pure pine forests at comparable age (Müller 2011, 2012).

In Lower Saxony, forest conversion from evergreen to deciduous forests has a great potential to increase deep seepage rates at the landscape level. Currently, 57 % of the forests in Lower Saxony are evergreen and 43 % are deciduous. The most important tree species is Scots pine (*Pinus sylvestris*, 29 %). Further important tree species are Norway spruce (*Picea abies*, 17 %), European beech (*Fagus sylvatica*, 14 %) and Oak (*Quercus robur*, *Quercus petraea*, 13 %) (Niedersächsisches Ministerium für Ernährung Landwirtschaft und Verbraucherschutz 2014). Recently, an increasing share of pure Scots pine forests in Lower Saxony is under conversion into mixed forests. For the conversion into near-natural and site-appropriate deciduous and mixed forests, European beech has been the most important target species in Northwest Germany so far (Rumpf & Petersen 2008).

Pine forests are usually converted at an age of at least 80 years. In the beginning, the stand density of the pine is reduced and young beech trees are planted, often after previous soil preparation. The pine is regularly thinned by removing weak trees, which promotes tree growth of dominant pine trees and also of young and vigorous beech trees. In the medium to long term, the mixed forest can be converted either into a pure beech forest by entirely removing the pine trees, or it remains a complex mixed forest.

The effect of these forest conversion practices on deep seepage in Lower Saxony has only been investigated in a few studies: Ringe et al. (2000) assessed deep seepage in a pure pine and a mixed pine and beech forest close to Hannover in 1998 and 1999. Schultze & Scherzer (2015) investigated the effect of forest conversion from pine forests to mixed forests with oak and Douglas fir on deep seepage in eastern Lower Saxony solely based on unsupervised modelling. The investigations of Müller (2012) are comprehensive, but not directly transferable to Lower Saxony as the climate conditions in Lower Saxony differ from those in Northeast Germany.

Accurate information about the effect of forest conversion on deep seepage amounts under different geographic conditions representative for Lower Saxony form the basis for answering many practical questions: These information can, for example, provide a basis for deciding how much money forest owners need and receive for converting their forests in order to increase the ecosystem service of deep seepage. Moreover, many evergreen forests in Lower Saxony need to be converted into mixed and deciduous forests as adaptation to changing climate conditions. Only stable forests that are adapted to the specific geographic and environmental conditions will be healthy in the future and will fulfil the broad range of forest functions.

Therefore, this study aims to quantify the effect of forest conversion from pure pine to pure beech forests on deep seepage in Lower Saxony. Thereby, mixed forests are of particular interest as they have been studied only in very few studies so far compared to pure evergreen and pure deciduous forests. In addition to mixed pine and beech, also a mixed pine

and Douglas fir (*Pseudotsuga menziesii*) forest is investigated, as Douglas fir has recently been a frequently selected target tree species for forest conversion (Fischer 2008).

Scots pine has a wide ecological range, a low nutrient demand and primarily grows on sandy soils in the lowlands of Lower Saxony. Therefore, three comparable study sites have been selected at representative sandy and nutrient-poor soils, representing climatically different regions of the Lower Saxonian lowlands: Sandkrug in western Lower Saxony receives more than 800 mm of precipitation per year, Wibbese in the eastern part of Lower Saxony receives only 600 mm of precipitation per year, and Elze in central Lower Saxony is located in between. These study sites represent typical forest sites in the Northwest German lowlands, where pine forests can potentially be converted into mixed forests.

At these study sites, in total 9 experimental forest plots have been selected to represent pure pine forests as well as different conversion stages with beech and Douglas fir. For these forest plots, deep seepage has been investigated in 2019 and 2020: Based on stand precipitation and soil moisture measurements, deep seepage has been modelled with the hydrological model *LWF-Brook90*.

Based on research findings e.g. from Müller (2012), Ringe et al. (2000), Schultze & Scherzer (2015), it is hypothesized that

- Resulting deep seepage will be lowest in pure pine forests and highest in pure beech forests.
- For the mixed pine and beech forests, it is assumed that deep seepage will be lower than in pure beech forests, but higher than in pure pine forests.
- Deep seepage is assumed to be lower in mixed forests with two evergreen species (pine and Douglas fir) than in mixed forests with an evergreen (pine) and a deciduous tree species (beech).
- Deep seepage is expected to increase in the pine stand in Wibbese after thinning

These hypotheses are further specified for the locations Sandkrug, Elze and Wibbese in the chapters 3.1.1, 3.1.2 and 3.1.3.

2 Theory and current state of research

2.1 Forest conversion from Scots pine to European beech

In Northwest Germany, **Scots pine** (*Pinus sylvestris*) is one of the economically most important tree species for forestry. Most of the pine forests are the result of afforestation of heathland and clear cuttings after World War II (Leuschner & Ellenberg 2017, Niedersächsisches Ministerium für Ernährung Landwirtschaft und Verbraucherschutz 2014). The Scots pine has a wide ecological amplitude and naturally grows on nutrient-poor and sandy soils or in less wet areas opposed to central parts of bogs in Northwest German lowlands (Leuschner & Ellenberg 2017).

Recently, an increasing share of pure Pine forests in Lower Saxony is under **conversion into mixed forests**. Forest conversion aims to (actively) change the structure of an existing forest by primarily changing the composition of tree species (Rumpf & Petersen 2008). In Germany, first forest conversions have started in the 1980s as a result of increasing immission-related damages to forests (Ulrich 1986). The most important motivation for the conversion of spruce forests into mixed forests was initially the reduction and spreading of operational and economical risks (Otto 1986). In recent decades, the motivation for forest conversion has become more differentiated: In comparison to monocultures, mixed forests are beneficial in terms of biodiversity, forest health, and economic production (Liu et al. 2018), because they are more resilient towards changing climate and environmental conditions due to their broader ecological amplitude (De Boeck et al. 2017, Paul et al. 2019). Thereby, the multifunctionality of forests for future generations should be ensured. Most of the forestry programs of the federal states (e. g. LÖWE guidelines in Lower Saxony) as well as in subsidy guidelines for private forests, forest conversion from evergreen to deciduous and mixed forests has been set as a target of near-natural forest management (Niedersächsische Landesforsten 2018).

For the conversion of coniferous forests into near-natural and site-appropriate deciduous and mixed forests, **European beech** (*Fagus sylvatica L.*) has been the most important target species in Northwest Germany so far (Rumpf & Petersen 2008). Being a common broadleaved tree species in Central Europe ever since, European beech has an extremely wide ecological amplitude (Ruhm et al. 2016): European beech occurs over a broad range of soil types, its climatic amplitude includes annual average air temperatures ranging from 4°C to 12°C and precipitation sums between 450 and 2000 mm $year^{-1}$. European Beech forests are naturally ubiquitous in Central Europe and occur even along the Atlantic coast and in Southern and Eastern Europe (Leuschner & Ellenberg 2017). Further favourable target tree species are oak (*Quercus rubra*, *Quercus petraea*), birch (e. g. *Betula pendula*) or Douglas fir (*Pseudotsuga menziesii*) (Böckmann et al. 2019, Schröder et al. 2018).

Forests can be converted either by **natural regeneration** or by **artificial regeneration** (planting or sowing). By natural regeneration, the next tree generation develops from seeds of mature trees and the target tree species is promoted through specific silvicultural measures. Wherever natural regeneration is not possible because of excessive competing vegetation or the target tree species is not in sufficient proximity, the target tree species needs to be planted or sowed artificially (Bayerische Staatsforsten 2022).

Rumpf & Petersen (2008) only recommend **forest conversion of pine forests** at an age of at least 80 years. In the beginning, the stand density of the pine is reduced in order to increase light availability. Then, young beech trees are planted, for example on a 2 m x 1 m grid. This planting system leads to a favourable qualitative development of the beech trees. If necessary, a fence is needed to protect the young trees from game browsing. The Scots pine is regularly thinned by removing weak trees, which promotes tree growth of dominant Scots pine trees and also of young and vigorous beech trees. According to Rumpf & Petersen (2008), a very strong reduction in the target stocking of pine only slightly promoted diameter growth of the beech trees, but led to considerable growth-loss of mature pines. Weak beech trees are also harvested to create additional space in which vigorous beech trees can grow into (Schröder et al. 2018). In the medium to long term, this results in a pure beech forest. Schröder et al. (2018) state that the Scots pine trees could be entirely removed even at an early forest conversion stage. As possible disadvantages, the remaining unprotected beech trees could be damaged by wind, snow, late frost and sun. On the other hand, an early removal of the pine layer can accelerate the growth of dominant beech trees and it can reduce the risk of pine trees being threatened by age-related pests (Schröder et al. 2018).

The pronounced drought in 2018 and 2019 has led to a large-scale dieback of forests in Central Europe. These developments raise general questions regarding the **adaptability of the main tree species to changing climate and environmental conditions**. Pine is considered being relatively drought-tolerant, but also suffers from the consequences of climate change. For example, the Diplodia tip blight disease (Bußkamp et al. 2020), favoured by drought stress and heat occurs more frequently in Northern Germany (Rohde et al. 2020). Under drought conditions, beech trees suffer from leaf senescence, crown mortality and bark exudation. Once a tree is weakened, it is particularly exposed to pests and pathogens and has an increased mortality risk. However, vital and dead tree individuals grow in direct proximity to each other. This indicates that not only location and environmental effects but also genetic disposition are important for a single tree's ability to adapt to changing climate conditions (Mergner et al. 2020). A glance at the effect of drought on beech trees in the past reveals that the majority of tree individuals recovered quickly and showed normal growth rates already two years after drought (Scharnweber et al. 2011).

The geographic origin (provenance) of tree individuals is often discussed to play an important role in drought tolerance. The current state of knowledge does not reveal a clear relationship between drought tolerance and provenance: Drought-related mortality correlated significantly with climatic factors as the mean growing season precipitation at population origins, rather than with geographic margins of the beech range (Bolte et al. 2016). Nguyen et al. (2017), however, did not find a positive correlation between low precipitation and increased drought resistance by investigating beech seedlings from provenances with different precipitation sums. Müller & Finkeldey (2017) found provenances from lower precipitation areas performing worse than provenances from higher precipitation areas with respect to drought tolerance in a field study in Northern Germany. Instead, they detected a minor genetic structure among provenances and a high genetic diversity within provenances. Kriebitzsch & Veste (2012) found a significantly high genetic variability within each population and only occasionally between different populations. Czajkowski & Bolte (2006) found highly drought resistant tree individuals in two different provenances, which indicates that forests are able to adapt to droughts by selection processes. Hosius et al. (2019) also found that poorly adapted parent individuals can create well-adapted descendants. A

study investigating the adaptive capacity of Sitka spruce (*Picea sitchensis*) even implies that tree individuals are also able to mutate their DNA within one life cycle to adapt to changing environmental conditions (Hanlon et al. 2019). Thiel et al. (2014) recommends to mix provenances being adapted to a variety of different climatic factors, such as drought or frost. A great provenance variety may act as functional insurance in future drought-prone forests (Thiel et al. 2014). Hajek et al. (2016) conclude that European beech has a high potential capacity to cope with changing climate and environmental conditions due to the high degree of **intra-population genetic variability**.

At the stand level, an increased tree species richness widens the forest's tolerance and increases its ability to successfully cope with changing environmental conditions. Mixing tree sizes and ages further strengthen the resistance of the forest. As genetic variation within tree species drives their adaptive capacity, it is advisable to maintain or increase the genetic variation by natural regeneration, enrichment with other provenances and exertion of variable selective pressure on single trees (Spathelf et al. 2014). At the stand scale, specific thinning practices promote the growth of vigorous tree individuals that are more resistant to biotic pests. Further adaptive strategies include persistence of current forest types, local adaptation due to environmental pressure and migration or substitution of species (Bussotti et al. 2014). Further recommendations to adapt forests to changing climate conditions are given by Spellmann (2020) and Höltermann & Jessel (2020).

2.2 The water cycle in forest ecosystems

Water cycles in various aggregate states between atmosphere, pedosphere and biosphere. The water balance of forest ecosystems is largely affected by tree, shrub and soil vegetation and is separated into the following terms of the water balance equation (Bartsch & Röhrig 2016):

$$P - I_T - I_G - SF - T_T - T_G - E_S - OF - IF - S = SWS \quad (1)$$

where precipitation (P), tree interception evaporation (I_T), ground vegetation interception evaporation (I_{SV}), stem flow (SF), tree transpiration (T_T), ground vegetation transpiration (T_{SV}), soil evaporation (E_S), overland flow (OF), interflow (IF), seepage flux (S) and soil water storage (SWS). A detailed overview of the hydrologic cycle in forest ecosystems is given in Figure 1.

Water enters the hydrological system as **precipitation**. Precipitation occurs in various aggregate states and forms, such as rain, snow, hail, dew, hoarfrost or fog. The forests that are present worldwide receive mean annual precipitation sums from 300 mm to more than 6000 mm (Bartsch & Röhrig 2016). In the lowlands of Lower Saxony, mean annual precipitation sums range between 500 mm and 800 mm.

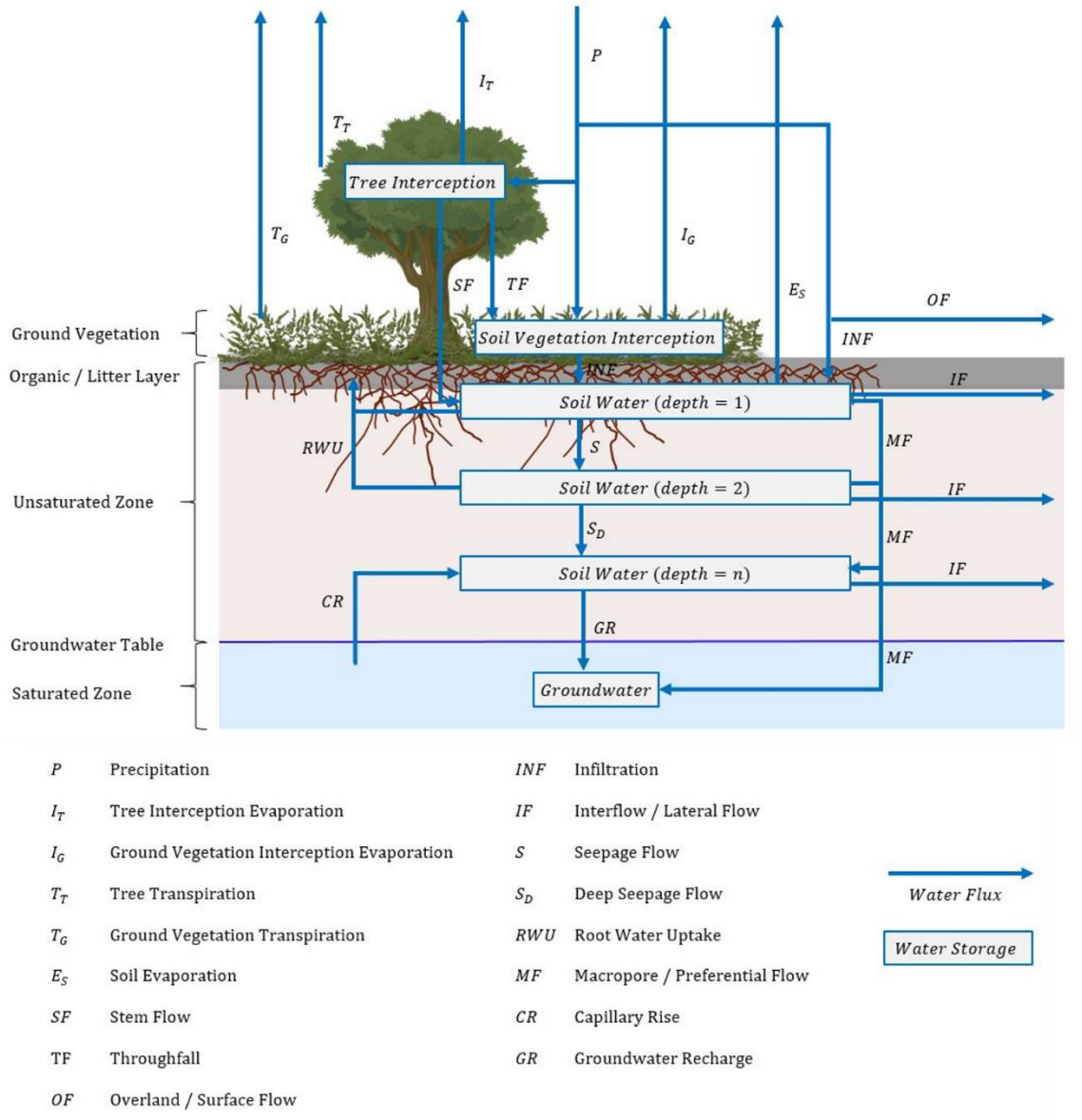

*Figure 1: Components of the **water cycle in a forest ecosystem** (modified after Hörmann et al. (2003)).*Water fluxes are shown as arrows and water storages are shown as boxes.

In forest ecosystems, leaves, needles, twigs and branches in the tree layer catch a variable portion of precipitation. This water is to a certain extent stored on vegetated surfaces and evaporates back into the atmosphere (**interception evaporation**). Interception evaporation rates are largely affected by weather conditions, location and tree species (Carlyle-Moses & Gash 2011, Ellenberg et al. 1986, Müller 2012, Peck & Mayer 1996). When water input is greater than the storage capacity of the vegetated surface, water either drips off and falls to the ground (**throughfall**) or is routed to the ground via twigs, branches and stems (**stemflow**). The sum of precipitation that reaches the ground including throughfall and stemflow, is referred to as **stand precipitation** (Bartsch & Röhrig 2016). Throughfall is highly variable in both time and space: Throughfall correlates with canopy openness and the spatial variability within a forest increases with tree age as trees naturally die off or are removed during forest intervention (Müller 2019). Stemflow is significantly affected by tree species, tree age, crown and bark morphology, woody biomass amount, branch number, branch inclination and weather conditions. Especially precipitation sum and intensity as well as stem and bark conditions control stemflow amounts (Levia et al. 2015, Müller 2019).

Relevant for the precipitation distribution on the forest floor is not only the stemflow amount, but also the distribution of stemflow from trees in the forest. The distribution of stemflow in the forest is linked to number and diameter of trees and thus to stand density. In beech forests, for example, this distribution is more important for moisturizing the forest soil than the absolute stemflow amount. Moreover, high stemflow amounts moisturize the soil also in relatively dry periods and in winter time, stemflow mostly directly becomes deep seepage (Müller 2012).

Apart from the tree layer, also the **ground vegetation** including shrubs, herbs and litter intercept a certain portion of precipitation (Gerrits & Savenije 2011, Helvey & Patric 1965, Putuhena & Cordery 1996). Note, that interception and stand precipitation values reported in the literature may (not) consider tree, shrub and/or ground vegetation.

Apart from interception evaporation, **evaporation** processes generally occur, where water is exposed to unsaturated air: Water evaporates from water surfaces, bare soil, rain droplets and to a lesser extent from snow surfaces. The amount of water evaporating from bare soil (**soil evaporation**) depends on soil texture: Coarse soil material dries out more quickly but to a lesser depth than fine textured soil. In general, meteorological variables such as water vapour deficit of air, solar radiation and wind control the amount of water that evaporates to the atmosphere (Bartsch & Röhrig 2016).

The vegetation in a forest ecosystem is part of the biosphere and connects the atmosphere and pedosphere. Many plants transport water from their roots to their leaves, driven by the difference in water potential between the soil and atmosphere (**transpiration**). The maximum possible amount of water that can be transpired under given site conditions and an unlimited water supply is defined as potential transpiration. The water amount that transpires under given weather and soil water conditions is defined as actual transpiration. If the water potential of the atmosphere is lower than in the intercellular space within the leaves, water vapour diffuses through the stomata and to a much lesser extent through the cuticula to the atmosphere. The decreased water potential within the leaves causes a compensational water flux from higher water potential in the roots to lower water potential in the leaves, and consequently from the soil into the roots. The plant can actively regulate transpiration by opening and closing their stomas, which also serves as a protection mechanism to avoid excessive water consumption during warm and dry air conditions. Under dry conditions, the plant extracts water from the soil until the water potential reaches the permanent wilting point. At this point, water is so strongly bound to soil particles that it is no longer available for plants (Larcher 2001). Transpiration rates depend on both meteorological conditions and plant physiological and soil characteristics and thus differ significantly among geographical locations and species (Jochheim et al. 2004, Larcher 2001, Leuschner et al. 2004, Müller 2012, Peck & Mayer 1996). Apart from the tree vegetation, ground vegetation substantially contributes to total transpiration in forest ecosystems (Lüttschwager et al. 1999, Müller 1967, Müller n. d.). Transpiration, evaporation and interception are often combined in one term that is referred to as **evapotranspiration**.

Stand precipitation either infiltrates into the soil (**infiltration**) or flows laterally at the soil surface (**overland flow**). Overland flow usually occurs if the soil surface is inclined or sealed, frozen or heavily compacted and thus less permeable. Moreover, overland flow occurs during heavy rainfall events when the top soil layer is saturated and water is routed laterally. However, infiltration plays a far more important role on vegetated forest ground

than overland flow. Tree and soil vegetation as well as crown density mainly affect water input into the soil. Especially tree species and the distribution of single trees in the forest control occurrence and amount of stemflow and thus local water input (Schwärzel 2012). The presence, form, thickness and water storage capacity of an organic layer thereby further controls water infiltration and overland flow. The infiltration rate depends on precipitation type and intensity, soil porosity, soil moisture and soil organic material content (Neary et al. 2009).

A major share of infiltrating water is temporarily stored in the soil matrix. Adhesive intermolecular forces between solid soil particles and water molecules alone (**adsorption**) and in combination with cohesion between liquid water molecules (**capillary forces**) hold water in the soil matrix. The soil water content **or soil moisture** is defined as water proportion per unit soil volume (volumetric soil water content) or soil mass (gravimetric soil water content). The amount of soil water that is held back against gravity is referred to as field capacity. The adsorption water is not readily available for plants because of strong adhesive forces that cannot be overcome in the root systems of plants (Amelung et al. 2018). Soil moisture in forest soils is highly variable within very short distances (Morgenstern et al. 2011). These heterogeneous patterns result from several factors, such as tree and ground vegetation, crown density, soil texture, root distribution and inclination, which interact and vary in a complex manner (Brocca et al. 2007, Chifflard et al. 2003, Morgenstern et al. 2011, Western et al. 1998). Tree and soil vegetation extract water with their roots from various depths. They are heterogeneously distributed in space and can cause local soil moisture minima (Morgenstern et al. 2011). Spatial variations of soil texture as well as the occurrence of impermeable soil layers further affect spatial soil moisture patterns.

The majority of infiltrated water percolates, driven by gravity, vertically into deeper soil layers (**seepage**). Soil texture and the presence of macropores determine how easily the water passes the soil downwards: Fine textured soils with small pores such as clay are less permeable than sandy soils with wide pores. Decaying roots, shrinking cracks and bioturbation can form macropores, through which water preferentially moves downwards (**preferential flow**). Preferential flow pathways are very common in forest soils and can increase both the infiltration rate and the deep percolation rate (Alaoui et al. 2011, Clothier et al. 2008, Guo & Lin 2018, van der Heijden et al. 2013, Zhang et al. 2016). Vertical changes in soil texture or impermeable layers such as rock formations within the soil reduce drainage velocity or even blocks vertical drainage. At the surface of these layers, water either accumulates temporarily (**stagnant water**) or flows laterally (**lateral flow**). Lateral flow either exfiltrates to the surface (**throughflow**) or enters a stream prior to becoming groundwater (**interflow**). The remaining water percolates into deeper soil layers below the root zone (**deep seepage**) and may eventually reach the groundwater (**groundwater recharge**) (Bartsch & Röhrig 2016).

In general, the above-mentioned water fluxes are present in every hydrological system in forested areas. The scale of single fluxes and the relation between several fluxes vary with climate, vegetation and soil type (Bartsch & Röhrig 2016).

2.3 Methods to determine the water cycle in forest ecosystems

Many hydrological fluxes of the forest water cycle can be measured directly or indirectly. This chapter reviews current methods that are used to estimate these hydrological fluxes.

2.3.1 Measuring the hydrological cycle in forest ecosystems

Water input in the hydrological system of forests (**precipitation**) is measured with a rain gauge in an open space without tree vegetation.

Throughfall in forests has been measured in various research studies within the last 130 years (Delfs 1955, Mitscherlich 1971, Müller 2019, Peck 2004). The methodology to assess stand precipitation has experienced only little changes over time, however, the technical equipment has improved significantly (Müller 2019). Stand precipitation is measured with rainfall collectors or gutters (Clarke et al. 2016). Zimmermann & Zimmermann (2014) and Clarke et al. (2016) suggest to assess stand precipitation with single rainfall collectors that are located equidistantly on a grid in the stand. Measurements with single collectors require regular cleaning and maintenance and are thus very laborious when many collectors are used. Thimonier (1998) found that the number of collectors and their spatial distribution in the forest stand is more important than the collector type. Gutters have a larger surface and their handling with respect to cleaning and maintenance is less laborious compared to single rainfall collectors. So far, a harmonized sampling strategy for stand precipitation measurement with gutters does not exist. Thimonier (1998) suggests to favour multiple shorter gutters over one long gutter to minimize evaporation losses. The DVWK (1986) suggests to use two to four gutters per plot with a length of 10.05 m, a width of 0.16 m and an inclination of 1:10. For example, the State Institute of Bavaria for Forestry and Silviculture (LWF) uses two of these gutters according to DVWK (1986) per plot. In general, the rainfall collectors should represent stand precipitation variability (Zimmermann et al. 2016). Müller (2019) states that stand precipitation amounts correlate with canopy openness and spatial stand precipitation patterns are influenced by tree species composition, the location and constitution of single trees.

Stemflow is usually measured with tubes that are split in half and wrapped around the trunk of a tree. The gap between tube and trunk is sealed with silicone to ensure water tightness. The collected water is then routed to a tipping bucket (automatic measurement) or a tank, where it is stored until the amount is manually measured. Stemflow is usually measured for several neighbouring trees. There is no harmonized sampling strategy for measuring stemflow yet, however, the methodology used is mostly similar and described in detail in several research papers dealing with stemflow measurements (Coenders-Gerrits et al. 2010, Levia & Germer 2015, Müller 2019). A comprehensive review of stemflow measurements in forests is given in Levia & Germer (2015).

The **soil moisture** can be measured directly in the laboratory by measuring the weight of water as proportion of the total soil sample (gravimetric method). This method, however, is destructive, time-consuming and does not deliver continuous measurements. On the other hand, the soil water content can be measured indirectly by measuring variables that are affected by the soil water content. Common soil moisture sensors measure the dielectric permittivity by measuring the travelling time of an electromagnetic wave back and forth on the probe (time-domain-reflectometry, TDR), or the dielectric properties of the reflected electromagnetic wave in the frequency domain (frequency-domain-reflectometry, FDR). Other sensor methods are based on the resistivity of the soil towards electronic currents, neutron scattering within the soil and soil thermal properties. Bittelli (2011) gives a comprehensive overview about soil moisture measurement techniques.

Soil moisture sensors, especially those based on relative electrical permittivity of the bulk soil, are widely used to continuously measure the soil water content in the field. However, both absolute soil water content values and relative reactions over time are often not accurately measured by these measurement systems. Raw soil moisture values can be improved by systematic calibration procedures. These procedures are, however, not harmonized and time-consuming so far (Jackisch et al. 2020).

Forest soils are highly inhomogeneous and soil water contents can vary significantly over small distances (Morgenstern et al. 2011, Schwärzel et al. 2009). Therefore, many soil moisture sensors are needed to approximate the mean soil water content of a forest soil. Schwärzel et al. (2009) suggest to measure soil moisture with a horizontal and vertical distance between 10 and 30 cm to capture soil moisture heterogeneity and to detect preferential flows.

Deep seepage can be estimated either directly by field measurements or indirectly with hydrological models. Direct measurements aim to assess the water flow through a defined area in a presumably undisturbed environment. Deep seepage flow rates are measured in a depth of several meters below the root zone.

Lysimeters are measurement tools to directly measure deep seepage rates (see Figure 2). A lysimeter consists of a soil monolith on top of a collecting device that collects seepage water. The soil monolith is encased in a container and thus hydrologically isolated from the surrounding soil. Depending on the research question, the soil is either naturally layered and undisturbed, or artificially layered (Müller 2017). Lysimeters allow accurate investigations of water quantity and quality, however, their installation is very costly and needs a long adaptation period.

In order to assess the water balance of forests, the lysimeter is planted with trees. Forest lysimeters are usually several meters deep and have an area of at least 100 m² to minimize boundary effects that occur along the encasing. They are installed representatively within a forest stand. Forest lysimeters are rare and can be found, e.g., in Eberswalde (Müller 2017), St. Arnold (Harsch et al. 2009) and Colbitz (Glugla et al. 1982) in Germany. The Lysimeter Research Group (2019) gives an overview of further existing forest lysimeters in Europe.

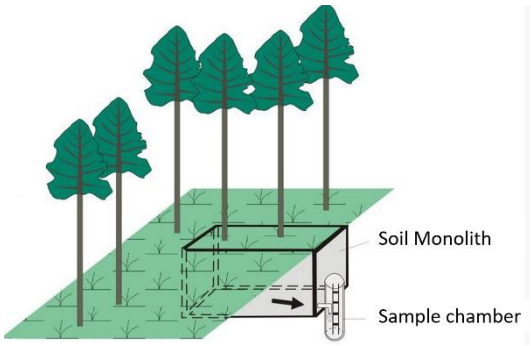

*Figure 2: Schematic illustration of a **forest lysimeter:** This lysimeter type is for example installed by the Thünen Institute for Forest Ecosystem Research in Eberswalde, Northeast Germany (Thünen Institut 2021).*

Seepage amounts can also be assessed by using tracer hydrological methods, if seepage or groundwater samples can be collected. Stable isotopes are frequently used as tracers of hydrological processes in order to determine groundwater ages and recharge rates. They do not undergo radioactive decay and only change as a result of certain processes, such as evaporation or mixing of water from different sources. They are useful to identify water sources, to evaluate interactions of different water types and to understand geochemical reactions in groundwater systems (Hendriksson et al. 2013).

In tracer hydrology, oxygen and hydrogen stable isotopes are often used. Different water sources (e.g. precipitation, surface water and groundwater) have distinct stable isotopic ratios due to natural fractionation processes. Groundwater, for example, is isotopically distinct from precipitation due to selective recharge or isotopic fractionation effects related to evapotranspiration and runoff. The contribution of precipitation on groundwater recharge can be assessed by comparing the isotopic compositions of oxygen and hydrogen in precipitation and groundwater samples (Hendriksson et al. 2013).

Another prominent hydrological tracer is tritium, which is a radiogenic isotope of hydrogen. Since large amounts of tritium had been released to the atmosphere from nuclear bomb testing in the 1950s and 1960s, it has been used as a tracer in hydrology. Tritium rapidly oxidizes into tritiated water (usually within one year) and enters the hydrological cycle via precipitation. It acts similarly in the water cycle as other water molecules. It naturally decays radioactively to its stable daughter helium with a half-life of 12.3 years. Timing and rates of groundwater recharge, flow and mixing can be assessed based on the distribution of tritium and its rate of decay (Hendriksson et al. 2013). This method has frequently been used to investigate groundwater recharge rates (e.g. Röper et al. (2012)).

A common method is the chloride mass-balance method (Allison & Hughes 1978, Bazuhair & Wood 1996, Eriksson & Khunakasem 1969), which is based on the mass balance of chloride considering long-term chloride concentrations in precipitation and soil water. The chloride concentration in soil water increases due to evaporation and the relationship between chloride concentrations in precipitation and soil water is thus a measure of seepage. Increasing evaporation rates increase the accuracy of resulting recharge rates. However, this method can be erroneous if precipitation is not the only chloride source or if chloride concentrations experience an increase or decrease due to dissolution or plant uptake (Leibundgut & Seibert 2011).

2.3.2 Modelling the hydrological cycle in forest ecosystems

Deep seepage rates in forests are often estimated indirectly by using **hydrological models**. In order to answer the research question of this study, the hydrological model should be able to successfully simulate all relevant components of the hydrological water cycle in forests, including interception, soil water content in various depths and deep seepage of forest stands with different vegetation characteristics.

Within the last decades, many hydrological models have been developed and have been proven to successfully represent forest hydrological systems. Hydrological models approximate all terms of the water balance equation, including deep seepage, based on meteorological, vegetation and soil data. Hydrological models can simulate water fluxes from single points to entire watersheds. A hydrological model used frequently for water balance studies in forests is Brook90 in various extensions (Federer 2019, Hammel & Kennel 2001, Schmidt-Walter et al. 2020b). Further hydrological models used to model forest water balances are e. g. FORHYCS (Speich et al. 2020), TOPMODEL (Beven & Kirkby 1979), WaSiM-ETH (Schulla 2021) or COUPMODEL (Jansson & Karlberg 2004). COUPMODEL for example, is able to represent multiple canopy layers representing for example ground vegetation and canopies of different tree species (Jansson & Karlberg 2004). A systematic review of hydrological modelling in forest ecosystems is provided by Golden et al. (2015).

LWF-Brook90 fulfils these requirements and has proven to successfully model the water balance in German forests many times (Groh et al. 2013, Hammel & Kennel 2001, Müller 2019, Schmidt-Walter et al. 2020b, Weis et al. 2020). Therefore, **LWF-Brook90** is used for water balance modelling in this study. LWF-Brook90 is a one-dimensional, process-based model for water balance simulation on a daily basis. Detailed information about general model conception, processes and parameters are described in Federer (2019), Hammel & Kennel (2001) and Schmidt-Walter et al. (2020a). LWFBrook90 is based on Brook90, a soil vegetation atmosphere transfer model that simulates soil water movement, evapotranspiration and local runoff for small and homogeneous watersheds or for single plots (Federer 2019). Hammel & Kennel (2001) modified the model (LWF-Brook90) by specifying soil parameterization, phenology and stand development over time. Recently, Vorobevskii et al. (2020) and Schmidt-Walter et al. (2020a) have implemented LWF-Brook90 in R, which is an open-source software environment for statistical computing and graphics and has facilitated data management and analyses across all scientific disciplines (R Core Team 2017). The R package 'LWFBrook90R' is available on the comprehensive R Archive Network (CRAN) and can be directly downloaded. Thus, the hydrologic community can now use this interface to run LWF-Brook90 and process model output flexibly and user-specifically (Schmidt-Walter et al. 2020b).

LWF-Brook90R incorporates the main hydrological fluxes and storages of a forest hydrological system (Figure 3): Water enters the system as rain or snow precipitation. Snow is either stored in the snow interception storage (INTS) and finally evaporates to the atmosphere (snow interception evaporation), or it enters the snowpack as snow throughfall. From the snowpack, snow either evaporates to the atmosphere (snowpack evaporation) or melts (snowmelt). Rainfall is partly stored in the rain interception storage (INTR) and eventually evaporates to the atmosphere (rain interception evaporation). The remaining share of rain (rain throughfall) reaches the soil or, if a snowpack is present, is added to the snowpack as liquid water. Snowmelt and rain reaching the ground either infiltrate into the soil or contributes to overland flow, which eventually routes water to streamflow. Water infiltrating into the soil can either enter one or more soil layers (soil water storage). Infiltrating water can also be routed directly to streamflow (bypass flow). Only from the uppermost soil water storage, water can evaporate to the atmosphere (soil evaporation). From any soil water storage, water either drains to the next lower soil water storage (vertical drainage), or directly flows to the stream flow (downslope flow), or transpires via plant roots to the atmosphere (transpiration). Only from the lowest soil water storage, water drains into the groundwater storage. From the groundwater, water either seeps further down (deep seepage from groundwater) or flows to the stream flow via downslope flow. Snow interception evaporation, rain interception evaporation, snowpack evaporation, soil evaporation and transpiration add up to total evapotranspiration. Overland flow, bypass flow and downslope flow add up to stream flow (Federer 2019, Hammel & Kennel 2001).

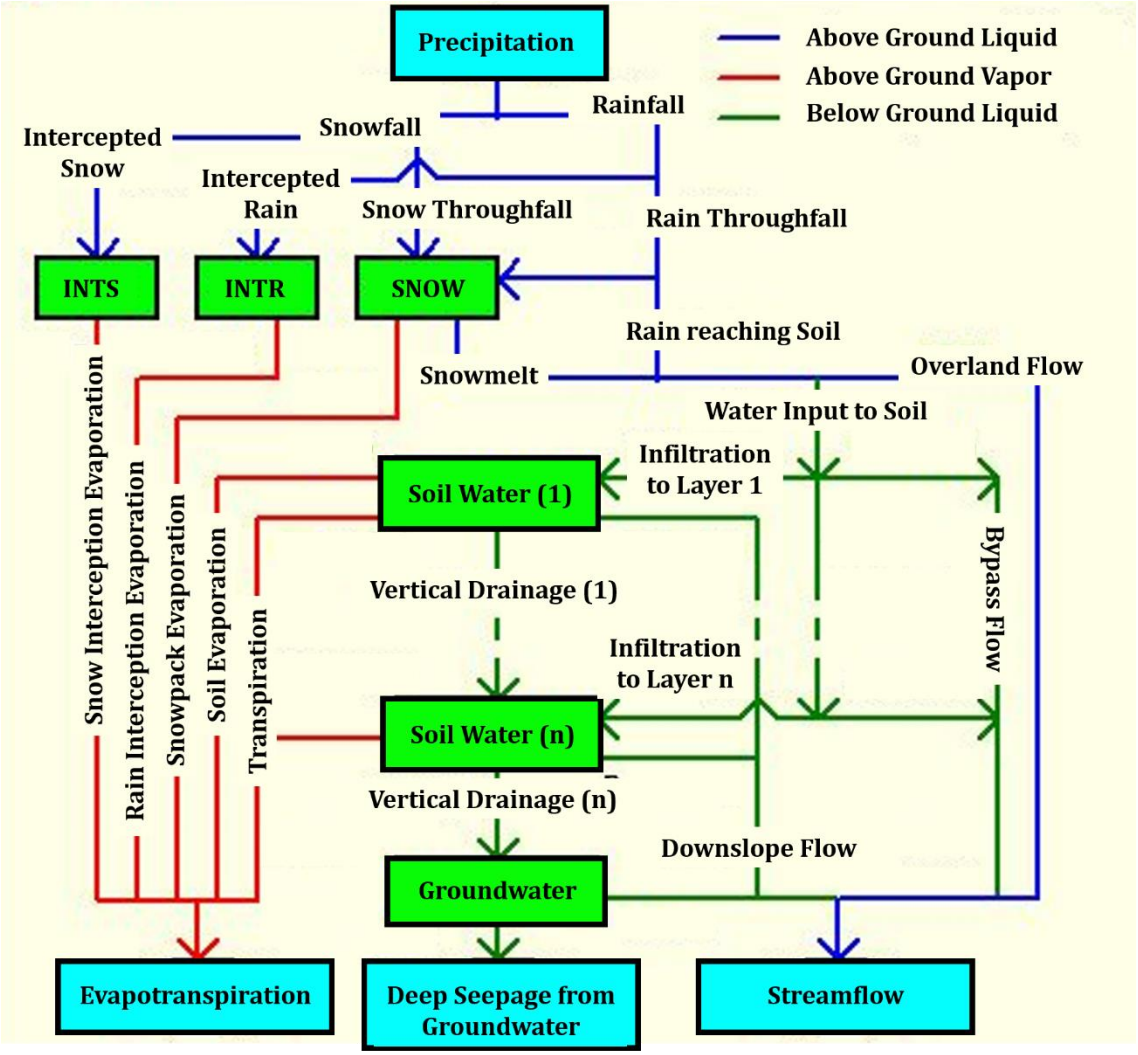

*Figure 3: Modelled water fluxes (arrows) and water storages (boxes) in **LWF-Brook90**, modified according to (Federer 2019).*

Figure 4 shows the workflow of LWF-Brook90R: The model requires climate data (daily precipitation, temperature, water vapour pressure, solar radiation, wind) and soil data (sand, silt, clay and gravel content, bulk density and organic carbon content). LWFBrook90R provides pedotransfer functions to estimate soil hydraulic parameters from physical soil data. In the model options, the user specifies basic technical settings with regard to simulation time period, type of radiation input, precipitation time interval and the method used to derive water retention characteristics and unsaturated hydraulic conductivity. In the model parameter settings, the user can specify any of the more than 100 parameters (see Table 67 in the appendix) that control the modelled hydrological cycle. For forest ecosystems, especially vegetation parameters are essential, as the forest canopy governs many water fluxes in forests, such as interception evaporation and transpiration. For example, reliable information about the leaf and woody area and its temporal dynamics are needed (Fleck et al. 2016). The Leaf Area Index (LAI) and Stem Area Index (SAI) are defined as one-sided leaf area and woody area per unit ground area, respectively (Chen & Black 1991, Watson 1947). The sum of LAI and SAI is referred to as Plant Area Index (PAI). LAI and SAI can be estimated directly by either harvesting biomass or collecting litter fall samples. These direct methods are highly accurate but destructive and time-consuming. Indirect methods such as digital hemispherical photography (DHP), the plant canopy analyzer or remote sensing techniques

are less tedious and well established in forest sciences. However, indirect methods derive LAI and SAI based on highly variable light regimes and radiation, which can cause substantial measurement errors. The choice of an appropriate method for LAI derivation depends on accuracy, time and labor capacity along with the tolerable degree of canopy disturbance (Fleck et al. 2016). Given the climate and soil data, the model options and model parameters, the package core function first specifies and determines phenology, leaf area index, root density depth distribution and daily vegetation properties. With these model parameters including soil, climate and vegetation properties, the model LWF-Brook90 is run and user-specifically selected output files (results) are returned (Schmidt-Walter 2019).

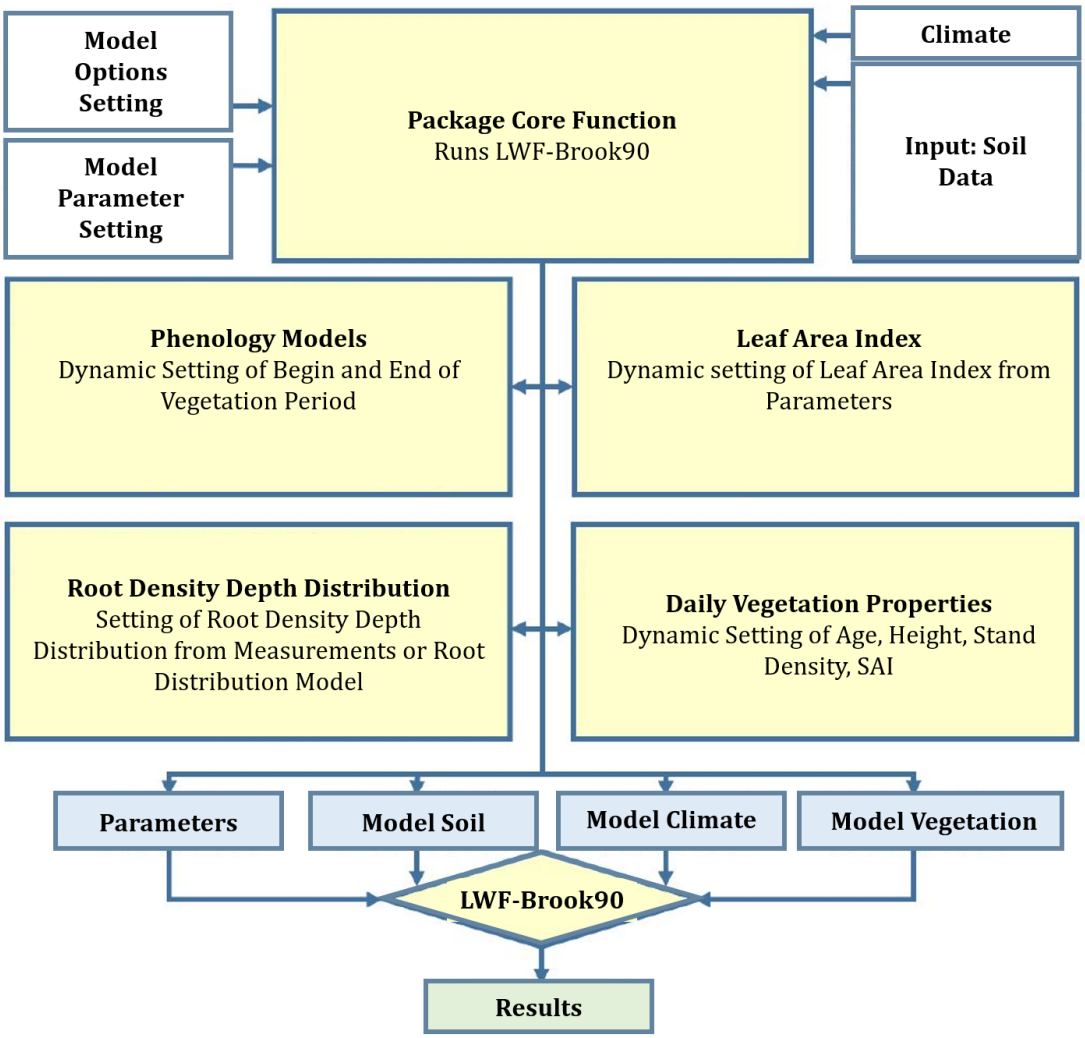

*Figure 4: The **LWFBrook90R workflow:** Model functions (yellow boxes), model parameters that can be specified by the user (white boxes), model input objects (blue boxes) that are constructed within the package core function and passed to the model LWF-Brook90, which finally returns the model results (green box). The figure is modified according to Schmidt-Walter (2019).*

Once a hydrological model is set up with site-specific weather, soil and vegetation data, the model can be used to calculate the water balance without further supervision (Ahrends et al. 2018, Schultze & Scherzer 2015). However, hydrological processes interact and depend on various state variables in a complicated manner. They behave often highly complex and non-linear and can to a certain extent be described only conceptually in hydrological models. Thus, hydrological models represent real hydrologic systems incompletely and in a simplified way. Corresponding model parameters are often arbitrary and cannot be estimated directly. They can be derived indirectly by finding a parameter set that produces a good

agreement between modelled and observed state variables. This procedure is referred to as model calibration. Recently, measured soil water storage (Schmidt-Walter et al. 2020b), soil moisture in various depths (Groh et al. 2013, Hammel & Kennel 2001, Müller 2019), matric potential, stand precipitation (Groh et al. 2013, Müller 2019), stream discharge (Armbruster et al. 2004), seepage rates from lysimeters (Klein 2000, Müller 2019) and remote sensing data (Tapia-Arenas et al. 2020) have been used for model calibration and validation.

Model calibration is a multi-step process: First, measured state variables, such as groundwater level, stream discharge, soil moisture or evapotranspiration are selected for model calibration. Second, important model parameters that are adjusted during model calibration are identified. This can be a difficult decision to make, as hydrological models often have tens to hundreds of parameters. A **sensitivity analysis** identifies relevant model parameters: It distinguishes unimportant model parameters from those that significantly influence model results and thus highlights parameters that are well suited for model calibration (Pianosi et al. 2016, Saltelli et al. 2008, Song et al. 2015). Sensitivity analyses are usually applied prior to the modelling process itself and can give valuable insights into model structure and behaviour (Song et al. 2015). Moreover, sensitivity analyses enable the modeller to assess the robustness of simulation results to uncertain input parameters or model assumptions (Paton et al. 2013).

The idea of sensitivity analyses is to run the model repeatedly with varying input parameter values within a reasonable range. The simulation output of each model run is then compared with observations and the corresponding parameter set is depending on the degree of agreement accepted (*behavioural* parameter set) or discarded (*non-behavioural* parameter set). After a sufficiently high number of simulations, each parameter is checked for its influence on model output: Parameter values from behavioural parameter sets form the behavioural probability distribution, and those from non-behavioural parameter sets form the non-behavioural probability distribution. If behavioural and non-behavioural probability distributions differ significantly, the model output is sensitive towards this parameter.

Sensitivity analyses can be divided into local and global sensitivity analyses. Local sensitivity analyses vary input factors around a specific value, whereas model parameters are varied within the entire parameter space in a global sensitivity analysis. Corresponding parameter ranges need to be specified by the modeller. Expert knowledge about plausible input values and variations is thus critical for meaningful sensitivity analyses (Pianosi et al. 2016). Furthermore, parameters can be varied one, several or all at a time. Simultaneous variations of multiple model parameters allow to characterize interactions between multiple input parameters. This, however, requires big sample sizes and thus significant computational resources. Devak & Dhanya (2017) give a comprehensive overview about existing sensitivity analysis methods and their characteristics. Systematic sensitivity analyses for LWF-Brook90 have been rare so far. Groh et al. (2013) conducted a global sensitivity analysis of LWF-Brook90 model performance referenced by observations of soil moisture. Schmidt-Walter et al. (2020b) investigated model input effects on model performance based on observed soil water storage.

Once the calibration parameters are selected, they can be adjusted during **model calibration**. The calibration parameters are varied within predefined ranges, until the resulting modelled and measured state variables are in good agreement. Model calibration can be

done manually by successively adjusting model parameters, however, manual calibration is cumbersome and to some extent subjective. Recent computational advances, however, make automatic calibration techniques such as Monte Carlo and Bayesian Inference easily available.

Recently, **Bayesian techniques** have been increasingly used for calibrating hydrological models (Hartig et al. 2012, Schmidt-Walter et al. 2020b, van Oijen 2017). Working with probability density functions, Bayesian approaches provide a statistical framework for sophistically quantifying uncertainties in model parameters and model predictions (Post et al. 2017, Raj et al. 2018, Schmidt-Walter et al. 2020b). Bayesian inference is based on the posterior distribution $p(\theta|D)$. The posterior distribution is the joint probability distribution of the vector of model parameters (θ) given the observed data (D). The posterior distribution is constructed by combining the prior distribution of the model parameters ($p(\theta)$), which represents pre-existing knowledge about the model parameters, and the likelihood function ($p(D|\theta)$), which is the distribution of observed data given the model parameters. Thereby, Bayesian inference adopts pre-existing knowledge through the prior distribution and updates the posterior distribution as additional data becomes available (Jeremiah et al. 2011, Marshall et al. 2004). The posterior distribution of the model parameters is calculated following Bayes theorem (Hogg & Foreman-Mackey 2018):

$$p(\theta|D) = \frac{1}{Z} p(D|\theta) p(\theta) \qquad (2)$$

Z is a constant often reffered to as marginal likelihood (Hogg & Foreman-Mackey 2018). Most hydrological models, unfortunately, have many parameters and act nonlinear and complex. Therefore, the posterior distribution may have multiple local modes and discontinuous derivates and cannot be solved analytically (Bates & Campbell 2001). To successfully summarize the posterior probability density function, **Monte Carlo methods** are routinely employed (Gelman et al. 1995). In particular, sampling methods such as Markov Chain Monte Carlo (MCMC) algorithms are frequently used. MCMC algorithms generate a random, correlated sample from the posterior distribution of model parameter values given the observed data (Bates & Campbell 2001, Micevski & Kuczera 2009). They generate a random walk through parameter space with a stable frequency stemming from a fixed probability distribution. To visit configurations with a stable frequency, a MCMC algorithm generates trial moves from the current position of the Markov chain to a new state (Vrugt et al. 2009). Several MCMC algorithms have been developed to efficiently explore the parameter space, such as the Random walk Metropolis (Metropolis et al. 1953), Metropolis-Hastings (Hastings 1970, Metropolis et al. 1953), Shuffled Complex Evolution Metropolis (SCEM) algorithm (Vrugt et al. 2003) and the Differential Evolution Adaptive Metropolis (DREAM) algorithm (Vrugt & Ter Braak 2011, Vrugt et al. 2009, Vrugt et al. 2008b). Hydrological models have successfully been calibrated by applying MCMC methods, for example by using the SCEM algorithm (Groh et al. 2013) or the DREAM algorithm (Schmidt-Walter et al. 2020b).

The calibrated model is then **validated** whether it is able to reproduce measured state variables outside of the calibration period. In this validation period, a successfully calibrated model reliably reproduces observed state variables. However, a good fit must result from plausible reasons and parameters must act as intended. Therefore, the model parameterization resulting from model calibration must be carefully checked for plausibility (Schaefli & Gupta 2007). A successfully calibrated and validated model can then be used to determine the entire hydrological cycle, including seepage rates.

2.4 Measuring the effect of forest type on the water cycle

Tree species affect the components of the water cycle in forest ecosystems differently. Here, species-specific effects of Scots pine and European beech on the water cycle are reviewed.

2.4.1 Species-specific vegetation data

In the literature, **LAI** values in Scots pine stands range between 1.1 and 3.4 (Bealde et al. 1982, Bréda 2003, Lovynska et al. 2018, Soudani et al. 2002). LAI values in beech stands are generally higher and vary between 2.6 and 9.5 in beech forests of varying ages (Bréda 2003, Černý et al. 2018, Kram 1998, Leuschner et al. 2006, Meier & Leuschner 2008).

In the literature, vertical relative **rooting depth distributions** are reported for pine for example by Scherfose (1990) and for beech by Hertel (1999). So far, comparing root depth distributions of pine and beech at the same site are lacking so far. At sandy soils in Northwest Germany, the vast majority of pine and beech roots is distributed in the uppermost organic soil layer (Hertel 1999, Scherfose 1990). In the organic layer of pine forests, Scherfose (1990) found 63 % to 77 % of the total root biomass in the upper 1 m soil column. The root density in the mineral soil decreases significantly with depth: For beech, the mean fine root density of beech in 50 cm depth is only 7 % of the mean fine root density found in the uppermost soil layers. Even though relative root densities are very low in deeper soil layers, roots are present down to a depth of almost 3 m (Hertel 1999). Steinmann (2015) reports that 10 % of beech fine roots are found below 270 cm depth. Compared to the root depth distributions of other evergreen species (Douglas fir, Norway spruce, larch) investigated by Steinmann (2015), beech shows a higher root density in greater depths. Jackson et al. (1996), on the other hand, report a lower root density in deeper soil layers for temperate deciduous forests compared to temperate evergreen forests: In the upper 50 cm of the soil, 82 % and 70 % of fine root biomass of temperate deciduous and evergreen forests is found. Below 100 cm depth, only 3 % and 9 % of fine root biomass of temperate deciduous and evergreen forests is found, respectively.

Steinmann (2015) found a mean maximum rooting depth of 2.8 ± 0.74 m for beech. Hertel (1999) found a maximum rooting depth for beech in North Germany of 2.8 m. Steinmann (2015) found the maximum rooting depth of pine and beech to range between 3 and 4 m depth.

2.4.2 Interception and stemflow of tree vegetation

Interception is largely affected by tree species and thus by horizontal and vertical stand structure, tree age, tree height, leaf area and seasonal leaf development (Hörmann et al. 1996, Müller 2019).

Interception is higher in evergreen forests than in broadleaved and mixed evergreen and deciduous forests (Ellenberg et al. 1986, Müller 2012, Peck & Mayer 1996). Meesenburg et al. (2014) report a difference in interception evaporation of 80 mm between evergreen and deciduous forests with comparable leaf area indices. For evergreen species, interception does not vary significantly between summer and winter and ranges from 25 % to 40 % (Bartsch & Röhrig 2016). In deciduous forests, interception varies seasonally with leaf fall and leaf unfolding and is thus higher in summer than in winter. Stemflow amounts are usu-

ally higher in deciduous forests than in evergreen forests (Müller 2019). Table 1 summarizes a selection of studies that investigated throughfall, interception and stemflow in pine and beech forests.

Pine has a dense crown with needles that are wettable from all sides. The stem surface is rough and has therefore a high water storage capacity. The interception storage capacity is in the order of 1 – 2 mm in mature forests (Federer 2019). Müller (2019) investigated **stemflow** amounts in pure pine forests in Eberswalde, Germany. He found stemflow amounts accounting for 5 % of the annual precipitation sum (625 mm) in a 35 years old pine forest. In older pine forests, the bark becomes rougher and stemflow amounts decrease to only 1 to 2 % of annual precipitation. This is in good agreement with e. g. Alvera (1976), who found a stemflow rate of 0.8 % of annual precipitation (858 mm) in a pine forest in Northeast Spain. Thus, stem flow only contributes very little to stand precipitation in pine forests.

Interception in pine forests has been investigated in various research studies and varies considerably depending on stand characteristics and weather conditions. Müller (2019) investigated the interception in pine forests of different ages and with different stem numbers in Eberswalde (Northeast Germany) between 2010 and 2016. He found mean throughfall values of 61.2 % of gross precipitation in winter (276.1 mm) and 69.4 % of gross precipitation in summer (390.6 mm). He also investigated interception rates in an 84 years old pine stand and found an interception rate of 32 %. Moreover, he investigated interception rates in mixed beech/oak and pine forests and found interception rates between 31 % and 34 % in those parts that are dominated by pine.

Ahrends & Penne (2010) reviewed interception in 78 pine stands in Germany and found a mean interception of 31 % and thus a mean throughfall rate of 69 % of mean precipitation (665 mm) of all stands. However, interception of the different forests varied between 15 % and 59 %, throughfall thus varied between 41 % and 85 % of site-specific precipitation. Alvera (1976) found a throughfall of 73.1 % of gross precipitation (858 mm) in a pine forest in Northeast Spain. Cape et al. (1991) found throughfall in pine forests in northern Britain ranging between 51 % and 78 %. Herrmann et al. (2006) found throughfall rates of 57 % to 68 % in a pine forest in Northwest Germany. In a pure pine forest in Sandkrug, Germany, throughfall rates of 69.7 % between 1996 and 1999 (713 mm) and 64.6 % in 2002 (758 mm) have been found (Mohr 2001, Mohr et al. 2005). Throughfall and interception rates vary considerably for pine forests, mostly between 25 % and 35 %.

Beech leaves are flat with a smooth surface. They are thus only wettable at one side and water can easily slide off the leaves. The interception storage of flat beech leaves is thus only small. Zhao et al. (2019) indicate leaf interception storage capacities being half of needle interception storage capacities per unit LAI. Schmidt-Walter (2019) suggests a storage capacity of 0.76 mm for beech. The inclined branches and twigs act as a funnel and route water towards the smooth stem and generate stemflow. In comparison to pine, the interception storage capacity of beech is considerably smaller (Müller 2019, Zhao et al. 2019). During the dormant season in winter, beech loses its leaves, which reduces interception evaporation compared to the vegetation period in summer (Müller 2019).

Müller (2019) investigated **stemflow** amounts in pure beech forests in Eberswalde, Germany. He found stemflow accounting for 11.8 % and 15.7 % of the annual precipitation sum (625 mm) in 35 years and 140 years old beech forests, respectively. Staelens et al. (2008) found a stemflow rate of 8 % in an 85 years old beech forest and Mosello et al. (2002) found a stemflow rate of 6.4 % of annual gross precipitation in a forest dominated by beech in Northwest Italy. Ringe et al. (2000) found stemflow rates of 1.4 %, 1.6 % and 3.2 % in a mixed pine and beech stand for the years 1998, 1999 and 2000, respectively. Müller (2019) showed that stemflow rates correlate positively with diameter at breast height. Levia et al. (2015) compared two groups of beech trees producing a comparably low and high stem flow amount. They found that trees that produce higher stem flow rates have straighter boles, higher branch inclination angles, less foliage, more branches and more woody biomass per unit projected crown area than those trees producing less stemflow amounts.

*Table 1: Overview of **Throughfall** (TF), **Interception** (I_T) and **Stem Flow** (SF) rates in % of gross precipitation (P) for Scots pine and European beech stands. In addition, the age of the investigated forests (age) and time period (period) in which the investigations took place as well as annual precipitation (P) are given if available.*

	Species	Period	Age [a]	P [mm a^{-1}]	TF [% of P]	I_T [% of P]	SF [% of P]
Müller (2019)	Scots Pine	1993-2016	39 – 45	656	66	34	-
Müller (2019)	Scots Pine	1993-2016	82 – 87	651	70	30	-
Mohr (2001)	Scots Pine	1996-1999	52	713	69.7	30.3	-
Mohr (2005)	Scots Pine	2002	65	758	64.6	35.4	-
Cape et al. (1991)	Scots Pine	-	-	-	51 – 78	22 – 49	-
Hermann et al. (2006)	Scots Pine	03/2001 – 02/2002	90	962	57 – 68	32 – 43	-
Alvera (1976)	Scots Pine	-	-	858	73.1	26.1	-
Müller (2019)	European beech	1993-2016	39 – 45	656	79	21	-
Müller (2019)	European beech	1993-2016	102 – 105	659	77	23	-
Staelens et al. (2007)	European beech	05/2002 – 05/2004	85	1448	71	21	8
Staelens et al. (2007)	European beech	leafed period	85	769.9	63	31	6.4
Staelens et al. (2007)	European beech	leafless period	85	677.9	80	10	9.5
Rothe et al. (2002)	European beech	1994-1997	90	892	70.0 (incl. stemflow)	30.0	-
Mosello et al. (2002), NW Italy	European beech	-	-	1139	73.9	19.7	6.4

Müller (2019) investigated **throughfall** in beech forests in Eberswalde, Northeast Germany. For beech forests of several age classes, he found a mean throughfall of 84.1 % of gross precipitation in winter and 81.2 % of gross precipitation in summer between 2010 and 2016. Furthermore, he found throughfall to account for 79 % and 77 % of gross precipitation in a 45 years and 105 years old beech forest. Moreover, he found interception rates between 21 % and 24 % in one part of a mixed beech and pine forest that is dominated by beech. Mosello et al. (2002) investigated interception processes in a forest dominated by beech in Northwest Italy and found a throughfall rate of 73.9 %. Rothe et al. (2002) found throughfall rates of 70 % in a 90 years old beech forest including stemflow. Staelens et al. (2008) found throughfall rates of 63 % in the leafed and 80 % of gross precipitation in the leafless period. Compared to pine, interception in beech forests is lower than in pine forests and mostly less

than 30 % of annual precipitation. Stemflow rates are considerably higher and range between 5 % and 10 % in beech forests being older than 30 years.

Müller (2019) also investigated interception rates in a chronosequence from a pure pine forest to various **mixed beech and pine** forests to a pure beech forest (See Figure 5). In the research period, gross precipitation was 600 mm. He found a stand precipitation rate of 68 % (408 mm) in the pure Scots pine (84a) forest. In the first conversion stage with 38 years old Scots pine and 10 years old beech, the stand precipitation rate increased to 71 % (426 mm). In the second stage with 76 years old pine and 33 years old beech, the stand precipitation rate further increased to 74 % (444 mm). In an older mixed forest with pine (114a) and beech (53a), the stand precipitation rate decreased to the same level as in the pure pine stand (86 %, 408 mm). In a pure beech forest (101 a), the stand precipitation rate increased to 76 % (456 mm). Stand precipitation rates thus increase slightly in mixed stands, due to lower interception evaporation of beech compared to pine that result from different crown architectures and different surfaces of needles, leaves and bark (Müller 2012).

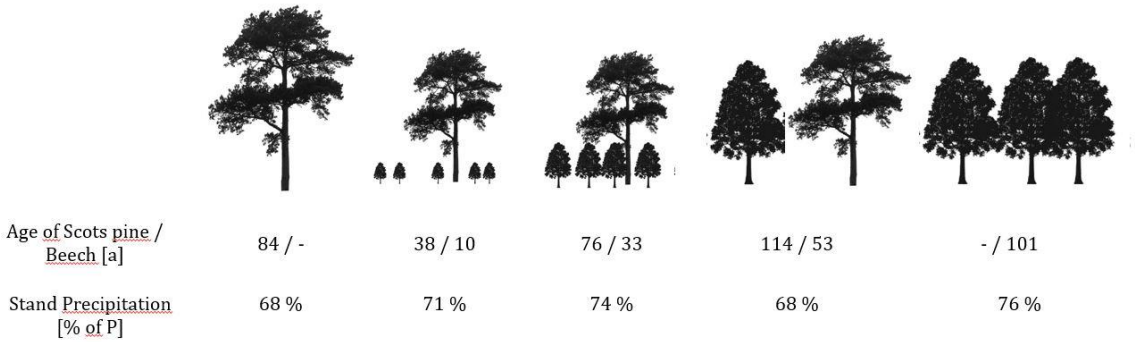

Figure 5: ***Stand precipitation rates in pine, beech and mixed pine and beech forests****: Stand Precipitation rates in % of annual precipitation in a chronosequence from a pure pine forest to various mixed beech and pine forests to a pure beech forest (from left to right), modified according to (Müller 2012).*

Ringe et al. (2000) investigates stand precipitation amounts in a pure pine forest and a mixed pine and beech forest close to Hannover, Lower Saxony. They found stand precipitation rates of 84 % for the pure pine and 90 % for the mixed pine for the period between 1998 and 2000.

In general, absolute amounts of interception, throughfall, stemflow and stand precipitation vary with precipitation sum and intensity. Therefore, absolute values are only directly comparable for measurements from the same location and thus with comparable precipitation characteristics, and from the same time period.

2.4.3 Transpiration of tree vegetation

Transpiration accounts for a substantial share of total evapotranspiration and is directly controlled by tree species, soil vegetation, weather conditions, vegetation structure, precipitation input and soil structure (Köstner 2001). The actual transpiration can be estimated by using lysimeters (Müller 2019), porometers (von Willert et al. 1995) and sap flow measurements (Köstner et al. 1998, Köstner et al. 2008). Even though transpiration is still only poorly constrained by measurements, a first comprehensive and global transpiration data set (SAPFLUXNET) obtained from sap flow measurements is presented by Poyatos et al. (2021).

Müller (2019) estimated transpiration rates in forests using lysimeters. He found mean evapotranspiration rates expressed as proportion of gross precipitation of 71 % for pine and 64 % for beech at an age between 15 and 27 years between 1990 and 2016. Thereby, transpiration amounts increase with increasing tree timber stock for pine and additionally with increasing leaf mass for beech. Müller (2012) investigated transpiration rates in different forests in Northeast Germany in the summer and found transpiration rates in % of gross precipitation (360 mm) of 41 % in a 84 years old pure Scots pine forest, 61 % in a mixed Scots pine (51 a) and European beech (11 a) forest, 70 % in a mixed Scots pine (76 a) and European beech (33 a) forest, and 71 % in a pure beech forest (101 a).

Lüttschwager et al. (1999) investigated tree transpiration in the growing season (April – September) in a 45- and two 65-years-old pine stands in Northern Germany. They found 106 mm and 94 mm in the 45-years-old pine stand in 1994 and 1995, respectively. In the first 65-years-old pine stand, they found 82 mm in 1994 and 90 mm in 1995. In the second 65-years-old pine stand, they found 113 mm in 1994 and 122 mm in 1995.

Köstner (2001) and Peck & Mayer (1996) summarize results of transpiration rates observed in spruce, pine and beech forests in Central Europe. For spruce, transpiration rates of 30 % of total evaporation are found, and for beech, transpiration rates of 40 % of total evaporation are found. Absolute transpiration rates, however, vary considerably.

2.4.4 Evapotranspiration of forest ground vegetation

Shrub, herb and litter layers play an important role in the water balance of forests. There is only little information on the water consumption of ground vegetation. Several studies investigated the water storage capacity of the forest floor (Helvey & Patric 1965, Putuhena & Cordery 1996). Rather than only the storage capacity, various studies investigated evapotranspiration rates of forest floor and shrub vegetation. Table 2 summarizes ground vegetation evapotranspiration rates that are found in the literature. Müller & Seyfarth (1999) developed weighable lysimeters to estimate evapotranspiration rates from ground vegetation in Northeast German pine forests. Müller (2011) presents evapotranspiration rates for ground vegetation covers with various compositions of wood small-reed (*Calamagrostis epigejos* (L.) Roth), wavy hair-grass (*Avenella flexuosa* (L.) Drej.), European blueberry (*Vaccinium myrtillus* L.) and red raspberry (*Rubus idaeus*) in pine forests in Northeast Germany. He found evapotranspiration rates of more than one third for wood small-reed and 30 % of the annual gross precipitation for wavy hair-grass. These rates are higher than those of mixed grass-shrub layers such as red raspberry and wavy-hair grass (25%) or European blueberry and wavy-hair grass (20%). Lüttschwager et al. (1999) found that ground vegetation contributes approximately 50 % to stand transpiration in summer in several pine tree forests in Northern Germany. Soudani et al. (2002) partitioned stand LAI of a 50 years old Scots pine stand with a dense herb and shrub layer into a tree LAI, herb LAI and shrub LAI. They found the tree, shrub and herb layer to account for 58 %, 11 % and 31 % of total LAI, respectively. For grassland, evapotranspiration rates vary significantly in the literature (Beard 1956, Clark 1940, Haynes 1940, Kittredge 1948).

*Table 2: Selected **ground vegetation evapotranspiration** rates [% of annual P] from literature.*

Soil vegetation species	Evapotranspiration [% of annual P]	Source
Wood small-reed (*Calamagrostis epigejos* (L.) Roth)	>33	Müller (2011)
Wavy hair-grass (*Avenella flexuosa* (L.) Drej.)	30	Müller (2011)
Big bluestem (*Andropogon gerardi*)	57-84	Clark (1940)
Buffalo grass (*Bouteloua dactyloides*)	17-74	Clark (1940)
Kentucky bluegrass (*Poa pratensis*)	56	Haynes (1940)
Grassland	13	Beard (1956)
Grassland	26	Kittredge (1948)
Red raspberry (*Rubus idaeus*), wavy hair-grass (*Avenella flexuosa* (L.) Drej.)	25	Müller (2011)
European blueberry (*Vaccinium myrtillus* L.), wavy hair-grass (*Avenella flexuosa* (L.) Drej.)	20	Müller (2011)

In dense forest stands, ground vegetation is mostly absent. Instead, the forest floor is covered with a litter layer consisting of needles and leaves. Litter does not transpire actively, however, it intercepts considerable water amounts. Table 3 summarizes interception loss values of litter that are found in the literature. Helvey & Patric (1965) investigated the interception loss from the forest floor in a poplar forest and found an interception loss of 18 % of annual net precipitation. Thamm & Widmoser (1995) and Brechtel (1969) found an interception loss between 12 % and 28 %, and 16 % of annual net precipitation for a beech forest floor, respectively. Coenders-Gerrits et al. (2010) found mean interception values between 10 % and 35 % of annual gross precipitation for a beech forest floor. Müller (2011) found an evaporation rate of 12% of annual gross precipitation in a dense (unspecified) forest stand without any ground cover. A comprehensive review of forest floor interception values can be found in Gerrits & Savenije (2011).

*Table 3: Selected **litter interception** values [% of annual P or stand precipitation (*)] from literature.*

Litter and Vegetation	Interception [% of annual P or stand precipitation (*)]	Source
Poplar (USA, NY)	18 *	Helvey & Patric (1965)
Beech forest (*Asperulo-Fagetum*)	12-28 *	Thamm & Widmoser (1995)
Beech forest (USA, NY)	16 *	Brechtel (1969)
Beech (Fagus sylvatica)	10-35	Coenders-Gerrits et al. (2010)

2.4.5 Deep seepage and groundwater recharge rates below forests

Since 1992, Müller (2019) has explored the effect of forest conversion on deep seepage in pure and mixed pine (*Pinus sylvestris L.*), beech (*Fagus sylvatica L.*), larch (*Larix decidua L.*) and Douglas fir (*Pseudotsuga menziesii (Mirb.) Franco*) stands on sandy and nutrient-poor soils. Müller (2019) has measured interception evaporation, soil moisture and deep seepage. The resulting comprehensive dataset has revealed compelling effects of tree species composition and stand age on deep seepage rates. Details of the experimental design as well as a synthesis and discussion of the results can be found in Müller (2005, 2011, 2012, 2019).

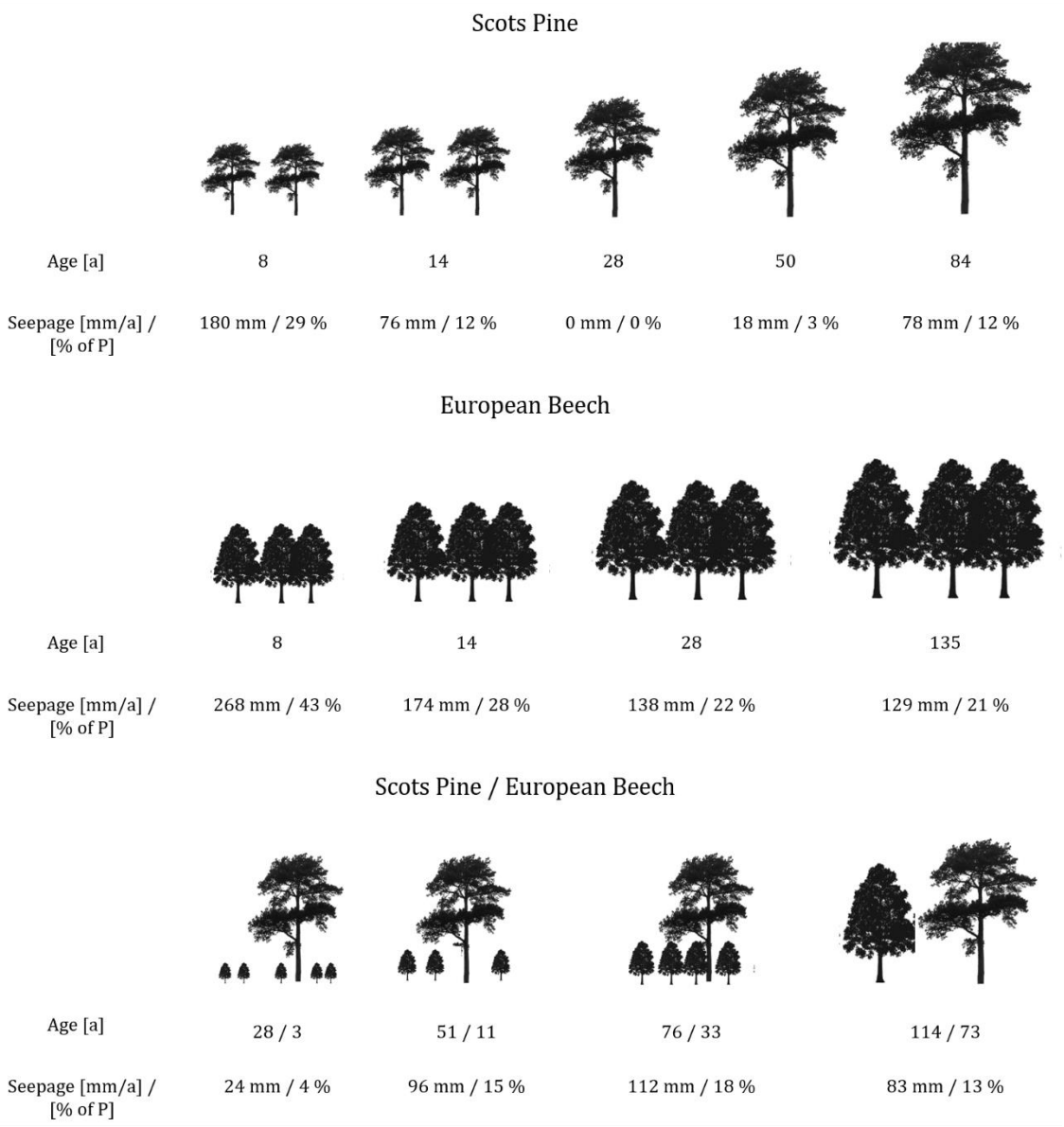

Figure 6: ***Deep seepage rates in pine, beech and mixed pine and beech forests****: Deep seepage rates (in mm/a and % of annual precipitation = 620 mm) in pine, beech and mixed pine and beech forests of various ages in Northeast Germany, edited according to Müller (2011).*

Figure 6 shows deep seepage rates in pure pine, pure beech and mixed pine and beech forests of varying ages, respectively. Deep seepage rates are given in % of mean annual precipitation (620 mm). In pure pine forests, deep seepage rates decrease with age. In a young pine forest (8 a), deep seepage accounts for 29 % of precipitation. Until an age of approximately 30 years, the deep seepage rate decreases to zero due to high interception losses and transpiration rates. Natural decay of single trees and managed thinning reduces the stem number continuously and thus increases deep seepage. In a 84-years old pine stand, 12 % of gross precipitation seeps into deeper soil layers (Müller 2011).

In pure beech forests, deep seepage rates decrease with age as observed in pine forests. Transpiration increases with age due to the increasing leaf area, but at the same time, stemflow increases with age, too. Deep seepage rates decrease from initially 43 % at an age of 8 years to 22 % at an age of 18 years. In a 135 years old beech forest, deep seepage rates

remain at a similar level (21 %). Deep seepage rates in beech forests of any stage are higher than in pine forests of comparable age (Müller 2011).

In mixed pine and beech forests, deep seepage rates range between those of pure pine and beech forests. In a mixed forest with 3 to 11 years old beech in a mature pine forest, the beech trees play a minor role. Their interception loss is small and stemflow is still negligible. The thinning of the pine, however, decreases interception rates and thus increases deep seepage rates. In a mixed forest with 51 years old pine and 11 years old beech, evapotranspiration is 85 % and seepage is 15 % of annual gross precipitation. In a mixed forest with 76 years old pine and 33 years old beech trees, the decreasing stem number of the pine and the increasing beech leaf area increases overall interception evaporation only slightly. As the beech trees grow up, stemflow plays an increasingly important role. This slightly increases deep seepage rates, even though interception rates increase slightly. In a mature mixed forest with 114 years old pine and 73 years old beech, interception evaporation increases compared to earlier conversion stages. Evapotranspiration rates are higher than in pure beech forests, however, they are not higher than in pure pine forests of comparable age classes. Corresponding deep seepage rates are in the order of that in pure pine stands or slightly higher (Müller 2012).

Further research studies in Germany underpin the findings of Müller (2011, 2012) in pure deciduous and evergreen forest forests. Natkhin (2011) found higher deep seepage rates in a pure beech forest (114 mm/a) than in a pine forest (45 mm/a) in Northeast Germany. Further studies compared seepage rates of other evergreen (*Pinus strobus*, *Picea abies*) and deciduous forests (*Fagus sylvatica*, *Quercus robur*) and found higher deep seepage rates for deciduous than for evergreen forests (Ellenberg et al. 1986, Harsch et al. 2009, Prietzel & Bachmann 2011, Schmidt-Walter et al. 2020b, Schultze & Scherzer 2015). Specific deep seepage amounts, however, depend on annual precipitation sums and temporal precipitation patterns. Therefore, deep seepage rates vary considerably from year to year and can even fail to occur in considerably dry years (Müller 2012).

Ringe et al. (2000) investigated deep seepage rates in a pure pine and a mixed pine and beech forest in Fuhrberg, Lower Saxony. They found deep seepage rates of 208 mm and 248 mm for the pure pine and the mixed forest for the period 1998-1999, respectively. For the period 1999 to 2000, they found deep seepage rates of 142 mm and 158 mm for the pure pine and the mixed forest, respectively. The difference between both forests thus differs from year to year.

Klinck et al. (2012) report annual deep seepage rates in pine forests ranging between 20 mm a^{-1} and 285 mm a^{-1} in Augustendorf in western Lower Saxony. They report annual deep seepage rates between 85 mm a^{-1} and 400 mm a^{-1} in Fuhrberg in central Lower Saxony. They investigated deep seepage rates also in a pure beech forest and found annual deep seepage rates ranging between 215 mm a^{-1} and 610 mm^{-1} in Lüss (Lüneburg Heath). The rates in Fuhrberg and Lüss are probably too high, as they are measured only in 100 cm and 60 cm depth.

Mohr et al. (2005) investigated deep seepage rates in pine forests in Northwest Germany. They found mean deep seepage rates of 38% in Augustendorf (gross precipitation = 825 mm), 52% in Holdorf (gross precipitation = 754 mm) and 51% in Sandkrug (gross precipitation = 758 mm) for the years 2002 and 2003. Klinck et al. (2012) reported annual deep seepage rates for a pine forest in Augustendorf between 1994 and 2009. They found a mean

annual deep seepage rate of 140 mm a^{-1} and a maximum deep seepage rate of 285 mm a^{-1} in 1994 and a minimum deep seepage rate of 20 mm a^{-1} in 1996. They also investigated deep seepage rates in a pine forest in Fuhrberg, Lower Saxony, between 1993 and 2007. There, they found a mean deep seepage rate of 203 mm a^{-1}, a minimum deep seepage rate of 85 mm a^{-1} in 1997 and a maximum deep seepage rate of 400 mm a^{-1} in 2007. They also report deep seepage rates for a pure beech forest in Lüss between 1993 and 2009 with deep seepage rates ranging from 215 mm a^{-1} to 610 mm a^{-1} with a mean annual deep seepage rate of 347 mm a^{-1}.

In East Lower Saxony, Spellmann et al. (2017) investigated deep seepage rates in forests growing on sandy soils with low water holding capacities. Spellmann et al. (2017) report a long-term mean deep seepage rate of 213 mm a^{-1} in forests located in the district of Uelzen. Schultze & Scherzer (2015) determined deep seepage rates in several forest types of varying ages in the Drawehn hill range by using the hydrological model *LWF-Brook90* over a time period of 60 years. They compared deep seepage rates of these forests to those of a pure pine stand. They found a positive effect on deep seepage rates in pure oak and mixed pine and oak forests. They found, in turn, negative effects on deep seepage rates in mixed forests with pine and Douglas fir, and Douglas fir and beech. Table 4 shows modelled changes in deep seepage rates for the different forest types in comparison to a pure pine forest.

Table 4: Modelled change in annual deep seepage rate [mm] in converted forest plots of different ages compared to a pure pine forest in Northeast Lower Saxony (Schultze & Scherzer 2015).

Time after forest conversion	10a	20a	30a	40a	50a	60a
Pinus sylvestris, Pseudotsuga menziesii	-13	-37	-30	-16	-44	-46
Pseudotsuga menziesii, Fagus sylvatica	+15	-13	-4	+1	-22	-29
Quercus robur, Pinus sylvestris	+46	+75	+95	+67	+72	+80
Quercus robur	+57	+97	+124	+99	+97	+98

3 Methods

3.1 Study sites

The study sites were selected under the premise that they are as transferable as possible to many forest sites in Northwest Germany. Therefore, different geographical regions and different forest conversion stages are selected, but with similar soil conditions: Three study locations are selected in the western (Sandkrug), central (Elze) and eastern part (Wibbese) of the low lands in Lower Saxony. Figure 7 shows the study site locations in Lower Saxony and Table 5 summarizes their geographical information. At these study sites, pure and mixed forests of pine and beech grow on sandy, nutrient-poor and groundwater distant soils in water protection areas. The climate shows a gradient from oceanic conditions in the western part of Lower Saxony to increasingly sub-continentally influenced conditions in the eastern part. Climate conditions in Lower Saxony are temperate, humid and predominantly governed by westerly winds from the North Sea (Zöller 2017). Mean annual temperatures are 9.2°C in Sandkrug and Wibbese and 9.6°C in Elze. Mean monthly temperatures change seasonally and vary between 1°C in winter and 18°C in summer. The temperature amplitude in east Lower Saxony is slightly higher than in the western part (Deutscher Wetterdienst 2020b, 2020c, 2020d). Precipitation is usually abundant throughout the year, however, considerable dry periods occasionally occur especially in spring and summer (Sutmöller et al. 2019). Mean annual precipitation sums decrease eastwards due to an increasing continental influence and range between 800 mm in Sandkrug and only 550 mm to 650 mm in Wibbese (Deutscher Wetterdienst 2020b, 2020d, 2020e). Precipitation usually occurs in form of rain and sometimes thunderstorms, hail or snowfall.

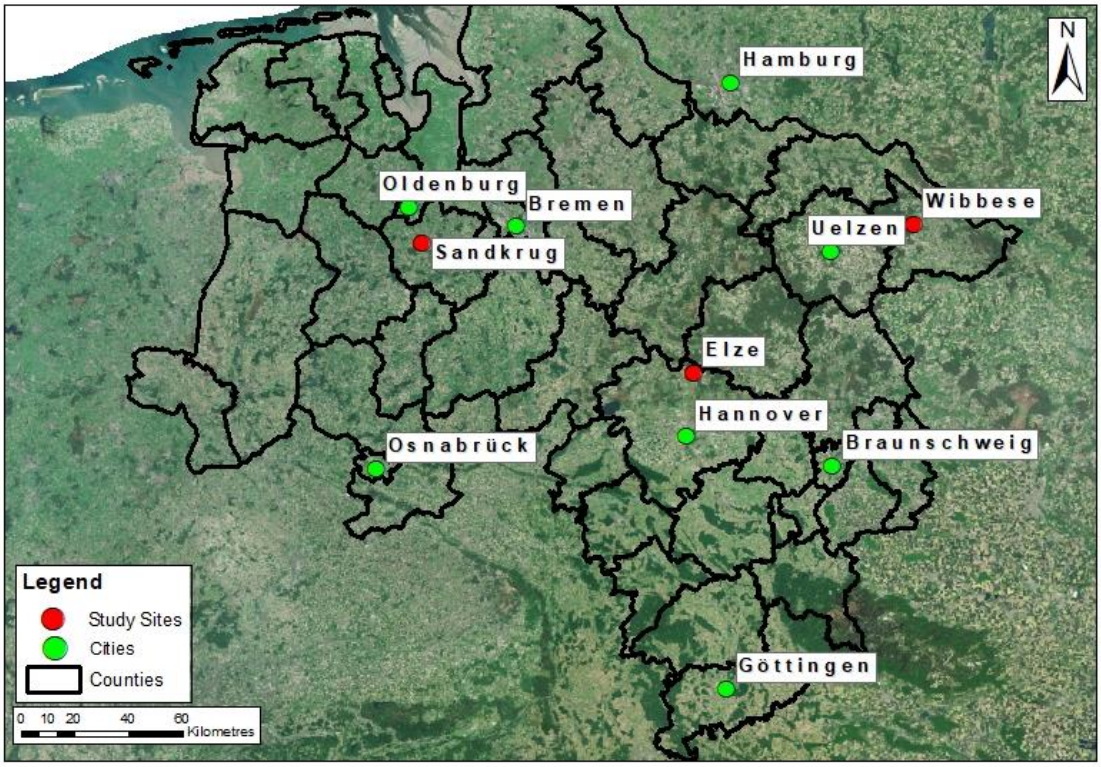

Figure 7: ***Location of the study sites*** *Sandkrug, Elze and Wibbese (shown in red) in Lower Saxony.*

*Table 5: **Study site details**: Geographic location, height above sea level, height of groundwater table above sea level, depth to groundwater table from surface, soil type and mean precipitation at the study sites Sandkrug, Elze and Wibbese (DWD 2020b, 2020c, 2020d, 2020e, NIBIS Kartenserver 2014a, 2014c).*

	Sandkrug	Elze	Wibbese
Geographic Location [°]	8.289 E 53.016 N	9.772 E 52.588 N	11.001 E 53.067 N
Height [m.a.s.l.]	15	40	70
Groundwater Surface Elevation [m.a.s.l.]	7.5 – 10	30 – 32.5	30 - 32.5
Depth to Groundwater [m below ground surface]	5 – 7.5	7.5 – 10	37.5 - 40
Soil Type	Podzol-Regosol	Podzol	Cambisol-Podzol
Mean Precipitation [mm a^{-1}]	800 mm a^{-1}	700 mm a^{-1}	610 mm a^{-1}

The study sites are located in North German Geest regions that have been formed during the Saale cold period around 126.000 to 310.000 years ago. In Geest regions, sandy material from glacial deposits dominate the predominantly occurring soils. These soil materials have usually been altered and formed by periglacial processes during the Vistula glacial period around 115.000 to 11.600 years ago. Until today, predominantly the soil types Regosol, Podzol and Cambisol have developed under humid climate conditions (Meschede & Warr 2019).

Thus, largely comparable conditions are present on the test plots Sandkrug, Elze and Wibbese, with approx. 90- to 100-year-old pure pine stands in different conversion stages on sandy, groundwater-distant soils. These conditions are favourable to investigate the research questions.

In the following, the forest plots at each study site are described by the stand parameters height, number of stems per hectare (stand density, SD), diameter at breast height (DBH), Basal Area (BA) and Kraft's classes of trees. The assessment details of these stand parameters are given in Table 6. Additionally, the species composition and degree of coverage of ground vegetation is surveyed by applying the Braun-Blanquet cover-abundance scale (Reichelt 1973).

*Table 6: Detailed information about **stand parameters**: Tree height, number of stems per hectare (SD), diameter at breast height (DBH), basal area (BA) and Kraft's classes of trees.*

Parameter	Unit	Method / Formula
Height	m	Geometric method (West 2015)
SD	stems ha^{-1}	Counting stems per defined area (West 2015)
DBH	cm	Measuring DBH at 130 cm with a girth tape (BMELV 2011, West 2015)
BA	m^2 ha^{-1}	Sum of the cross-sectional area at breast height of all tree trunks per area (West 2015) $BA = \sum \pi * (\frac{DBH}{2})^2$
Kraft's classes of trees	-	Visual estimation of tree height relative to the height of surrounding trees according to the classification after Kraft (1884): Dominant (1), codominant (2), subdominant (3), suppressed (4), dying (5).

3.1.1 Sandkrug

The study site 'Sandkrug' is located within a large forested area ('Osenberge') in an old moraine area (Delmenhorster Geest). During the Vistula cold period, strong and continually blowing winds separated moraine particles by size and formed a large inland dune area. Since the middle age, the area has been intensively used: Livestock grazed in the forests (silvopasture) and over time, wide-spread heathland developed. This heath was then used

in the "plaggen" agriculture as bedding for cattle and ultimately as fertilizer. Due to these management activities, large unvegetated sandy areas and inland dunes developed. In the 19th century, the unvegetated areas were afforested (Meschede & Warr 2019). Today, a 70-year-old even aged pine (*Pinus sylvestris*) stand grows at the study site 'Sandkrug'. This pure pine stand is referred to as reference state (SREF). In the immediate vicinity of the reference plot, the pine stand has been thinned 20 years ago and European beech (*Fagus sylvatica*) has been planted. Today, this is a mixed pine and beech stand (mixed pine beech plot, SB20). The forest observation plots SREF and SB20 are shown in Figure 8. Table 7 shows the forest parameters age, height, DBH, SD, BA and social class for SREF and SB20. More detailed values of these stand parameters are given in Table 52 (appendix).

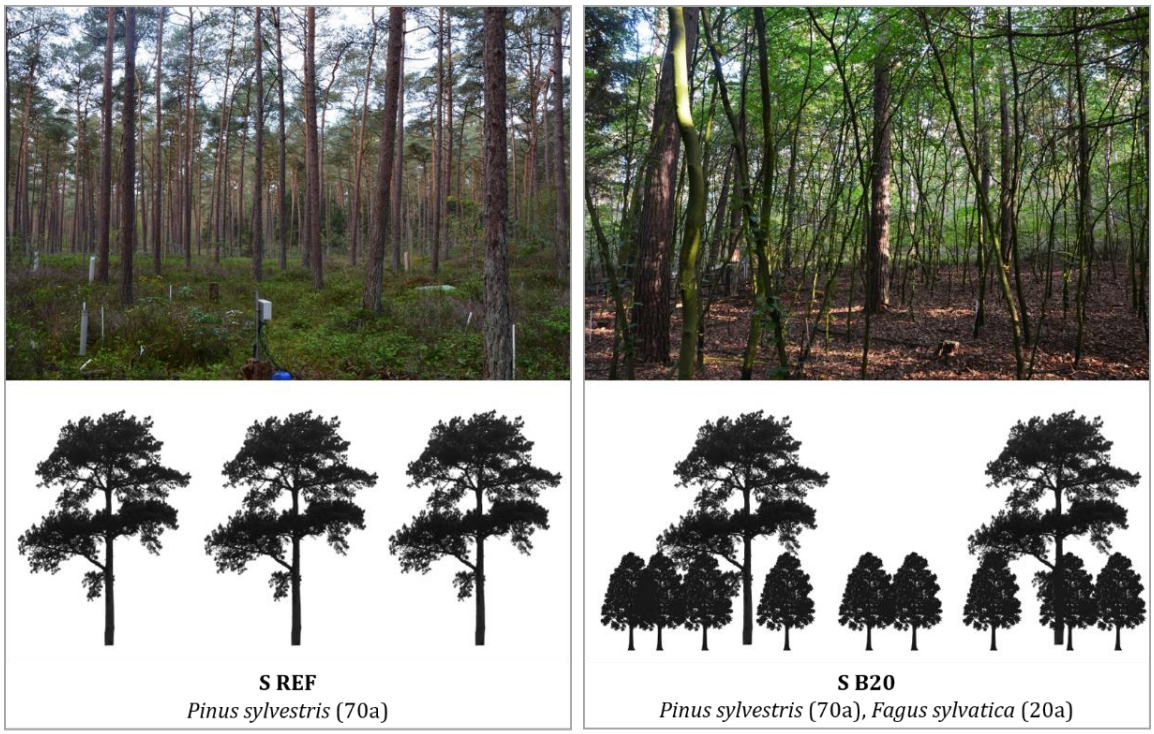

*Figure 8: Forest observations plots **SREF** (left) and **SB20** (right) in Sandkrug.*

The stand density of the pine in SB20 (389 ha^{-1}) is lower than in SREF (612 ha^{-1}) due to several thinnings within the last decades. However, according to Kraft's social class, the share of dominating pine tree individuals with dense and wide crowns is higher in SB20 than in SREF, which is also well reflected in a higher mean diameter at breast height (DBH) in SB20 (30.4 cm) than in SREF (26.9 cm). The beech grows comparably dense in SB20 showing a stem number of 4496 ha^{-1} and a small DBH of 4.5 cm. Based on stem number and diameter at breast height, total basal area (BA) is 35.5 m^2 ha^{-1} for pine in SREF and adds up to 40.1 m^2 ha^{-1} for pine and beech in SB20. The mean tree height of the pine is comparable in SREF and SB20 (23.0 m), the beech trees are considerably smaller (7.0 m).

*Table 7: **Stand parameters in Sandkrug** (DBH = diameter at breast height, SD = stocking density, BA = basal area, Social class = Kraft's classes of trees, mean value).*

Plot	Species	Age [a]	Height [m]	DBH [cm]	SD [ha^{-1}]	BA [m^2 ha^{-1}]	Social class
S REF	Pine	70	23.0	26.9	612	35.5	2.21
S B20	Pine	70	23.0	30.4	389	32.0	2.00
	Beech	20	7.0	4.5	4496	8.1	-

Ground vegetation coverage and species composition is given in Table 53 (appendix). Ground vegetation differs significantly between SREF and SB20 (see Figure 9). In SREF, the forest floor is dominated by mosses and shrubs. The red stemmed feather-moss (*Pleurozium schreberi*), the hair moss (*Polytrichastrum formosum*) and the European blueberry (*Vaccinum myrtillus*) dominate the ground vegetation. Occasionally, other species such as oak (*Quercus petraea*), honeysuckle (*Lonicera periclymenum*) and rowan (*Sorbus aucuparia*) occur. Leaf and needle litter is also present but plays only a minor role in ground cover compared to the aforementioned species. In SB20, the dense understory layer of European beech significantly reduces light availability. The ground vegetation is thus very sparse and leaf litter and sporadically occurring mosses dominate ground cover.

*Figure 9: Dominating **ground cover in SREF and SB20**: Ground cover is dominated by European blueberry and mosses in SREF (left) and by leaf litter in SB20 (right).*

Based on the literature findings and the tree and ground vegetation characteristics, the general hypotheses are specified for Sandkrug as follows:

Stand precipitation and deep seepage rates increase from SREF to SB20.

3.1.2 Elze

The study site 'Elze' is situated on an outwash plain in the Aller glacial valley that has been formed 200. 000 years ago. Originally, a large braided river system originating from the inland glacier took up large parts of the valley. The glacial water transported huge amounts of sand and gravel-sized material, which then sedimented under slower flow conditions (Meschede & Warr 2019). The sandy soils have been used for grazing, agriculture and forestry in the past, which is typical for this region. The forest observation plots are located within the extensive forested area 'Rundshorn'. The reference plot is an 80-year-old even aged pine (*Pinus sylvestris*) forest (EREF). In the immediate vicinity of the reference plot, two pine stands of the same age have been thinned 5 and 15 years ago, respectively, and beech (*Fagus sylvatica*) has been planted. These mixed pine-beech stands are referred to as EB5 and EB15, respectively. One further pine stand has been thinned 25 years ago and beech was planted. Since then, the pine has been thinned regularly and has eventually been removed in 2017, hence, this stand is today a pure even-aged beech stand (EB25). These four stands cover a time span of 25 years of forest conversion from the initial evergreen to the pure deciduous forest. The forest observation plots are shown in Figure 10. Table 8 shows the forest parameters age, height, DBH, SD, BA and social class for EREF, EB5, EB15 and EB25. More detailed values of these stand parameters are given in Table 52 (appendix).

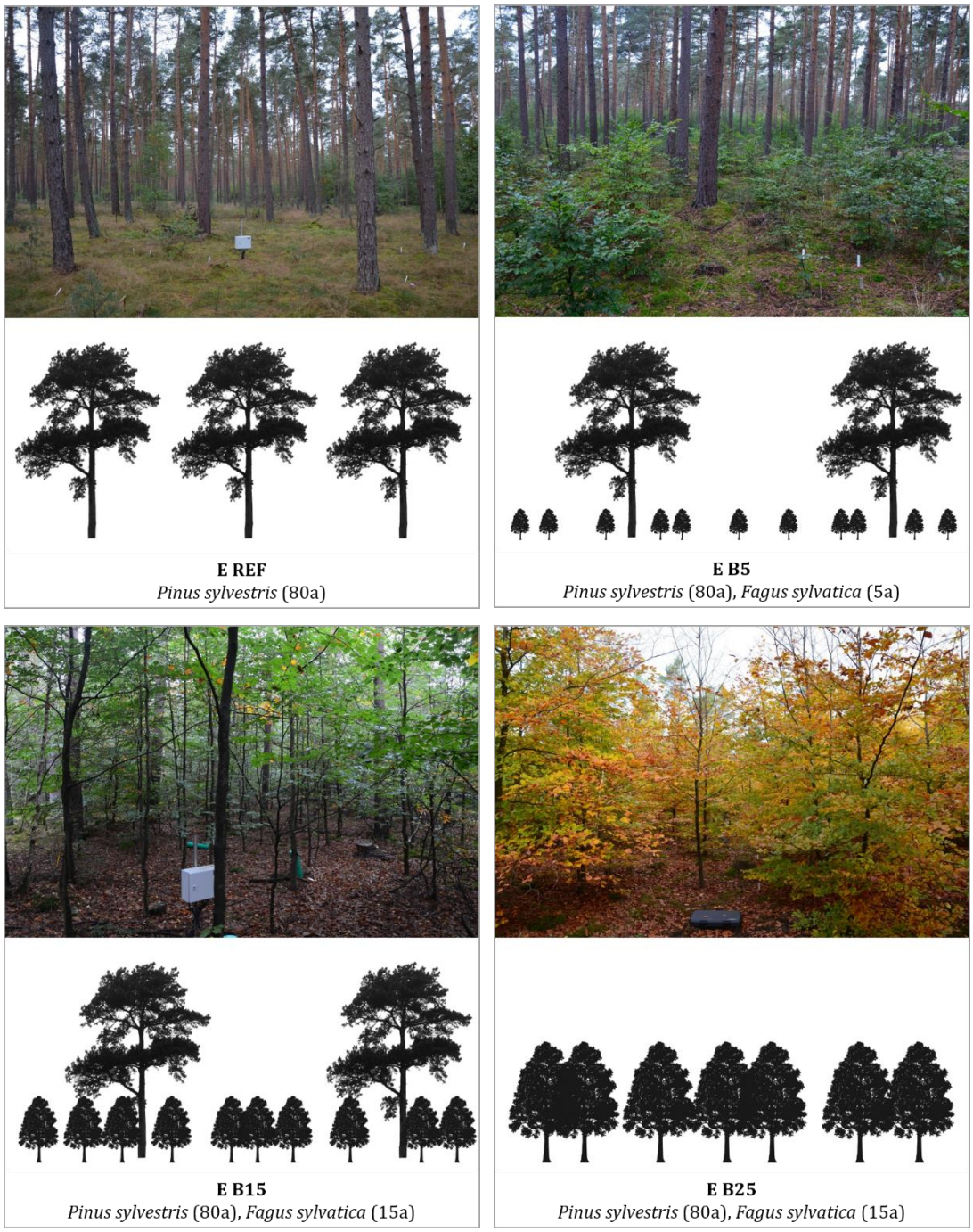

Figure 10: ***Forest observation plots EREF*** *(upper left),* ***EB5*** *(upper right),* ***EB15*** *(lower left) and* ***EB25*** *(lower right) in Elze.*

Thereby, stem numbers of Scots pine decrease from EREF (419 ha^{-1}) to EB5 (385 ha^{-1}) to EB15 (285 ha^{-1}) and eventually 0 ha^{-1} in EB25. At the same time, the mean DBH increases with decreasing stem numbers by removing comparably weak tree individuals from 32 cm in EREF and EB5 to 36.5 cm in EB15. The share of dominant trees according to Kraft's social class also increases with lower stem numbers. Mean tree heights of pine are comparable and range between 20 m and 22 m. Stem numbers of beech decrease with increasing age from 4507 ha^{-1} in EB5 to 3084 ha^{-1} in EB15 to 1908 ha^{-1} in EB25 due to natural decay and thinning. At the same time, the mean DBH increases from only a few cm in EB5 to 4.5 cm in EB15 to almost 7 cm in EB25. Mean tree heights of beech increase with increasing age from 1.6 m in EB5 to 7.0 m in EB15 to 7.5 m in EB25.

The resulting total basal area first decreases from 34.3 m^2 ha^{-1} in E REF to 30.6 m^2 m^{-1} in EB5 due to decreasing pine stem numbers and only a negligibly small share of beech. In E B15, total Scots pine and European beech basal area sums up to 34.5 m^2 ha^{-1}, even though the pine basal area remains stable. The beech basal area increases with tree growth from 5.5 m^2 ha^{-1} in E B15 to 7.3 m^2 ha^1 in E B25.

Table 8: ***Stand parameters in Elze*** *(DBH = diameter at breast height, SD = stocking density, BA = basal area, Social class = mean Kraft's classes of trees).*

Plot	Species	Age [a]	Height [m]	DBH [cm]	SD [ha^{-1}]	BA [m^2 ha^{-1}]	Social class
E REF	Pine	80	22.0	31.8	419	34.3	1.98
E B5	Pine	80	21.6	31.7	385	30.6	1.94
	Beech	5	1.6	-	4507	-	-
E B15	Pine	80	20.2	36.5	285	29.0	1.5
	Beech	15	7.0	4.5	3084	5.5	-
E B25	Beech	25	7.5	6.7	1908	7.3	-

Figure 11: Dominating ***ground cover in EREF, EB5, EB15 and EB25****: Ground cover dominated by mosses, wavy hair grass and European blueberry in EREF (upper left) and EB5 (upper right). In EB15 (lower left) and EB25 (lower right), ground cover is dominated by leaf litter and mosses.*

Ground vegetation coverage and species composition is given in Table 53 (appendix). Ground vegetation differs significantly between EREF, EB5, EB15 and EB25 (see Figure 11). Generally, soil vegetation density decreases with the growing understory layer of beech. In EREF and EB5, the forest floor is dominated by mosses and shrubs. The red stemmed feather-moss (*Pleurozium schreberi*), the European blueberry (*Vaccinum myrtillus*) and the wavy hair-grass (*Avenella flexuosa*) dominate the ground vegetation. Occasionally, other species such as oak (*Quercus petraea*) and rowan (*Sorbus aucuparia*) occur. In EB5, natural rejuvenation of pine has spread after the planting of beech. In order to protect the beech

from the massive natural rejuvenation of the pine, the small pine trees had been removed in the beginning of the research period. Other sporadic woody plants such as oak or shrubs were retained. Leaf and needle litter is also present but plays only a minor role in ground cover compared to the aforementioned species. In EB15 and EB25, the dense understory layer of beech significantly reduces light availability. The ground vegetation is thus very sparse and leaf litter and sporadically occurring mosses dominate ground cover. However, sporadic moss cushions (e.g. *Brachytecium rutabulum*, *Dicranum scoparium*, *Hypnum cupressiforme*, *Polytrichastrum formosum*) are present.

Based on the literature findings and the tree and ground vegetation characteristics, the general hypotheses are specified for Elze as follows:

Stand precipitation and deep seepage rates increase from EREF to EB5 to EB15 to EB25.

3.1.3 Wibbese

Wibbese is located at the eastern edge of the Göhrde-Drawehn hill range between Lüneburg Heath and Wendland. The Drawehn hill range is an end moraine that has been formed at the glacier margin during the Saale cold period. Unsorted clastic sediments with a broad grain-sized spectrum accumulated at the end of the inland glacier and fluvial and fluvio-glacial processes such as meltwater erosion and wind-blown sand deposition then further formed the landscape (Meschede & Warr 2019). At the study site 'Wibbese', a 70-year-old even aged pine (*Pinus sylvestris*) stand is located within an extensive forested area and represents the current state (reference plot, WREF). Adjacent to the reference plot, the stand has been planted with beech (*Fagus sylvatica*) and Douglas fir (*Pseudotsuga menziesii*), respectively. These plots are referred to as mixed pine and beech plot (WB5) and mixed pine and Douglas fir plot (WD5). The forest observation plots are shown in Figure 12. Table 9 shows the forest parameters age, height, DBH, SD, BA and social class for WREF, WB5 and WD5. More detailed values of these stand parameters are given in Table 52 (appendix).

Table 9: ***Stand parameters in Wibbese*** *(DBH = diameter at breast height, SD = stocking density, BA = basal area, Social class = mean Kraft's classes of trees). In March 2020, the pine stand in WB5 and WD5 has been thinned and corresponding stand parameters after thinning are given in parentheses.*

Plot	Species	Age [a]	Height [m]	DBH [cm]	SD [ha^{-1}]	BA [$m^2\ ha^{-1}$]	Social class
W REF	Pine	70	27.8	31.2	494	45.1	2.5
W B5	Pine	70	27.8	32.1 (32.1)	640 (460)	53.1 (38.4)	2.4
	Beech	5	1.6	-	3847	-	-
W D5	Pine	70	27.8	39.4 (39.4)	500 (300)	62.4 (37.3)	1.9
	Douglas fir	5	2.2	-	3387	-	-

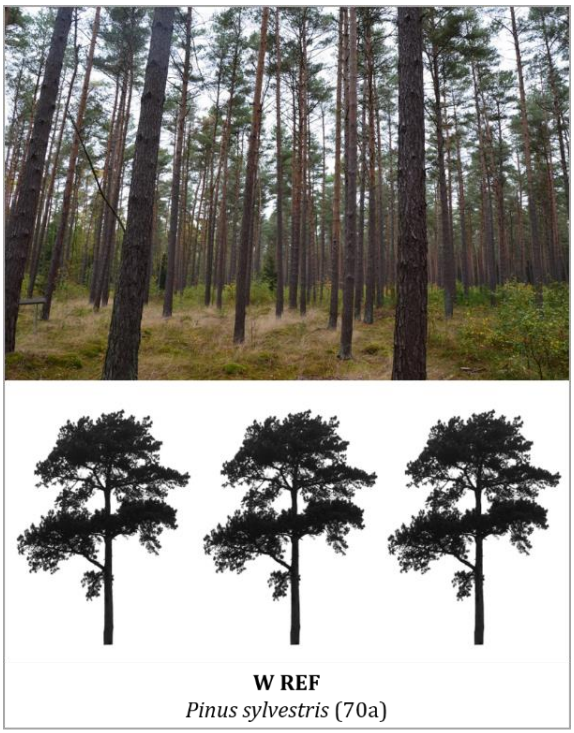

Figure 12: ***Forest observation plots WREF*** *(top),* ***WB5*** *(bottom left) and* ***WD5*** *(bottom right) in Wibbese.*

Stem numbers are similar in WREF and WD5 (500 ha^{-1}) and slightly higher in WB5 (640 ha^{-1}). Mean DBH is comparable in WREF (31.2 cm) and WB5 (32.1 cm), but considerably higher in WD5 (39.4 cm). The resulting basal area of pine is thus higher in W D5 than in WB5 and WREF. According to Kraft's social classes, the pine trees are more dominant in WD5 than in WB5 and WREF. Mean tree height of pine is 28 m and is comparable in all three plots. Compared to pine, stem numbers of beech (3847 ha^{-1}) and Douglas fir (3387 ha^{-1}) are comparably high. Their mean heights are comparably small with 1.6 m (beech) and 2.2 m (Douglas fir). In March 2020, the pine has been thinned in WB5 and WD5, which has reduced stem

numbers from 640 ha^{-1} to 460 ha^{-1} in WB5 and from 500 ha^{-1} to 300 ha^{-1} in WD5. Hence, stem numbers after thinning are lower in WB5 and WD5 compared to WREF.

Ground vegetation coverage and species composition is given in Table 53 (appendix). Ground vegetation is similar in WREF, WB5 and WD5 (see Figure 13): The forest floor is dominated by mosses and shrubs. The red stemmed feather-moss (*Pleurozium schreberi*) and the wavy hair-grass (*Avenella flexuosa*) dominate the ground vegetation. Occasionally, other species such as oak (*Quercus petraea*) and rowan (*Sorbus aucuparia*) occur. In WB5 and WD5, the European beech (*Fagus sylvatica*) and Douglas fir (*Pseudotsuga menziesii*) are still very small and are still part of the ground vegetation. Leaf and needle litter is also present but plays only a minor role in ground cover compared to the aforementioned species.

*Figure 13: Dominating **ground cover in WREF, WB5 and WD5:** Ground cover dominated by wavy hairgrass, mosses and European blueberry in WREF (top), WB5 (lower left) and WD5 (lower right).*

Based on the literature findings and the tree and ground vegetation characteristics, the general hypotheses are specified for Wibbese as follows:

Before thinning, stand precipitation and deep seepage rates increase from WD5 to WB5 to WREF, as the pine tree layer in WD5 and WB5 is slightly denser than in WREF and beech and Douglas fir also intercept and transpire small water amounts.

After thinning, stand precipitation and seepage rates increase from WREF to WD5 to WB5 as a result of the thinned pine tree layer.

Stand precipitation and deep seepage in the mixed forest with an evergreen and a deciduous tree species (WB5) is higher than in the mixed forest with two evergreen tree species (WD5).

3.2 In situ measurements

Extensive measurements of weather variables, stand precipitation, soil moisture and vegetation parameters are conducted on the test plots. Since August 2018, meteorological parameters are continuously measured in Sandkrug, Elze and Wibbese. Continuous soil moisture measurements started in Elze and Wibbese in August 2018 and in Sandkrug in December 2018. The measurement of stand precipitation in Sandkrug started already in 2018 and in Elze and Wibbese in spring 2019. Site-specific vegetation and soil data were acquired between 2018 and 2020.

3.2.1 Meteorological parameters

Meteorological parameters are measured in an open space close to the forest plots at each study site. The distances between the meteorological observation site and the forest plots are 0.3 km in Elze, 0.6 km in Sandkrug and 1.7 km in Wibbese. The assessed meteorological parameters are temperature, relative humidity, solar radiation and precipitation. In Sandkrug, only precipitation is assessed at the open spaced site, the remaining variables are assessed next to the forest monitoring plots. Table 10 gives detailed information about the meteorological sensors used. Temperature, relative humidity and solar radiation are measured at a height of 2 m, precipitation is measured at a height of 1 m. Measured precipitation is validated by simultaneously measuring precipitation sums with a manual Hellmann type rain gauge. Figure 14 shows exemplarily the meteorological observation site in Wibbese.

Figure 14: ***Meteorological observation site*** *in Wibbese showing the meteorological measuring instruments (from left to right): Rain gauge with tipping bucket, rain sampling gutter, Hellmann rain gauge, data logger with temperature, humidity and solar radiation sensor.*

Wind speed data are derived from surrounding weather observation stations of the German Weather Service (DWD): Wind speed is obtained from Friesoythe-Altenoythe for Sandkrug, from Hannover for Elze and from Seehausen for Wibbese. Meteorological **data gaps** are also filled by data from surrounding DWD weather stations: In Sandkrug, solar radiation data are obtained from Bremen and temperature, relative humidity and precipitation data are obtained from Großenkneten. In Elze, solar radiation data are obtained from Braunschweig, temperature and relative humidity data are obtained from Hannover and precipitation data are obtained from Elze-Berkhof. In Wibbese, solar radiation, temperature and relative humidity data are obtained from Seehausen and precipitation data are obtained from Zernien.

*Table 10: Technical **details of the meteorological sensors** for temperature, relative humidity and precipitation.*

	Unit	Range	Accuracy	Sensor
Temperature	°C	-30°C … +70°C	± 0.2K	Combined temperature and air humidity sensor
Relative Humidity	%	0% … 100%	± 2%	
Precipitation	mm	0 … 8 mm/min	No information	Rain gauge with tipping bucket (Lambrecht)
				Hellmann rain gauge

3.2.2 Stand precipitation and soil moisture

Stand precipitation and soil moisture are measured continuously at every forest plot. Figure 15 illustrates the measurement design of stand precipitation and soil moisture.

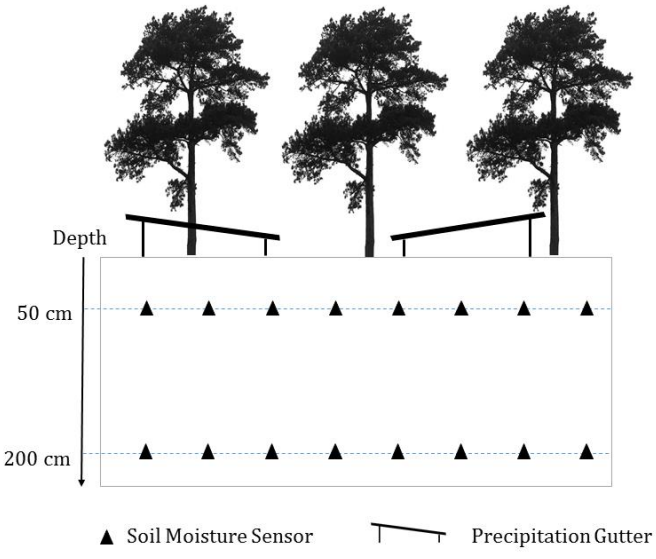

*Figure 15: Schematic illustration of **stand precipitation** and **soil moisture measurements** at a forest plot.*

Stand precipitation is measured with stainless steel gutters of 2 m length, 0.1 m width and an inclination of 5 °. A frame of 10 cm height on top of the gutter serves as splash guard. In total, 8 precipitation gutters are installed per plot and the gutter locations are selected with respect to the crown situation. The mean area of tree crown cover classes in each forest stand is determined by adopting a simplified version of the classification method used by Penne (2009): Photographs of the tree crown situation within the stand are taken at a regular grid and the pixels are classified into the classes "crown", "transition zone" and "gap", based on thresholds set by visual estimation. Then, the number of sensors located under certain crown cover conditions is calculated based on their respective share (Table 54 in the appendix). This systematic crown cover mapping revealed that the share of crown cover classes 'crown', 'transition zone' and 'gap' is approximately one third each for most of the plots. The gutters are arranged in two to four transects and they are connected

by a flexible tube that routes the precipitated water to a reservoir (see Figure 16). A wire mesh prevents leaves and litter from clogging the gutter outlet. This gutter design minimizes evaporation and splash losses and ensures a quick water outflow. The simulation of larger transects by using several short gutters is advantageous, as the amount of litter falling into the gutter that could potentially block the outlet is reduced. Regular maintenance is due every 2 to 4 weeks and includes removing litter from the gutters, flushing the tubes and cleaning the wire meshes. The stand precipitation sum is assessed every 2 weeks by measuring the stored precipitation amount and dividing it by the total surface of the gutters. In spring 2021, the reservoir was replaced by a tipping bucket connected to a data logger that allows continuous stand precipitation measurement.

Figure 16: ***Measurement of stand precipitation****: Gutters (left, used in Elze and Wibbese) and single rainfall collectors (right, used in Sandkrug) are used to measure stand precipitation.*

In Sandkrug, stand precipitation is measured with 16 rain collectors (see Figure 16) with a respective collecting area of 200 cm^2. These collectors are already used since 1998 to assess atmospheric nitrogen deposition. In summer 2020, precipitation gutters were additionally installed. Since then, stand precipitation is both measured with single collectors and precipitation gutters. The stand precipitation measurement interval is two to four weeks.

Soil Moisture is measured in a depth of 50 cm and 200 cm by using the soil moisture sensor SMT-100 (Umwelt-Geräte-Technik GmbH, Müncheberg, Germany, see Figure 17), which combines the methods of Time-Domain-Reflectometry (TDR) and Frequency-Domain-Reflectometry (FDR). The measured relative permittivity of the soil is translated into the volumetric soil water content according to the regression equation formulated by Topp et al. (1980). The SMT-100 sensor measures the volumetric soil moisture content in a range of 0 and 60% with a resolution of 0.1% and an accuracy of ± 3% (Umwelt Geräte Technik GmbH 2020b). Measurement inaccuracies can occur when the sensor has only poor contact to the soil because of air filled cavities (Umwelt Geräte Technik GmbH 2020a). Therefore, an insertion tool with a thinner rod than that of the sensor was used during sensor installation to safeguard a good contact of soil and sensor. Additionally, the hole was drilled with an inclination of 30° into the soil to minimize soil disturbances and preferential flow generation that could affect local soil water content. Soil moisture heterogeneity in forest soils is considered by installing 8 sensors per plot and depth. The sensor locations are selected with regard to the crown cover conditions. Figure

Figure 17: ***Measurement of soil moisture****: SMT-100 sensor used to measure the volumetric soil moisture content (Umwelt Geräte Technik GmbH 2020b).*

18 shows the locations of soil moisture sensors and stand precipitation gutters at the forest plots in Sandkrug, Elze and Wibbese.

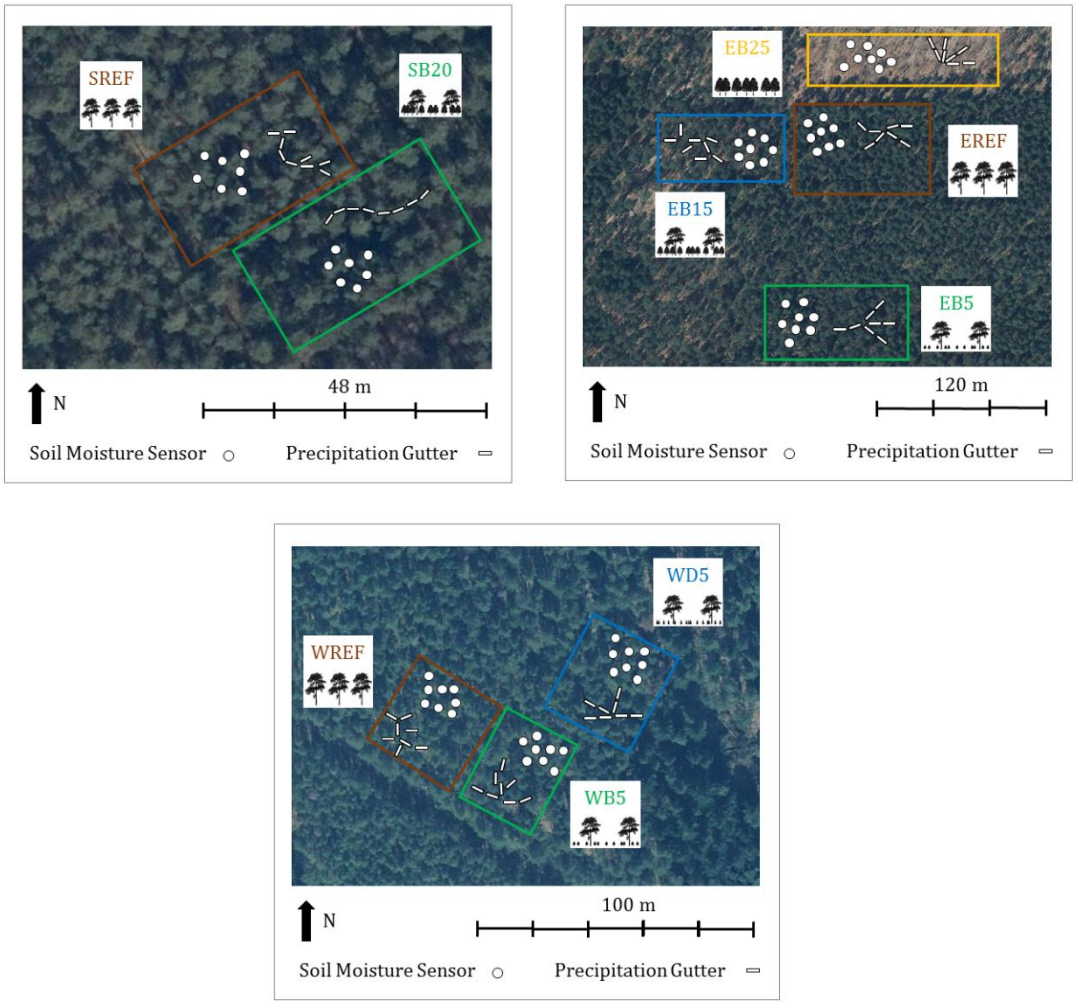

Figure 18: ***Location of soil moisture sensors and stand precipitation gutters*** *at the forest plots in Sandkrug (upper left), Elze (upper right) and Wibbese (bottom).*

3.2.3 Phenology and Leaf Area Index

The tree leaf area and its temporal development depends on tree species and forest management and is therefore characteristic for each forest plot. Phenology and leaf area of soil vegetation is not measured.

The **phenology** of the beech is estimated by visiting the plots regularly every 2 to 3 weeks. Thereby, the dates of budburst and leaf fall start are estimated by setting them to the mid of the time period in which the leaves have started to unfold or to fall. The lengths of leaf unfolding and leaf fall time periods are estimated visually. For pine, temporal dynamics of needle growth and fall are not assessed.

The **Leaf Area Index (LAI)** is regularly assessed for each forest plot every 3 to 6 months, but at least once in summer and winter to assess minimum and maximum LAI. The LAI is differently assessed for evergreen and deciduous trees: For evergreen forests (pine and Douglas fir), PAI, LAI and SAI are estimated by using Digital Hemispherical Photography (DHP), which is a widely applied method to assess the leaf area in forests (Chianucci & Cutini 2012, Jonckheere et al. 2004, Rich 1990). For deciduous forests (beech), PAI, LAI and SAI

are assessed based on litter fall sampling as described in the ICP Forest Manual Part XVII Canopy Leaf Area (Fleck et al. 2016). For mixed evergreen and deciduous forests, a combination of both techniques is used.

Figure 19: ***Example of DHP*** *with a field of view of 120° separated into ten rings before (left) and after (right) pixel classification into vegetation (black) and non-vegetation (white).*

Digital Hemispherical Photographs are acquired and analyzed as suggested by the ICP Forest Manual Part XVII Canopy Leaf Area (Fleck et al. 2016): Digital hemispherical photographs are taken at each soil moisture sensor and stand precipitation gutter, which yields 16 photographs per plot. These photograph locations are identical for every acquisition date. The photos are taken by a Nikon D50 camera with a fish-eye lens (Sigma 4.5 mm) at a height of 1 m above the ground. The top of the photograph points northwards. The correct horizontal and vertical orientation of the photograph is ensured by using a tripod and a water level bubble. The photographs are taken under uniform sky conditions before sunrise, after sunset or at days with a uniformly overcast sky to ensure comparable light conditions during photograph acquisition. The pictures are slightly underexposed to minimize the effect of canopy gaps blooming over the dark parts of the image. In order to estimate the plot LAI from these 16 single photographs, the software *Hemisfer* (Schleppi et al. 2007, Thimonier et al. 2010) is used. *Hemisfer* estimates potential radiation above vegetation and actual radiation below the canopy based on the photograph. Based on this radiation difference, *Hemisfer* estimates PAI, LAI and SAI: First the field of view of each photograph is set to 120°, which restricts the analysis to a circular angle of 60° around the zenith. This area is divided into ten rings of 6° width each. Second, the threshold distinguishing canopy from non-canopy pixels is calculated according to Ridler & Calvard (1978) separately for each ring to account for varying light conditions within the picture (see Figure 19). In a third step, the PAI is calculated according to Norman & Campbell (1989) and corrected for clumping-effects (Chen & Cihlar 1995). Hemisfer automatically summarizes the PAI for all 16 photographs and gives one synthesized PAI value for the plot. In order to separate this PAI into LAI and SAI, the species-specific needle-to-shoot area ratio (γ) and woody to total plant area ratio (α) are used. Tagesson (2006) found species-specific values of γ = 1.7 and α = 0.14 for Scots pine. LAI and SAI are then calculated as follows:

$$LAI = PAI * \gamma * (1 - \alpha) = PAI * 1.7 * (1 - 0.14) \quad (3)$$

$$SAI = PAI * \gamma * \alpha = PAI * 1.7 * 0.14 \quad (4)$$

Litter fall is sampled as described in the ICP Forest Manual Part XVII Canopy Leaf Area (Fleck et al. 2016). As deciduous trees, beech trees lose their foliage every year. This litter can be collected and its leaf area can be directly measured. By the end of July, the maximum amount of leaves in the canopy is formed (Bréda & Granier 1996). Consequently, the area of the falling leaves until the tree is bare in winter equals to the maximum leaf area in summer. Litter is collected both in rain gauges and litter traps. The litter traps are distributed in the forest with respect to canopy closure. The total sampling area (litter trap area + rain channel area, A_{traps}) is 3.1 m² in E B15, 2.8 m² in E B25 and 2.9 m² in S B20. Every two to four weeks, leaf litter is collected and immediately separated from needles and twigs. The sample is then stored at 4°C in a plastic bag until leaf area analysis. Litter is collected during the entire leaf fall period in autumn and winter until all leaves have fallen off.

*Figure 20: Scanned **litter fall** sample.*

Every litter sample is separately analyzed to construct the temporal LAI development during the leaf fall period. From every sample, a subsample of 100-200 leaves is selected, the rest is referred to as main sample. This sub sample is then scanned (see Figure 20) and the leaf area of this litter sub sample (A_s) is measured by using the software *ImageJ* (Schneider et al. 2012). Then, both sub sample and main sample are dried at 105°C until weight constancy to obtain dry masses of main (m_m) and sub sample (m_s). Then, the specific leaf area of the sub sample (SLA_s) is calculated:

$$SLA_s[m^2 * g^{-1}] = A_s/m_s \quad (5)$$

The leaf area of the main sample A_m is then calculated based on SLA_s and m_m:

$$A_m[m^2] = SLA_s * m_m \quad (6)$$

The total leaf area of the sample (A_t) is then calculated by adding up A_m and A_s:

$$A_t[m^2] = A_m + A_s \quad (7)$$

The corresponding LAI of this sample (LAI_{sample}) is then calculated by dividing the total leaf area of the sample by the total sampling area A_{traps}:

$$LAI_{sample}[m^2 * m^{-2}] = A_t/A_{traps} \quad (8)$$

In this manner, the LAI of every sample during the leaf fall period is calculated and the sum of all LAI values gives the maximum LAI (LAI_{max}) of the year:

$$LAI_{max} = \sum_{i=1}^{n} LAI_{sample\ i} \quad (9)$$

Table 8 summarizes the methods that are used to derive LAI and SAI for each forest plot. For SREF, EREF, EB5, WREF, WB5 and WD5, both LAI and SAI are derived based on DHP. For EB25, the SAI (SAI_{EB25}) is derived from DHP in winter:

$$SAI_{EB25} = PAI_{EB25,winter} \quad (10)$$

The minimum LAI in winter is assumed to be zero, as SAI_{EB25} also includes remaining dead leaves on the trees during winter. The maximum summer LAI ($LAI_{EB25,max}$) is assessed by using the litter fall method.

For mixed coniferous and broadleaved stands (EB15, SB20), the coniferous share (LAI_c) and the deciduous share (LAI_d) of the total LAI is assessed separately. LAI_d is assessed by litter fall sampling (Fleck et al. 2016) between August 2020 and January 2021. This value is also used for 2019, as litter was not collected during that year. LAI_c is assessed by DHP (Fleck et al. 2016) in winter time, when the leaves haven fallen off. However, beech stems and twigs contribute to PAI in winter, therefore, the woody to total area ratio needs to be adjusted towards a higher contribution of woody surfaces to the PAI. The woody to total area ratio for pine (α_p) is increased according to the ratio of beech basal area (BA_b) to pine basal area (BA_p) to calculate the woody to total area ratio for the mixed stand (α_m):

$$\alpha_m = \alpha_p + \left(\alpha_p * \frac{BA_b}{BA_p}\right) \quad (11)$$

LAI_c is then calculated based on the PAI from DHP, the needle-to-shoot area index for pine γ_p and α_m:

$$LAI_c = PAI * \gamma_p * (1 - \alpha_m) \quad (12)$$

LAI_c is assumed to be constant throughout the year. The minimum LAI ($LAI_{min,mixed}$) is assumed to be LAI_C and the maximum LAI ($LAI_{max,\ mixed}$) is assumed to be the sum of LAI_c and LAI_d:

$$LAI_{Min,mixed} = LAI_c \quad (13)$$

$$LAI_{Max,mixed} = LAI_c + LAI_d \quad (14)$$

The SAI of mixed stands (SAI_m) is assumed to be constant throughout the year and is calculated based on the PAI from DHP, the needle-to-shoot area index for pine γ_p and the woody to total area ratio adjusted for mixed stands (α_m):

$$SAI_m = PAI * \gamma_p * \alpha_m \quad (15)$$

Table 11 summarizes briefly the methods used to determine PAI, LAI and SAI at the forest plots.

*Table 11: Summary of **methods used to derive LAI** at the forest plots (Digital Hemispherical Photography (DHP) and/or Litter Fall Sampling (LFS)).*

	SREF	SB20	EREF	EB5	EB15	EB25	WREF	WB5	WD5
DHP	x	x	x	x	x	x	x	x	x
LFS		x			x	x			

3.2.4 Soil

Soil physical properties such as particle size distribution, bulk density and organic carbon content influence the water holding capacity of a soil as well as horizontal and vertical water movement (Amelung et al. 2018). These soil data are acquired for each forest plot.

During sensor installation, soil materials from the sensor locations were checked for homogeneity. The grain size distribution of the soil samples was roughly investigated by means of the finger test as described in Sponagel (2005). First, the soil sample was moistened slightly. Then, by squeezing and rolling the sample between thumb and fingers, the soil texture was estimated by evaluating plasticity, rolling capacity and roughness of the sample (Amelung et al. 2018, Sponagel 2005).

For a detailed analysis of the **grain size distribution**, three soil cores down to a depth of 200 cm within each plot were extracted by means of a gauge auger. By applying the finger test (Sponagel 2005), these soil cores were segmented into sub samples with similar grain size distributions. Every sub sample was stored in a plastic bag and labelled uniquely with plot name, number of soil core and depth. In the laboratory, the *LA-950 Laser Particle Size Analyser* (Company *Horiba,* Horiba Scientific (2020)) was used to estimate the particle size distribution of the soil samples. Beforehand, soil samples that contain considerably high organic material amounts are treated with hydrogen peroxide (H_2O_2) until the organic matter is destroyed. Then, the soil samples are homogenised by undirected stirring and three teaspoons of the soil material are extracted from the sample. The sub sample is then sieved to extract the gravel fraction (diameter > 2mm). Then, the sub sample is dispersed in demineralised water. From this sample, a sub sample is transferred into the water tank of the *LA-950*. The *LA-950* continuously stirs the sample and sends a laser beam through the sample. Depending on intensity and angle of the backscattered light, the LA-950 returns the grain size distribution of the sub sample (Horiba Scientific 2020). In total, the particle size distribution of three sub samples of the dispersed soil sample is assessed and the mean value of those three samples gives the particle size distribution of the soil sample.

In addition to grain size distribution, the **bulk density** of the soil down to a depth of 100 cm is assessed for every forest plot. For this purpose, one soil profile of 100 cm depth is dug at every forest plot. Then, three soil samples are collected with a sampling ring in 10cm, 30cm, 50cm and 100cm depth and stored in a plastic bag. In the laboratory, the samples are dried in the laboratory until weight constancy. The corresponding bulk density d_b is then calculated by calculating the ratio of the dry soil sample mass m_d to the sampling ring volume of 100 cm^3:

$$d_b[\frac{g}{cm^3}] = \frac{m_d}{100\ cm^3} \tag{16}$$

The bulk density of the specific depth and the specific plot is then calculated as average value of the three parallel samples.

Additionally, the organic carbon content C_{org} of the soil is estimated. Therefore, a sub sample of 5 g absolutely dry soil material (m_{ad}) from the bulk density sample is extracted and placed in a weighed porcelain crucible (m_{pc}). The sample is then placed in the furnace at 500°C for 4 hours. It afterwards cools down in a desiccator and is subsequently weighed (m_b). The ignition loss (IL) is then calculated according to (Blume et al. 2011):

$$IL\ [\text{mass} - \%] = \frac{(m_{ad} - m_b)}{m_{ad} * 100} \tag{17}$$

The organic carbon content is then considered being 50 % of the IL (Blume et al. 2011):

$$C_{org}[\text{mass} - \%] = \frac{IL}{2} \quad (18)$$

3.3 Modelling

3.3.1 Modelling strategy

Figure 21 shows schematically the modelling strategy used in this study. The modelling strategy is based on modelling strategies used by Groh et al. (2013), Hammel & Kennel (2001), Müller (2019), Schmidt-Walter et al. (2020b). For each forest plot, an individual model is set up with both general and plot-specific basic model settings (A). Then, a sensitivity analysis is run to assess the effect of individual model parameters on model performance (B). Thereby, model parameters are investigated whether they affect modelled stand precipitation and/or soil moisture. Model parameters that influence interception processes in the model are then manually calibrated against measured stand precipitation (C). Then, the model's ability to reproduce measured stand precipitation outside the calibration period is checked (D). Once the interception parameters are successfully calibrated, the soil hydraulic parameters of all forest plots at a site are adjusted simultaneously against measured soil moisture using automatic calibration techniques (E). Then, the remaining important evapotranspiration and soil water flow parameters that affect modelled soil moisture are adjusted (F). In the next step, the calibrated model is validated by means of measured soil moisture data (G). Finally, when the model is successfully calibrated, the modelled water fluxes including the deep seepage rate are analysed (H).

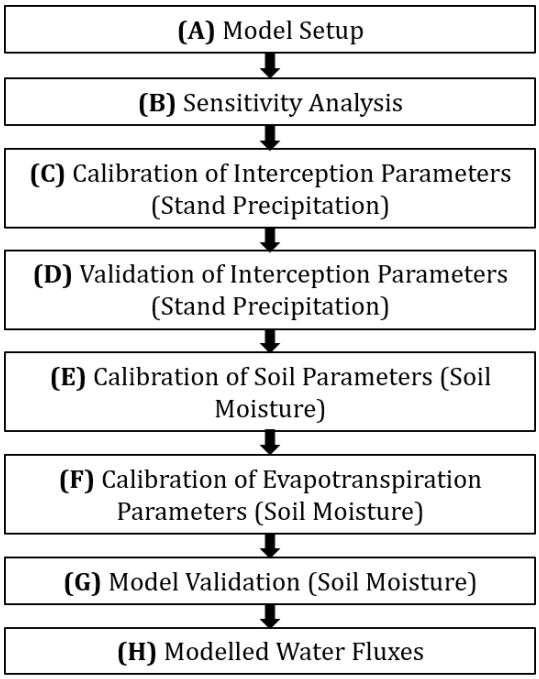

*Figure 21: The **modelling workflow** used for water balance modelling based on methodologies used by Groh et al. (2013), Hammel & Kennel (2001), Müller (2019), Schmidt-Walter et al. (2020b).*

3.3.2 Model setup

The model set up is identical for all forest observation plots apart from site-specific soil, weather and vegetation data. For each plot geographic coordinates are specifically set (see Table 14). LWF-Brook90R requires minimum, maximum as well as mean air temperature, vapour pressure, solar radiation and wind speed on a daily basis. Precipitation is provided on an hourly basis in an extra data file (see Table 12). Vapour pressure (e) is calculated based on mean air temperature (T), relative humidity (RH) and the saturation vapour pressure (e_s) (Magnus equation, Sonntag (1990)):

$$e_s\ [Pa] = 611.2 * e^{\frac{17.62*T}{243.12+T}} \quad (19)$$

$$e\ [\text{k}Pa] = \frac{RH * \frac{e_s}{100}}{1000} \quad (20)$$

Table 12: ***Meteorological input data*** *required as input for LWF-Brook90.*

Parameter	Description	Unit
tmin	Minimum temperature	°C
tmax	Maximum temperature	°C
tmean	Mean temperature	°C
prec	Precipitation sum	mm
vappres	Vapour Pressure	kPa
globrad	Global radiation sum	MJ/m^2
wind	Mean wind speed	m/s

Table 13: ***Soil input data*** *required as input for LWF-Brook90.*

Parameter	Description	Unit
horizon	Horizon symbol	-
upper	Upper soil layer boundary	m
lower	Lower soil layer boundary	m
texture	Soil texture according to German soil texture classification system	-
bd	Bulk density of fine earth	g/cm^3
gravel	Fraction of coarse material	%
sand	Sand content	Mass-%
silt	Silt content	Mass-%
clay	Clay content	Mass-%
c_org	Organic carbon content	Mass-%

LWF-Brook90 requires various soil input data that are given in Table 13. Every soil consists of one organic topsoil layer and 25 mineral soil layers down to a depth of 300 cm. The mineral soil layers are grouped into two different soil materials, with soil layers having similar soil properties being aggregated by calculating weighed mean values of measured sand, silt and clay content as well as bulk density and organic carbon content. For every study site (Sandkrug, Elze, Wibbese), the plot-specific soils are aggregated to one mean soil that is then used for soil water modelling. For these site-specific soils, the soil hydraulic parameters for mineral soil are parameterized according to Van Genuchten (1980) (MvG). LWF-Brook90R provides pedotransfer functions (PTFs) that are integrated within the model (Puhlmann & Von Wilpert 2011, Wessolek et al. 2009, Wösten et al. 1999, Wösten et al. 2001). These PTFs base on soil texture values according to the German Soil classification system KA5 (Wessolek et al. 2009) or measured clay, sand and silt contents and bulk density (Puhlmann & Von Wilpert 2011, Wösten et al. 1999). In this study, the pedotransfer function according to Wösten et al. (1999) is used to derive the MvG parameters. The hydraulic parameters of the humus layer are estimated according to Hammel & Kennel (2001).

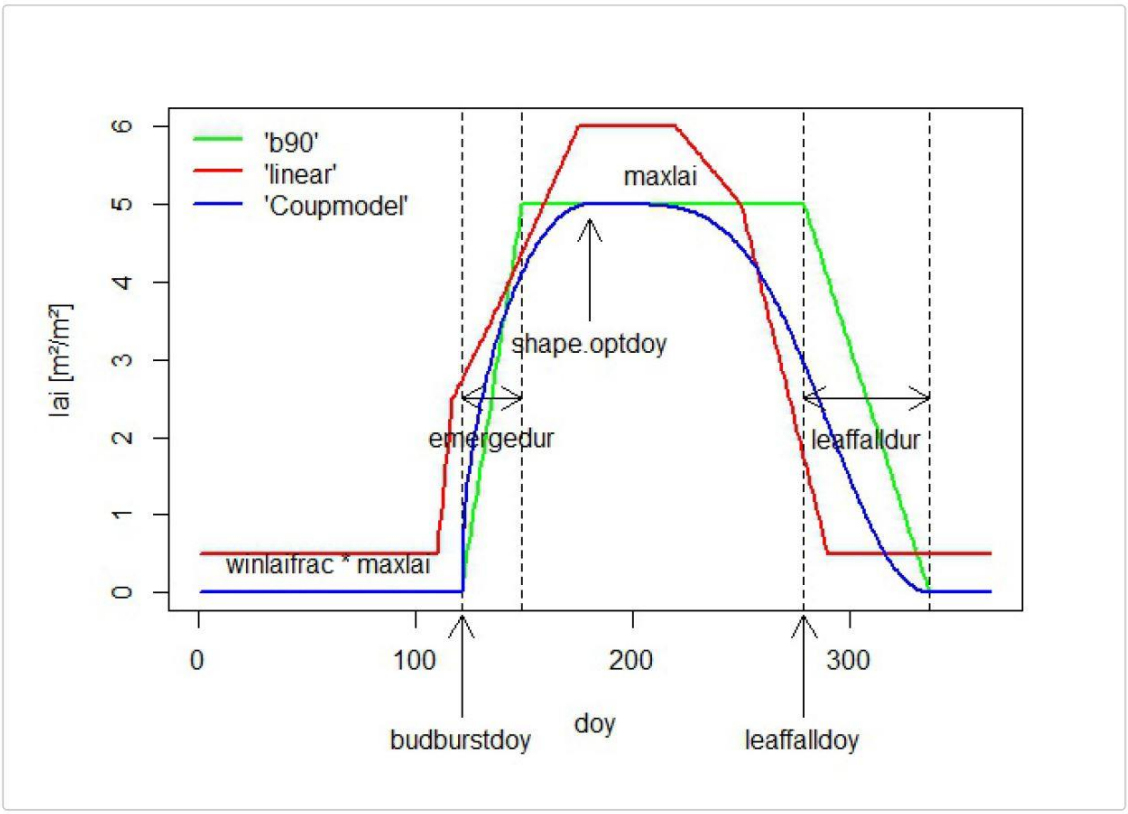

*Figure 22: Seasonal **LAI construction methods** ('b90', 'linear' and 'Coupmodel') in LWF-Brook90R (Schmidt-Walter et al. 2020a).*

The aboveground vegetation in the model is characterized by the parameters LAI, SAI, tree height and stand density. SAI is assumed being constant over time and is provided based on measurements. Tree height is also assumed being constant over time and is based on measurements. Tree height of mixed forest stands is calculated as weighed mean based on the basal area of the respective species (see Table 14). For LAI time series construction, LWF-Brook90R provides the methods 'linear', 'b90' and 'Coupmodel' (Jansson & Karlberg 2004), which require at least one LAI value per year to construct a daily time series of LAI values (see Figure 22). Here, the linear method is used: Pairs of DOY and LAI are provided and the model interpolates linearly between these dates to construct time series with daily steps. The maximum LAI is not varied from year to year in the simulation period. In coniferous forests, the LAI is set to a constant value without intra-annual variation. In mixed and deciduous stands, the seasonal course of the LAI is constructed based on phenological observations. During leaf unfolding and leaf fall, the LAI value increases and decreases linearly between minimum (winter) and maximum (summer) LAI. For tree height, SAI and stand density, constant values are used at all plots for the entire simulation period.

In order to simulate the thinning in Wibbese, the LAI construction method 'b90' is used in combination with the model parameter '*densef*'. In the model, *maxlai* is reduced by the same extent as measured LAI of WB5 ($LAI_{WB5,\ obs}$) and WD5 ($LAI_{WD5,obs}$) have been reduced relatively to the measured LAI of WREF ($LAI_{WREF,\ obs}$) . *Maxlai* and *sai* are simultaneously reduced by reducing the stand density parameter *densef*. The target LAI for WB5 ($LAI_{WB5,\ mod,\ after\ thinning}$) and WD5 after thinning ($LAI_{WD5,mod,after\ thinning}$) in the model are calculated based on the LAI of WREF in the model ($LAI_{WREF,\ mod}$) as follows:

$$LAI_{WB5,mod,after\ thinning} = LAI_{WREF,mod} * \frac{LAI_{WB5,obs,after\ thinning}}{LAI_{WREF,obs}} \quad (21)$$

$$LAI_{WD5,mod,after\ thinning} = LAI_{WREF,mod} * \frac{LAI_{WD5,obs,after\ thinning}}{LAI_{WREF,obs}} \quad (22)$$

Correspondingly, the resulting values for *densef* are calculated based on the model LAI values of WB5 and WD5 before thinning ($LAI_{WB5,\ mod,\ before\ thinning}$, $LAI_{WD5,\ mod,\ before\ thinning}$) as follows:

$$densef_{WB5} = \frac{LAI_{WB5,mod,after\ thinning}}{LAI_{WB5,mod,before\ thinning}} \quad (23)$$

$$densef_{WD5} = \frac{LAI_{WD5,mod,after\ thinning}}{LAI_{WD5,mod,before\ thinning}} \quad (24)$$

For considering roots, LWF-Brook90R provides the methods '*table*', '*betamodel*', '*linear*' and '*constant*' to approximate the root density depth distribution down to the maximum root depth (see Figure 23). Here, the method '*betamodel*' is used: It calculates the root density depth distribution as follows (Gale & Grigal 1987):

$$y = 1 - \beta^d \quad (25)$$

Y is the cumulative root fraction down to soil depth d and β is the depth coefficient. As shown in Figure 23, smaller values of β correspond to a greater proportion of roots in the upper soil layers, and vice versa (Schmidt-Walter et al. 2020a).

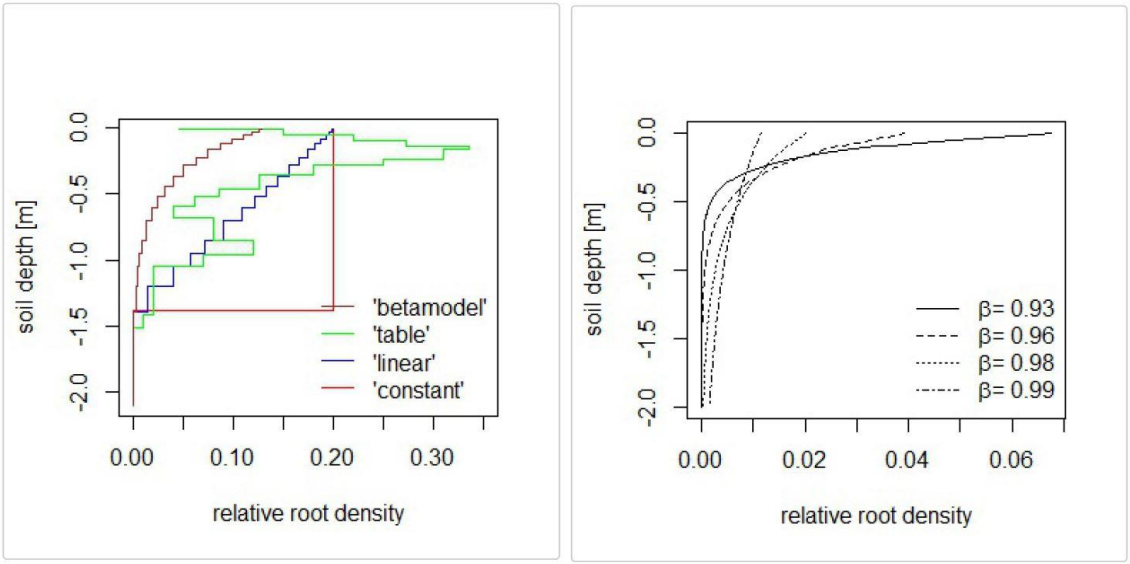

Figure 23: ***Relative root depth distribution construction in LWF-Brook90****: Methods to define relative root depth distributions ('betamodel', 'table', 'linear', 'constant', left) and the effect of the depth coefficient β on root density depth distribution calculation based on betamodel (right, Gale & Grigal (1987), Schmidt-Walter et al. (2020a)).*

Surface flow is prevented as precipitation input usually infiltrates entirely into plane forest soils. Impermeable soil layers routing water laterally within the soil matrix are not present, hence, lateral water flow paths are turned off. Water is allowed to infiltrate directly into

deeper soil layers via macropore and preferential flow (ilayer > 1). The soil moisture measurements indicate that plant roots extract water down to a depth of at least 200 cm, the maximum rooting depth is therefore set to 250 cm depth for all forest plots. For the bottom soil layer, free drainage to groundwater is assumed because groundwater levels are low and an intermediate state between free and no drainage would be difficult to justify (Hammel & Kennel 2001). Table 14 summarizes the model parameterization for each forest plot.

A spin-off period of 1 year (01/2018 – 12/2018) is set for every model run. The simulation period lengths are one year for calibration (01/2019 – 12/2019) and 10 months for validation (01/2020 – 10/2020).

Table 14: ***Initial plot-specific model parameterization****: Plot-specific geographic coordinates and tree height.*

	Sandkrug		Elze				Wibbese		
	S REF	S B20	E REF	E B5	E B15	E B25	W REF	W B5	W D5
Coordinates (X) [°]	8.29	8.29	9.77	9.77	9.77	9.77	11.0	11.0	11.0
Coordinates (Y) [°]	53.02	53.02	52.59	52.59	52.59	52.59	53.07	53.07	53.07
Tree Height [m]	23.00	19.77	22.00	21.60	18.10	7.50	27.80	27.80	27.80

3.3.3 Sensitivity analysis

The sensitivity analysis is run as described in Schmidt-Walter et al. (2020b). Based on suggestions from Groh et al. (2013), Schmidt-Walter et al. (2020b) and Müller (2019), 29 parameters are selected with parameter ranges based on literature values. Table 15 gives unit, description, value range and literature source for the value range for every model parameter investigated in the sensitivity analysis. The investigated model parameters include interception parameters (*maxlai*, *sai*, *lwidth*, *cintrl*, *cintrs*, *frintlai*, *frintsai*), evapotranspiration parameters (*alb*, *radex*, *cvpd*, *glmax*, *r5*, *t1*, *t2*, *rssa*, *betaroot*, *maxrootdepth*, *maxrlen*, *fxylem*, *mxkpl*, *psicr*), soil hydraulic parameters (MvG parameters *alpha* and *npar*, saturated hydraulic conductivity) and infiltration parameters (*ilayer*, *infexp*). An adequate sample size is critical for a meaningful sensitivity analysis. Stable sensitivity estimates usually require higher sample numbers for sensitive parameters than for less sensitive variables (Nossent et al. 2011). In the literature, sample sizes of n = 15.000 (Groh et al. 2013) and n = 50.000 (Schmidt-Walter et al. 2020b) are reported for LWF-Brook90R. Here, a sample size of n = 20.000 is used. For each parameter, samples are generated from random uniform distributions within predefined ranges (see Table 15).

Table 15: ***Parameters selected for sensitivity analysis*** *and corresponding unit, description, prior ranges (Min., Max.) and literature sources of the prior ranges.*

Parameter	Unit	Description	Min.	Max.	Literature Sources for Parameter Range
cintrl	mm	Maximum interception storage of rain per unit LAI	0.05	0.75	Federer (2015a), Schmidt-Walter et al. (2020b)
cintrs	mm	Maximum interception storage of rain per unit SAI	0.05	0.75	Federer (2015a), Schmidt-Walter et al. (2020b)
frintlai	-	Intercepted fraction of rain per unit LAI	0.1	0.2	-
frintsai	-	Intercepted fraction of rain per unit SAI	0.1	0.2	-
lwidth	m	Average leaf width	0.004	0.1	Federer (2015), Müller (2019)
maxlai	$m^2\ m^{-2}$	Maximum leaf area index	-25%	+25%	-
sai	$m^2\ m^{-2}$	Stem area index	-25%	+25%	-
alb	-	Albedo of soil/vegetation surface without snow	0.1	0.3	Schmidt-Walter et al. (2020b)
radex	-	Extinction coefficient for solar radiation and net radiation in the canopy	0.4	0.7	Schmidt-Walter et al. (2020b)
cvpd	kPa	Vapour pressure deficit at which leaf conductance is halved	0.5	3	Körner (1995), Federer (2015a), Schmidt-Walter et al. (2020b)
glmax	$m\ s^{-1}$	Maximum leaf vapour conductance when stomata are fully open	0.005	0.025	Federer (2015a), Hinckley et al. (1978), Körner (1995), Körner et al. (1979)
r5	$W\ m^2$	Solar radiation level at which leaf conductance is half of its value at nominal maximum solar shortwave radiation possible on a leaf	50	400	Federer (2015a), Körner (1995), Schmidt-Walter et al. (2020b)
t1	°C	Lower suboptimal temperature threshold for stomata opening – temperature relation	5	15	Federer (2015a), Körner (1995), Schmidt-Walter et al. (2020b)
t2	°C	Upper suboptimal temperature threshold for stomata opening – temperature relation	20	35	Federer (2015a), Körner (1995), Schmidt-Walter et al. (2020b)
rssa	$s\ m^{-1}$	Soil evaporation resistance at field capacity	20	1500	Federer (2015a), Schmidt-Walter et al. (2020b), Shuttleworth & Gurney (1990)
betaroot	-	Vertical root distribution β-coefficient	0.9	0.999	Schmidt-Walter et al. (2020b)
maxrootdepth	m	Maximum root depth	-2.5	-1.0	-
maxrlen	$m\ m^{-2}$	Total length of fine roots per unit ground area	500	11000	Newman (1974), Safford (1974), Safford & Bell (1972)
fxylem	-	Fraction of internal plant resistance to water flow that is in the xylem	0.01	0.9	Hunt et al. (1991)
mxkpl	$mm\ d^{-1}\ MPa^{-1}$	Maximum internal conductivity for water flow through the plants	1	30	Abdul-Jabbar et al. (1984), Hunt et al. (1991)
psicr	MPa	Critical leaf water potential at which stomates close	-4	-0.5	Federer (2015a), Hinckley et al. (1978)

alpha_1	-	Empirical MVG parameter alpha for upper soil layer	5	70	(Ad-hoc-Arbeitsgruppe Boden 1999, Gupta et al. 2021, Wösten et al. 1999)
alpha_2	-	Empirical MVG parameter alpha for lower soil layer	5	70	(Ad-hoc-Arbeitsgruppe Boden 1999, Gupta et al. 2021, Wösten et al. 1999)
npar_1	-	Empirical MVG parameter n for upper soil layer	1.2	2	(Ad-hoc-Arbeitsgruppe Boden 1999, Gupta et al. 2021, Wösten et al. 1999)
npar_2	-	Empirical MVG parameter n for lower soil layer	1.2	2	(Ad-hoc-Arbeitsgruppe Boden 1999, Gupta et al. 2021, Wösten et al. 1999)
sc_ksat_1	-	Scaling factor for saturated hydraulic conductivity for the upper soil layer	-0.5	0.5	Schmidt-Walter et al. (2020b)
sc_ksat_2	-	Scaling factor for saturated hydraulic conductivity for the lower soil layer	-0.5	0.5	Schmidt-Walter et al. (2020b)
ilayer	-	Number of layers from top to which infiltration is distributed	1	25	Number of soil layers
infexp	-	Shape parameter for distribution of infiltration in first ilayer	0	2	Federer (2015a)

For *maxlai* and *sai*, measured LAI and SAI values from winter 2019/2020 and summer 2020 are used in Sandkrug and Elze. In Wibbese, measured LAI and SAI values from summer 2019 before thinning are used. The corresponding parameter ranges for each forest plot are shown in Table 16.

Table 16: ***Ranges for the parameters maxlai and sai*** *in the sensitivity analysis based on measurements.*

	Sandkrug		Elze				Wibbese		
	S REF	S B20	E REF	E B5	E B15	E B25	W REF	W B5	W D5
maxlai (max)	3.5	6.2	3.9	3.6	7.3	6.5	2.0	2.1	2.3
maxlai	2.8	4.98	3.1	2.9	5.8	5.2	2.6	2.8	3.1
maxlai (min)	2.1	3.7	2.3	2.2	4.4	3.9	3.3	3.5	3.9
sai (max)	0.6	0.8	0.6	0.6	0.6	0.6	0.6	0.6	0.6
sai	0.5	0.6	0.5	0.5	0.5	0.5	0.5	0.5	0.5
sai (min)	0.4	0.4	0.4	0.4	0.4	0.4	0.4	0.4	0.4

The spin-off period is 01/2018 – 12/2018 and the sensitivity analysis is run from 01/2019 to 12/2019. Model simulations are compared with observed stand precipitation and soil moisture in 50 cm and 200 cm depth. The model performance is evaluated by calculating the Nash Sutcliffe Efficiency (NSE, Nash & Sutcliffe (1970)):

$$NSE = 1 - \frac{\sum_{t=1}^{t}\left(Q_{sim}^{t} - Q_{obs}^{t}\right)^{2}}{\sum_{t=1}^{t}(Q_{obs}^{t} - \bar{Q}_{obs})^{2}}, \qquad (26)$$

where t is the total number of time steps, Q_{sim}^{t} the modelled value at time t, Q_{obs}^{t} the observed value at time t, and $\bar{Q}_{obs}$ the mean observed value. An NSE of 1 indicates perfect correspondence between simulations and observations. NSE values between 0 and 1 are generally viewed as acceptable levels of performance and values < 0 indicate that the model

simulation is a worse predictor than observation mean, which indicates unacceptable performance (Knoben et al. 2019, Moriasi et al. 2007, Schaefli & Gupta 2007).

Based on the NSE, a parameter set is accepted (*behavioural*) or discarded (*non-behavioural*). Groh et al. (2013) define a parameter set as behavioural when its NSE is among the highest 10% NSE values. Schmidt-Walter et al. (2020b), in turn, define all parameters above a "hard" threshold of NSE = 0.8 being behavioural. Here, a parameter set is defined as behavioural when its NSE is above the 99.5 % confidence level.

Behavioural and non-behavioural parameter distributions are then tested for sensitivity by using the two-sample Kolmogorov-Smirnov test (Massey 1951). The test calculates the maximum distance between the behavioural and non-behavioral empirical cumulative distribution function (D_{max}). According to Harlin & Kung (1992), a parameter is 'highly important' if $D_{max} > 0.2$, 'important' if $0.1 \leq D_{max} \leq 0.2$, and 'unimportant' if $D_{max} \leq 1$.

Parameters that are important or highly important at most of the plots are further adjusted during model calibration, the remaining parameters are set to default or species-specific literature values.

3.3.4 Manual calibration of interception parameters

Important model parameters affecting model performance with regard to stand precipitation at most of the forest plots are manually adjusted in to safeguard comparability and to account for species-specific interception characteristics. Federer (2019) gives some recommendations for manually calibrating LWF-Brook90.

Species-specific interception characteristics are mostly associated with interception storage capacities and evaporation rates of intercepted water, for which ranges are found in the literature. Interception storage capacities are in the order of 1 – 2 mm in mature forests (Federer 2019). Schmidt-Walter et al. (2019) suggest a storage capacity of 0.76 mm for beech and Zhao et al. (2019) indicate leaf interception storage capacities being half of needle interception storage capacities per unit LAI. Therefore, interception parameters are adjusted in a way that storage capacities range between 1 and 2 mm in pine forests, between 0.5 and 1 mm in beech forests and between 0.5 and 2 mm in mixed forests. Evaporation of intercepted water is controlled by the model parameter *lwidth*. For *lwidth*, species-dependent values are reported in the literature. *Lwidth* is suggested to be 0.004 m for evergreen species (Federer 2019, Schmidt-Walter et al. 2019, Müller 2019) and 0.05 m (Schmidt-Walter et al. 2019), 0.06 m (Müller 2019) or 0.1 m (Federer 2019) for beech. *Lwidth* is thus calibrated within this parameter range.

3.3.5 Automatic calibration of soil and evapotranspiration parameters

Automatic calibration is used to adjust sensitive soil hydraulic and evapotranspiration parameters with respect to observed soil moisture in 50 cm and 200 cm. For automatic calibration, Bayesian Interference is used.

The joint posterior model parameter distribution is estimated using the DREAM algorithm (Vrugt et al. 2009). DREAM uses several chains to robustly and efficiently explore the parameter space. It is able to sample even multimodal posterior probability density functions with several local optimal solutions, which are frequently encountered in hydrological modelling (Vrugt et al. 2009). The between- and within-variance of the different parallel chains

is compared by the Gelman-Rubin scale-reduction factor (Gelman & Rubin 1992), which assesses the convergence of parameters to a stationary posterior distribution. The MCMC evolution is either repeated until this scale-reduction factor has reached a certain value (e. g. Groh et al. (2013)) or it is repeated for a fixed number of iterations (e. g. Schmidt-Walter et al. (2020b)). For further reading, a general discussion about applying MCMC techniques by Hogg & Foreman-Mackey (2018) and the work of Vrugt et al. (2009) discussing technical details of the DREAM algorithm are recommended.

The DREAM algorithm implemented in the R package 'DREAM' (Guillaume & Andrews 2012) is used to automatically calibrate sensitive soil and evapotranspiration parameters Based on literature values, feasible parameter ranges and starting points (initial values), at which the sampler starts to explore the parameter space within the predefined ranges are defined. The prior probability for the parameters $prior$ is calculated by summing up the Gaussian likelihood densities of each parameter:

$$prior = \sum_{i=1}^{n} log10\left(\frac{1}{\sqrt{2 * \pi} * \sigma} * e^{\frac{-(x_i-\mu_i)^2}{2*\sigma^2}}\right) \tag{27}$$

Where n is the number of parameters, x_i is the parameter value, μ_i is the initial value and σ is a standard deviation of 50. Then the Gaussian likelihood of a model simulation for a given state variable is calculated as follows:

$$logp = \sum_{i=1}^{n} log10\left(\frac{1}{\sqrt{2 * \pi} * \sigma} * e^{\frac{-\frac{(obs_i-mod_i)^2}{\overline{obs}}}{2*\sigma^2}}\right) \tag{28}$$

Where n is the number of state variable observations, σ is the standard deviation, obs_i is the observed state variable at a given time step, mod_i is the modelled state variable at a given time step, $\overline{obs}$ is the mean of all observed state variable values. The overall Gaussian likelihood of a model simulation is then calculated by summing up the weighted likelihood values of the state variables:

$$logp_{mod} = \frac{logp_{sp}}{len_{sp}} * len_{th50} + logp_{th50} + logp_{th200} + prior \tag{29}$$

Where $logp_{sp}$, $logp_{th50}$ and $logp_{th200}$ are the likelihood values for stand precipitation, soil moisture (50 cm) and soil moisture (200 cm), and len_{sp} and len_{th50} are the number of stand precipitation and soil moisture observations, respectively. By weighing the likelihood of stand precipitation, all three likelihood values have the same weight.

When the Gelman-Rubin scale-reduction factor falls below a value of 1.1, the parameters have converged to a stationary posteriori distribution function. The first half of the sampled parameter sets is then discarded and a random sample is drawn from the remaining parameter sets to display the best parameter set and its 95%-confidence bounds. By running the model with all parameter sets from this sample, the confidence bounds of the modelled state variables are displayed uncertainty ranges for all modelled water fluxes that originate from parameter sampling are provided. Additionally, the model prediction uncertainty based on the standard deviation is calculated, which is usually much larger than parameter uncertainty.

Model performance is evaluated by calculating the NSE and the Mean Absolute Error (MAE). The MAE indicates error in the units of the state variable and thus eases the analysis of the results (Moriasi et al. 2007). MAE values less than half the standard deviation of the measured data are considered being acceptable. The MAE is calculated as follows:

$$MAE = \frac{\sum_{t=1}^{n} \left| Q_{sim}^{t} - Q_{obs}^{t} \right|}{n} \quad (30)$$

where n is the total number of time steps, Q_{sim}^{t} the modelled value at time t and Q_{obs}^{t} the observed value at time t.

3.3.6 Model validation

The calibrated model is tested, whether it is able to reproduce observations of stand precipitation, and soil moisture in 50 cm and 200 cm depth in other periods than the calibration period. Therefore, each model is run within the validation period from 01/2020 to 10/2020, with a spin-off period from 01/2018 to 12/2019. In this validation period, the model's ability to reproduce measured stand precipitation and soil moisture in 50 cm and 200 cm depth is evaluated by means of resulting NSE and MAE values.

3.3.7 Resulting water balance components

With the calibrated model, the resulting water balance components interception evaporation, soil evaporation, transpiration and deep seepage are calculated. They are given as monthly and total sums in the entire modelling period 01/2019 – 10/2020.

In Wibbese, the effect of thinning on the water balance components in WB5 and WD5 compared to the reference state (WREF) is investigated by calculating and comparing sums for the period before (01/2019 – 02/2020) and after thinning (04/2020 – 10/2020). In addition, the plot-specific thinning effect is investigated by modelling the water fluxes with two different model parameter sets in the period 04/2020 – 10/2020: The first model parameter set is the same as used for the period before thinning (no thinning), and the second parameter set is the same as used for the period after thinning (thinning).

4 Results

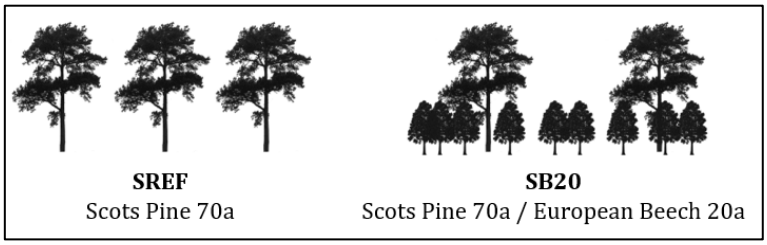

*Figure 24: **Abbreviations** (**SREF**, **SB20**) used for the investigated forest plots in Sandkrug.*

4.1 Sandkrug

4.1.1 Precipitation measurements

*Table 17: **Precipitation** sums and their absolute and relative deviations from multi-annual mean values in Sandkrug.*

Period	Sum [mm]	Abs. deviation [mm]	Rel. deviation [%]
08/2018 – 12/2018	212.9	-143.1	-40.2
01/2019 – 12/2019	845.4	44.4	5.5
01/2020 – 10/2020	600.9	-57.1	-8.7

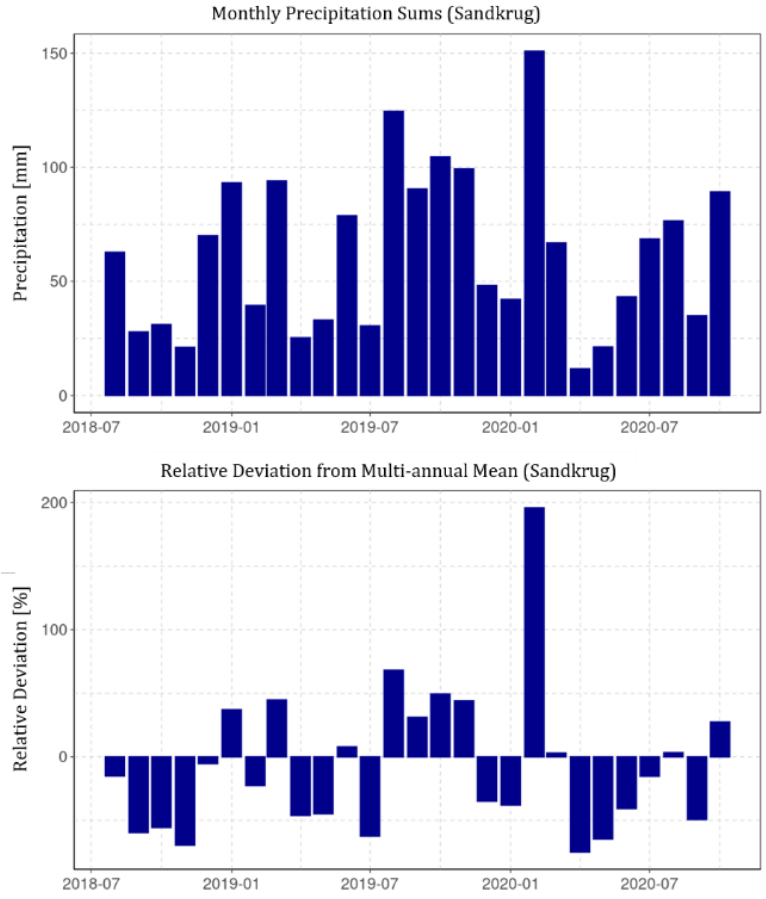

*Figure 25: Measured **monthly precipitation** sums (top) and their relative deviations from mean multi-annual precipitation sums (bottom) in Sandkrug between 08/2018 and 10/2020.*

Precipitation is measured in Sandkrug since August 2018. Table 17 shows measured precipitation sums in Sandkrug between 08/2018 and 10/2020 aggregated for every year and corresponding absolute and relative deviations from mean multi-annual precipitation sums in Grossenkneten. Figure 25 shows monthly precipitation sums and their relative deviation from multi annual mean precipitation measured in Grossenkneten between 08/2018 and 10/2020. Daily precipitation sums are shown in Figure 68 (appendix).

The period between August 2018 and December 2018 was remarkably dry with lower precipitation sums compared to the multi-annual average. The precipitation sum in 2019 corresponds to the long-term average. However, precipitation was unevenly distributed throughout the

year: Precipitation was below average between January and July, and above average between August and November. The precipitation sum in the period between January 2020 and October 2020 was slightly lower than the multi-annual mean precipitation sum in this period. February 2020 was an exception as precipitation summed up to almost 200 % of the multi annual mean precipitation sum. Overall precipitation was below average, with seven months not even reaching 50 % of mean precipitation.

4.1.2 Soil measurements

The study site Sandkrug (Figure 26) is located on a deep and sandy Podzol-Regosol (NIBIS Kartenserver 2014a). A 10 cm thick layer of organic material covers the mineral soil (O horizon). Below the organic layer, there is a 5 to 10 cm thick bleached eluviation soil horizon (Ae). From this grey colored horizon, aluminum (Al) and iron (Fe) leaches in suspension to the illuviation horizon (Bs) below. In this horizon in a depth of 10 to 30 cm, the Al and Fe molecules are deposited and give the horizon its characteristic red-brown color. As typical for forest soils, the boundaries between soil horizons are interrupted by preferential flow pathways along roots and are thus not horizontally uniform. The Bs horizon then goes progressively over into the parent dune material below (C horizon). The eluviation and illuviation horizons are less thick in S B20 compared to S REF. The observation sites in Sandkrug are groundwater distant, the groundwater table lies approximately 5 m below the surface (NIBIS Kartenserver 2014c).

*Table 18: Depth-specific **soil texture** in Sandkrug derived from grain size distribution analysis (Ss = pure sand, Su2 = slightly silty sand).*

Depth [cm]	SREF	SB20
0-10	Ss	Ss
10-20	Su2	Ss
20-30	Su2	Ss
30-40	Ss	Ss
40-50	Ss	Ss
50-60	Ss	Ss
60-70	Ss	Ss
70-80	Ss	Ss
80-90	Ss	Ss
90-100	Ss	Ss
100-110	Ss	Ss
110-120	Ss	Su2
120-130	Ss	Su2
130-140	Ss	Su2
140-150	Ss	Su2
150-160	Ss	Su2
160-170	Ss	Ss
170-180	Ss	Ss
180-190	Ss	Ss
190-200	Ss	Ss

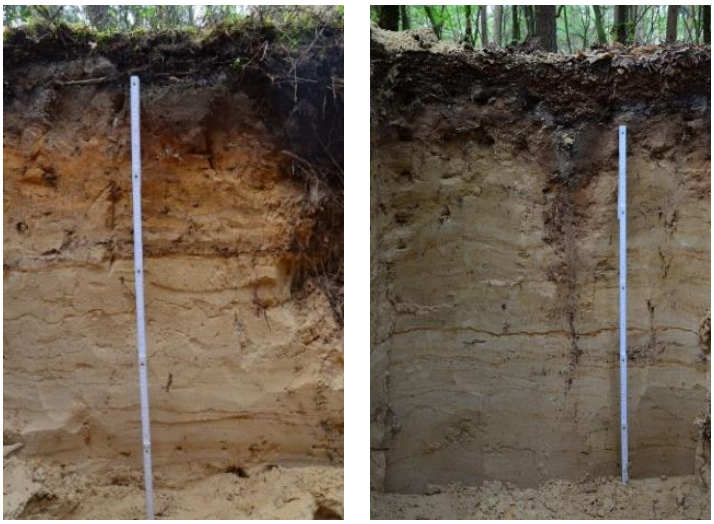

*Figure 26: **Soil profiles** in Sandkrug (left: S REF, right: S B20) down to a depth of 100 cm.*

The results of the grain size distribution analysis for SREF and SB20 are summarized in Table 18. Corresponding detailed information about sand, silt and clay content (Figure 69) as well as gravel content (Table 58), bulk density (Table 59) and organic carbon content (Table 60) analyses are provided in the appendix.

The dominating soil texture classes in SREF and SB20 are pure sand (Ss) and slightly silty sand (Su2). The sand fraction is dominated by fine and medium sand. Noteworthy quantities of silt only occur between 10 cm and 30 cm depth in SREF and in deeper soil layers below 100 cm in S B20. In both plots, the gravel content is negligible in the entire soil column. Soil texture is generally comparable in both observation plots.

For each plot, soil layers with similar soil properties were combined into a total of two soil layers with weighed mean soil properties. These simplified plot-specific soils are then aggregated to one site-specific soil for Sandkrug (Table 61, appendix) by calculating the average of the plot-specific soil properties. This site-specific soil is used as model soil for the site Sandkrug.

4.1.3 Phenology & Plant Area Index measurements

Based on regular LAI measurements and phenological observations, the development of the tree canopy is monitored. Table 19 gives approximations of bud burst dates, leaf unfolding periods, leaf fall start dates and leaf shedding periods for beech in SB20 based on in situ observations every two weeks. In 2019, the bud burst date of beech is in the end of April and leaves unfold until the end of May. Leaves start to fall in the mid of October. The leaf fall period ends in the beginning of December 2019. In 2020, the bud burst date of beech is already in mid-April and thus two weeks earlier than in 2019. The corresponding leaf unfolding period lasts until mid-May. Pronounced drought stress during summer causes the beech to partly drop its leaves already in August 2020. Some rain in the end of August alleviates the drought and the early leaf fall is stopped. The remaining leaves then start to fall in mid-October until the majority of leaves has fallen in mid-December 2020.

*Table 19: Assessment of **phenology**: Time periods of leaf unfolding and leaf fall of European beech in SB20 in 2019 and 2020 based on observations (time interval: 2 to 4 weeks).*

	leaf unfolding 2019	leaf fall 2019	leaf unfolding 2020	leaf fall 2020
Date	29.04.2019 – 28.05.2019	16.10.2019 – 04.12.2019	15.04.2020 – 14.05.2020	19.08.2020 – 10.12.2020
DOY	120 - 150	290 - 340	105 - 135	230 - 340

Table 55 (appendix) shows measured LAI values for European beech in SB20 based on litter fall sampling in summer and autumn 2020. More than 50 % of the leaves have fallen off due to drought conditions in August 2020, reducing beech LAI from 2.09 to 0.74. From mid-October to the beginning of December, the LAI is further reduced to approximately zero. Table 57 (appendix) shows the total LAI and SAI values of both pine and beech for SB20 in summer and autumn 2020. Table 56 (appendix) then gives final LAI and SAI values for SREF and SB20 in the period 2019 – 2020. Figure 27 shows these measured LAI and SAI as sum (LAI + SAI = PAI) in SREF and SB20 in 2019 and 2020. PAI values differ substantially between S REF and S B20. In winter, when the beech has shed its leaves, PAI values in S REF and S B20 are between 3.0 and 3.6 with slightly higher values in S B20 than in SREF. When the beech trees unfold their leaves in spring, the PAI increases to a value of 5.6. In S REF, the canopy shows higher values in summer (3.7, 4.0) than in winter (3.2, 3.0). The PAI in SREF thus varies between 3.0 and 4.0 throughout the year.

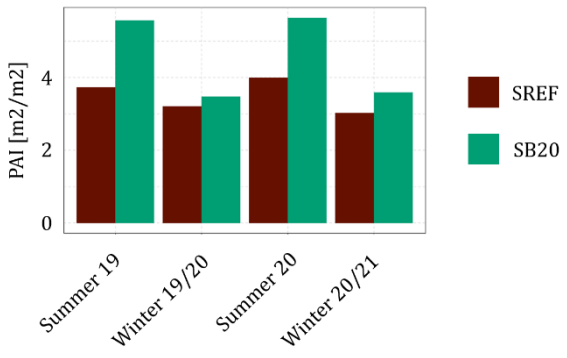

*Figure 27: Total **Plant Area Index** (PAI = LAI + SAI) in SREF (pine) and SB20 (pine, beech). The minimum (winter) and (maximum) PAI are given for 2019 and 2020.*

4.1.4 Stand precipitation measurements

The total number of measured stand precipitation sums is 19 in 2019 and 18 in 2020 in both plots. Figure 28 shows average interception in SREF and SB20. Interception values are aggregated for summer 2019 (n = 11), winter 2019/2020 (n = 6), summer 2020 (n = 11) and the entire calibration (01/2019-12/2019, n = 19) and validation (01/2020-10/2020, n = 18) period. Thereby, summer is defined as period between 01/05 an 30/09, and winter is defined as period between 01/12 and 30/04. Detailed stand precipitation and interception loss data are provided in Table 64 (appendix).

Measured stand precipitation sums are the highest in SREF and the lowest in SB20 all year round. Correspondingly, interception losses in SREF are lower than in SB20: Mean interception losses are 37.7 % (SREF) and 50.6 % (SB20) in 2019 and 38.3 % (SREF) and 50.2 % (SB20) in 2020. In summer 2019, interception in SREF (42.4 %) is considerably lower than in SB20 (58.2 %). In winter 2019/2020, this difference decreases because the beech trees in SB20 shed their leaves, but interception in SREF (38.4 %) is still lower than in SB20 (44.1 %). In summer 2020, the interception rate in SB20 increases with leaf growth to 49.1 % and is considerably higher than in SREF (34.3 %). Table 64 (appendix) shows single interception values of stand precipitation sums in periods of 2 to 4 weeks length. These interception values vary significantly over time and are the result of varying precipitation intensities and patterns.

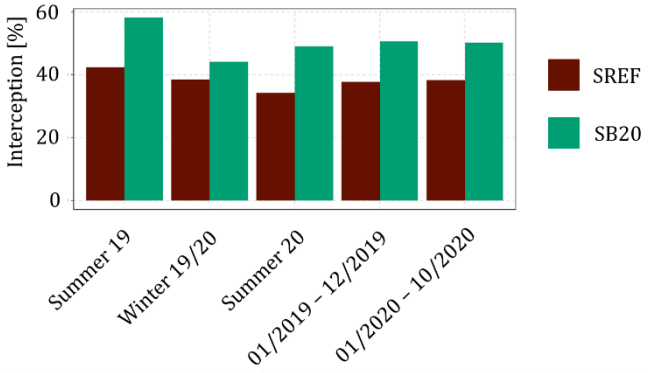

*Figure 28: **Mean interception** rates in SREF and SB20 in summer 2019 (n = 11), winter 2019/2020 (n = 6), summer 2020 (n = 11), and the periods 01/2019-12/2019 (n = 19) and 01/2020-10/2020 (n = 18).*

4.1.5 Soil moisture measurements

Figure 29 shows mean daily soil moisture values in 50 cm and 200 cm depth in SREF and SB20 as well as daily precipitation sums between January 2019 and October 2020. The corresponding soil moisture profiles of the single soil moisture sensors are provided in Figure 70 in the appendix.

The soil moisture level is different in both plots: In 50 cm depth, the soil moisture level is slightly higher in SB20 than in SREF. This difference is particularly large in the beginning of 2019, but it becomes smaller later in 2019 and remains relatively small until the end of the observation period. In 200 cm depth, the soil moisture level in SB20 is higher than in SREF throughout the entire period.

The soil moisture shows a characteristic behavior in SREF and SB20. In 50 cm depth, the soil moisture course is similar in both plots: In winter 2018/2019, soil moisture was comparably high, with soil moisture values between 12 % and 15 % in SB20 and between 8 % and 10 % in SREF. Precipitation events caused small soil moisture peaks in this period. In spring and summer 2019, the soil moisture decreased in both plots to a low soil moisture level of approximately 5 % due to evapotranspiration of the vegetation. A thunderstorm

with abundant rainfall caused a sharp increase in soil moisture in June (10 % in SREF, almost 20 % in SB20), which then dropped very quickly within only a few days. In August, several rain events caused an increase in soil moisture in both plots, with the increase more pronounced in SB20 than in SREF. Another significant rain event with almost 50 mm of rain within a few hours in August caused a rapid increase in soil moisture in both plots. In October, the soil moisture sustainably increased to a higher level between 10 % and 12 % due to abundant rainfall and remained on this level during winter 2019/2020. Heavy rain caused pronounced soil moisture peaks of 12 % to 15 % in November 2019 and February 2020. From March 2020 onwards, the soil moisture decreased continuously to a level between 5 % and 7 % and remained at this low level until the end of the observation period. Rain fall caused only few soil moisture peaks, which are more pronounced in SB20 than in SREF. Until the end of the observation period, the soil moisture did not sustainably increase to a higher level as in autumn 2019.

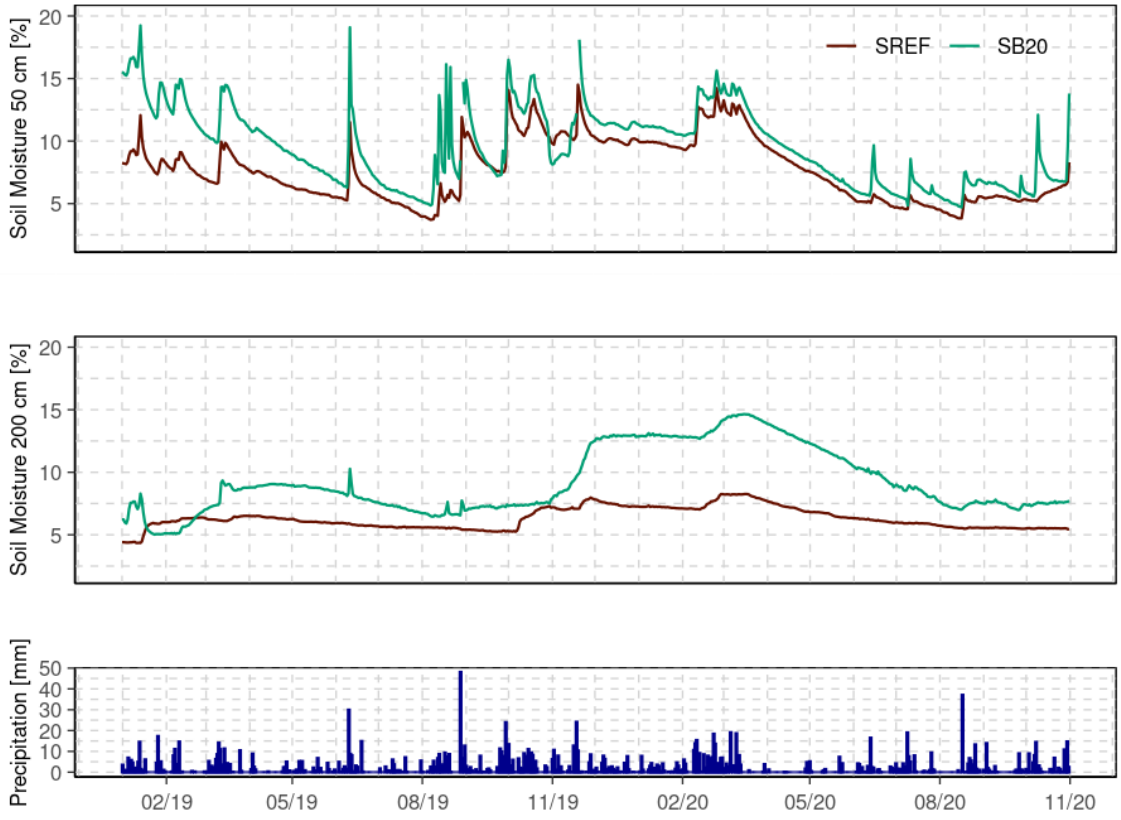

Figure 29: ***Soil moisture observations*** *(daily mean of 7 soil moisture sensors) in 50 cm (top) and 200 cm depth (middle) as well as daily precipitation sums (bottom) in Sandkrug.*

In 200 cm depth, the soil moisture course of both plots shows some significant differences. In winter 2018/2019, the soil moisture increases sustainably in both plots. In SREF, the soil moisture increases in mid-January from below 5 % to between 6 % and 7 %. In SB20, the soil moisture increases later (mid-February) but more strongly from 5 % to almost 10 %. In spring and summer 2019, soil moisture decreases in both plots successively to 5 % in SREF and to 7 % in SB20. Abundant rainfall in June and August caused small short-term peaks in SB20, which are not visible in SREF. In autumn 2019, abundant precipitation caused a sustainable soil moisture increase in both plots. In SREF, soil moisture increased in the beginning of October from 5 % to 8 %, and in SB20 soil moisture increased one month later from 7 % to 13 %. From then on, soil moisture remained at this relatively high level throughout

the winter at both plots. In February 2020, soil moisture increased even more due to abundant rain fall. In spring and summer 2020, soil moisture decreased successively to a level of 7 % in SB20 and 5 % in SREF without any major peaks until the end of the observation period.

For statistical analyses, descriptive statistical measures are calculated for mean daily soil moisture values of 7 soil moisture sensors per plot in the observation period between 01/2019 and 10/2020: Mean 5 % confidence level (CI5), median, mean 95 % confidence level (CI95), mean 90% interquartile range (IQR90), mean standard deviation (SDEV), minimum (Min), maximum (Max) and mean range between lowest and highest daily soil moisture value of all sensors (range). Table 20 show these descriptive statistical measures of soil moisture in 50 cm and 200 cm depth. The soil moisture level in SREF is lower than in SB20 in 50 cm and 200 cm depth. In 50 cm depth, the corresponding soil moisture ranges between 2.0 % and 28.2 % in SREF and between 2.4 % and 32.4 % in SB20. In 200 cm depth, the corresponding soil moisture values range between 3.0 % and 10.1 % in SREF and between 3.8 % and 23.1 % in SB20. Thus, soil moisture variability in SREF is higher than in SB20 in both depths.

*Table 20: **Statistical measures** calculated from daily mean **soil moisture** values of the 8 soil moisture sensors in **50 cm and 200 cm depth** between 01/2019 and 10/2020: Mean 5 % confidence level (CI5), median, mean 95 % confidence level (CI95), mean 90% interquartile range between CI5 and CI95 (IQR90), mean standard deviation (SDEV), minimum (Min), maximum (Max) and mean range between lowest and highest daily soil moisture value of all sensors (range).*

	CI5 [Vol-%]	Median [Vol-%]	CI95 [Vol-%]	IQR95 [Vol-%]	SDEV [Vol-%]	Min [Vol-%]	Max [Vol-%]	Range [Vol-%]
				50 cm depth				
S REF	5.4	6.7	8.6	3.2	2.3	2.0	28.2	6.4
S B20	7.7	9.1	9.9	2.2	1.6	2.4	32.4	4.0
				200 cm depth				
S REF	5.1	6.1	6.7	1.6	1.1	3.0	10.1	2.9
S B20	6.8	8.4	9.7	2.9	2.1	3.8	23.1	5.4

4.1.6 Sensitivity analysis

Table 21: NSE values at the 99.5 % confidence level separating behavioural from non-behavioural model runs.

	S REF	S B20
stand precipitation	0.995	0.959
soil moisture (50 cm)	0.690	0.461
soil moisture (200 cm)	-0.117	0.178

The sensitivity analysis reveals the importance of individual model parameters for model performance with regard to stand precipitation and soil moisture in 50 cm and 200 cm depth in Sandkrug. The threshold between behavioural and non-behavioural model runs is set to the 99.5% confidence level. Corresponding NSE values are given in Table 21. Figure 30 shows insensitive parameters in white, moderately sensitive parameters in orange and highly sensitive parameters in red. Those parameters selected for model calibration are marked with an x.

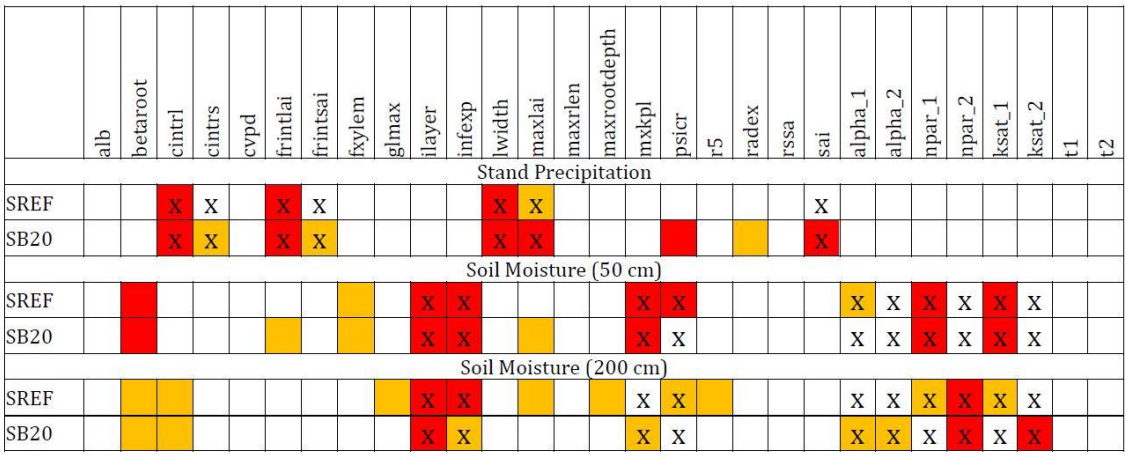

Figure 30: ***Results of the sensitivity analysis*** *with regard to stand precipitation, soil moisture (50 cm) and soil moisture (200 cm) in Sandkrug. Highly important parameters are shown in red, moderately important parameters are shown in orange and unimportant parameters are shown in white. Model parameters selected for model calibration with respect to stand precipitation, soil moisture in 50 cm and 200 cm depth are marked with an X.*

In SREF and SB20, those **model parameters that control interception evaporation** are sensitive with respect to observed stand precipitation. The fraction of rain intercepted per unit LAI (*frintlai*), leaf rain interception storage per unit LAI (*cintrl*) and leaf width (*lwidth*) are highly important in SREF and SB20. The maximum LAI (*maxlai*) is moderately important in SREF and highly important in SB20. The other model parameters are not sensitive in SREF. In SB20, however, the critical leaf water potential at which stomates close (*psicr)* and the stem area index (*sai)* are highly sensitive and the leaf rain interception storage per unit SAI (*cintrs)*, the extinction coefficient for solar radiation and net radiation in the canopy (*radex)* and the fraction of intercepted rain per unit SAI (*frintsai)* are moderately important.

Maxlai and *sai* are directly linked to *frintlai*, *frintsai*, *cintrl* and *cintrs* and hence simultaneously affect interception storage capacity and the fraction of precipitation that is added to this storage. Thus, these parameters are included into calibration, even if *cintrs* and *frintsai* are less important parameters. *Lwidth* determines the canopy boundary resistance and thus affects the amount of water that evaporates from the canopy interception storage to the atmosphere: Increasing *lwidth* increases the canopy boundary resistance and thus reduces interception evaporation, and vice versa. Therefore, *lwidth* is also considered in the calibration process. Additionally, interception evaporation rates are also constrained by the available amount of energy, which is controlled by the surface albedo (*alb*) and the extinction coefficient for photosynthetically-active radiation within the canopy (*radex*). These parameters are, however, only of limited importance for modelled stand precipitation.

Soil moisture in 50 cm depth is mostly affected by soil and evapotranspiration parameters in SREF and SB20. The empirical MvG parameters *alpha*, *npar* and *ksat* affecting soil water movement and soil water content are moderately to highly important. Maximum depth (*ilayer*) and vertical distribution with depth (*infexp*) of macro pore-assisted infiltrating water are also highly important model parameters. The remaining important parameters control soil water removal through evapotranspiration (*betaroot*, *mxkpl*, *psicr*). *Betaroot* controls the root depth density distribution and thus the amount of water that can be extracted from specific soil depths. Within the plant, water flow from root to leaf is affected by the maximum plant internal conductivity (*mxkpl*). *Psicr* is the critical leaf water potential at which stomates close and thus controls evapotranspiration rates when the soil is dry. For **soil moisture in 200 cm depth**, parameters affecting vertical soil water movement are

most important: *Ilayer*, *infexp*, *npar* and *ksat* are highly important at mostly both plots. Evapotranspiration parameters are of less importance for soil moisture in 200 cm depth. Therefore, the MvG parameters *alpha*, *npar* and *ksat*, as well as *mxkpl*, *psicr*, *infexp* and *ilayer* are included in model calibration with respect to soil moisture in 50 cm and 200 cm depth. Even though betaroot is a sensitive parameter, it is set to a fixed value according to Jackson et al. (1996).

Parameters found having an overall negligible effect on modelled stand precipitation and soil moisture are the albedo of soil / vegetation surface without snow (*alb*), vapor pressure deficit at which leaf conductance is halved (*cvpd*), the fraction of internal plant resistance to water flow that is in the xylem (*fxylem*), the maximum leaf vapor conductance when stomates are fully open (*glmax*), total length of fine roots per unit ground area (*maxrlen*), maximum root depth (*maxrootdepth*), solar radiation at which leaf conductance is half of its value at nominal maximum solar shortwave radiation possible on a leaf (*r5*), extinction coefficient for solar radiation and net radiation in the canopy (*radex*), soil evaporation resistance at field capacity (*rssa*) and the lower and upper suboptimal temperature threshold for stomata opening-temperature relation (*t1*, *t2).* These parameters are fixed to literature values according to Federer (2019) and Jackson et al. (1996) (see Table 22). For SB20, weighed mean values of conifers and broadleaves based on the specific stand basal area of both species are used.

Table 22: ***Fixed model parameter values*** *based on literature values (Federer 2019) of parameters being identified as unimportant in the sensitivity analysis. For SB20, parameter values are weighed mean values based on the specific stand basal area of pine and beech.*

	alb [-]	cvpd [kPa]	fxylem [-]	glmax [m s^{-1}]	maxrlen [$m\ m^{-2}$]	maxrootdepth [m]	r5 [$W\ m^{2}$]	radex [-]	rssa [$s\ m^{-1}$]	t1 [°C]	t2 [°C]	betaroot [-]
SREF	0.14	2	0.5	0.0053	3000	-2.5	100	0.5	100	10	30	0.976
SB20	0.157	2	0.5	0.0053	3000	-2.5	100	0.542	100	10	30	0.974

4.1.7 Calibration and validation of interception evaporation parameters

Model interception parameters are manually adjusted in a way that storage capacities range between 1 and 2 mm in SREF and between 0.5 and 2 mm in SB20. In SREF, modelled stand precipitation is initially too low in winter. Decreasing *maxlai* yields a better fit for the winter period, however, stand precipitation is then overestimated in summer. Therefore, *maxlai* is not further changed but *lwidth* is increased from 0.004 m to 0.05 m, which yields a good fit both in summer and winter. An increased *lwidth* increases the canopy boundary resistance and thus reduces interception evaporation. In SB20, the different interception characteristics of needles and leaves are considered by slightly decreasing the interception storage capacity (*cintrl*, *cintrs*) and increasing *lwidth* to 0.07 m. The resulting modelled stand precipitation was slightly too high in winter. Thus, the minimum LAI is then increased from 2.9 to 3.9, which yields a good fit. The resulting parameter values from calibrating stand precipitation and the corresponding modelled interception storage capacities for each plot are given in Table 23. Figure 31 shows the seasonal PAI course between 01/2019 and 10/2020 after model calibration.

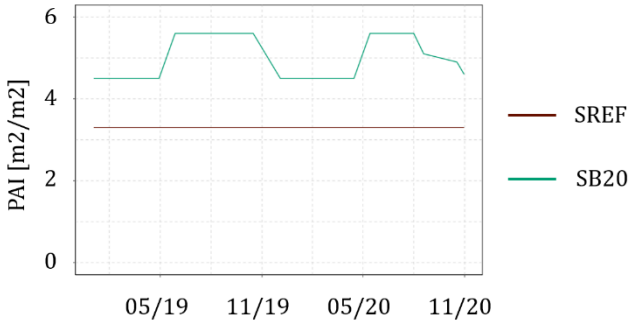

*Figure 31: Course of the **PAI** in the model **after calibration** of model interception parameters between 01/2019 and 10/2020.*

*Table 23: **Calibrated interception parameter values** from calibrating stand precipitation and the associated modelled interception storage in SREF and SB20.*

		cintrl [mm]	cintrs [mm]	frintlai [-]	frintsai [-]	lwidth [m]	maxlai [m^2 m^{-2}]	minlai [m^2 m^{-2}]	sai [m^2 m^{-2}]	storage capacity [mm]
SREF	Min	0.05	0.05	0.1	0.1	0.004	2.1	2.1	0.4	1.0
	Max	0.75	0.75	0.2	0.2	0.1	3.5	3.5	0.6	2.0
	Best Fit	**0.3**	**0.3**	**0.17**	**0.17**	**0.05**	**2.8**	**2.8**	**0.5**	**0.99**
SB20	Min	0.05	0.05	0.1	0.1	0.004	3.7	2.2	0.4	0.5
	Max	0.75	0.75	0.2	0.2	0.1	6.2	3.9	0.8	2.0
	Best Fit	**0.25**	**0.25**	**0.18**	**0.18**	**0.07**	**4.98**	**3.9**	**0.6**	**1.4**

Figure 32 shows modelled and observed cumulated stand precipitation and gross precipitation sums after model calibration for SREF and SB20 in the calibration and validation period. Table 24 shows observed and modelled stand precipitation sums, interception rates and error measures for SREF and SB20 in the calibration and validation period.

*Table 24: **Observed and modelled stand precipitation** characteristics for SREF and SB20 in the calibration (01/2019 – 12/2019) and validation period (01/2020 – 10/2020): Total observed and modelled sums (Sum_{Obs} , Sum_{Mod}), mean observed and modelled interception rates (Int_{Obs}, Int_{Mod}), modelled interception rates in summer (Int_{summer}) and winter (Int_{winter}) and the error measures NSE and MAE.*

	Sum_{Obs} [mm]	Sum_{Mod} [mm]	Int_{Obs} [%]	Int_{Mod} [%]	Int_{summer} [%]	Int_{winter} [%]	NSE	MAE [mm]
Calibration period (01/2019 – 12/2019)								
SREF	495.8	491.2	38.1	38.8	36.5	31.9	99.5	1.2
SB20	410.2	414.6	51.2	54.1	51.5	39.5	98.5	2.0
Validation period (01/2020 – 10/2020)								
SREF	390.4	391.3	38.4	38.6	34.9	40.7	97.7	2.8
SB20	330.9	328.1	50.4	53.5	49.5	51.5	97.1	2.8

The model reproduces measured stand precipitation well in SREF and SB20 in the calibration period. Corresponding error measures show an NSE close to 100 and a low MAE. Thereby, the model reliably reproduces higher interception rates in SB20 compared to SREF as well as the seasonal variation in interception due to leaf fall and leaf unfolding in SB20. In the validation period, the model also reproduces modelled stand precipitation well. In summer, there is a small deviation between observed and modelled stand precipitation, however, the difference is only small. The accurate modelling performance is reflected in a NSE value close to 100 and a low MAE, however, the goodness of fit is slightly lower than in the calibration period.

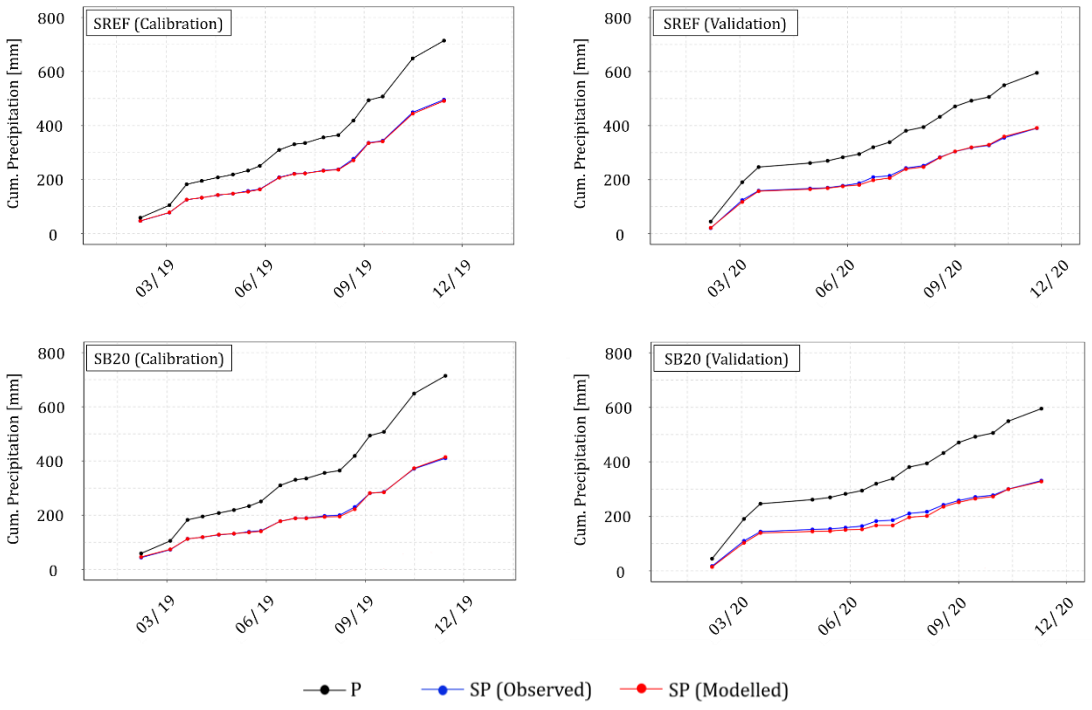

*Figure 32: **Modelled** (red) and **observed** (blue) **cumulated stand precipitation** (SP) as well as cumulated precipitation (P) in SREF and SB20 in the calibration period (01/2019 – 12/2019) and validation period (01/2020 – 10/2020).*

4.1.8 Calibration and validation of soil and evapotranspiration parameters

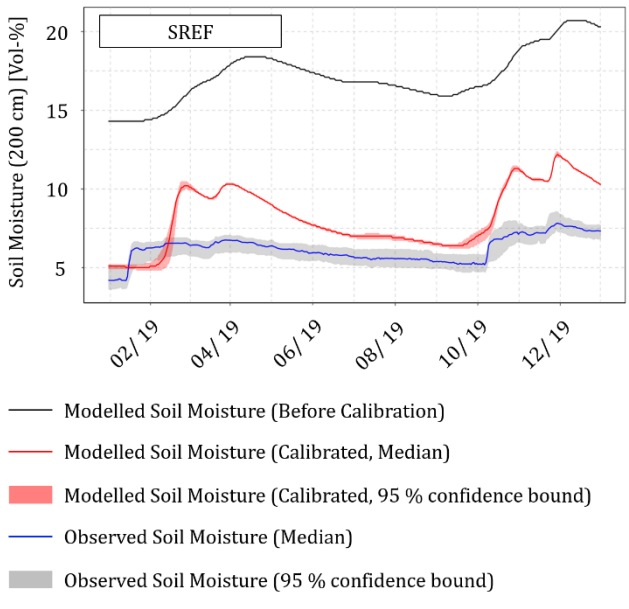

*Figure 33: The **effect of calibrating the empirical MvG parameters** alpha and npar and the saturated hydraulic conductivity (ksat) on the modelled soil moisture in 200 cm depth in SREF. The observed median soil moisture is shown in blue and the corresponding 95 % confidence bound is shown in grey. The modelled soil moisture with original soil hydraulic parameters is shown in black. The modelled soil moisture (median, 95 % confidence bound) is shown in red.*

After successfully calibrating the interception evaporation model parameters, the soil and evapotranspiration model parameters are calibrated with respect to soil moisture in 50 cm and 200 cm depth. First, the empirical MvG parameters alpha, npar and the saturated hydraulic conductivity ksat of the model soil for the study site Sandkrug are calibrated automatically by using the DREAM algorithm (Vrugt et al. 2009). The remaining soil hydraulic parameters saturated water content (ths), residual water content (thr) and the empirical MvG parameters m (mpar) and l (tort) are not calibrated. For ths, thr and mpar, the parameter values resulting from the PTF (Wösten et al. 1999) are used, and tort is set to 0.5 (Ad-hoc-Arbeitsgruppe Boden 1999, Wösten et al. 1999). Table 25 shows the original parameter values of alpha, npar and ksat as derived by the PTF (Wösten et al. 1999), the minimum (Min) and maximum (Max) value defining the respective calibration range, and the median parameter values after calibration. The best fit of the calibrated empirical MvG parameter alpha is close to the minimum of the predefined parameter range. The best fit values of the MvG parameter npar and the saturated hydraulic conductivity (ksat) are located at the maximum of the predefined parameter limits. Figure 33 exemplarily shows the effect of calibrating the empirical MvG parameters alpha and npar as well as the saturated hydraulic conductivity (ksat) on the modelled soil moisture in 200 cm depth in SREF in the calibration period (01/2019 – 12/2019). Before calibrating the soil hydraulic properties, modelled soil moisture is considerably higher than observed soil moisture. After calibrating the soil hydraulic properties, the soil moisture level of modelled and observed soil moisture is in better agreement. Table 26 shows the soil hydraulic parameter values as used for further calibration.

*Table 25: **Original values of the empirical MvG parameters** alpha and npar as well as the saturated hydraulic conductivity (ksat) for the upper (1) and the lower soil layer (2) as derived by the PTF (Original) for the soil in Sandkrug, their calibration range (Min, Max) and the median parameter value after model calibration.*

	Original	Min	Max	Median
alpha1	5.99	5	70	5.09
alpha2	5.05	5	70	9.92
npar1	1.19	1.2	2	1.84
npar2	1.62	1.2	2	2.0
ksat1	1186	-0.5	+0.5	0.49 (3665)
ksat2	739	-0.5	+0.5	0.5 (2337)

Table 68 (appendix) shows the resulting soil file as used for further model calculations.

*Table 26: Depth-specific **soil hydraulic parameters**: Saturated water content (ths), residual water content (thr), empirical MvG parameters (alpha, npar, mpar, tort) and the saturated hydraulic conductivity (ksat) of the soil in Sandkrug. Ths, thr and mpar are derived from the PTF (Wösten et al. 1999) and tort is set to 0.5 (Ad-hoc-Arbeitsgruppe Boden 1999, Wösten et al. 1999). Alpha, npar and ksat are calibrated.*

Depth [m]	ths	thr	alpha	npar	mpar	ksat	tort
Organic layer	0.848	0	98.0	1.19	0.16	98000	0.5
0 – 1.15	0.393	0	5.09	1.84	0.38	3665	0.5
1.15 – 1.65	0.398	0	9.92	2.0	0.35	2337	0.5
1.65 – 3.0	0.393	0	5.09	1.84	0.38	3665	0.5

Table 27 shows the calibration results for the adjusted evapotranspiration and infiltration model parameters *mxkpl*, *psicr*, *infexp* and *ilayer* for SREF and SB20, respectively.

*Table 27: **Calibration results for evapotranspiration and infiltration parameters** in SREF and SB20: Predefined parameter range (Min, Max) and model calibration results (median, 5 % (CI5) and 95 % confidence level (CI95) for the model parameters mxkpl (maximum internal conductivity for water flow through the plants), psicr (critical leaf water potential at which stomates close) and the infiltration parameters infexp and ilayer.*

		mxkpl [mm d^{-1} MPa^{-1}]	psicr [MPa]	infexp [-]	ilayer [-]
SREF	Min	2	-3	0.1	1
	Max	15	-1.5	2	20
	CI5	2.27	-2.97	1.46	11
	Median	3.25	-2.24	1.77	12
	CI95	5.56	-1.5	1.99	13
SB20	Min	2	-3	0.1	1
	Max	15	-1.5	2	20
	CI5	2.0	-1.53	1.77	8
	Median	2.01	-1.51	1.94	9
	CI95	2.04	-1.50	2	10

The calibrated maximum internal conductivity for water flow through the plants (*mxkpl*) is low for SREF and SB20 and ranges between 2 and 5.5 mm d^{-1} MPa^{-1}. Thereby, *mxkpl* is slightly lower in SB20 than in SREF, which reduces the potential transpiration rate in SB20 compared to SREF. The critical leaf water potential at which stomates close (*psicr*) ranges within the entire parameter space in SREF between -1.5 and -3 MPa, and is -1.5 MPa in SB20. Thus, drought stress conditions stop the transpiration flow in SB20 earlier than in SREF. The calibrated infiltration depth (*ilayer*) ranges between the soil layers 11 (90 cm) and 13 (110 cm) in SREF and between 8 (60 cm) and 10 (80 cm) in SB20. The corresponding infiltration distribution within this depth (*infexp*) ranges between 1.46 and 1.99 in SREF and between 1.77 and 2 in SB20. Modelled infiltration is hence slightly deeper in SREF than in SB20 and a major proportion of infiltrating water is directly distributed into deeper soil layers within the infiltration depth in both plots.

Figure 34 shows observed and **modelled soil moisture in 50 cm depth** after model calibration in SREF and SB20 in the calibration period (01/2019 – 12/2019) and validation period (01/2020 – 10/2020). In 50 cm depth, modelled soil moisture is in good agreement with mean observed soil moisture in SREF (NSE = 77.7, MAE = 0.94 Vol-%). In SB20, the modelled soil moisture in 50 cm depth shows a systematic offset in the beginning of the calibration period, with mostly lower soil moisture values than observed. This is reflected by a negative NSE (-129) and a MAE of 1.9 Vol-%. In the second half of the calibration period,

the deviation decreases considerably. The temporal courses of modelled and observed soil moisture in 50 cm agree mostly well in both plots. The timing of soil moisture peaks is well reproduced, however, the magnitude is sometimes too small. The modelled soil moisture decrease in spring and summer is steeper than observed in SREF and slightly less steep than observed in SB20. In the validation period, modelled soil moisture in 50 cm depth mostly agrees with mean observed soil moisture in SREF (NSE = 81.6, MAE = 1.0 Vol-%), showing a slightly higher deviation than in the calibration period. The temporal courses of modelled and observed soil moisture in 50 cm agree well in winter, but show major deviations in summer. Modelled soil moisture decreases faster in spring and summer than in the observations and shows several peaks in summer, which are not present in the observations. Timing and magnitude of soil moisture peaks as well as soil moisture decrease in spring and summer are well reproduced in winter, but less satisfactorily reproduced in summer. In SB20, modelled soil moisture in 50 cm depth is in better agreement with observed soil moisture (NSE = 53.0, MAE = 1.2 Vol-%) than in the calibration period. Modelled soil moisture is slightly too low in winter and slightly too high in summer. The temporal courses of modelled and observed soil moisture in 50 cm agree mostly well: Timing and magnitude of soil moisture peaks and decrease are well reproduced. In general, soil moisture dynamics in 50 cm depth are well reproduced in both plots in the calibration and validation period.

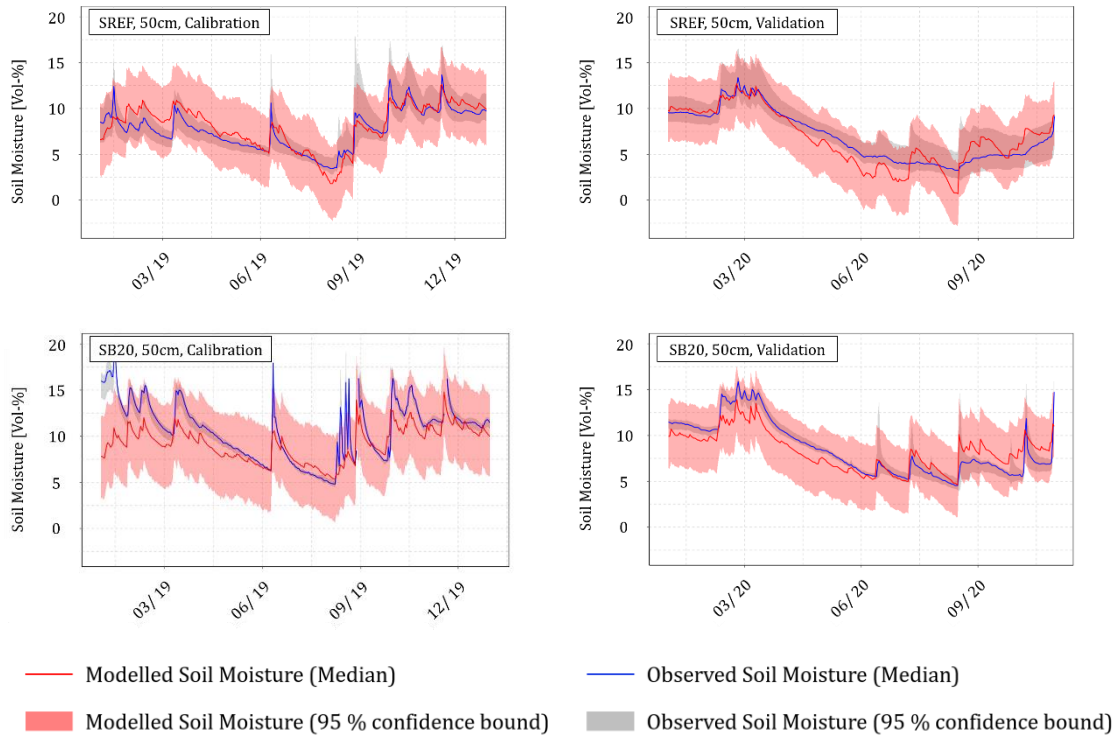

Figure 34: ***Observed and modelled soil moisture in 50 cm depth after model calibration in SREF and SB20*** *in the calibration period (01/2019 – 12/2019) and validation period (01/2020 – 10/2020). Median and 90 % confidence bound of modelled soil moisture are given as solid line and envelope in red, respectively. Median and 90 % confidence bound of observed soil moisture are given as solid line and envelope in blue and grey, respectively.*

Figure 35 shows observed and **modelled soil moisture in 200 cm depth** after model calibration in SREF and SB20 in the calibration period (01/2019 – 12/2019) and validation period (01/2020 – 10/2020). In SREF, modelled soil moisture in 200 cm depth is less well reproduced by the model (NSE = 29.7, MAE = 1.7 Vol-%) than in 50 cm depth. The deviation is especially high in winter, as soil moisture peaks are considerably higher in the model than

in the observations. The temporal course is not satisfactorily represented in the beginning of the calibration period, as the sharp soil moisture increase in January is modelled two months later than observed. In autumn and winter 2019, however, the temporal delay between modelled and observed soil moisture increase in October is considerably smaller. In SB20, observed soil moisture in 200 cm depth is well reproduced by the model (NSE = 60.2. MAE = 1.1 Vol-%). The temporal courses of modelled and observed soil moisture in 200 cm agree mostly well. Timing and magnitude of soil moisture peaks as well as soil moisture decrease in spring and summer are well reproduced. The small observed soil moisture peaks in summer, however, are not reproduced by the model. In the validation period, modelled soil moisture in 200 cm depth in SREF is in better agreement with observations than in the calibration period (NSE = 49.3, MAE = 1.4 Vol-%). Even though the soil moisture level is too high in winter, it is in good agreement with observations in summer. The temporal course is better represented than in the calibration period: The timing of the soil moisture increase in February is in good agreement with observed soil moisture, however, the modelled peak is higher than in the observations. The modelled soil moisture decrease in spring and summer is steeper than in the observations. In SB20, modelled soil moisture in 200 cm depth is systematically lower than observed (NSE = -96.1, MAE = 2.9 Vol-%). The temporal courses of modelled and observed soil moisture in 200 cm agree mostly well. The timing and magnitude of soil moisture peaks as well as the soil moisture decrease in spring and summer are well reproduced. However, the slight soil moisture increase in autumn is not reproduced by the model. In general, soil moisture dynamics in 200 cm depth are well reproduced in both plots in the calibration and validation period.

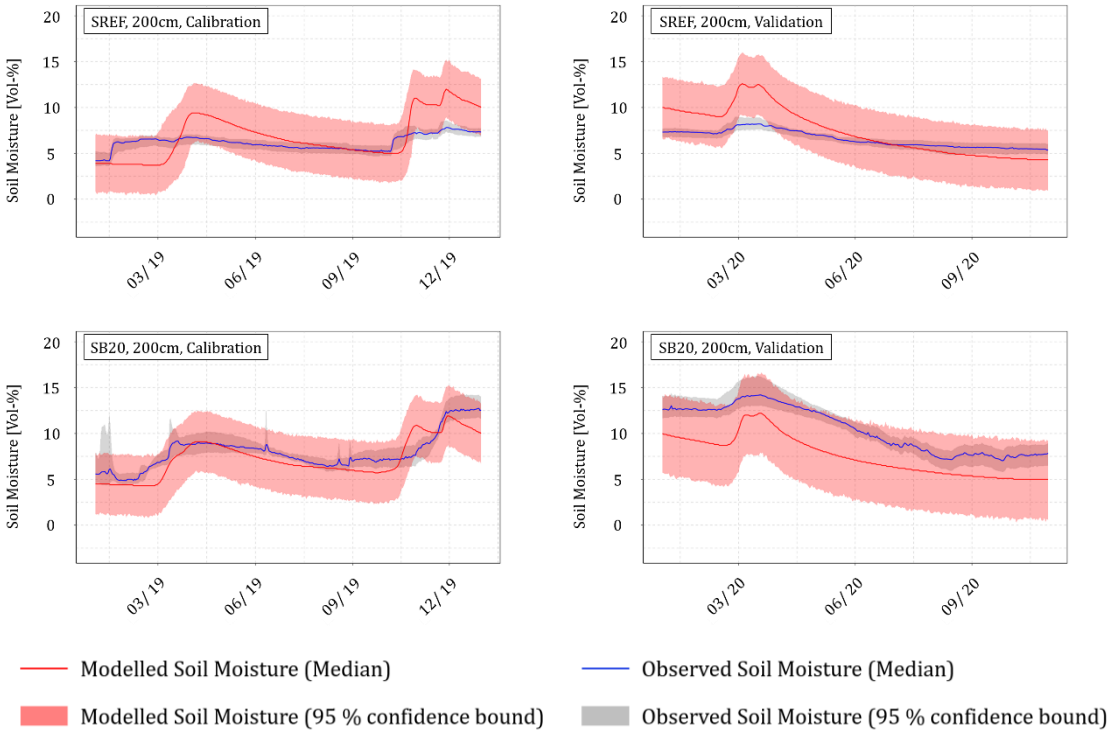

Figure 35: ***Observed and modelled soil moisture in 200 cm depth after model calibration in SREF and SB20*** *in the calibration period (01/2019 – 12/2019) and validation period (01/2020 – 10/2020). Median and 90 % confidence bound of modelled soil moisture are given as solid line and envelope in red, respectively. Median and 90 % confidence bound of observed soil moisture are given as solid line and envelope in blue and grey, respectively.*

4.1.9 Modelled water balance and deep seepage rates

With the successfully calibrated model, all terms of the water balance are calculated for SREF and SB20. Figure 36 shows monthly precipitation (P), interception evaporation (I_T), transpiration (T_T), ground evaporation (E_S) and deep seepage (S_D) sums in the entire calibration and validation period (01/2019 – 10/2020). The water fluxes show a characteristic seasonal course in SREF and SB20: Transpiration is negligible in winter and increases significantly in spring and summer with rising temperatures. Thereby, transpiration rates are higher in SREF than in SB20. Interception is an important process all year round in both plots. Interception sums are especially high in months with high precipitation sums. Ground evaporation only plays a negligible role in both plots in the entire period. The seasonal course of deep seepage is the result of the interplay of precipitation and evapotranspiration: In January and February 2019, deep seepage is negligible as precipitation has not entirely filled the soil water storage yet. In spring 2019, deep seepage occurs in SREF and SB20 as a result of precipitation input and low evapotranspiration rates. In spring 2019, as transpiration rates increase with rising temperatures and increasing solar radiation input, deep seepage rates decrease quickly to a level near zero. In summer 2019, evaporation and transpiration rates are high and deep seepage is only negligible. In autumn 2019, high precipitation sums occur and lead to a sudden increase in deep seepage rates in late autumn. Abundant precipitation and low evapotranspiration rates in winter 2019/2020 cause a continuous deep seepage flow in both plots. With rising evapotranspiration rates and only little

*Figure 36: **Monthly water budgets** in SREF and SB20: Precipitation (P), transpiration (T_T), interception (I_T), soil evaporation (E_S) and deep seepage (S_D) sums in the period 01/2019 – 10/2020.*

precipitation in spring 2020, deep seepage rates decrease quickly and remain negligible in late spring and summer 2020. Until the end of October 2020, deep seepage rates are at a level near zero.

Figure 37 shows median sums of precipitation (P), interception (I_T), stand precipitation (SP), transpiration (T_T), soil evaporation (E_S) and deep seepage (S_D) for SREF and SB20 in the entire modelling period (01/2019 – 10/2020). The precipitation sum is 1467 mm. In SREF, stand precipitation sums up to 1004 mm, which is 68 % of precipitation. The corresponding interception rate is 32 %. In SB20, stand precipitation is 58 % of precipitation and thus 15 % lower than in SREF. Correspondingly, the interception rate in SB20 is 42 % and thus 32 % higher than in SREF. Transpiration accumulates to 559 mm in SREF, which is 38 % of precipitation. Transpiration in SB20 is 27 % of precipitation and thus 29 % lower than in SREF. Soil evaporation is very low in both plots being 2 % of precipitation. The deep seepage sum is 368 mm in SREF, which accounts for 25 % of precipitation. In SB20, deep seepage is at the same level (367 mm).

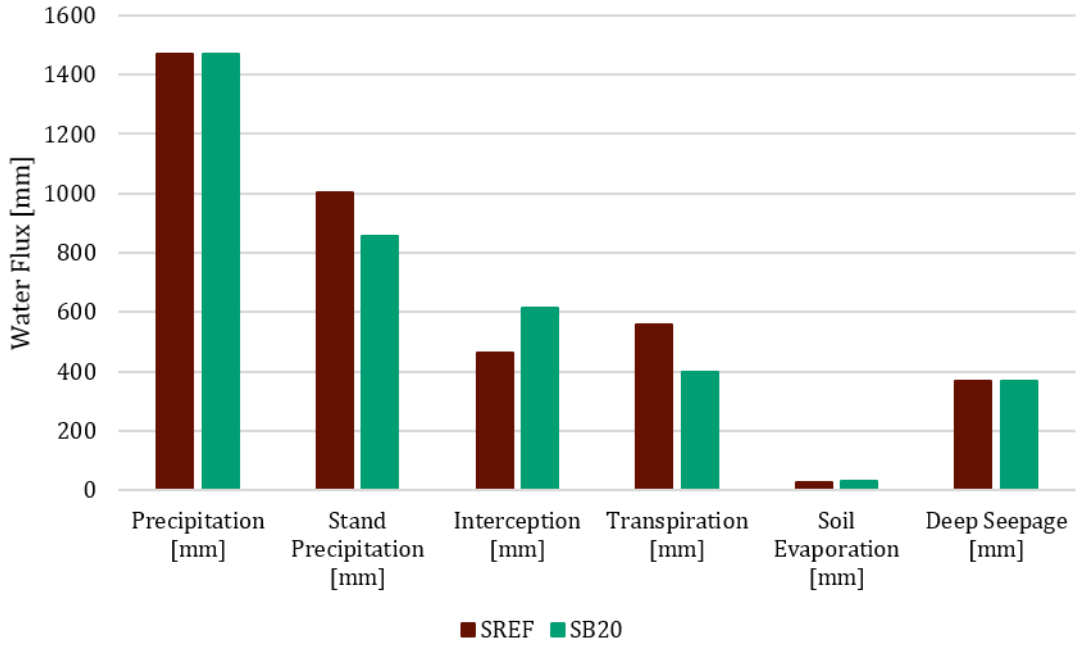

Figure 37: ***Total modelled water fluxes in SREF and SB20:*** *Precipitation (P), transpiration (T_T), interception (I_T), soil evaporation (E_S) and deep seepage (S_D) sums in the period 01/2019 – 10/2020.*

4.2 Elze

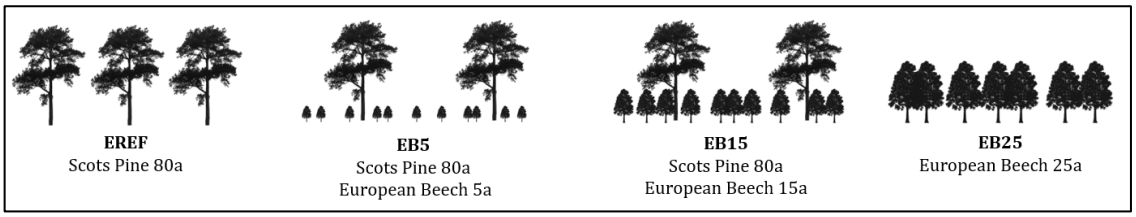

*Figure 38: **Abbreviations** (EREF, EB5, EB15, EB25) used for the investigated forest plots in **Elze**.*

4.2.1 Precipitation measurements

*Table 28: **Precipitation** sums and their deviations from multi-annual mean values in Elze.*

Period	Sum [mm]	Abs. deviation [mm]	Rel. deviation [%]
08/2018 – 12/2018	191.5	-112.5	-37.0
01/2019 – 12/2019	663.7	-37.3	-5.3
01/2020 – 10/2020	509.8	-66.2	-11.5

Precipitation is measured in Elze since August 2018. Table 28 shows measured precipitation sums in Elze between 08/2018 and 10/2020 aggregated for every year and corresponding absolute and relative deviations from mean multi-annual precipitation sums in Elze-Wedemark. Figure 39 shows monthly precipitation sums and their relative deviations from multi annual mean precipitation measured in Elze-Wedemark between 08/2018 and 10/2020. Daily precipitation sums are shown in Figure 68 (appendix). The period between August 2018 and December 2018 was remarkably dry, with a precipitation sum lower than the multi-annual precipitation mean. The precipitation sum in 2019 corresponds to the long-term average. However, precipitation was unevenly distributed throughout the year: Precipitation was mostly below average throughout the year, but was significantly above average in October. The period between January 2020 and October 2020 was slightly drier than multi-annual observations. However, February 2020 was very wet with a precipitation sum exceeding 150 % of the multi annual mean precipitation

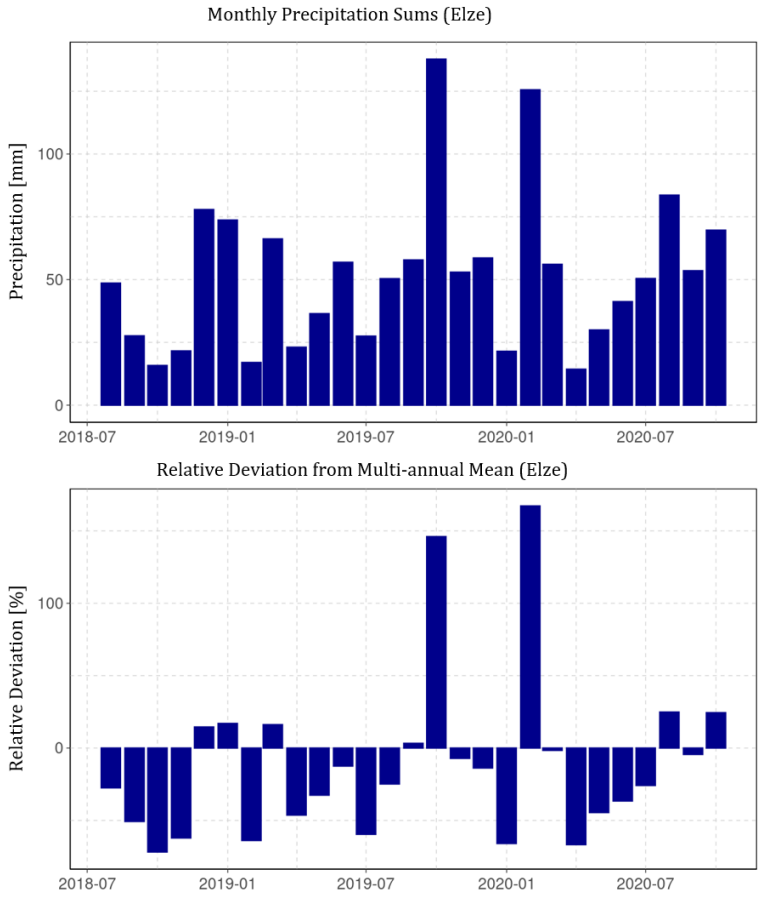

*Figure 39: Measured **monthly precipitation** sums (top) and their relative deviations from mean multi-annual precipitation sums (bottom) in Elze between 08/2018 and 10/2020.*

sum, and precipitation in August and September was also above average. Overall precipitation was below average between 08/2018 and 10/2020, with seven months not even reaching 50 % of the mean precipitation.

4.2.2 Soil measurements

*Table 29: Depth-specific **soil textures** in Elze derived from grain size distribution analysis (Ss = pure sand, Su2 = slightly silty sand, Su3 = medium silty sand).*

Depth	EREF	EB5	EB15	EB25
0-10	Su3	Su2	Su3	Su2
10-20	Su3	Su3	Su2	Su2
20-30	Su3	Su3	Su2	Su2
30-40	Su3	Su3	Su2	Su2
40-50	Su3	Su2	Su2	Su2
50-60	Su3	Su2	Su2	Su2
60-70	Su3	Ss	Su2	Su2
70-80	Su2	Ss	Su2	Su2
80-90	Su2	Ss	Ss	Su2
90-100	Ss	Ss	Ss	Su2
100-110	Ss	Ss	Ss	Su2
110-120	Ss	Ss	Ss	Su2
120-130	Ss	Ss	Ss	Su2
130-140	Ss	Ss	Ss	Su2
140-150	Ss	Ss	Ss	Su2
150-160	Ss	Ss	Ss	Su2
160-170	Ss	Ss	Ss	Ss
170-180	Ss	Ss	Ss	Ss
180-190	Ss	Ss	Ss	Ss
190-200	Ss	Ss	Ss	Ss

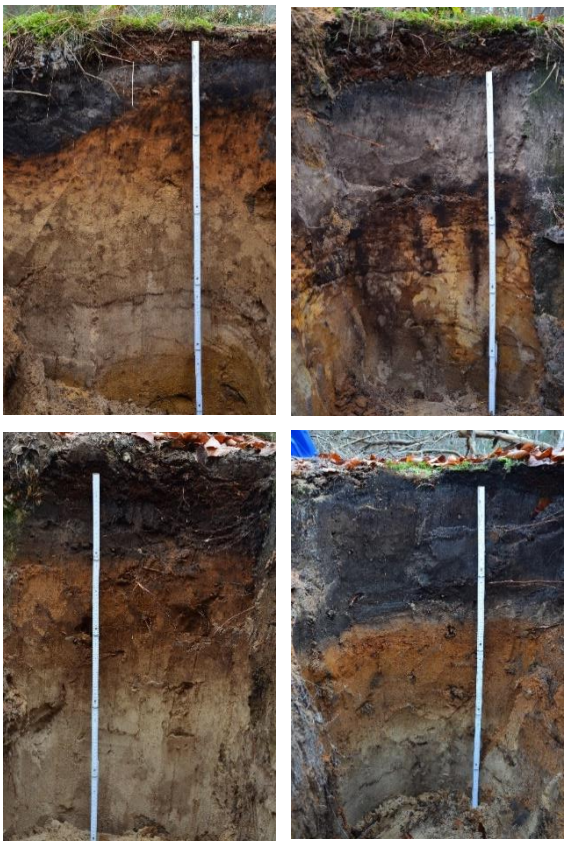

*Figure 40: **Soil profiles** in E REF (upper left), E B5 (upper right), E B15 (lower left), E B25 (lower right) down to a depth of 100 cm.*

The observation plots in Elze (Figure 40) are located on a deep Podzol-Regosol (NIBIS Kartenserver 2014a). In the past, this area was not only used for forestry, but also for grazing and agriculture. Historic maps from the late 19th century show that this area was heathland at that time (Nibis Kartenserver 2014b). Due to these changes in land use, windthrow and forest management activities such as scarification and subsoiling, the top soil layer is partly altered and disturbed. The humus layer is approximately 8 cm thick. The mineral soil horizons differ in their thickness among the forest plots. In E REF, the Ae horizon is only a few centimeters thick and partly disturbed. The transition zone from the Bs horizon to the C horizon is approximately in 40 cm depth. In E B5, the Ae horizon is considerably thicker (30 cm) than in E REF. The Bs horizon below is partly crusted due to the accumulation of iron oxides and has an irregular shaped transition zone to the C horizon below. In E B15, a considerably thick Ah horizon can be found instead of the Ae horizon. The horizon boundaries can be found in 20 cm (Ah/Bs) and in 60 cm (Bs/C). In E B25, the illuviation horizon is 30 cm thick, homogeneous due to ploughing and rich in organic material (Aeh). The Bs horizon can be found between 30 cm and 70 cm depth. All four observation plots are groundwater distant, the groundwater table is approximately 5 m below the surface (NIBIS Kartenserver 2014c).

The results of the grain size distribution analysis in EREF, EB5, EB15 and EB25 are summarized in Table 29. Corresponding detailed information about sand, silt and clay content

(Figure 69) as well as gravel content (Table 58), bulk density (Table 59) and organic carbon content (Table 60) analyses are provided in the appendix.

In Elze, the predominantly occurring soil materials are pure sand (Ss) in lower soil layers, and slightly (Su2) and medium silty sand (Su3) in the upper soil layers. The sand fraction is dominated by fine and medium sand at all plots, coarse sand fractions are generally low and increase with soil depth. The soil in E B15 contains the highest proportion of coarse sand material. The silt fraction is slightly different at the observation plots. Significant silt amounts of up to 20 % are present in the upper soil layers above 100 cm (E REF), 80 cm (E B15) and 40 cm depth (E B5). Higher silt contents of up to 30 % are present in the uppermost soil layers in EREF. In E B25, significant silt amounts are present in almost the entire soil column. Gravel and clay amounts are generally low and account for less than 5 % at all plots.

For each plot, soil layers with similar soil properties were combined into a total of two soil layers with weighed mean soil properties. These simplified plot-specific soils are then aggregated to one site-specific soil for Elze (Table 62, appendix) by calculating the average of the plot-specific soil properties. This site-specific soil is used as model soil for the site Elze.

4.2.3 Phenology & Plant Area Index measurements

Based on regular LAI measurements and phenological observations, the development of the tree canopy is monitored.

Table 30: ***Time periods of leaf unfolding and leaf fall of European beech*** *in EB15 and EB25 in 2019 and 2020 based on observations (time interval: 2 to 4 weeks).*

	leaf unfolding 2019	leaf fall 2019	leaf unfolding 2020	leaf fall 2020
Date	29.04.2019 – 28.05.2019	02.10.2019 – 04.12.2019	15.04.2020 – 14.05.2020	25.08.2020 – 15.12.2020
DOY	120 - 150	275 - 340	105 - 135	235 - 350

Table 30 gives approximations of bud burst dates, leaf unfolding periods, leaf fall start dates and leaf shedding periods for beech in EB15 and EB25 based on in situ observations every two to four weeks. In 2019, the bud burst date of beech is in the end of April and leaves unfold until the end of May. Leaves start to fall in the beginning of October. The leaf fall period ends in the beginning of December 2019. In 2020, the bud burst date of beech is already in mid-April and thus two weeks earlier than in 2019. The corresponding leaf unfolding period lasts until mid-May. Pronounced drought stress during summer causes the beech to partly drop its leaves already in August 2020. Some rain in the end of August alleviates the drought and the early leaf fall is stopped. The remaining leaves then start to fall in mid-October until the majority of leaves has fallen off in mid-December 2020. In E B25, a small proportion of brown leaves remained at the trees during winter 2020/2021.

Table 55 (appendix) shows measured LAI values for beech in EB15 and EB25 based on litter fall sampling in summer and autumn 2020. Approximately 15 % (EB25) and 40 % (EB15) of the leaves have already fallen off in late summer 2020 due to drought conditions, reducing the beech LAI from 5.19 to 4.43 in EB25 and from 3.35 to 1.98 in EB15. From mid-October to the end of November, beech LAI is further reduced to approximately zero in both plots. Table 57 (appendix) shows total LAI values of both pine and beech for EB15 in summer and autumn 2020. Table 56 (appendix) then gives final LAI and SAI values for EREF, EB5, EB15 and EB25 in the period 2019 – 2020. Figure 41 shows these measured LAI and

SAI as sum (LAI + SAI = PAI) in 2019 and 2020. PAI values differ substantially between pine, beech and mixed stands. In summer 2019, PAI values are at a comparable level in EREF (2.6) and EB5 (2.8). In EB25 and EB15, PAI values are considerably higher with 5.4 and 6.3, respectively. In winter 2019/2020, when the beech has shed its leaves, PAI values range from 0.5 (EB25) to 3.6 (EREF), with EB15 (3.0) and EB5 (3.4) in between. In summer 2020, PAI values are again the highest in EB15 (6.3) and EB25 (5.7), and considerably lower in EREF (4.9) and EB5 (4.2). In winter 2020/2021, the measurements confirm the order in PAI values from the former winter, with the highest PAI in EREF (4.0) and the lowest PAI in EB25 (0.7), with EB5 (3.6) and EB15 (3.0) in between.

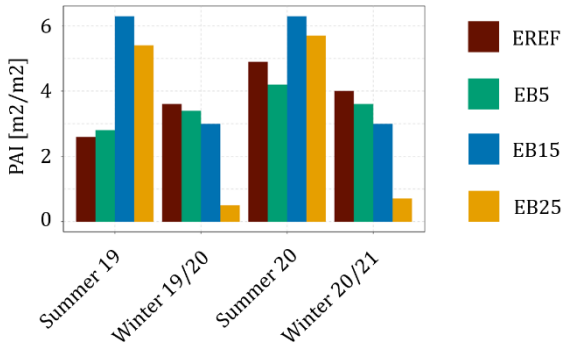

Figure 41: ***Total PAI*** *(LAI + SAI) in EREF (Scots Pine) and EB5, EB15 and EB25 (Scots Pine, European Beech). The minimum (winter) and (maximum) PAI are given for 2019 and 2020.*

The order is mostly consistent over time: In summer, PAI is highest in EB15 and EB25 and considerably lower in EREF and EB5. In winter, PAI is highest in EREF, EB5 and EB15 and considerably lower in EB25. This is the result of the seasonal course of the beech trees in EB15 and EB25. The PAI value in EREF is higher than in EB5 most of the time, which is not true for summer 2019. However, the difference between EREF and EB5 is only small.

4.2.4 Stand precipitation measurements

The total number of measured stand precipitation sums is 7 in EB5, 9 in EB15 and EB25 and 10 in EREF in 2019. In 2020, the number of measured stand precipitation sums is 5 in EB5, 10 in EB15 and 11 in EREF and EB25. Technical problems led to some measurement errors in EB5, which causes a comparably small sample size. Therefore, interception rates are in a first step only analyzed for EREF, EB15 and EB25 based on those dates where data were simultaneously available for EREF, EB15 and EB25 (see Table 31, Figure 42). Second, interception rates are analyzed for EB5 and compared to EREF, EB15 and B25 based on those measurements dates where data were available for all plots (see Table 31, Figure 43). Detailed stand precipitation and interception data are provided in Table 65 (appendix).

Figure 42 shows average interception loss values in EREF, EB15 and EB25. Interception values are aggregated for summer 2019 (n = 5), winter 2019/2020 (n = 4), summer 2020 (n = 5) and the periods 01/2019 – 12/2019 (n = 8) and 01/2020 – 10/2020 (n = 10). Thereby, summer is defined as period between 01/05 and 30/09, and winter is defined as period between 01/12 and 30/04.

Table 31: ***Interception measurement dates*** *for which data are simultaneously available either for EREF, EB15 and EB25 (left column) and simultaneously available for EREF, EB5, EB15 and EB25 (right column). Measurement dates are classified into summer and winter.*

EREF, EB15, EB25		EREF, EB5, EB15, EB25	
2019	2020	2019	2020
2019-05-15 (summer)	2020-01-09 (winter)	2019-05-15 (summer)	2020-04-07 (winter)
2019-07-16 (summer)	2020-02-19 (winter)	2019-07-16 (summer)	2020-05-14 (summer)
2019-08-01 (summer)	2020-04-07 (winter)	2019-08-01 (summer)	2020-06-30 (summer)
2019-09-10 (summer)	2020-05-14 (summer)	2019-09-10 (summer)	2020-10-08
2019-09-26 (summer)	2020-06-30 (summer)	2019-09-26 (summer)	
2019-10-02	2020-07-30 (summer)	2019-12-03 (winter)	
2019-11-12	2020-08-25 (summer)		
2019-12-03 (winter)	2020-09-17 (summer)		
	2020-10-08		
	2020-11-11		

Measured stand precipitation sums are highest in EB25 and considerably lower in EREF and EB15. Correspondingly, interception losses in EB25 are lower than in EREF and EB15: Mean interception losses are 18 % in EB25 and 28 % in EB15 and EREF in 2019. In 2020, mean interception losses are 11 % in EB25, 25 % in EB15 and 26 % in EREF. In summer 2019, interception in EB25 (21 %) is considerably lower than in EB15 (31 %) and EREF (31 %). In winter 2019/2020, this difference between EB25 on the one hand and EB15 and EREF increases because the beech trees in EB25 shed their leaves. Additionally, the interception rate in EB15 (29 %) is considerably lower than in EREF (35 %) due to leaf fall. In summer 2020, the interception rate in EB25 increases with leaf unfolding and leaf growth to 14 %, which is still considerably lower than in EB15 (26 %) and EREF (24 %).

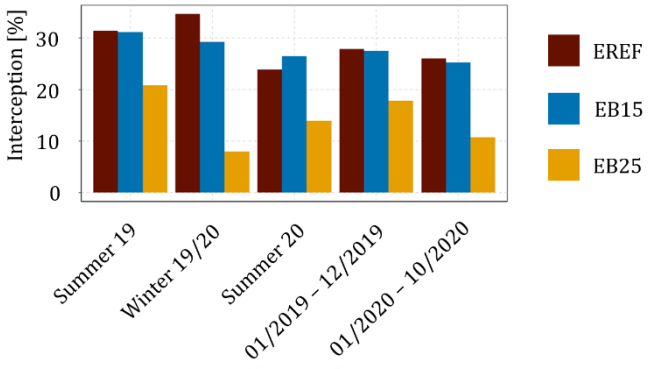

Figure 42: ***Mean interception*** *rates in EREF, EB15 and EB25 in summer 2019 (n = 5), winter 2019/2020 (n = 4), summer 2020 (n = 5), and the periods 01/2019-12/2019 (n = 8) and 01/2020-10/2020 (n = 10).*

Figure 43 shows average interception loss values in EREF, EB5, EB15 and EB25. Interception values are aggregated for summer 2019 (n = 5), winter 2019/2020 (n = 2), summer 2020 (n = 2) and the periods 01/2019 – 12/2019 (n = 6) and 01/2020 – 10/2020 (n = 4). Due to only few available data points, the following analysis only gives an approximate estimate on how interception rates of EB5 fits into the range of interception rates of EREF, EB15 and EB25.

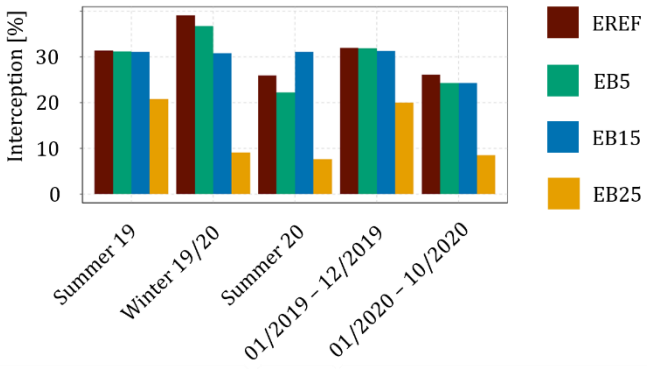

*Figure 43: **Mean interception** rates in EREF, EB5, EB15 and EB25 in summer 2019 (n = 5), winter 2019/2020 (n = 2), summer 2020 (n = 2), and the periods 01/2019-12/2019 (n = 6) and 01/2020-10/2020 (n = 4).*

In summer 2019, the interception rate of EB5 is at the same level as interception rates in EREF and EB15. In winter 2019/2020, the interception rate of EB5 is between those of EREF and EB15. In summer 2020, the interception rate of EB5 is lower than in EREF. Compared to EREF, the interception rate of EB5 is slightly lower all year round. Compared to EB15, the interception rate in EB5 is slightly lower in summer and slightly higher in winter. However, considering interception measurements of single dates reveal that interception rates in EB5 are sometimes higher and sometimes lower than in EREF (see Table 65 in the appendix).

4.2.5 Soil moisture measurements

Figure 44 shows mean daily soil moisture values in 50 cm and 200 cm depth in EREF, EB5, EB15 and EB25 as well as daily precipitation sums between January 2019 and October 2020. The corresponding soil moisture profiles of the single soil moisture sensors are provided in Figure 70 in the appendix.

The soil moisture level of all plots is mostly comparable in 50 cm depth. In 200 cm depth, the soil moisture level is most of the time highest in EB25 and lowest in EB15. In summer 2020, however, the soil moisture level in EB5 is higher than in EB25.

The soil moisture shows a characteristic course that partially differs among the plots. In 50 cm depth, the soil moisture course is similar in all plots: In winter 2018/2019, soil moisture was comparably high, with soil moisture values between 10 % and 12 %. Precipitation events caused small soil moisture peaks in this period. In spring and summer 2019, the soil moisture decreased to a low soil moisture level between 4 % and 6 % due to evapotranspiration of the vegetation. In EB25, soil moisture started to decrease later than in EREF, EB5 and EB15, because the beech leaves unfold later in spring. Thus, water consumption through evapotranspiration starts earlier in plots with evergreen pine and cause the soil moisture to drop earlier than in EB25. During summer, scattered precipitation events caused small soil moisture peaks in almost all plots, except for EB5. In EB25, these soil moisture peaks occur more frequently than in the other plots. In October, the soil moisture sustainably increased to a higher level between 10 % and 12 % due to abundant rainfall and remained on this level during the winter 2019/2020. Technical problems caused fluctuations in soil moisture values in November and eventually data loss in December and January in EREF, EB15 and EB25. Heavy rain caused pronounced soil moisture peaks between 12 % and 14 % in February 2020 in all plots. From March 2020 onwards, the soil moisture decreased continuously to a level between 4 % and 6 % and remained at this low level until August 2020. In this period, there are no significant differences between the forest plots. Abundant rain fall

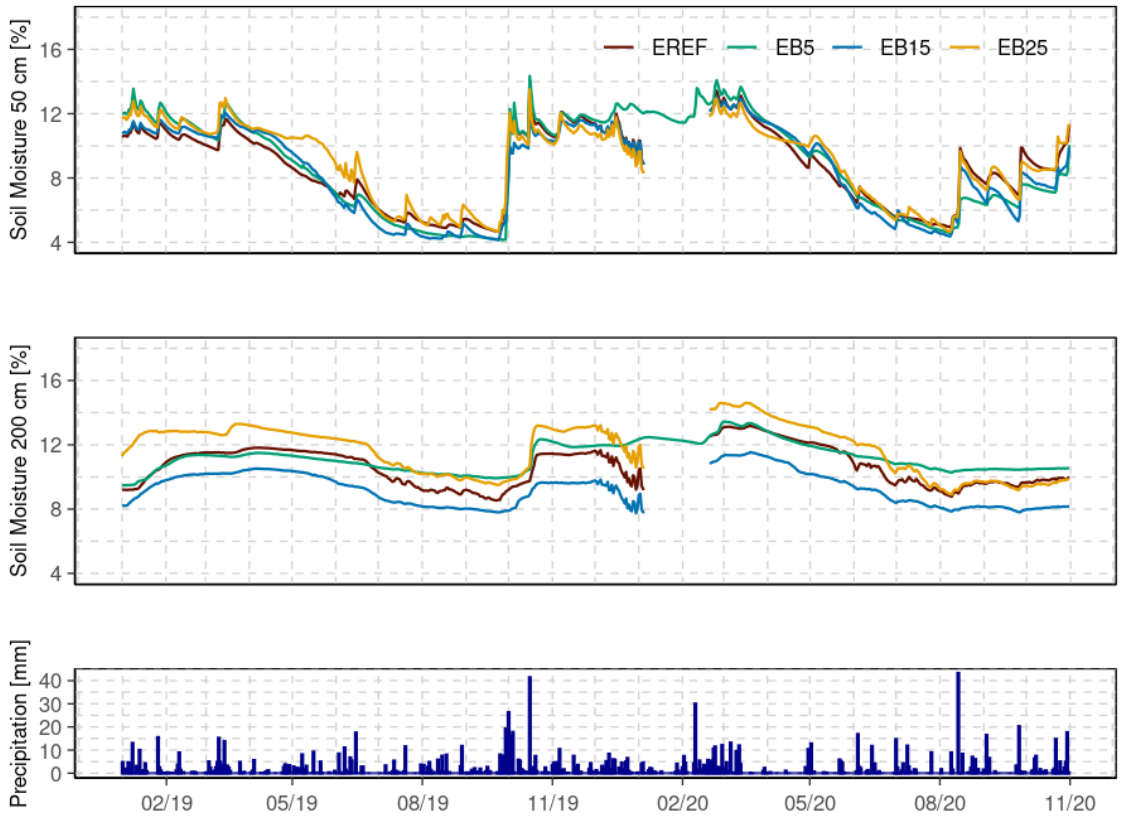

Figure 44: ***Soil moisture*** *observations (daily mean from 8 sensors) in 50 cm (top) and 200 cm depth (middle) as well as daily precipitation sums (bottom) in Elze.*

with almost 50 mm within one day caused a considerable soil moisture peak in all plots, with a less pronounced peak in EB5 than in the other plots. Until the end of the observation period, the soil moisture fluctuates between 6 % and 10 % in all plots due to occasional rain events. However, the increase in soil moisture in autumn 2020 is not as sharp as in autumn 2019.

In 200 cm depth, the soil moisture courses of all plots are to some extent different. In winter 2018/2019, soil moisture is already quite high in EB25 (11% - 12 %) and below 10 % in EREF, EB5 and EB15. In the beginning of January 2019, soil moisture increases sustainably in EB15 to 10 % and in mid-January also in EREF and EB5 to approximately 12 %. In spring and summer 2019, soil moisture decreases in all plots successively to 8 % in EB15, 9 % in EREF and 10 % in EB5 and EB25. In the end of June, soil moisture suddenly drops in EREF, EB15 and EB25, while soil moisture decrease remains linear in EB5. Abundant rain fall in August and September caused a slight increase in soil moisture in all plots. This increase intensifies with abundant precipitation in autumn 2019. From then on, soil moisture values remain at a comparably high level in winter (10 % in EB15, 12 % in EREF and EB5, and 13 % in EB25). Technical problems caused fluctuations in soil moisture values in November and eventually data loss in December and January in EREF, EB15 and EB25. In February 2020, soil moisture increased even more to 11 % in EB15, 13 % in EB5 and EREF and 15 % in EB25. In spring and summer 2020, soil moisture decreased successively to a level of 8 % in EB15 and 10 % in EB5 without any major peaks until the end of the observation period.

For statistical analyses, descriptive statistical measures are calculated for mean daily soil moisture values of 8 soil moisture sensors per plot in the observation period between 01/2019 and 10/2020: Mean 5 % confidence level (CI5), median, mean 95 % confidence

level (CI95), mean 90% interquartile range (IQR90), mean standard deviation (SDEV), minimum (Min), maximum (Max) and mean range between lowest and highest daily soil moisture value of all sensors (range). Table 32 show these descriptive statistical measures of the soil moisture in 50 cm and 200 cm depth.

The soil moisture level is similar for all plots in 50 cm depth. In 200 cm depth, the soil moisture level decreases from EB25 to EB5 to EREF to EB15. For all plots, the soil moisture level and variability in 50 cm depth are slightly lower than in 200 cm depth. Soil moisture variability in 50 cm depth is highest in EB5 and lowest in EREF and EB25. Soil moisture values range between 3.1 % and 27.4 % in EB5, between 3.3 % and 27.0 % in EB15, between 3.6 % and 23.1 % in EREF and between 4.1 % and 21.5 % in EB25. In 200 cm depth, soil moisture variability is highest in EB5 and lowest in EB25. In this depth, soil moisture values range between 5.1 % and 15.0 % in EB15, between 5.3 % and 19.6 % in EREF, between 5.4 % and 18.7 % in EB25 and between 6.1 % and 19.9 % in EB5.

*Table 32: **Statistical measures** calculated from daily mean **soil moisture** values of the 8 soil moisture sensors in **50 cm and 200 cm depth** between 01/2019 and 10/2020: Mean 5 % confidence level (CI5), median, mean 95 % confidence level (CI95), mean 90% interquartile range between CI5 and CI95 (IQR90), mean standard deviation (SDEV), minimum (Min), maximum (Max) and mean range between lowest and highest daily soil moisture value of all sensors (range).*

	CI5 [Vol-%]	Median [Vol-%]	CI95 [Vol-%]	IQR95 [Vol-%]	SDEV [Vol-%]	Min [Vol-%]	Max [Vol-%]	Range [Vol-%]
				50 cm depth				
E REF	7.8	8.5	9.3	1.5	1.0	3.6	23.1	3.0
E B5	7.5	8.6	10.4	2.8	2.1	3.1	27.4	6.2
E B15	7.3	8.2	9.3	1.9	1.4	3.3	27.0	4.0
E B25	8.2	8.7	9.6	1.4	1.0	4.1	21.5	3.0
				200 cm depth				
E REF	9.1	10.3	12.3	3.3	2.4	5.3	19.6	6.9
E B5	8.9	11.0	13.5	4.6	3.3	6.1	19.9	10.5
E B15	8.1	9.0	10.5	2.5	1.8	5.1	15.0	5.1
E B25	10.3	11.8	13.0	2.7	2.0	5.4	18.7	5.7

4.2.6 Sensitivity analysis

Table 33: NSE values at the 99.5 % confidence level separating behavioural from non-behavioural model runs.

	E REF	E B5	E B15	E B25
stand precipitation	0.995	0.969	0.987	0.995
soil moisture (50 cm)	0.843	0.837	0.857	0.700
soil moisture (200 cm)	0.029	0.374	0.210	0.483

The sensitivity analysis reveals the importance of individual model parameters for model performance with regard to stand precipitation and soil moisture in 50 cm and 200 cm depth in Elze. The threshold between behavioural and non-behavioural model runs is set to the 99.5% confidence level. Corresponding NSE values are given in Table 33. Figure 45 shows insensitive parameters in white, moderately sensitive parameters in orange and highly sensitive parameters in red.

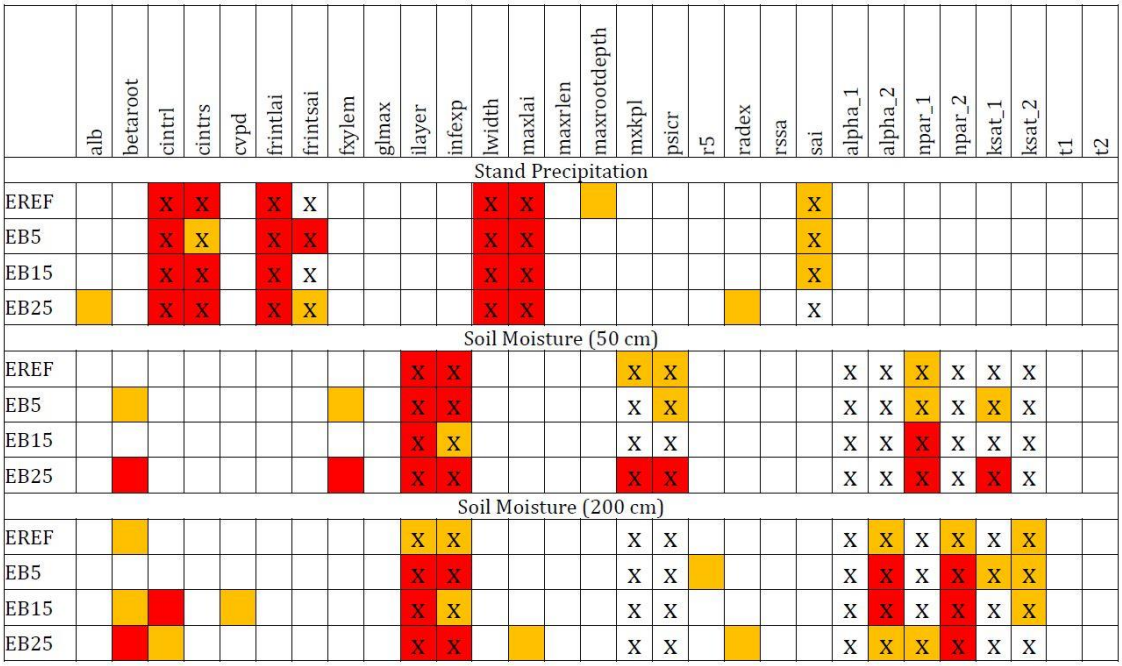

*Figure 45: **Results of the sensitivity analysis** with regard to stand precipitation, soil moisture (50 cm) and soil moisture (200 cm) in Elze. Highly important parameters are shown in red, moderately important parameters are shown in orange and unimportant parameters are shown in white. Model parameters selected for model calibration with respect to stand precipitation, soil moisture in 50 cm and 200 cm depth are marked with an X.*

In EREF, EB5, EB15 and EB25, those **model parameters that control interception evaporation** are sensitive with respect to observed stand precipitation. The leaf interception storage per unit LAI (*cintrl*) and SAI (*cintrs*), the fraction of rain intercepted per unit LAI (*frintlai*), leaf width (*lwidth*) and maximum LAI (*maxlai*) are highly important for most of the plots. The fraction of rain intercepted per unit SAI (*frintsai*) and stem area index (*sai*) are moderately important for most of the plots. As described in the sensitivity analysis results for Sandkrug, the model parameters *cintrl*, *cintrs*, *frintlai*, *frintsai*, *lwidth*, *maxlai* and *sai* are calibrated with respect to stand precipitation.

Soil moisture in 50 cm depth is mostly affected by soil and evapotranspiration parameters in EREF, EB5, EB15 and EB25. The MvG parameters *npar* and *ksat* affect soil water movement and soil water content and are moderately to highly important. Maximum depth (*ilayer*) and vertical distribution with depth (*infexp*) of macro pore-assisted infiltrating wa-

ter are also highly important model parameters. The remaining important parameters control soil water removal through evapotranspiration (*betaroot*, *fxylem*, *mxkpl*, *psicr*). For **soil moisture in 200 cm depth**, parameters affecting vertical soil water movement are most important: *Betaroot*, *ilayer*, *infexp*, *alpha*, *npar* and *ksat* are highly important at most of the plots. Other evapotranspiration parameters are of less importance for soil moisture in 200 cm depth. Therefore, the MvG parameters *alpha*, *npar* and *ksat*, as well as *mxkpl*, *psicr*, *infexp* and *ilayer* are included in model calibration with respect to soil moisture in 50 cm and 200 cm depth. Even though betaroot is a sensitive parameter, it is set to a fixed value according to Jackson et al. (1996).

As in Sandkrug, parameters found having an overall negligible effect on modelled stand precipitation and soil moisture are *alb*, *cvpd*, *glmax*, *maxrlen*, *maxrootdepth*, *r5*, *radex*, *rssa*, *t1* and *t2.* These parameters are fixed to literature values according to Federer (2019) and Jackson et al. (1996) (see Table 34). For EB15, weighed mean values of conifers and broadleaves based on the specific stand basal area of both species are used.

Table 34: ***Fixed model parameter values*** *based on literature values (Federer 2019) of parameters being identified as unimportant in the sensitivity analysis. For EB15, parameter values are weighed mean values based on the specific stand basal area of Scots pine and European beech.*

	alb [-]	cvpd [kPa]	fxylem [-]	glmax [m s^{-1}]	maxrlen [m m^{-2}]	maxrootdepth [m]	r5 [W m^{-2}]	radex [-]	rssa [s m^{-1}]	t1 [°C]	t2 [°C]	betaroot [-]
EREF	0.14	2	0.5	0.0053	3000	-2.5	100	0.5	100	10	30	0.976
EB5	0.14	2	0.5	0.0053	3000	-2.5	100	0.5	100	10	30	0.976
EB15	0.146	2	0.5	0.0053	3000	-2.5	100	0.516	100	10	30	0.974
EB25	0.18	2	0.5	0.0053	3000	-2.5	100	0.6	100	10	30	0.966

4.2.7 Calibration and validation of interception evaporation parameters

Model interception parameters are manually adjusted in a way that storage capacities range between 1 and 2 mm in EREF and EB5, between 0.5 and 2 mm in EB15 and between 0.5 mm and 1 mm in EB25. Initially, modelled stand precipitation is initially too low at all plots. To increase modelled stand precipitation, the storage capacity and canopy cover would have been needed to be set to unrealistically low values. In order to maintain realistic interception storages and canopy cover properties, interception evaporation is reduced by increasing *lwidth* from 0.004 m to 0.05 m in the Scots pine stands EREF and EB5. For the pure beech stand EB25, *lwidth* = 0.1 m yielded a reliable result and *lwidth* is set to 0.08 m for EB15. With *lwidth* adjusted, stand precipitation is still too low at all plots. Reducing the fraction of rain that is intercepted by vegetation surfaces per unit LAI (*frintlai*) and SAI (*frintsai*) to 10 % improved overall model performance in all plots. Then, *maxlai* is adjusted to finely tune stand precipitation. *Maxlai* is changed from 3.1 to 2.8 in EREF and from 2.9 to 3.2 in EB5 to reproduce slightly higher interception rates in EB5 compared to EREF. In EB15, interception rates are generally too high and thus the interception storage capacity per unit LAI (*cintrl*) and SAI (*cintrs*) is reduced to 0.1 mm. Interception rates are nevertheless still too high in summer, thus, *maxlai* is reduced to 5 in summer. In EB25, interception rates are too high and thus the storage capacity per unit LAI (*cintrl*) and SAI (*cintrs*) is reduced to 0.05 mm. SAI is increased from 0.5 to 1.0 to account for dead leaves remaining at the tree in winter, which yields a good fit in winter. *Maxlai* is reduced from 5.2 to 4 to yield appropriate

stand precipitation in summer. The resulting storage capacity of 0.25 mm in EB25 is lower than literature values, however, it seems realistic as the beech trees are comparably small and young. The resulting parameter values from calibrating stand precipitation and the corresponding modelled interception storage capacities for each plot are given in Table 35. Figure 46 shows the seasonal PAI course between 01/2019 and 10/2020 after model calibration.

Table 35: ***Calibrated interception parameter values*** *from calibrating stand precipitation and the associated modelled interception storage in EREF, EB5, EB15 and EB25.*

		cintrl [mm]	cintrs [mm]	frintlai [-]	frintsai [-]	lwidth [m]	maxlai [m² m⁻²]	minlai [m² m⁻²]	sai [m² m⁻²]	storage capacity [mm]
EREF	Min	0.05	0.05	0.1	0.1	0.004	2.3	2.3	0.4	1.0
	Max	0.75	0.75	0.2	0.2	0.1	3.9	3.9	0.6	2.0
	Best Fit	**0.3**	**0.3**	**0.1**	**0.1**	**0.05**	**2.8**	**2.8**	**0.5**	**0.99**
EB5	Min	0.05	0.05	0.1	0.1	0.004	2.2	2.2	0.4	1.0
	Max	0.75	0.75	0.2	0.2	0.1	3.6	3.6	0.6	2.0
	Best Fit	**0.3**	**0.3**	**0.1**	**0.1**	**0.05**	**3.2**	**3.2**	**0.5**	**1.11**
EB15	Min	0.05	0.05	0.1	0.1	0.004	4.4	2.2	0.4	0.5
	Max	0.75	0.75	0.2	0.2	0.1	7.3	3.7	0.6	2.0
	Best Fit	**0.1**	**0.1**	**0.1**	**0.1**	**0.08**	**5.0**	**2.5**	**0.5**	**0.55**
EB25	Min	0.05	0.05	0.1	0.1	0.004	3.9	0	0.4	0.5
	Max	0.75	0.75	0.2	0.2	0.1	6.5	0	0.6	1.0
	Best Fit	**0.05**	**0.05**	**0.1**	**0.1**	**0.1**	**4.0**	**0**	**1.0**	**0.25**

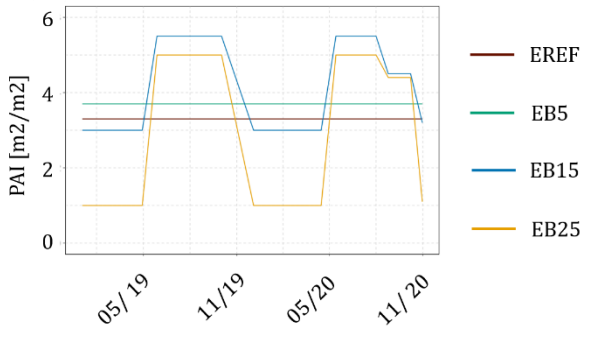

Figure 46: ***Course of the PAI*** *in the model after calibration of model interception parameters in Elze between 01/2019 and 10/2020.*

Figure 47 shows modelled and observed stand precipitation sums after model calibration for EREF, EB5, EB15 and EB25 in the calibration and validation period. Table 36 shows observed and modelled stand precipitation sums, interception rates and error measures for EREF, EB5, EB15 and EB25 in the calibration and validation period.

The model reproduces measured stand precipitation well in EREF, EB5, EB15 and EB25 in the **calibration period**. Corresponding error measures show an NSE close to 100 and a low MAE with values less than 2 mm. Thereby, the model reproduces reliably decreasing interception rates as observed from EB5 to EREF to EB15 to EB25. Seasonal variations in interception rates in EB15 and EB25 with higher interception rates in summer than in winter are also well reproduced by the model. In the **validation period**, the model also reproduces modelled stand precipitation well. The deviation between modelled and observed stand precipitation is slightly higher than in the calibration period, which is reflected in slightly higher MAE and lower NSE values. Measured and modelled stand precipitation sums and interception rates are in

good agreement for all plots showing only minor deviations: Modelled interception rates are slightly higher than observed in EB5 and EB25. As in the calibration period, the model is able to reproduce different interception rates in EREF, EB5, EB15 and EB25, as well as the seasonal variation in interception loss due to leaf fall and leaf unfolding in EB15 and EB25.

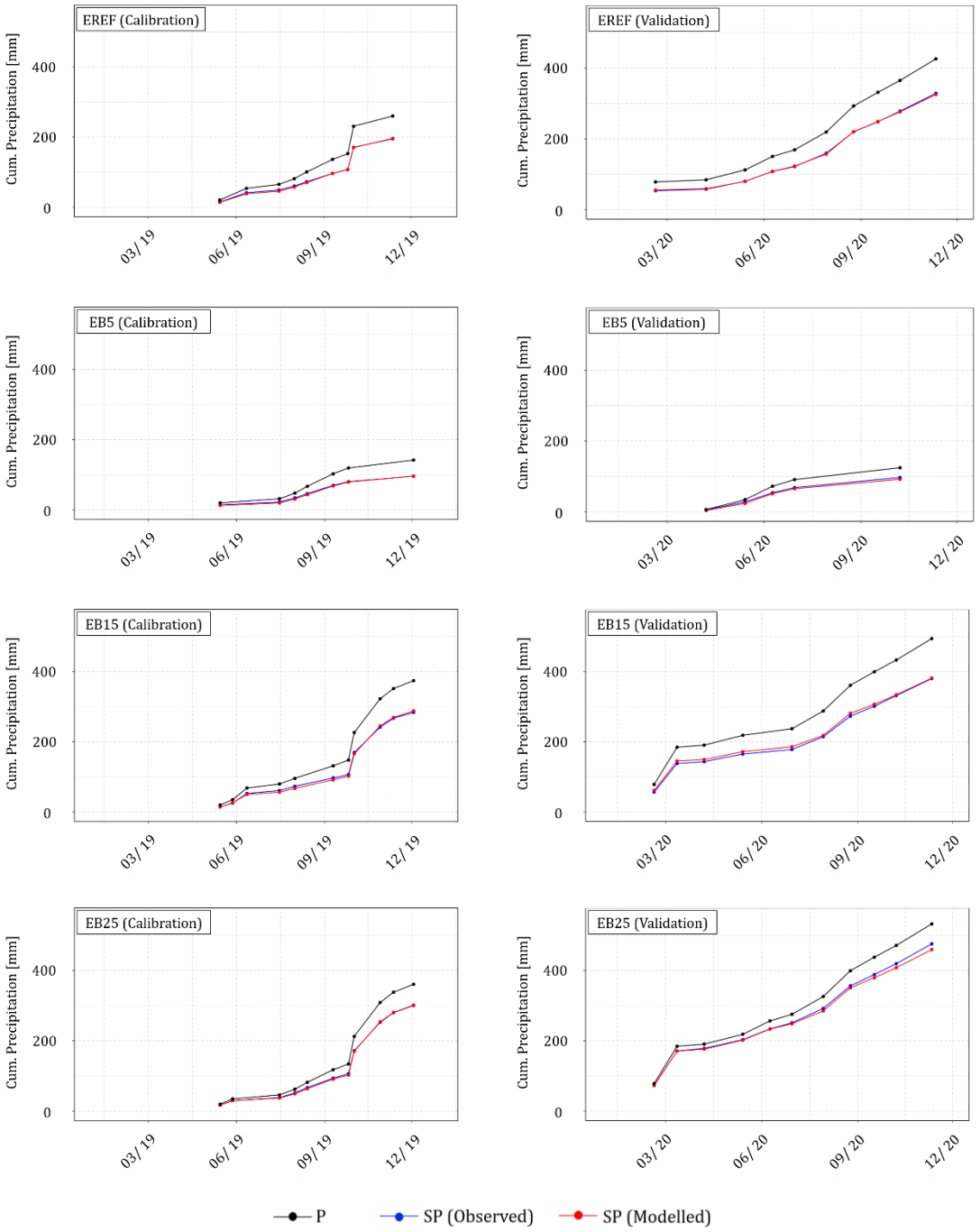

*Figure 47: **Modelled** (red) and **observed** (blue) **cumulated stand precipitation** (SP) as well as cumulated gross precipitation (P) in EREF, EB5, EB15 and EB25 in the calibration period (01/2019 – 12/2019) and validation period (01/2020 – 10/2020).*

Table 36: ***Observed and modelled stand precipitation characteristics*** *for EREF, EB5, EB15 and EB25 in the calibration (01/2019 – 12/2019) and validation period (01/2020 – 10/2020): Total observed and modelled sums (Sum_{Obs} , Sum_{Mod}), mean observed and modelled interception rates (Int_{Obs}, Int_{Mod}), modelled interception rates in summer (Int_{summer}) and winter (Int_{winter}) and the error measures NSE and MAE.*

	Sum_{Obs} [mm]	Sum_{Mod} [mm]	Int_{Obs} [%]	Int_{Mod} [%]	Int_{summer} [%]	Int_{winter} [%]	NSE	MAE [mm]
Calibration period (01/2019 – 12/2019)								
EREF	196.0	194.7	27.4	27.9	25.8	27.1	99.4	1.0
EB5	96.2	96.5	32.6	33.6	28.4	29.9	94.2	1.0
EB15	283.8	288.0	26.4	27.5	27.5	21.1	98.4	1.8
EB25	300.3	301.4	17.8	20.0	19.9	8.4	99.6	1.1
Validation period (01/2020 – 10/2020)								
EREF	328.9	325.7	26.1	27.6	22.6	31.7	98.8	1.6
EB5	96.8	91.7	25.9	31.7	25.0	35.2	94.8	1.7
EB15	380.3	381.7	25.5	27.0	24.1	24.3	98.3	2.5
EB25	475.8	459.4	12.4	18.1	17.6	9.0	99.0	2.1

4.2.8 Calibration and validation of soil and evapotranspiration parameters

Table 37: ***Original values of the empirical MvG parameters*** *alpha and npar as well as the saturated hydraulic conductivity (ksat) for the upper (1) and the lower soil layer (2) as derived by the PTF (Original) for the soil in Elze, their calibration range (Min, Max) and the median parameter value after model calibration.*

	Original	Min	Max	Median
alpha1	3.66	5	70	5.08
alpha2	6.68	5	70	7.17
npar1	1.48	1.2	2	1.85
npar2	1.76	1.2	2	1.66
ksat1	654	-0.5	+0.5	0.49 (2021)
ksat2	1812	-0.5	+0.5	0.48 (5472)

After successfully calibrating the interception evaporation model parameters, the soil and evapotranspiration model parameters are calibrated with respect to soil moisture in 50 cm and 200 cm depth. First, the empirical MvG parameters *alpha*, *npar* and the saturated hydraulic conductivity *ksat* of the model soil for the study site Elze are calibrated automatically by using the DREAM algorithm (Vrugt et al. 2009). The remaining soil hydraulic parameters saturated water content (*ths*), residual water content (*thr*) and the empirical MvG parameters m (*mpar*) and l (*tort*) are not calibrated. For *ths*, *thr* and *mpar*, the parameter values resulting from the PTF (Wösten et al. 1999) are used, and tort is set to 0.5 (Ad-hoc-Arbeitsgruppe Boden 1999, Wösten et al. 1999). Table 37 shows the original parameter values of *alpha*, *npar* and *ksat* as derived by the PTF (Wösten et al. 1999), the minimum (Min) and maximum (Max) value defining the respective calibration range, and the median parameter values after calibration. The best fit of the calibrated empirical MvG parameter *alpha* is close to the minimum of the predefined parameter range. The best fit value of the MvG parameter *npar* is well in the middle between the predefined parameter limits. The best fit of the saturated hydraulic conductivity (*ksat*) is located at the maximum of the predefined parameter limit. Figure 33 exemplarily shows

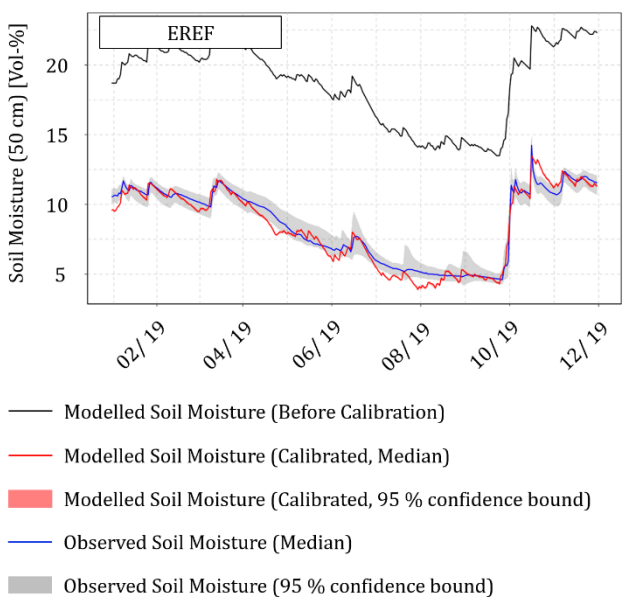

*Figure 48: The **effect of calibrating the empirical MvG parameters** alpha and npar and the saturated hydraulic conductivity (ksat) on the modelled soil moisture in 50 cm depth in EREF. The observed median soil moisture is shown in blue and the corresponding 95 % confidence bound is shown in grey. The modelled soil moisture with original soil hydraulic parameters is shown in black. The modelled soil moisture (median, 95 % confidence bound) is shown in red.*

the effect of calibrating the empirical MvG parameters *alpha* and *npar* as well as the saturated hydraulic conductivity (*ksat*) on the modelled soil moisture in 50 cm depth in EREF in the calibration period (01/2019 – 12/2019). Before calibrating the soil hydraulic properties, modelled soil moisture is considerably higher than observed soil moisture. After calibrating the soil hydraulic properties, the soil moisture level of modelled and observed soil moisture is in better agreement. Table 38 shows the soil hydraulic parameter values as used for further calibration. Table 69 in the appendix shows the resulting soil file as used for further model calculations.

*Table 38: Depth-specific **soil hydraulic parameters**: Saturated water content (ths), residual water content (thr), empirical MvG parameters (alpha, npar, mpar, tort) and the saturated hydraulic conductivity (ksat) of the soil in Elze. Ths, thr and mpar are derived from the PTF (Wösten et al. 1999) and tort is set to 0.5 (Ad-hoc-Arbeitsgruppe Boden 1999, Wösten et al. 1999). Alpha, npar and ksat are calibrated.*

Depth [m]	ths	thr	alpha	npar	mpar	ksat	tort
Organic layer	0.848	0	98.0	1.19	0.16	98000	0.5
0 – 0.95	0.435	0	5.08	1.85	0.33	2021	0.5
0.95 – 3.0	0.394	0	7.17	1.66	0.43	5472	0.5

Table 39 shows the calibration results for the adjusted evapotranspiration and infiltration model parameters *mxkpl*, *psicr*, *infexp* and *ilayer* for EREF, EB5, EB15 and EB25, respectively. The calibrated maximum internal conductivity for water flow through the plants (*mxkpl*) is low for all plots and ranges between 2 and 2.6 mm d^{-1} MPa^{-1}. These low conductivities reduce the potential transpiration rate in all plots. The critical leaf water potential at which stomates close (*psicr*) ranges close to the upper parameter space limit of -1.5 MPa in EREF and EB5, and in the lower half of parameter space between -1.9 and -1.5 MPa in EB15 and EB25. Thus, drought stress conditions stop the transpiration flow in EREF and EB5 earlier than in EB15 and EB25. The calibrated infiltration depth (*ilayer*) does not differ significantly between the plots: The infiltration depths range between 12 (100 cm) and 14 (120 cm). In EREF, EB5 and EB15, input water infiltrates rather uniformly into all soil layers down to the infiltration depth as *infexp* ranges between 0.8 and 1.2. In EB25, water preferably infiltrates into deeper soil layers within the infiltration depth with *infexp* ranging between 1.6 and 1.9.

Table 39: ***Calibration results for evapotranspiration and infiltration parameters*** *in EREF, EB5, EB15 and EB25: Predefined parameter range (Min, Max) and model calibration results (median, 5 % (CI5) and 95 % confidence level (CI95) for the model parameters mxkpl (maximum internal conductivity for water flow through the plants), psicr (critical leaf water potential at which stomates close) and the infiltration parameters infexp and ilayer.*

		mxkpl [mm d^{-1} MPa^{-1}]	psicr [MPa]	infexp [-]	ilayer [-]
EREF	Min	2	-3	0.1	1
	Max	15	-1.5	2	20
	CI5	2.0	-1.61	0.8	13
	Median	2.09	-1.53	0.93	13
	CI95	2.21	-1.5	0.98	14
EB5	Min	2	-3	0.1	1
	Max	15	-1.5	2	20
	CI5	2.0	-1.62	0.86	13
	Median	2.05	-1.52	0.98	14
	CI95	2.21	-1.5	1.15	14
EB15	Min	2	-3	0.1	1
	Max	15	-1.5	2	20
	CI5	2.0	-1.9	0.78	12
	Median	2.18	-1.68	0.94	13
	CI95	2.57	1.51	1.02	13
EB25	Min	2	-3	0.1	1
	Max	15	-1.5	2	20
	CI5	2.01	-1.91	1.64	13
	Median	2.36	-1.58	1.73	13
	CI95	2.56	-1.5	1.85	14

Figure 49 shows observed and **modelled soil moisture in 50 cm depth** after model calibration in EREF, EB5, EB15 and EB25 in the calibration period (01/2019 – 12/2019) and validation period (01/2020 – 10/2020). In 50 cm depth, modelled soil moisture is in good agreement with mean observed soil moisture in EREF (NSE = 93.7, MAE = 0.5 Vol-%), EB5 (NSE = 86.1, MAE = 0.75 Vol-%), EB15 (NSE = 89.9, MAE = 0.78 Vol-%) and EB25 (NSE = 93.2, MAE = 0.51 Vol-%). Modelled soil moisture levels are in good agreement with measured soil moisture levels. In EB5, modelled soil moisture is initially slightly lower than observed. The temporal courses of modelled and observed soil moisture in 50 cm agree mostly well. Modelled soil moisture shows more small peaks than in the observations, especially in spring and summer. The soil moisture decrease in spring and summer is well reproduced in EREF and EB5. In EB15, this decrease is interrupted by many small peaks, which are not present in the observations. Moreover, the soil moisture plateau at a low level of 5 Vol-% is not represented by the model, instead, modelled soil moisture further decreases until autumn. The timing and magnitude of the steep soil moisture increase in autumn 2019, however, is well reproduced by the model for all plots.

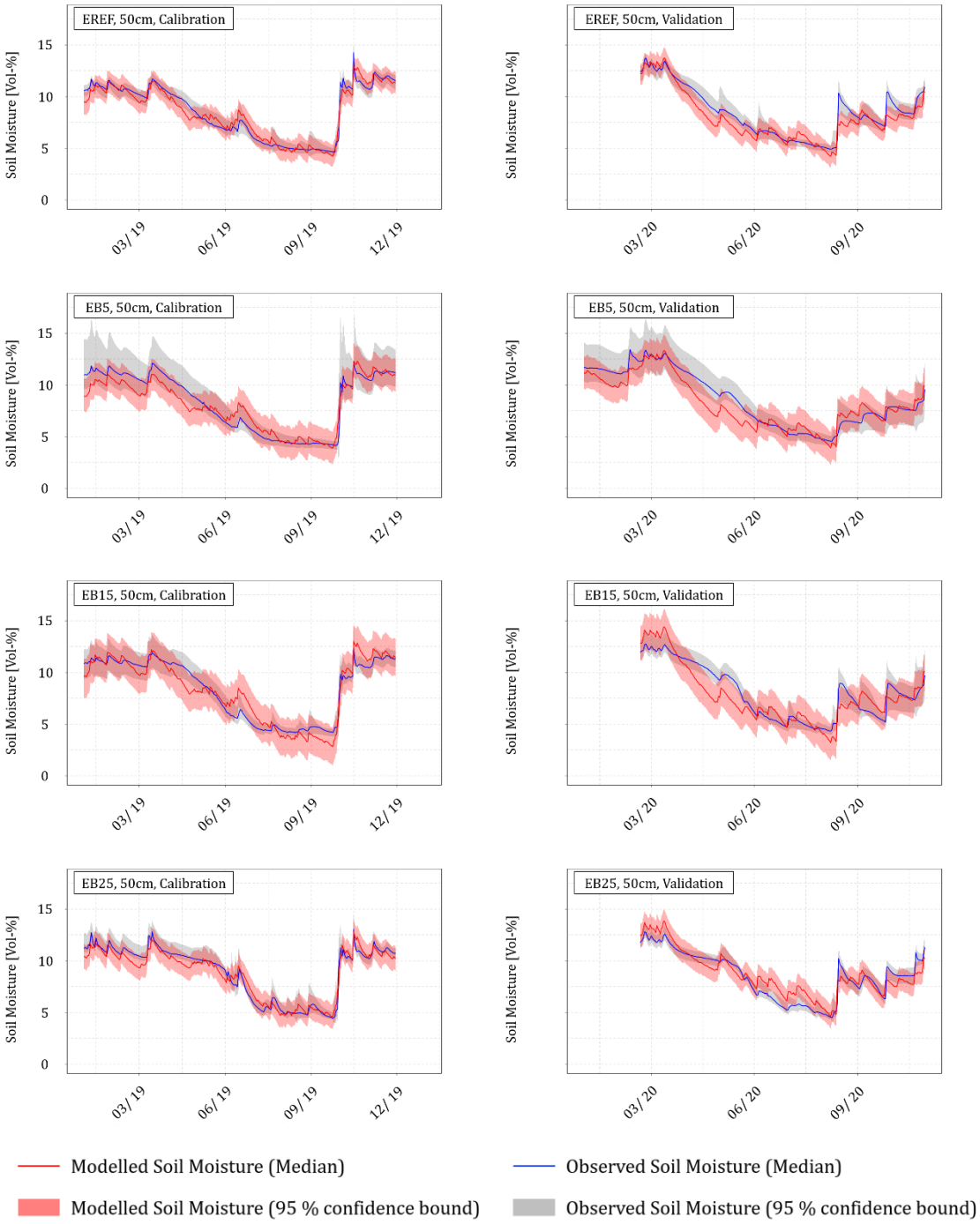

Figure 49: ***Observed and modelled soil moisture in 50 cm depth after model calibration in EREF, EB5, EB15 and EB25*** *in the calibration period (01/2019 – 12/2019) and validation period (01/2020 – 10/2020). Median and 90 % confidence bound of modelled soil moisture are given as solid line and envelope in red, respectively. Median and 90 % confidence bound of observed soil moisture are given as solid line and envelope in blue and grey, respectively.*

In the validation period, modelled soil moisture in 50 cm depth is in good agreement with mean observed soil moisture in EREF (NSE = 82.4, MAE = 0.75 Vol-%), EB5 (NSE = 81.0, MAE = 0.81 Vol-%), EB15 (NSE = 78.9, MAE = 1.0 Vol-%) and EB25 (NSE = 82.5, MAE = 0.75 Vol-%). However, deviations of modelled from observed soil moisture are slightly higher than in the calibration period. The temporal courses of modelled and observed soil moisture in 50 cm agree mostly well, however, modelled soil moisture decreases faster in spring than in the observations. Moreover, modelled soil moisture shows small peaks in summer that

are not present in the observations. However, both timing and magnitude of soil moisture peaks are mostly well reproduced. In general, soil moisture dynamics in 50 cm depth are well reproduced in both plots in the calibration and validation period.

Figure 50 shows observed and **modelled soil moisture in 200 cm depth** after model calibration in EREF, EB5, EB15 and EB25 in the calibration period (01/2019 – 12/2019) and validation period (01/2020 – 10/2020). In 50 cm depth, modelled soil moisture is in good agreement with mean observed soil moisture in EREF (NSE = 64.6, MAE = 0.51 Vol-%), EB5 (NSE = 29.2, MAE = 0.74 Vol-%), EB15 (NSE = 38.8, MAE = 0.8 Vol-%) and EB25 (NSE = 35.0, MAE = 0.81 Vol-%). Modelled soil moisture levels are in good agreement with measured soil moisture levels. In EREF, modelled soil moisture in 200 cm depth is higher than observed soil moisture in December 2019. In EB15, modelled soil moisture is mostly slightly higher than observed. In EB25, modelled soil moisture is mostly slightly lower than observed. Apart from that, the temporal soil moisture course is well represented: The timing of the sharp soil moisture increase is reproduced well in January 2019 and slightly too late in autumn 2019. The soil moisture starts to decrease in spring slightly earlier than observed. Despite these small deficiencies, the model reproduces soil moisture 200 cm depth accurately in the calibration period.

In the validation period, modelled soil moisture in 200 cm depth is in good agreement with mean observed soil moisture in EREF (NSE = 87.2, MAE = 0.52 Vol-%), EB5 (NSE = 32.3, MAE = 0.99 Vol-%), EB15 (NSE = 39.5, MAE = 1.3 Vol-%) and EB25 (NSE = 10.1, MAE = 1.0 Vol-%). The goodness-of-fit in the validation period is similar to the goodness-of-fit in the calibration period in EREF. In EB5, modelled soil moisture is lower than observed soil moisture, and higher than observed soil moisture in EB15. In EB25, modelled soil moisture is lower until July and higher than observations in autumn. The temporal course is well represented, however, the modelled soil moisture peak in March is higher than the observed peak in EREF and slightly later simulated than observed in EB15 and EB25. The overall decreasing trend of soil moisture in spring and summer is well reproduced, however, modelled soil moisture decreases faster than observed in EB25. The slight increase in autumn is slightly later reproduced by the model for all plots. Despite these small deficiencies, the model reproduces soil moisture in 200 cm depth accurately in the validation period.

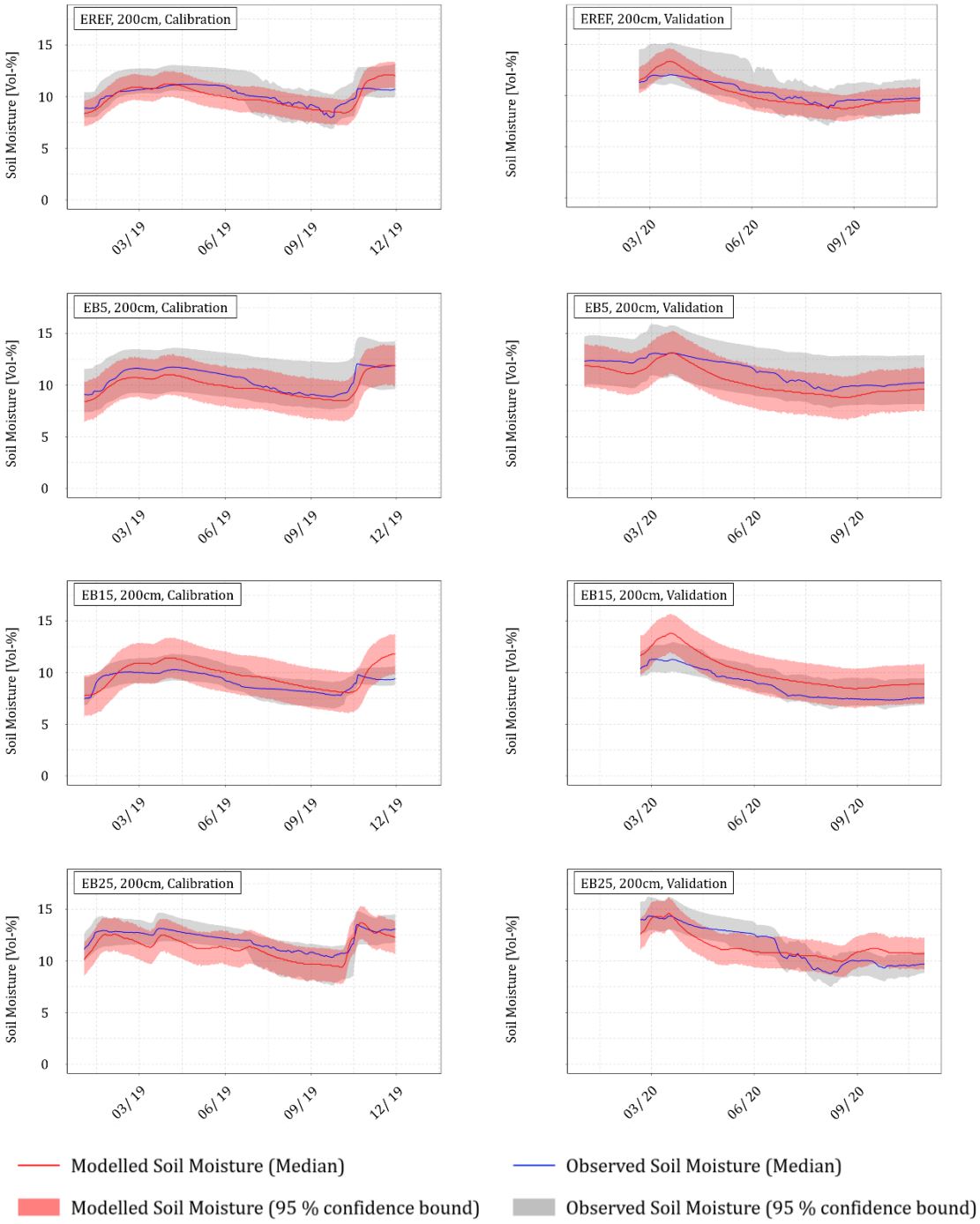

Figure 50: ***Observed and modelled soil moisture in 200 cm depth after model calibration in EREF, EB5, EB15 and EB25*** *in the calibration period (01/2019 – 12/2019) and validation period (01/2020 – 10/2020). Median and 90 % confidence bound of modelled soil moisture are given as solid line and envelope in red, respectively. Median and 90 % confidence bound of observed soil moisture are given as solid line and envelope in blue and grey, respectively.*

4.2.9 Modelled water balance and deep seepage rates

With the successfully calibrated model, all terms of the water balance are calculated for EREF, EB5, EB15 and EB25. Figure 51 shows monthly precipitation (P), interception evaporation (I_T), transpiration (T_T), ground evaporation (E_S) and deep seepage (S_D) sums in the entire calibration and validation period (01/2019 – 10/2020). The water fluxes show a characteristic seasonal course: Transpiration is negligible in winter and increases significantly in spring and summer with rising temperatures in EREF, EB5 and EB15. In EB25,

transpiration is zero in winter and starts to play an important role after budburst of the beech trees. Interception is an important process all year round in all plots. Interception sums are especially high in months with high precipitation sums. In EB25, however, interception only plays a minor role in winter when the leaves have fallen off. Ground evaporation only plays a negligible role in all plots in the entire period. The seasonal course of deep seepage is the result of the interplay of precipitation and evapotranspiration: In January 2019, deep seepage is negligible in EREF, EB5 and EB15 as precipitation has not entirely filled the soil water storage yet. In EB25, deep seepage flow is already comparably high in January. In late winter and early spring 2019, deep seepage occurs also in EREF, EB5 and EB15 as a result of precipitation input and low evapotranspiration rates. In spring 2019, as transpiration rates increase with rising temperatures and increasing solar radiation input, deep seepage rates decrease quickly to a low level. In summer 2019, evaporation and transpiration rates are high and deep seepage rates are low in all plots. However, deep seepage does not come to a complete standstill in summer. In autumn 2019, high precipitation sums occur and lead to a sudden increase in deep seepage rates in late autumn in all plots. Abundant precipitation and low evapotranspiration rates in winter 2019/2020 cause a continuous deep seepage flow until spring 2020. With rising evapotranspiration rates and only little precipitation in spring 2020, deep seepage rates decrease quickly and remain at a low level in late spring and summer 2020. These low deep seepage rates remain until the end of October 2020.

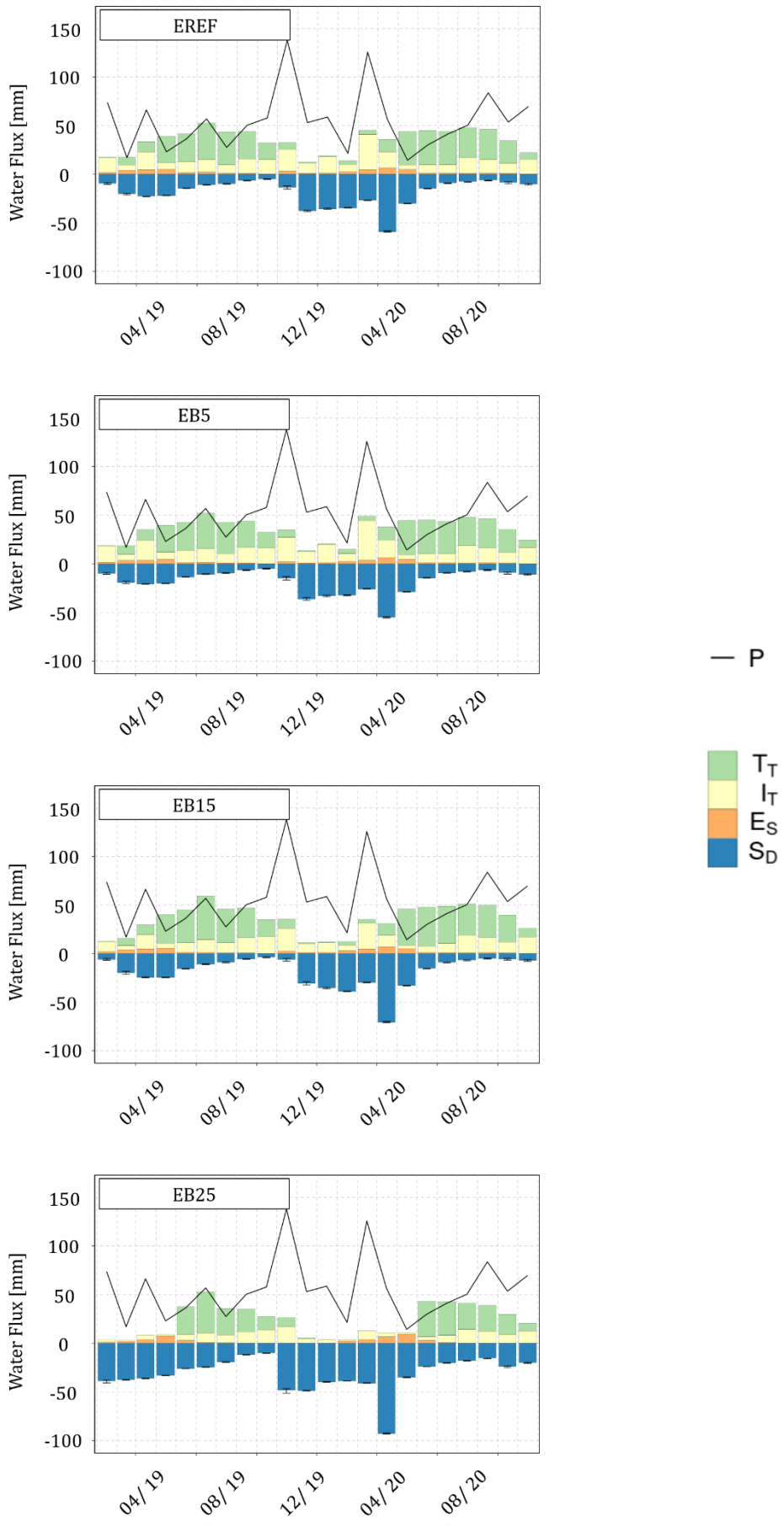

Figure 51: ***Monthly water budgets*** *in EREF, EB5, EB15 and EB25: Precipitation (P), transpiration (T_T), interception (I_T), soil evaporation (E_S) and deep seepage (S_D) sums in the period 01/2019 – 10/2020.*

Figure 52 shows median sums of precipitation (P), interception (I_T), stand precipitation (SP), transpiration (T_T), soil evaporation (E_S) and deep seepage (S_D) for EREF, EB5, EB15 and EB25 in the entire modelling period (01/2019 – 10/2020). The precipitation sum is 1146 mm. In EREF, stand precipitation sums up to 870 mm, which is 76 % of precipitation. The corresponding interception rate is 24 %. In EB5, stand precipitation is 73 % of precipitation and thus 4 % lower than in EREF. Correspondingly, the interception rate in EB5 is 27 % and thus 11 % higher than in EREF. In EB15, stand precipitation is 78 % of precipitation and thus 2 % higher than in EREF. Correspondingly, the interception rate in EB15 is 23 % and thus 7 % lower than in EREF. In EB25, stand precipitation is highest being 87 % of precipitation, which is 14 % higher than in EREF. The corresponding interception rate is 14 %, which is 44 % lower than in EREF. Transpiration is highest in EB15 (40 % of precipitation) and lowest in EB25 (26 % of precipitation). In EREF and EB5, transpiration is at the same level. Soil evaporation is very low in all plots being 4 % of precipitation. The deep seepage sum is 381 mm in EREF, which accounts for 33 % of precipitation. Deep seepage sums are at a comparable level in EB5 and EB15, being 4 % and 1 % lower than in EREF, respectively. In EB25, seepage sums up to 662 mm, which is 58 % of precipitation and more than 70 % higher than in EREF, EB5 and EB15.

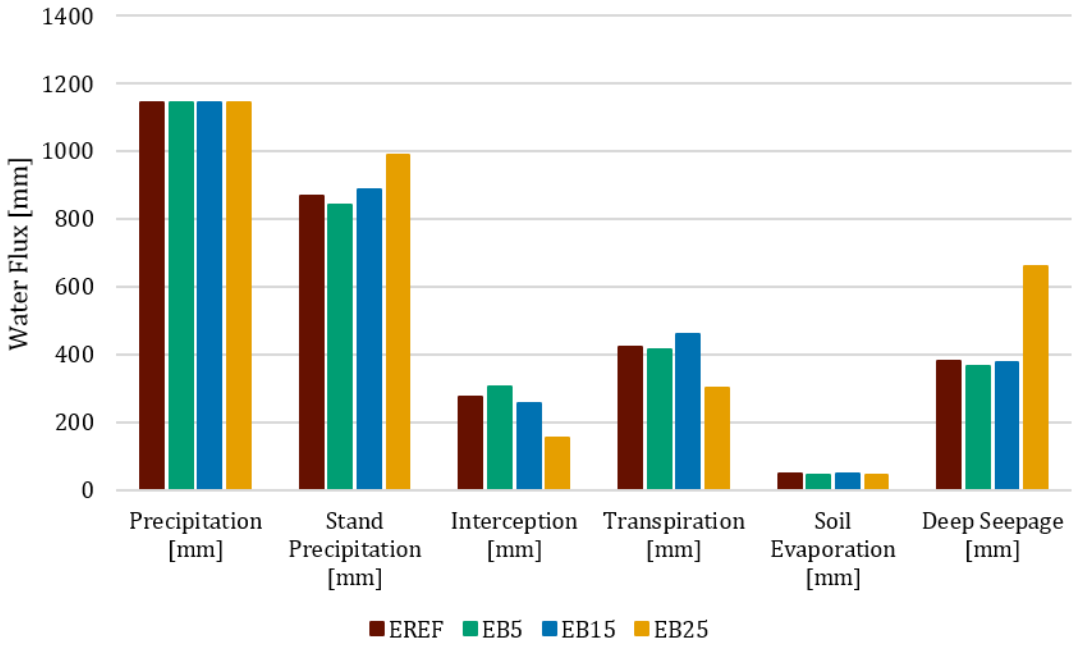

Figure 52: ***Total modelled water fluxes in EREF, EB5, EB15 and EB25:*** *Precipitation (P), transpiration (T_T), interception (I_T), soil evaporation (E_S) and deep seepage (S_D) sums in the period 01/2019 – 10/2020.*

4.3 Wibbese

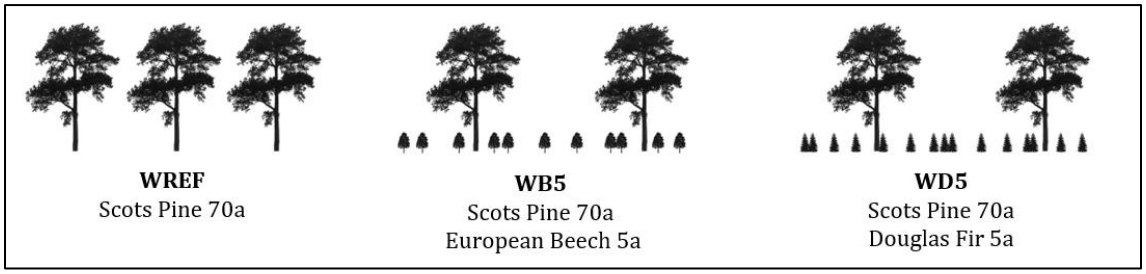

*Figure 53: **Abbreviations** (WREF, WB5, WD5) used for the investigated forest plots in **Wibbese**.*

4.3.1 Precipitation measurements

Precipitation is measured in Wibbese since August 2018. Table 40 shows measured precipitation sums in Wibbese between 08/2018 and 10/2020 aggregated for every year and corresponding absolute and relative deviations from mean multi-annual precipitation sums measured in Rosche-Stütensen and Lüchow. Figure 54 shows monthly precipitation sums and their relative deviations from multi annual mean precipitation measured in Rosche-Stütensen and Lüchow between 08/2018 and 10/2020. Daily precipitation sums are shown in Figure 68 (appendix).

*Table 40: **Precipitation** sums and their deviations from multi-annual mean values in Wibbese.*

Period	Sum [mm]	Abs. deviation [mm]	Rel. deviation [%]
01/2018 – 12/2018	138.1	-117.4	-45.9
01/2019 – 12/2019	627.4	21.9	3.6
01/2020 – 10/2020	528.3	21.3	4.2

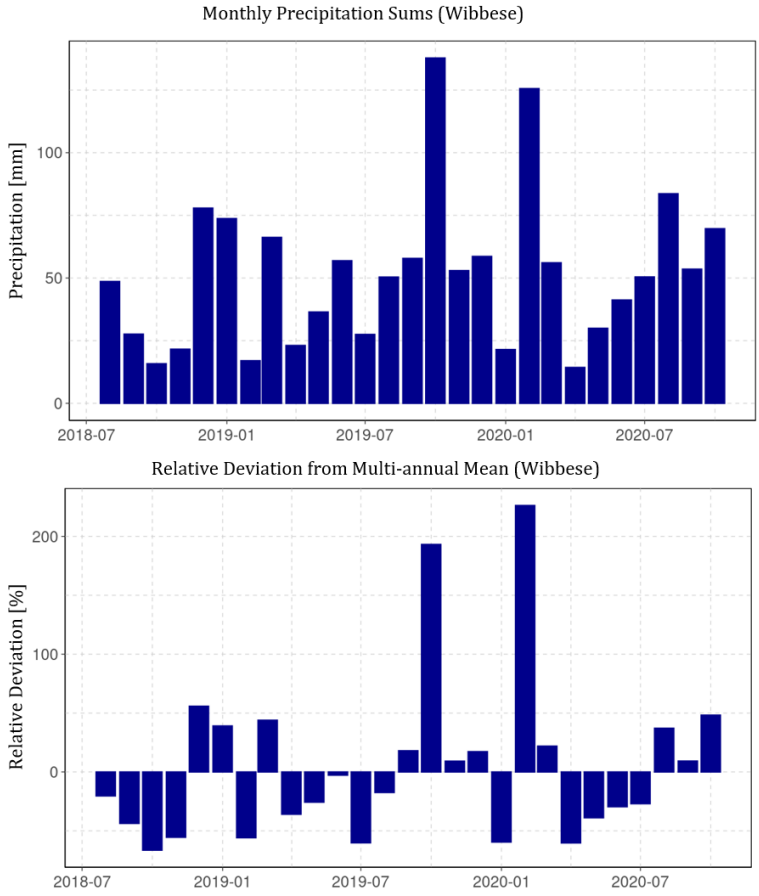

*Figure 54: Measured **monthly precipitation** sums (top) and their relative deviations from mean multi-annual precipitation sums (bottom) in Wibbese between 08/2018 and 10/2020.*

The period between August 2018 and December 2018 was remarkably dry, with precipitation summing up to only 55 % of the multi-annual mean precipitation sum. The precipitation sums in 2019 and 2020 correspond to the long-term average. However, precipitation was unevenly distributed within this period: Precipitation was mostly below average between 03/2019 and 08/2019 and between 04/2020 and 07/2020. Between 09/2019 and 03/2020, pre-

cipitation was mostly average with significant above average totals in October 2019 and February 2020. The period between August 2020 and October 2020 showed also above average precipitation sums. Overall precipitation between 08/2018 and 10/2020 was below average, with six months not even reaching 50 % of the mean precipitation.

4.3.2 Soil measurements

*Figure 55: **Soil profiles** in Wibbese (from left to right: W REF, W B5, W D5) up to a depth of 100 cm.*

The observation plots in Wibbese (see Figure 55) are located on a Cambisol-Podzol (NIBIS Kartenserver 2014a). The humus layer is 2 to 4 cm thick and thus comparably thin. The eluviation horizon is only a few centimeters thick and the illuviation horizon is only weakly pronounced in W REF and well pronounced in W B5 and W D5.

The results of the grain size distribution analysis in WREF, WB5 and WD5 are summarized in Table 41. Corresponding detailed information about sand, silt and clay content (Figure 69) as well as gravel content (Table 58), bulk density (Table 59) and organic carbon content (Table 60) analyses are provided in the appendix.

*Table 41: Depth-specific **soil textures** in Wibbese derived from grain size distribution analysis (Ss = pure sand, Su2 = slightly silty sand, Su3 = medium silty sand, Us = sandy silt).*

Depth	WREF	WB5	WD5
0-10	Su2	Su2	Us
10-20	Su2	Su2	Us
20-30	Su2	Su2	Us
30-40	Su2	Su2	Us
40-50	Su2	Su2	Su3
50-60	Ss	Ss	Su2
60-70	Ss	Ss	Su2
70-80	Ss	Ss	Su2
80-90	Ss	Ss	Su2
90-100	Ss	Su2	Su2
100-110	Ss	Su2	Su2
110-120	Ss	Su2	Su2
120-130	Su2	Ss	Ss
130-140	Su2	Ss	Ss
140-150	Ss	Ss	Su2
150-160	Ss	Ss	Su2
160-170	Ss	Ss	Su3
170-180	Ss	Ss	Su3
180-190	Ss	Ss	Su2
190-200	Ss	Ss	Su2

The soils in Wibbese are also dominated by sand, however soil materials differ slightly among the forest plots. In WREF and WB5, the predominantly occurring soil materials are pure sand (Ss) in lower soil layers, and slightly silty sand (Su2) in the upper soil layers. The sand fraction in WREF is dominated by fine and medium sand with only negligible amounts of coarse sand. In the depths between 0 cm and 50 cm and between 120 cm and 140 cm, noteworthy silt amounts of more than 20 % are present. Besides, silt contents are below 10 %. In WB5, coarse and medium sand contents are higher and fine sand contents are lower than in WREF. The silt content is slightly higher than in WREF and decreases with increasing soil depth. Clay contents are negligible in the entire soil column in both WREF and WB5. In WD5, the dominating soil material is

sand, however, sand contents are lower than in WREF and WB5 and only account for 60 % to 80 %. The content of coarse and medium sized sand is higher than in WREF and WB5, in turn, the fine sand content is lower. The silt content is with 20 % to 40 % comparably high. Several soil layers also contain small clay amounts of up to 5 %. The soil material in WD5 can generally be classified as loamy sand or sandy loam. Gravel amounts in the soils of WREF and WB5 are very low and slightly higher in WD5.

For each plot, soil layers with similar soil properties were combined into a total of two soil layers with weighed mean soil properties. These simplified plot-specific soils are then aggregated to one site-specific soil for Wibbese (Table 63, appendix) by calculating the average of the plot-specific soil properties. This site-specific soil is used as model soil for the site Wibbese.

4.3.3 Phenology & Plant Area Index measurements

Table 56 (appendix) gives final LAI and SAI values for WREF, WB5 and WD5 in the period 2019 – 2020 based on DHP measurements. Figure 56 shows these measured LAI and SAI as sum (LAI + SAI = PAI) in 2019 and 2020. In summer 2019, PAI is the lowest in WREF (3.0) and the highest in WD5 (3.6), with WB5 (3.3) in between. Thus, the PAI in WB5 and WD5 is 7 % and 20 % higher than in WREF, respectively. In March 2020, the pine stand is thinned in WB5 and WD5, which reduces the PAI considerably: In spring 2020 after thinning, the PAI in WB5 (2.9) and WD5 (3.3) is lower than in WREF (3.5). In summer 2020 and winter 2020/2021, the PAI is highest in WREF (4.1, 3.0) and lowest in WD5 (3.8, 2.4), with WB5 (4.0, 2.8) in between. Mean PAI values after thinning in WB5 and WD5 are 8 % and 11 % lower than in WREF, respectively. However, absolute PAI values vary in the observation period.

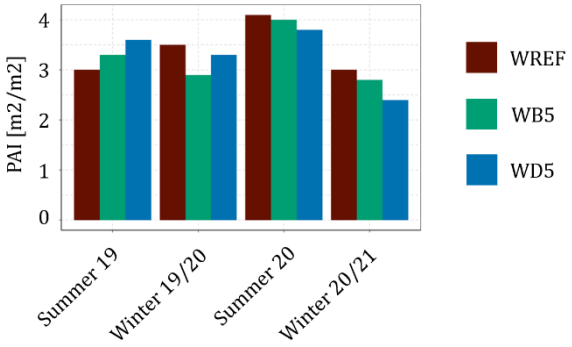

*Figure 56: **Total PAI** (LAI + SAI) in WREF (Scots Pine), WB5 (Scots Pine, European Beech) and WD5 (Scots Pine, Douglas Fir). The minimum (winter) and (maximum) PAI are given for 2019 and 2020.*

Table 42: ***Interception measurement dates*** *for which data are simultaneously available for WREF, WB5 and WD5. Measurement dates are classified into summer and winter.*

01/2019 – 02/2020	04/2020 – 10/2020
2019-05-14 (summer)	2020-05-05 (summer)
2019-05-28 (summer)	2020-06-09 (summer)
2019-07-04 (summer)	2020-07-30 (summer)
2019-08-01 (summer)	2020-08-20 (summer)
2019-08-14 (summer)	2020-09-17 (summer)
2019-10-02	2020-10-20
2019-10-22	2020-11-11
2019-11-13	
2019-12-04 (winter)	
2020-01-21 (winter)	
2020-02-19 (winter)	

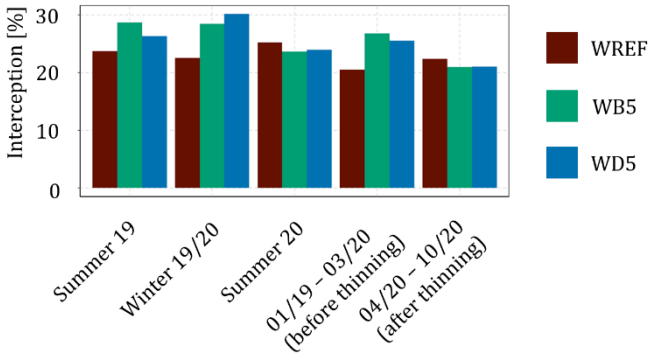

Figure 57: ***Mean interception*** *rates in WREF, WB5 and WD5 in summer 2019 (n = 5), winter 2019/2020 (n = 3), summer 2020 (n = 5), and the periods before thinning (01/2019-03/2020, n = 11) and after thinning (04/2020-10/2020, n = 7).*

4.3.4 Stand precipitation measurements

The total number of measured stand precipitation sums is 9 in WREF, WB5 and WD5 in 2019. In 2020, the number of measured stand precipitation sums is 12 in WREF and WD5, and 11 in WB5. Detailed stand precipitation and interception loss data are provided in Table 66 in the appendix.

Interception rates are analyzed for WREF, WB5 and WD5 based on those dates where data were available for all plots (see Table 42). Figure 57 shows average interception loss values in WREF, WB5 and WD5. Stand precipitation and interception values are aggregated for summer 2019 (n = 5), winter 2019/2020 (n = 3), summer 2020 (n = 5) and the entire period before thinning (01/2019 – 02/2020, n = 11) and after thinning (04/2020 – 10/2020, n = 7). Thereby, summer is defined as period between 01/05 an 30/09, and winter is defined as period between 01/12 and 30/04.

In summer 2019, measured interception rates are the highest in WB5 (29 %) and the lowest in WREF (24 %), with WD5 (26 %) in between. In winter 2019/2020, measured interception rates in WREF are still lowest (23 %), however, interception losses in WD5 (30 %) are slightly higher than in WB5 (29 %). Considering the entire period before thinning in March 2020, measured interception losses are highest in WB5 (27 %) and lowest in WREF (21 %), with WD5 (26%) in between. After thinning, measured interception losses decrease in WB5 and WD5 compared to WREF. In summer 2020 after thinning, measured interception is slightly higher in WREF (25 %) than in WD5 (24 %) and WB5 (24 %).

The differences in measured interception loss is generally small between WREF, WB5 and WD5. However, the thinning of the pine stand reduces interception in WB5 and WD5 considerably.

4.3.5 Soil moisture measurements

Figure 58 shows mean daily soil moisture values in 50 cm and 200 cm depth in WREF, WB5 and WD5 as well as daily precipitation sums between January 2019 and October 2020. The

corresponding soil moisture profiles of the single soil moisture sensors are provided in Figure 70 in the appendix.

The soil moisture level of all plots is mostly comparable in 50 cm depth, however, small differences occur in the end of 2019 and in the beginning of 2020. In 200 cm depth, the soil moisture level is initially higher in WREF than in WB5 and WD5, but is at a comparable level later on.

Soil moisture shows a characteristic course that partially differs among the plots. In 50 cm depth, the soil moisture course is similar in all plots: In winter 2018/2019, soil moisture was comparably high, with soil moisture values between 10 % and 12 %. Precipitation events caused small soil moisture peaks in this period. In spring and summer 2019, the soil moisture decreased to a low soil moisture level between 5 % and 8 %. In June, a significant soil moisture peak occurs in all plots due to heavy rain fall with almost 60 mm of rain within a few hours. During summer, scattered precipitation events caused small soil moisture peaks in almost all plots, except for WD5. In October, soil moisture sustainably increased to a higher level between 10 % and 12 % due to abundant rainfall and further increased to a level between 12 % and 14 % until the end of the winter 2019/2020 due to abundant rain fall in February 2020. From March 2020 onwards, soil moisture decreased continuously to a level between 5 % and 6 % (WREF) and between 7 % and 8 % in WB5 and WD5 and remained at this low level until September 2020. In this period, occasional soil moisture peaks occurred due to scattered rain fall. Until the end of the observation period, the soil moisture started to increase simultaneously in all plots and reached a level of 10 % in October. This increase, however, was not as sharp as in autumn 2019.

In 200 cm depth, the soil moisture courses of all plots are to some extent different. In winter 2018/2019, the soil moisture level is between 6 % (WB5, WD5) and 7 % (WREF) in all plots. In the mid of January 2019, soil moisture started to increase sustainably in WB5 and in the end of January also in WD5. Maximum soil moisture values range between almost 8 % (WB5) and 9 % (WREF, WD5). In spring and summer 2019, the soil moisture decreases in all plots successively to 6 % in WB5 and WD5 and to 8 % in WREF. Heavy rain fall with almost 60 mm of rain within a few hours in June causes a small soil moisture peak in WREF and WB5, which did not occur in WD5. Abundant rainfall in September and October caused an increase in soil moisture in all plots. This increase already started in the beginning of October in WREF, in mid-October in WB5 and in WD5 not until mid-December. From then on, soil moisture values remain at a comparably high level throughout the winter and reach a maximum in March 2020 (10 % in WB5, 11 % in WREF and WD5). In spring and summer 2020, soil moisture decreased successively to a level of 6 % in WB5 and 7 % in WREF and WD5 without any major peaks until the end of the observation period.

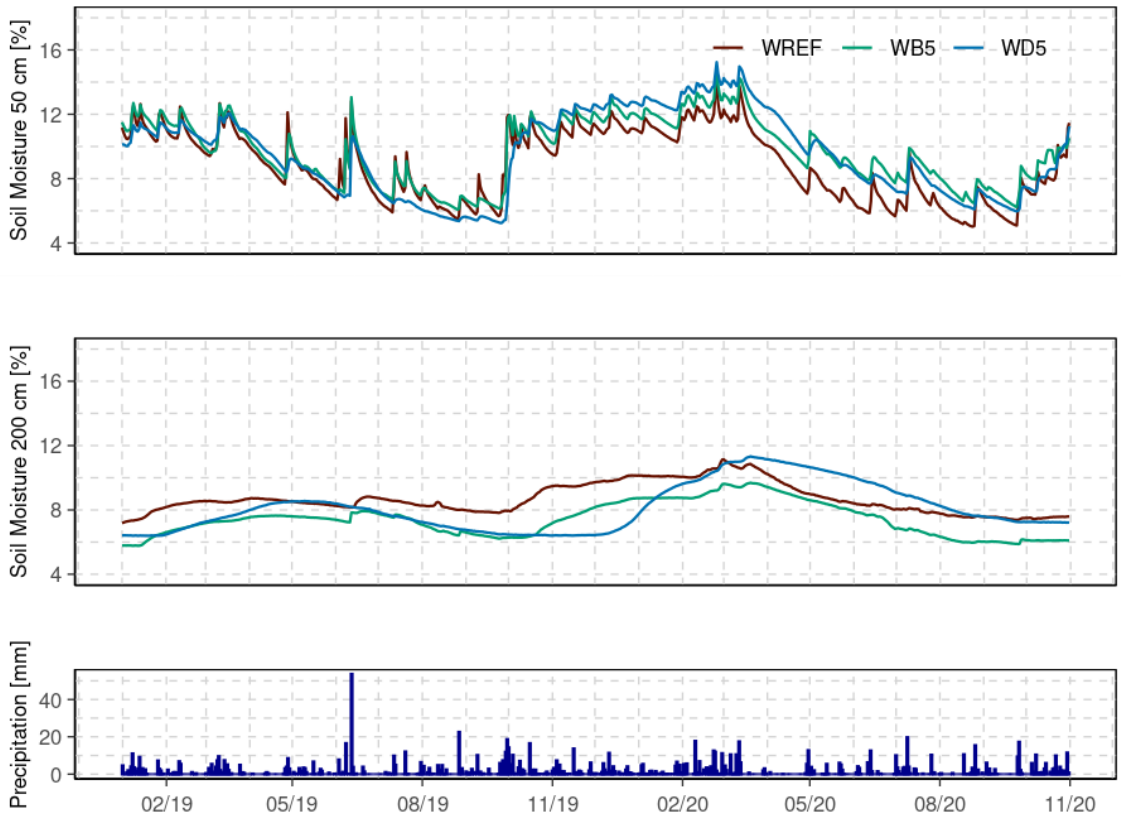

*Figure 58: **Soil moisture** observations (daily mean) in 50 cm (top) and 200 cm depth (middle) as well as daily precipitation sums (bottom) in Wibbese.*

For statistical analyses, descriptive statistical measures are calculated for mean daily soil moisture values of 8 soil moisture sensors per plot in the observation period between 01/2019 and 10/2020: Mean 5 % confidence level (CI5), median, mean 95 % confidence level (CI95), mean 90% interquartile range (IQR90), mean standard deviation (SDEV), minimum (Min), maximum (Max) and mean range between lowest and highest daily soil moisture value of all sensors (range). Table 43 show these descriptive statistical measures of the soil moisture in 50 cm and 200 cm depth.

In 50 cm depth, the soil moisture level is lowest in WREF and highest in WD5, soil moisture variability is highest in WB5 and lowest in WD5. Soil moisture values range between 3.3 % and 33.5 % in WREF, between 3.9 % and 22.9 % in WD5 and between 4.2 % and 26.8 % in WB5.

In 200 cm depth, the soil moisture level is highest in WREF and lowest in WB5. Soil moisture variability is highest in WD5 and lowest in WREF and WB5. Soil moisture values range between 3.6 % and 15.5 % in WB5, between 4.0 % and 19.3 % in WD5 and between 5.2 % and 13.7 % in WREF.

*Table 43: **Statistical measures** calculated from daily mean **soil moisture** values of the 8 soil moisture sensors in **50 cm and 200 cm depth** between 01/2019 and 10/2020: Mean 5 % confidence level (CI5), median, mean 95 % confidence level (CI95), mean 90% interquartile range between CI5 and CI95 (IQR90), mean standard deviation (SDEV), minimum (Min), maximum (Max) and mean range between lowest and highest daily soil moisture value of all sensors (range).*

	CI5 [Vol-%]	Median [Vol-%]	CI95 [Vol-%]	IQR95 [Vol-%]	SDEV [Vol-%]	Min [Vol-%]	Max [Vol-%]	Range [Vol-%]
				50 cm depth				
W REF	7.3	8.2	10.4	3.2	2.3	3.3	33.5	6.9
W B5	8.0	9.1	11.7	3.8	2.7	4.2	26.8	7.6
W D5	8.3	9.7	10.9	2.6	1.9	3.9	22.9	5.6
				200 cm depth				
W REF	7.7	8.8	9.7	2.0	1.4	5.2	13.7	3.7
W B5	6.4	7.2	8.5	2.1	1.5	3.6	15.5	4.9
W D5	6.8	8.0	9.6	2.8	2.0	4.0	19.3	6.4

4.3.6 Sensitivity analysis

*Table 44: **NSE values at the 99.5 % confidence level** separating behavioural from non-behavioural model runs.*

	W REF	W B5	W D5
stand precipitation	0.982	0.993	0.986
soil moisture (50 cm)	0.638	0.602	0.829
soil moisture (200 cm)	-0.071	-0.080	-0.069

The sensitivity analysis reveals the importance of individual model parameters for model performance with regard to stand precipitation and soil moisture in 50 cm and 200 cm depth in Wibbese. The threshold between behavioural and non-behavioural model runs is set to the 99.5% confidence level. Corresponding NSE values are given in Table 44. Figure 59 shows insensitive parameters in white, moderately sensitive parameters in orange and highly sensitive parameters in red. Those parameters selected for model calibration are marked with an x.

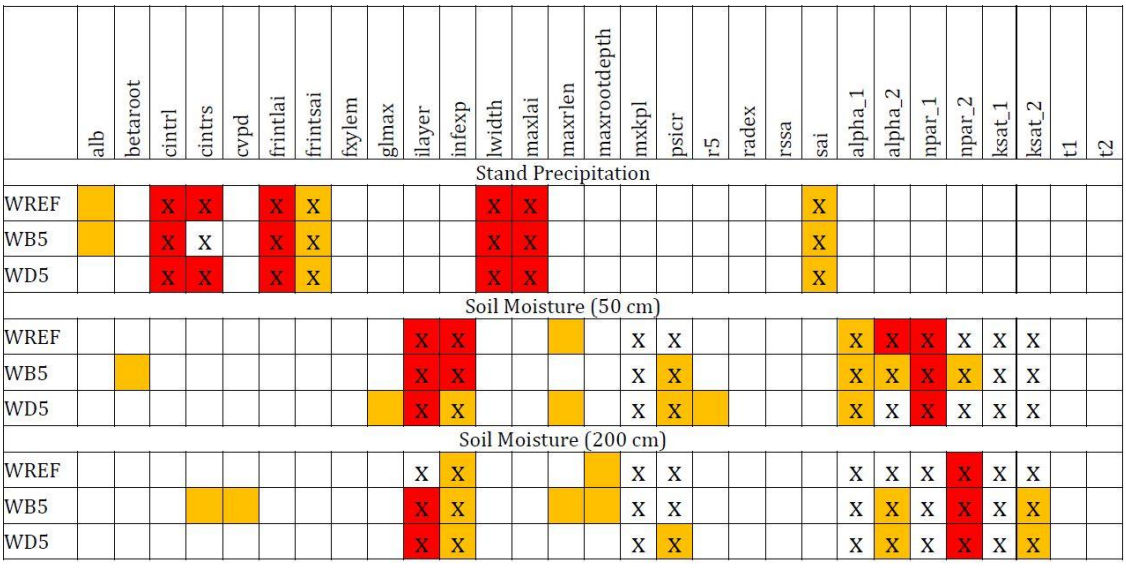

*Figure 59: **Results of the sensitivity analysis** with regard to stand precipitation, soil moisture (50 cm) and soil moisture (200 cm) in Wibbese. Highly important parameters are shown in red, moderately important parameters are shown in orange and unimportant parameters are shown in white. Model parameters selected for model calibration with respect to stand precipitation, soil moisture in 50 cm and 200 cm depth are marked with an X.*

In WREF, WB5 and WD5, those **model parameters that control interception evaporation** are sensitive with respect to observed stand precipitation. The leaf interception storage per unit LAI (*cintrl*) and SAI (*cintrs*), the fraction of rain intercepted per unit LAI (*frintlai*), leaf width (*lwidth*) and maximum LAI (*maxlai*) are highly important for most of the plots. The albedo (*alb*), fraction of rain intercepted per unit SAI (*frintsai*) and stem area index (*sai*) are moderately important for most of the plots. The other model parameters are not sensitive in most of the plots. As described in the sensitivity analysis results for Sandkrug and Elze, the model parameters *cintrl*, *cintrs*, *frintlai*, *frintsai*, *lwidth*, *maxlai* and *sai* are calibrated with respect to stand precipitation. Since *alb* is not calibrated in Sandkrug and Elze, it is set to fixed values in Wibbese, too, in order to maintain comparability.

Soil moisture in 50 cm depth is mostly affected by soil and evapotranspiration parameters in WREF, WB5 and WD5. The MvG parameters *alpha* and *npar* affect soil water movement and soil water content and are moderately to highly important. Maximum depth (*ilayer*) and vertical distribution with depth (*infexp*) of macro pore-assisted infiltrating water are also highly important model parameters. The remaining important parameters control soil water removal through evapotranspiration (*maxrlen*, *psicr*). For **soil moisture in 200 cm depth**, parameters affecting vertical soil water movement are most important: *iIayer*, *infexp*, *maxrlen*, *maxrootdepth*, *psicr*, *alpha*, *npar* and *ksat* are highly important at most of the plots. Other evapotranspiration parameters are of less importance for soil moisture in 200 cm depth. Therefore, the MvG parameters *alpha*, *npar* and *ksat*, as well as *mxkpl*, *psicr*, *infexp* and *ilayer* are included in model calibration with respect to soil moisture in 50 cm and 200 cm depth. Even though *glmax*, *maxrlen*, *r5* and *maxrootdepth* are to some extent important parameters, they are not calibrated, as they are not calibrated in Sandkrug and Elze either. These parameters, as well as the unimportant model parameters *alb*, *betaroot*, *cvpd*, *radex*, *rssa*, *t1* and *t2,* are set to fixed values according to Federer (2019) and Jackson et al. (1996) (see Table 45).

Table 45: ***Fixed model parameter values*** *based on literature values (Federer 2019) of parameters being identified as unimportant in the sensitivity analysis.*

	alb [-]	cvpd [kPa]	fxylem [-]	glmax [m s^{-1}]	maxrlen [m m^{-2}]	maxrootdepth [m]	r5 [W m^{-2}]	radex [-]	rssa [s m^{-1}]	t1 [°C]	t2 [°C]	betaroot [-]
WREF	0.14	2	0.5	0.0053	3000	-2.5	100	0.5	100	10	30	0.976
WB5	0.14	2	0.5	0.0053	3000	-2.5	100	0.5	100	10	30	0.976
WD5	0.14	2	0.5	0.0053	3000	-2.5	100	0.5	100	10	30	0.976

4.3.7 Calibration and validation of interception evaporation parameters

Model interception parameters are manually adjusted in a way that storage capacities range between 1 and 2 mm in WREF, WB5 and WD5.

Table 46: ***Calibrated interception parameter values*** *from calibrating stand precipitation and the associated modelled interception storage in WREF, WB5 and WD5.*

		cintrl [mm]	cintrs [mm]	frintlai [-]	frintsai [-]	lwidth [m]	maxlai [m^2 m^{-2}]	minlai [m^2 m^{-2}]	sai [m^2 m^{-2}]	storage capacity [mm]
WREF	Min	0.05	0.05	0.1	0.1	0.004	1.8	1.8	0.4	1.0
	Max	0.75	0.75	0.2	0.2	0.1	3.3	3.3	0.6	2.0
	Best Fit	**0.2**	**0.2**	**0.1**	**0.1**	**0.05**	**1.8**	**1.8**	**0.5**	**0.46**
WB5	Min	0.05	0.05	0.1	0.1	0.004	2.1	2.1	0.4	1.0
	Max	0.75	0.75	0.2	0.2	0.1	3.5	3.5	0.6	2.0
	Best Fit	**0.2**	**0.2**	**0.1**	**0.1**	**0.05**	**2.8**	**2.8**	**0.5**	**0.66**
WD5	Min	0.05	0.05	0.1	0.1	0.004	2.3	2.3	0.4	1.0
	Max	0.75	0.75	0.2	0.2	0.1	3.9	3.9	0.6	2.0
	Best Fit	**0.2**	**0.2**	**0.1**	**0.1**	**0.05**	**2.4**	**2.4**	**0.5**	**0.58**

In Wibbese, modelled stand precipitation is initially too low at all plots. To increase modelled stand precipitation, interception evaporation is reduced by increasing *lwidth* from 0.004 m to 0.05 m in all plots. Reducing both the interception storage per unit LAI (*cintrl*) and SAI (*cintrs*) to 0.2 mm and the fraction of rain that is intercepted by vegetation surfaces per unit LAI (*frintlai*) and SAI (*frintsai*) to 10 % further improves overall model performance in all plots. In WREF, however, stand precipitation is still too low. Therefore, *maxlai* is decreased from 2.6 to 1.8, which yields a good fit. For WB5, the initial *maxlai* of 2.8 yields the best fit. In WD5, *maxlai* is reduced from 3.1 to 2.4 to yield a good fit. The remaining interception characteristics are identical for all three plots. These model interception parameters result in lower storage capacities than reported in the literature for pine forests (1-2 mm, Federer (2019)) for WREF, WB5 and WD5.

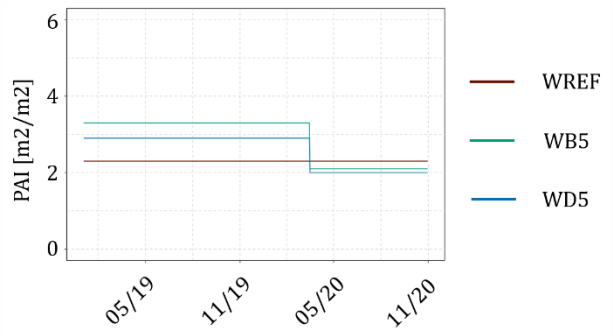

Figure 60: ***Course of the PAI in the model*** *after calibration of model interception parameters in Wibbese between 01/2019 and 10/2020.*

The resulting parameter values from calibrating stand precipitation and the corresponding modelled interception storage capacities for each plot are given in Table 46. Figure 60 shows the seasonal PAI course between 01/2019 and 10/2020 after model calibration.

Within the validation period, the pine layer has been thinned in WB5 and WD5 in March 2020. This is considered in the model by reducing *maxlai* to the same extent as the measured LAI of WB5 and WD5 has been reduced relatively to the measured LAI of WREF. *Maxlai* and *sai* are simultaneously reduced by reducing the stand density parameter *densef*. After thinning, the LAI in WB5 is 92 % of the LAI in WREF, and the LAI in WD5 is 89 % of the LAI in WREF. The reduced LAI values for WB5 and WD5 after thinning are thus calculated as follows:

$$LAI_{WB5,after\ thinning} = LAI_{WREF} * 0.92 = 1.8 * 0.92 = 1.656 \quad (31)$$

$$LAI_{WD5,after\ thinning} = LAI_{WREF} * 0.89 = 1.8 * 0.89 = 1.602 \quad (32)$$

Resulting LAI values correspond to 59 % of the former LAI value in WB5 and to 67 % of the former LAI value in WD5. The LAI is thus reduced by 41 % in WB5 and by 33 % in WB5 after thinning. Correspondingly, *densef* is set to 0.59 in WB5 and to 0.67 in WD5 after thinning.

Figure 61 shows modelled and observed stand precipitation sums after model calibration for WREF, WB5 and WD5 in the calibration and validation period. Table 47 shows observed and modelled stand precipitation sums, interception rates and error measures for WREF, WB5 and WD5 in the calibration and validation period.

Table 47: ***Observed and modelled stand precipitation characteristics*** *for WREF, WB5 and WD5 in the calibration (01/2019 – 12/2019) and validation period (01/2020 – 10/2020): Total observed and modelled sums (Sum_{Obs}, Sum_{Mod}), mean observed and modelled interception rates (Int_{Obs}, Int_{Mod}), modelled interception rates in summer (Int_{summer}) and winter (Int_{winter}) and the error measures NSE and MAE.*

	Sum_{Obs} [mm]	Sum_{Mod} [mm]	Int_{Obs} [%]	Int_{Mod} [%]	Int_{summer} [%]	Int_{winter} [%]	NSE	MAE [mm]
Calibration period (01/2019 – 12/2019)								
WREF	217.5	212.0	19.1	18.4	16.9	21.0	98.4	1.8
WB5	196.5	194.6	25.7	26.4	23.4	28.7	99.1	1.4
WD5	206.8	201.4	22.6	23.2	20.8	25.7	98.4	1.9
Validation period (01/2020 – 10/2020)								
WREF	367.6	362.3	22.8	19.9	18.7	20.3	98.4	2.1
WB5	353.9	356.6	24.1	21.4	15.9	24.8	98.1	2.2
WD5	350.7	361.7	25.2	20.1	15.9	22.7	97.8	2.7

The model reproduces measured stand precipitation well in WREF, WB5 and WD5 in the calibration period. Corresponding error measures show an NSE close to 100 and a low MAE with values less than 2 mm. Thereby, the model reproduces reliably higher interception rates in WB5 and WD5 compared to WREF. In the validation period, the model also reproduces modelled stand precipitation well. Modelled interception rates are slightly lower than observed, however, the general agreement is acceptable. The goodness of fit is slightly lower than in the calibration period, with MAE values ranging between 2 and 3 mm and slightly lower NSE values than in the calibration period. Overall, the model is able to reproduce the interception rates in WREF, WB5 and WD5, which are at a comparable level in the validation period.

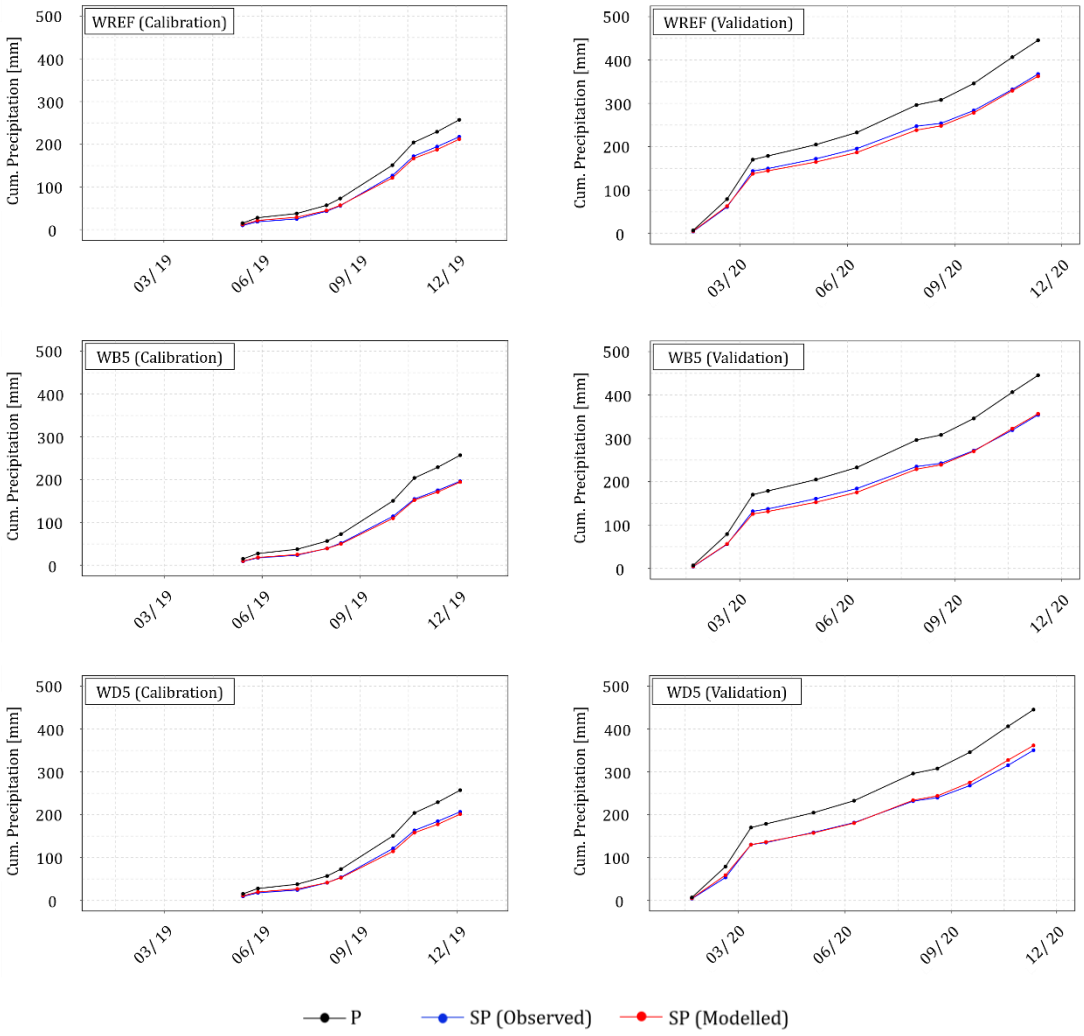

*Figure 61: **Modelled** (red) and **observed** (blue) **cumulated stand precipitation** (SP) as well as cumulated gross precipitation (P) in WREF, WB5 and WD5 in the calibration period (01/2019 – 12/2019) and validation period (01/2020 – 10/2020).*

4.3.8 Calibration and validation of soil and evapotranspiration parameters

*Table 48: Original values of the **empirical MvG parameters** alpha and npar as well as the saturated hydraulic conductivity (ksat) for the upper (1) and the lower soil layer (2) as derived by the PTF (Original) for the soil in Wibbese, their calibration range (Min, Max) and the median parameter value after model calibration.*

	Original	Min	Max	Median
alpha1	3.35	5	70	6.83
alpha2	4.99	5	70	5.03
npar1	1.47	1.2	2	1.71
npar2	1.57	1.2	2	2.0
ksat1	561	-0.5	+0.5	0.48 (1694)
ksat2	1001	-0.5	+0.5	0.5 (3165)

After successfully calibrating the interception evaporation model parameters, the soil and evapotranspiration model parameters are calibrated with respect to soil moisture in 50 cm and 200 cm depth. First, the empirical MvG parameters *alpha*, *npar* and the saturated hydraulic conductivity *ksat* of the model soil for the study site Wibbese are calibrated automatically by using the DREAM algorithm (Vrugt et al. 2009). The remaining soil hydraulic parameters saturated water content (*ths*), residual water content (*thr*) and the empirical MvG parameters m (*mpar*) and l

(*tort*) are not calibrated. For *ths*, *thr* and *mpar*, the parameter values resulting from the PTF (Wösten et al. 1999) are used, and tort is set to 0.5 (Ad-hoc-Arbeitsgruppe Boden 1999, Wösten et al. 1999). Table 48 shows the original parameter values of *alpha*, *npar* and *ksat* as derived by the PTF (Wösten et al. 1999), the minimum (Min) and maximum (Max) value defining the respective calibration range, and the median parameter values after calibration. The best fit of the calibrated empirical MvG parameter *alpha* is close to the minimum of the predefined parameter range. The best fit values of the MvG parameter *npar* and the saturated hydraulic conductivity (*ksat*) are located at the maximum of the predefined parameter limit.

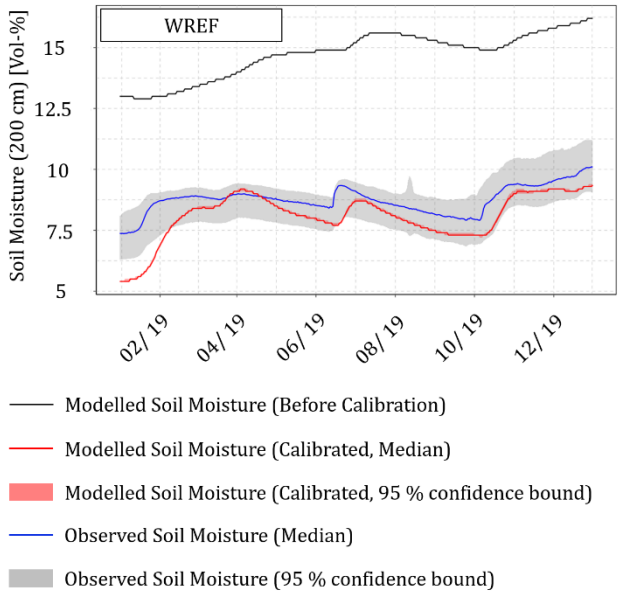

*Figure 62: The **effect of calibrating the empirical MvG parameters** alpha and npar and the saturated hydraulic conductivity (ksat) on the modelled soil moisture in 200 cm depth in WREF. The observed median soil moisture is shown in blue and the corresponding 95 % confidence bound is shown in grey. The modelled soil moisture with original soil hydraulic parameters is shown in black. The modelled soil moisture (median, 95 % confidence bound) is shown in red.*

Figure 62 exemplarily shows the effect of calibrating the empirical MvG parameters *alpha* and *npar* as well as the saturated hydraulic conductivity (*ksat*) on modelled soil moisture in 200 cm depth in WREF in the calibration period (01/2019 – 12/2019). Before calibrating the soil hydraulic properties, modelled soil moisture is considerably higher than observed soil moisture. After calibrating the soil hydraulic properties, the soil moisture level of modelled and observed soil moisture is in better agreement. Table 49 shows the soil hydraulic parameter values as used for further calibration. Table 70 in the appendix shows the resulting soil file as used for further model calculations.

*Table 49: Depth-specific **soil hydraulic parameters**: Saturated water content (ths), residual water content (thr), empirical MvG parameters (alpha, npar, mpar, tort) and the saturated hydraulic conductivity (ksat) of the soil in Wibbese. Ths, thr and mpar are derived from the PTF (Wösten et al. 1999) and tort is set to 0.5 (Ad-hoc-Arbeitsgruppe Boden 1999, Wösten et al. 1999). Alpha, npar and ksat are calibrated.*

Depth [m]	ths	thr	alpha	npar	mpar	ksat	tort
Organic layer	0.848	0	98.0	1.19	0.16	98000	0.5
0 – 0.5	0.435	0	6.83	1.71	0.32	1694	0.5
0.5 – 3.0	0.418	0	5.03	2.0	0.36	3165	0.5

Table 50: ***Calibration results for evapotranspiration and infiltration parameters*** *in WREF, WB5 and WD5: Predefined parameter range (Min, Max) and model calibration results (median, 5 % (CI5) and 95 % confidence level (CI95) for the model parameters mxkpl (maximum internal conductivity for water flow through the plants), psicr (critical leaf water potential at which stomates close) and the infiltration parameters infexp and ilayer.*

		mxkpl [mm d^{-1} MPa^{-1}]	psicr [MPa]	infexp [-]	ilayer [-]
WREF	Min	2	-3	0.1	1
	Max	15	-1.5	2	20
	CI5	2.0	-1.62	1.25	15
	Median	2.06	-1.54	1.34	16
	CI95	2.19	-1.5	1.56	16
WB5	Min	2	-3	0.1	1
	Max	15	-1.5	2	20
	CI5	2.0	-1.57	0.79	14
	Median	2.02	-1.52	0.88	14
	CI95	2.12	-1.50	0.95	15
WD5	Min	2	-3	0.1	1
	Max	15	-1.5	2	20
	CI5	2.0	-1.53	0.45	16
	Median	2.01	-1.51	0.48	17
	CI95	2.06	-1.5	0.54	17

Table 50 shows the calibration results for the adjusted evapotranspiration and infiltration model parameters *mxkpl*, *psicr*, *infexp* and *ilayer* for WREF, WB5 and WD5, respectively. The calibrated maximum internal conductivity for water flow through the plants (*mxkpl*) is low for all plots and ranges between 2 and 2.2 mm d^{-1} MPa^{-1}. These low conductivities reduce the potential transpiration rate in all plots. The critical leaf water potential at which stomates close (*psicr*) ranges close to the upper parameter space limit of -1.5 MPa for all plots. Thus, drought stress conditions stop the transpiration flow already at a comparably low leaf water potential at all plots. The calibrated infiltration depth (*ilayer*) ranges between 14 (120 cm) and 17 (150 cm) in all forest plots. The infiltration depth is slightly higher in WD5 compared to WREF and WB5. In WB5 and WD5, water predominantly infiltrates into the upper soil layers (*infexp* < 1), whereas water in infiltrates predominantly into deeper soil layers in WREF (infexp > 1). The calibrated models differ only slightly with respect to evapotranspiration and water infiltration among the forest plots in Wibbese.

Figure 63 shows observed and **modelled soil moisture in 50 cm depth** after model calibration in WREF, WB5 and WD5 in the calibration period (01/2019 – 12/2019) and validation period (01/2020 – 10/2020). In 50 cm depth, modelled soil moisture is in good agreement with mean observed soil moisture in WREF (NSE = 70.7, MAE = 0.57 Vol-%), WB5 (NSE = 56.0, MAE = 0.8 Vol-%) and WD5 (NSE = 57.3, MAE = 1.0 Vol-%) in the calibration period. The modelled soil moisture level is in good agreement with measured soil moisture levels in WREF and WB5. In WD5, modelled soil moisture is slightly lower than observed. The temporal courses of modelled and observed soil moisture in 50 cm agree mostly well. Modelled soil moisture peaks are not as high as in the observations in WREF and WB5. In WD5, modelled soil moisture shows small peaks in spring and summer that are not present in the observations. However, the timing of soil moisture peaks is mostly well reproduced at all plots.

In the validation period, modelled soil moisture in 50 cm depth is in good agreement with mean observed soil moisture in WREF (NSE = 84.0, MAE = 0.73 Vol-%), WB5 (NSE = 59.6, MAE = 0.79 Vol-%) and WD5 (NSE = 55.1, MAE = 1.1 Vol-%). The deviation of modelled from measured soil moisture is low, but slightly higher than in the calibration period in WREF and WD5. The modelled and observed soil moisture levels are at the same level in WREF. In WB5, modelled soil moisture is slightly higher than observed. In WD5, the soil moisture level is slightly underestimated by the model in winter and spring. Temporal moisture courses are comparable throughout the entire validation period. Modelled soil moisture peaks are not as high as in the observations in WREF and WB5. In WD5, modelled soil moisture shows small peaks in spring and summer that are not present in the observations. However, the timing of soil moisture peaks is mostly well reproduced at all plots. In general, soil moisture dynamics in 50 cm depth are well reproduced in both plots in the calibration and validation period.

Figure 64 shows observed and **modelled soil moisture in 200 cm depth** after model calibration in WREF, WB5 and WD5 in the calibration period (01/2019 – 12/2019) and validation period (01/2020 – 10/2020). In 200 cm depth, modelled soil moisture is in good agreement with mean observed soil moisture in WREF (NSE = 61.4, MAE = 0.45 Vol-%), WB5 (NSE = 56.0, MAE = 0.8 Vol-%) and WD5 (NSE = 18.0, MAE = 0.77 Vol-%) in the calibration period. The modelled soil moisture level is in good agreement with measured soil moisture levels in WREF. In WB5 and WD5, modelled soil moisture levels are lower than observed in January and February. During the rest of the year, modelled and observed soil moisture levels are in good agreement. The temporal soil moisture course is mostly well represented: Modelled soil moisture peaks in February, March, June and October are well represented in WREF. However, the magnitude of these soil moisture peaks is slightly higher in the model than in the observations. In WB5, the observed soil moisture increase in February and June are reproduced slightly later by the model. The observed increase in October, however, is well reproduced by the model. In WD5, the timing of the observed soil moisture increase in March is well reproduced, however, the soil moisture increases steeper in the model than in the observations. The soil moisture increase in autumn is earlier reproduced by the model than observed. The decreasing soil moisture in spring and summer is well reproduced in WREF, WB5 and WD5.

In the validation period, modelled soil moisture in 50 cm depth is in good agreement with mean observed soil moisture in WREF (NSE = 78.2, MAE = 0.45 Vol-%), WB5 (NSE = 69.7, MAE = 1.2 Vol-%) and WD5 (NSE = 61.7, MAE = 0.68 Vol-%). The deviation of modelled from measured soil moisture is low, but slightly higher than in the calibration period in WREF and WD5. In several months, modelled soil moisture is slightly lower than observed in WREF. In WB5, the model systematically overestimates the soil moisture level in the entire validation period. In WD5, the modelled soil moisture level is in good agreement in winter and slightly lower than observed from spring until autumn. The temporal course is mostly well represented: The modelled soil moisture peak in January in WD5 is earlier than observed, but the soil moisture peak in March is well represented in all plots. However, the magnitude of soil moisture peaks is slightly higher in the model than in the observations. The decreasing soil moisture in spring and summer, as well as the slight soil moisture increase in autumn are well reproduced by the model in WREF and WD5. In WB5, the sudden

decrease in July and August is not reproduced by the model. In general, soil moisture dynamics in 200 cm depth are well reproduced in both plots in the calibration and validation period.

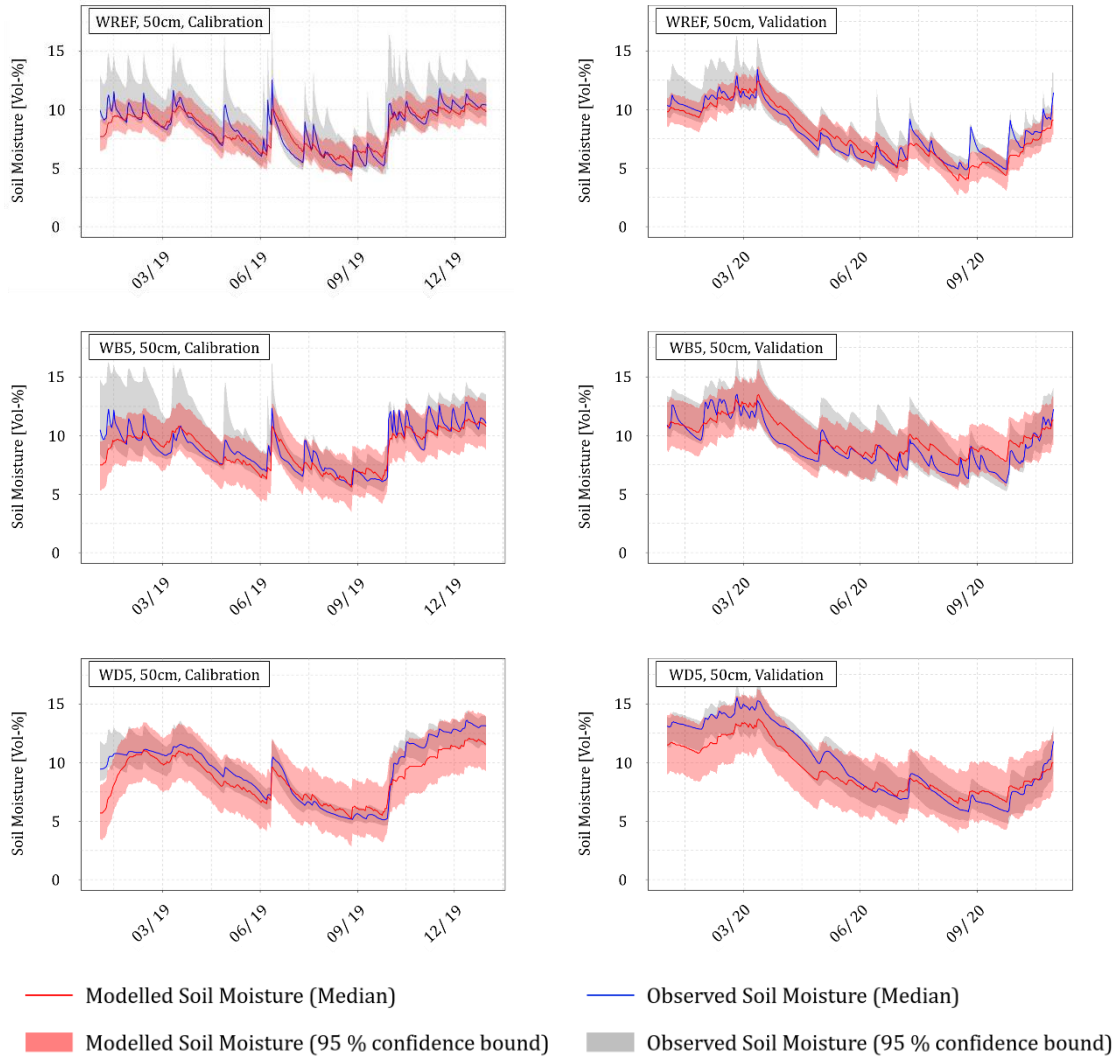

Figure 63: ***Observed and modelled soil moisture in 50 cm depth after model calibration in WREF, WB5 and WD5*** *in the calibration period (01/2019 – 12/2019) and validation period (01/2020 – 10/2020). Median and 90 % confidence bound of modelled soil moisture are given as solid line and envelope in red, respectively. Median and 90 % confidence bound of observed soil moisture are given as solid line and envelope in blue and grey, respectively.*

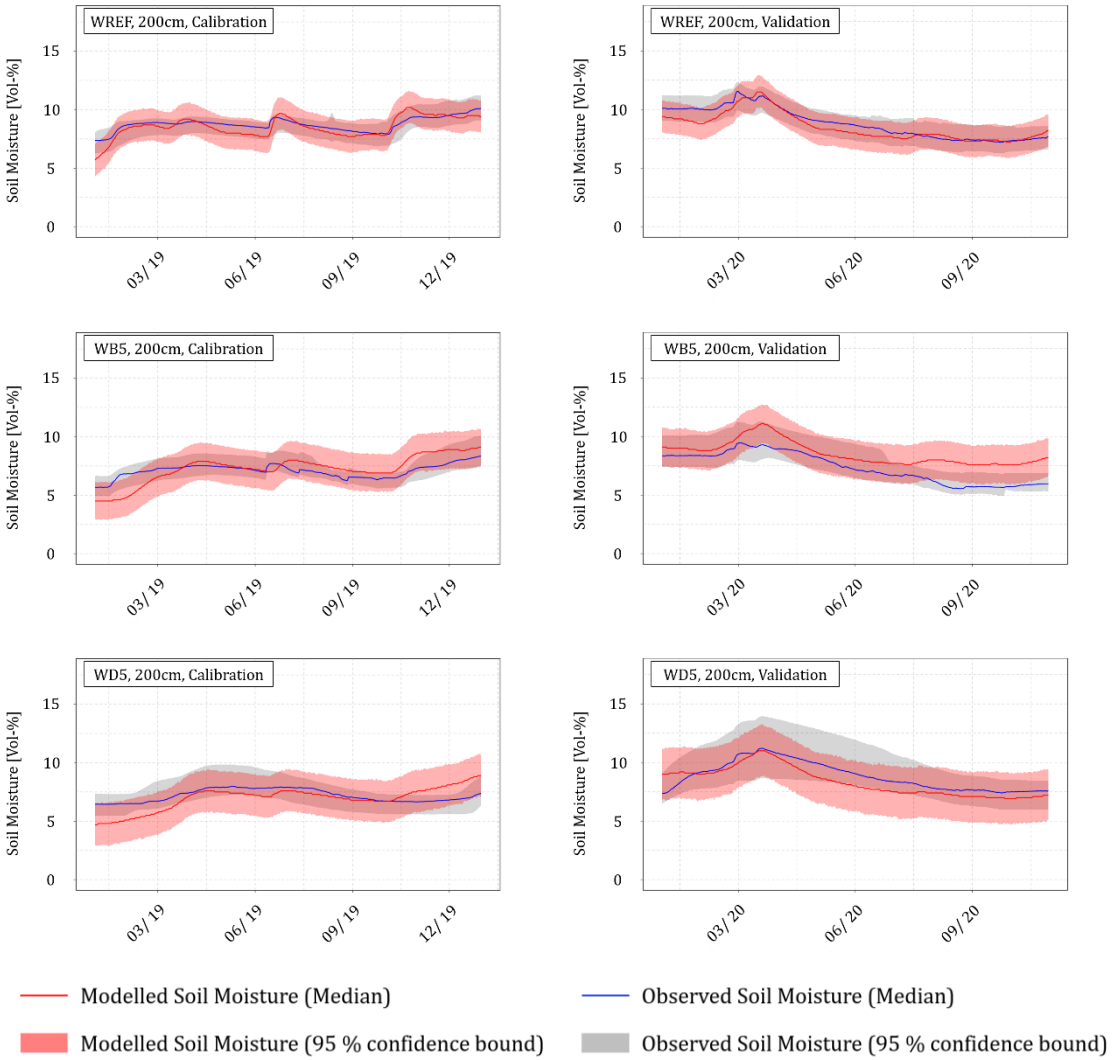

Figure 64: ***Observed and modelled soil moisture in 200 cm depth after model calibration in WREF, WB5 and WD5*** *in the calibration period (01/2019 – 12/2019) and validation period (01/2020 – 10/2020). Median and 90 % confidence bound of modelled soil moisture are given as solid line and envelope in red, respectively. Median and 90 % confidence bound of observed soil moisture are given as solid line and envelope in blue and grey, respectively.*

4.3.9 Modelled water balance and deep seepage rates

With the successfully calibrated model, all terms of the water balance are calculated for WREF, WB5 and WD5. Figure 65 shows monthly precipitation (P), interception evaporation (I_T), transpiration (T_T), ground evaporation (E_S) and deep seepage (S_D) sums in the entire calibration and validation period (01/2019 – 10/2020). The water fluxes show a characteristic seasonal course, which is similar in WREF, WB5 and WD5: Transpiration is negligible in winter and increases significantly in spring and summer with rising temperatures. Interception is an important process all year round in all plots. Interception sums are especially high in months with high precipitation sums. Soil evaporation only plays a negligible role in all plots in the entire period. The seasonal course of deep seepage is the result of the interplay of precipitation and evapotranspiration: In January 2019, deep seepage is low in WREF and negligible in WB5 and WD5 as precipitation has not entirely filled the soil water storage yet. In late winter and early spring 2019, deep seepage increases slightly in all plots as a result of precipitation input and low evapotranspiration rates. In spring 2019, as transpira-

tion rates increase with rising temperatures and increasing solar radiation input, deep seepage rates decrease to a lower level. In summer 2019, thunderstorms cause a rise in deep seepage rates, however, the seepage amounts remain at a comparably low level. With abundant precipitation sums in October 2019, deep seepage rates increase and remain at a comparably high level in winter 2019/2020 with a maximum in March 2020 after abundant rainfall in February 2020. In spring and summer 2020, deep seepage rates again decrease considerably to a very low level. Thereby, deep seepage rates in WREF are at a higher level than in WB5 and WD5.

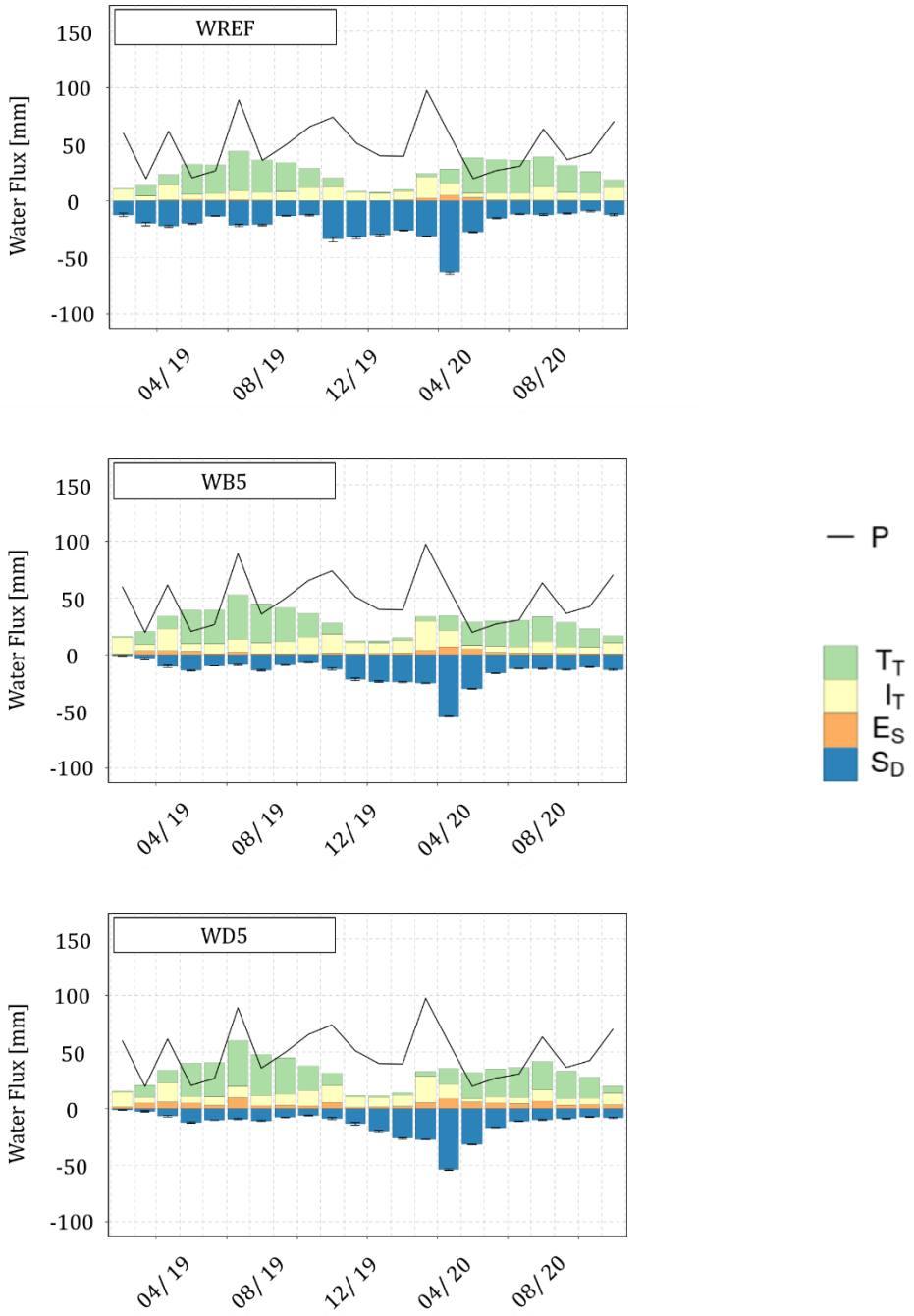

Figure 65: ***Monthly water budgets*** *in WREF, WB5 and WD5: Precipitation (P), transpiration (T_T), interception (I_T), soil evaporation (E_S) and deep seepage (S_D) sums in the period 01/2019 – 10/2020.*

Figure 66 shows median sums of precipitation (P), interception (I_T), stand precipitation (SP), transpiration (T_T), soil evaporation (E_S) and deep seepage (S_D) for WREF, WB5 and

WD5 in the entire modelling period (01/2019 – 10/2020). The precipitation sum is 1079 mm. In WREF, stand precipitation sums up to 889 mm, which is 82 % of precipitation. The corresponding interception rate is 18 %. In WB5, stand precipitation is 78 % of precipitation and thus 5 % lower than in WREF. Correspondingly, the interception rate in WB5 is 22 % and thus 23 % higher than in WREF. In WD5, stand precipitation is 80 % of precipitation and thus 3 % lower than in WREF. Correspondingly, the interception rate in WD5 is 20 % and thus 12 % higher than in WREF. Transpiration is at a similar level for all plots, being 35 to 37 % of precipitation. Soil evaporation is very low in all plots being 2 % of precipitation in WREF, 4 % in WB5 and 9 % in WD5. The deep seepage sum is 472 mm in WREF, which accounts for 44 % of precipitation. Deep seepage sums are at a comparable level in WB5 and WD5, being 26 % and 34 % lower than in WREF, respectively.

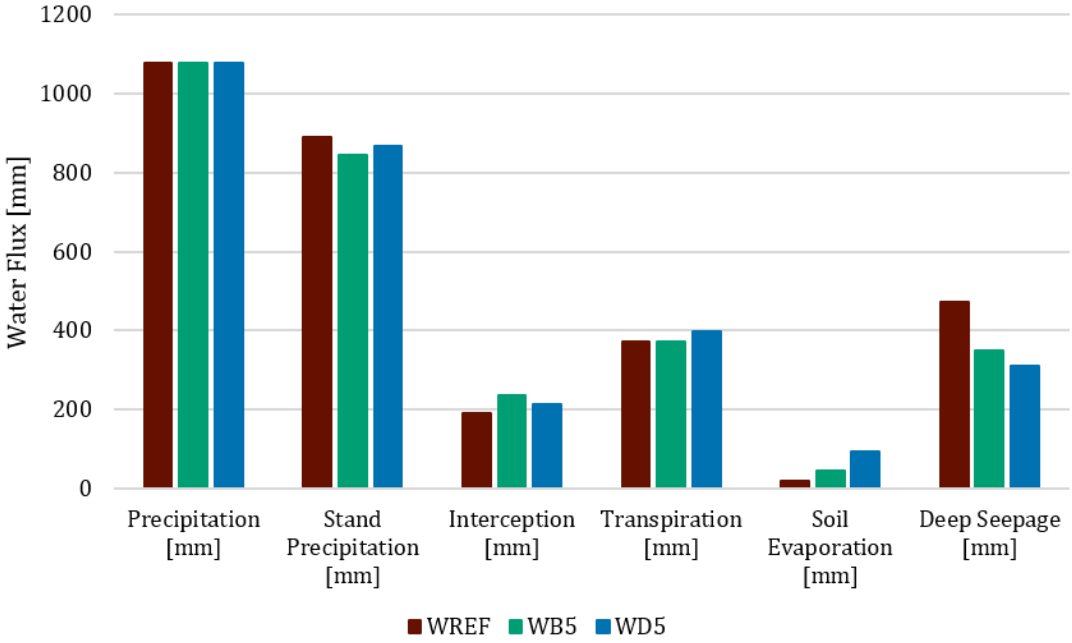

Figure 66: ***Total modelled water fluxes in WREF, WB5 and WD5:*** *Precipitation (P), transpiration (T_T), interception (I_T), soil evaporation (E_S) and deep seepage (S_D) sums in the period 01/2019 – 10/2020.*

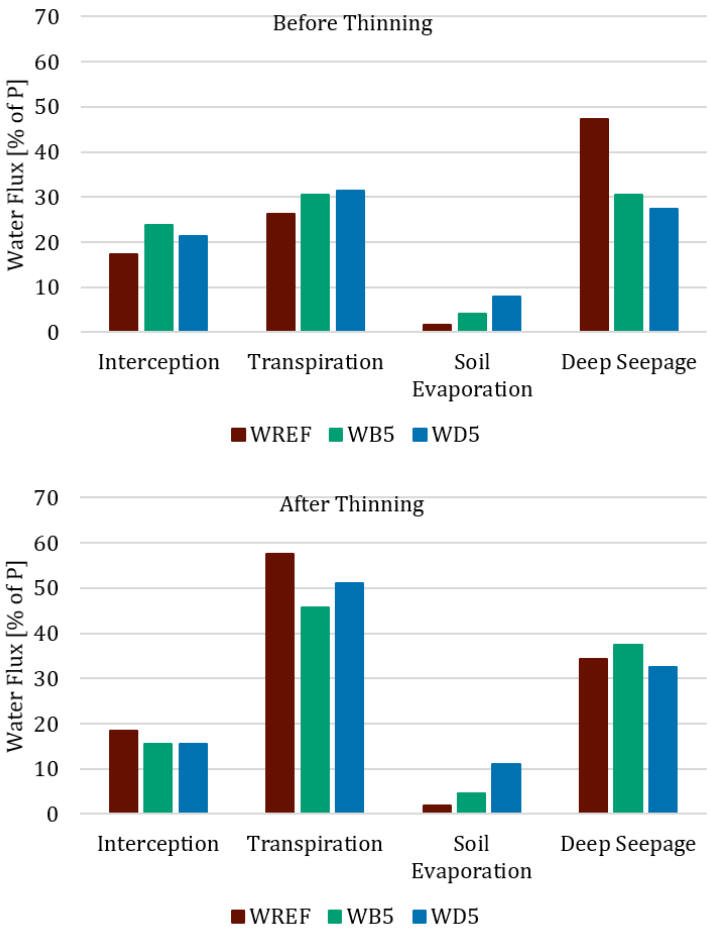

Figure 67: Modelled water fluxes in WREF, WB5 and WD5 before (top) and after thinning (bottom): Interception, transpiration. soil evaporation and deep seepage [% of P] in the period before thinning (01/2019 – 02/2020) and after thinning (04/2020 – 10/2020).

Figure 67 compares interception, soil evaporation, transpiration and deep seepage sums before thinning (01/2019 – 02/2020) and after thinning (04/2020 – 10/2020) between WREF, WB5 and WD5. Before thinning, interception is highest in WB5 and lowest in WREF with WD5 in between. After thinning, interception is slightly lower in WB5 and WD5 compared to WREF. Before thinning, transpiration is highest in WD5 and lowest in WREF, with WB5 in between. After thinning, transpiration is highest in WREF and slightly lower in WD5 and WB5. Ground evaporation only plays a minor role at all plots in both periods. Before thinning, deep seepage is highest in WREF and considerably lower in WB5 and WD5. After thinning, deep seepage is highest in WB5 and slightly lower in WREF and WD5. Thinning thus decreases transpiration and interception and increases deep seepage considerably.

Table 51: ***The effect of thinning on modelled water fluxes in WB5 and WD5****: Sums of precipitation, interception, stand precipitation, transpiration, ground evaporation and deep seepage [mm] in WB5 and WD5 for the period 04/2020-10/2020. Thereby, vegetation parameters before thinning (no thinning) and after thinning (thinning) are used. Additionally, the difference (Δ) between both scenarios is calculated.*

	no thinning	thinning	Δ
	WB5		
Gross Precipitation	290 mm	290 mm	-
Interception	73 mm	45 mm	-38 %
Stand Precipitation	217 mm	245 mm	+13 %
Transpiration	199 mm	173 mm	-13 %
Ground Evaporation	5 mm	8 mm	+65 %
Deep Seepage	84 mm	104 mm	+24 %
	WD5		
Gross Precipitation	290 mm	290 mm	-
Interception	66 mm	45 mm	-31 %
Stand Precipitation	224 mm	245 mm	+9 %
Transpiration	212 mm	203 mm	-4 %
Ground Evaporation	8 mm	13 mm	+60 %
Deep Seepage	86 mm	93 mm	+8 %

The effect of thinning on interception, evapotranspiration and deep seepage is investigated by modelling the water fluxes with two different model parameter sets in the period 04/2020 – 10/2020. The first model parameter set is the same as used for the period before thinning (no thinning), and the second parameter set is the same as used for the period after thinning (thinning). In the "no thinning" scenario, the thinning parameter *densef* is 1, which corresponds to a *maxlai* of 2.8 in WB5 and 2.4 in WD5. In the "thinning" scenario, the thinning parameter *densef* is 0.59 in WB5 and 0.67 in WD5, which corresponds to a *maxlai* of 1.656 in WB5 and 1.602 in WD5. Table 51 shows the resulting water fluxes of the scenarios "thinning" and "no thinning" as well as their difference for WB5 and WD5, respectively. Thinning of the pine stand led to a decrease in interception by 38 % in WB5 and by 31 % in WD5. Stand precipitation, at the same time, increased by 13 % in WB5 and by 9 % in WD5. Transpiration decreased by 13 % in WB5 and by only 4 % in WD5. Ground evaporation remained at a low level. Deep seepage rates increased by 24 % in WB5 and by 8 % in WD5.

5. Discussion

The research objective was to quantify the effect of forest conversion of coniferous pine forests on seepage amounts in Northwest Germany as accurately as possible. These results are transferable to a large share of forest locations in Northwest Germany. Hence, these data provide a profound basis on which the role that forest conversion may play in order to increase deep seepage rates at the landscape level can be discussed.

5.1 Discussion of measurement results

5.1.1 Discussion of vegetation parameter measurements

Stand density and **basal area** of the studied forests can be compared to similar forest plots in Northeast Germany described in Müller (2019). The selected **pure pine** forests can be compared to several similar forests from Northeast Germany. Stand densities are 600 ha^{-1} in Sandkrug, 400 ha^{-1} in Elze and 500 ha^{-1} in Wibbese. These stand densities are slightly lower than in comparative pure pine forests in Northeast Germany (700 ha^{-1} – 900 ha^{-1}). Corresponding basal areas are 36 m^2 ha^{-1} in Sandkrug, 34 m^2 ha^{-1} in Elze and 45 m^2 ha^{-1} in Wibbese. This is in a similar range as found for comparative Northeast German pine forests (26 m^2 ha^{-1} – 39 m^2 ha^{-1}), however, the basal area in Wibbese is slightly higher.

Stand densities and basal areas of the selected **mixed pine stands with beech and Douglas fir** can be compared to three comparable mixed pine and beech stands of varying ages in Northeast Germany. Stand densities for pine of the selected mixed pine stands with 5 years old beech and Douglas fir trees are 390 ha^{-1} in Elze (EB5), 640 ha^{-1} in WB5 and 500 ha^{-1} in WD5. In WB5 and WD5, stand densities are reduced to 460 ha^{-1} and 300 ha^{-1} after thinning, respectively. This is in good agreement with stand densities in mixed pine and beech forests in Northeast Germany (340 ha^{-1} – 590 ha^{-1}). Corresponding basal areas are 31 m^2 ha^{-1} in EB5, 53 m^2 ha^{-1} in WB5 and 62 m^2 ha^{-1} in WD5 (reduced to 38.4 m^2 ha^{-1} in WB5 and 37.3 m^2 ha^{-1} in WD5 after thinning). For mixed pine and beech forests in Northeast Germany, basal areas between 25 m^2 ha^{-1} and 35 m^2 ha^{-1} are reported. Thus, basal areas in Wibbese are higher than in comparable forests. Corresponding stand densities for beech and Douglas fir are 4500 ha^{-1} in EB5, 3800 ha^{-1} in WB5 and 3400 ha^{-1} in WD5. They are thus lower than 8200 ha^{-1} as found in a comparable mixed pine (51 a) and beech (11 a) forest in Northeast Germany.

Stand densities and basal areas for pine of the selected mixed pine stands with 15 to 20 years old beech trees can be compared to comparable mixed pine (76 a) and beech (33 a) forest in Northeast Germany. Stand densities are 390 ha^{-1} in SB20 and 290 ha^{-1} in EB15. This is lower than the pine stand density of 470 ha^{-1} in the comparable forest. Corresponding basal areas are 32 and 29 m^2 ha^{-1}, which is at the same level as the pine basal area of 32 m^2 ha^{-1} in the comparative forest. Corresponding beech stand densities are 4500 ha^{-1} in SB20 and 3100 ha^{-1} in EB15, which is denser than 2100 ha^{-1} in the comparable forest. Corresponding basal areas are 8.1 m^2 ha^{-1} in SB20 and 5.5 m^2 ha^{-1} in EB15, which is in good agreement with 7.3 m^2 ha^{-1} in the comparable forest.

The stand density of the selected **pure beech** forest in Elze (EB25) is 1908 ha^{-1} and the corresponding basal area is 7.3 m^2 ha^{-1}. This beech forest is younger than investigated pure beech forests from Müller (2019), but it can be compared to the mixed pine (76 a) and beech (33 a) forest instead. Both stand density and basal area are similar to the comparable forest.

Measured LAI values can be compared to literature values. In the **pine** stands in Sandkrug, Elze and Wibbese, measured LAI values mostly range between 2.5 and 3.5. These values correspond well with LAI values reported in the literature for Scots pine stands ranging between 1.1 and 3.4 (Bealde et al. 1982, Bréda 2003, Lovynska et al. 2018, Soudani et al. 2002). Literature LAI values of **beech** forests are generally higher than in pine stands and vary between 2.6 and 9.5 in beech forests of varying ages (Bréda 2003, Černý et al. 2018, Kram 1998, Leuschner et al. 2006, Meier & Leuschner 2008). The LAI of 5.2 found for EB25 is in good agreement with the LAI of 5.53 in a 22 years old beech stand found by Bartelink (1997). The SAI of 0.5 for E B25 is higher than reported literature values (SAI = 0.26 in a 19 years old beech stand, (Černý et al. 2018)). This high value can be explained by brown leaves that remain at the trees in E B25 during winter, which contribute to SAI. The results of the leaf area measurements in this study are in good agreement with leaf area values reported in the literature. However, measured LAI values vary within one year due to different light regimes as well as leaf and needle fall.

Significant **ground vegetation** in the form of shrubs, grasses and mosses is present in the pure pine forests. 5 years after forest conversion began, this ground vegetation is still present (EB5, WB5, WD5) and competes with parent trees and young emergent trees for water. Only about 10 to 15 years after the start of forest conversion does the ground vegetation slowly retreat, to disappear almost completely after a few years (SB20, EB15, EB25). Thus, after ground vegetation and tree vegetation compete for water during the first 15 years, this competition visibly dissipates in subsequent years.

5.1.2 Discussion of stand precipitation measurements

Measured stand precipitation or interception is one state variable used to calibrate the interception parameters of the model. In **Sandkrug**, interception is mostly higher than reported literature values: Mean interception in **SREF** in both 2019 and 2020 (38 %) is higher than most of the interception values reported for pine in the literature that range between 25 % and 35 % (Ahrends & Penne 2010, Alvera 1976, Mohr 2001, Mohr et al. 2005, Müller 2012). Mean interception in SREF is also slightly higher than interception in the same area found by Mohr (2001), Mohr et al. (2005) between 1996 and 1999 (30 %) and in 2002 (35 %). Mean interception in **SB20** in both 2019 (51 %) and 2020 (50 %) is higher than reported literature values for mixed pine and beech stands, which are usually lower than in pure pine stands. They are also considerably higher than the interception measured in a comparable mixed forest with pine (76 a) and young beech (33 a) of 26 % found by Müller (2012).

For Sandkrug, it was hypothesized that stand precipitation increases (and interception decreases) from SREF to SB20. Stand precipitation measurements, however, indicate that stand precipitation decreases from SREF to SB20. The stand densities of pine in SREF (SD = 612 ha^{-1}) and SB20 (SD = 389 ha^{-1}) would suggest a higher interception in SREF than in SB20. The beech, however, grows very dense in SB20 (SD = 4496 ha^{-1}), which increases interception rates in summer considerably. This is supported by summer PAI values that are considerably higher in SB20 than in SREF. In winter, however, beech trees lose their leaves and do not contribute substantially to winter PAI in SB20. Winter PAI in SB20 is slightly higher than in SREF, despite higher stem numbers of pine in SREF. In SB20, the majority of pine trees is more dominant according to Kraft's classification (Kraft 1884) than in SREF. These dominant trees with denser crowns intercept more precipitation than less dominant

trees. This causes higher interception rates in SB20 than in SREF, even though stem numbers in SB20 are lower than in SREF.

Interception in **Elze** is in good agreement with interception reported in the literature: Mean interception in **EREF** being 28 % (2019) and 26 % (2020) is well within the range between 25 % and 35 % found for pine in the literature (Ahrends & Penne 2010, Alvera 1976, Mohr 2001, Mohr et al. 2005, Müller 2012). Interception in **EB5** is similar to interception in EREF. This, however, does not agree with lower PAI and stand density measurements in EB5 compared to EREF. In EB5, individual pine trees are more dominant than in EREF, which might explain higher interception rates compared to EREF. However, only few stand precipitation data are available for EB5 so far and the results thus need to be interpreted carefully. Interception in **EB15** being 28 % (2019) and 25 % (2020) is slightly lower than in EREF, which corresponds well with slightly decreased interception values of 26 % in a comparable mixed forest of pine (76 a) and young beech (33 a) found by Müller (2012). This is also in good agreement with Ringe et al. (2000), who found a lower interception in a mixed pine and beech forest compared to a pure pine forest at a forest site nearby. Interception in **EB25** being 18 % (2019) and 11 % (2020) is lower than in EREF and is also lower than interception values between 20 % and 30 % found for beech in the literature (Mosello et al. 2002, Müller 2012, Staelens et al. 2008). However, the beech forest in EB25 is younger than those beech forests for which interception values are found in the literature. It is therefore plausible that interception in EB25 is lower than literature values. The interception of less than 10 % in EB25 in the leafless period, however, corresponds well with interception in a leafless beech forest investigated by Staelens et al. (2008).

Measured interception in Elze corresponds only to some extent with measured PAI: In summer, PAI is higher in EB25 than in EREF and EB5. In turn, interception in EB25 is lower than in EREF and EB5. This is the result of different interception storage capacities of needles and flat beech leaves. The storage capacity of needles is a multiple of the storage capacity of flat beech leaves (Zhao et al. 2019). Thus, interception in EB25 is lower than in EREF, even though PAI values are considerably higher. This also explains the only small difference in summer interception rates between EB15 and EREF, when PAI values in EB15 are also considerably higher than in EREF.

Interception in **Wibbese** is in good agreement with interception reported in the literature: Mean interception varies between 20 % and 30 % and is thus at the lower end of interception rates found for pine forests in the literature (Ahrends & Penne 2010, Alvera 1976, Mohr 2001, Mohr et al. 2005, Müller 2012). Between WREF, WB5 and WD5, differences in stand precipitation are found **before thinning**: Interception is highest in WB5 (27 %) and lowest in WREF (21 %), with WD5 (26%) in between. This is partly the result of different stand densities, which is highest in WB5 (SD = 640 ha^{-1}) and considerably lower in WREF (SD = 494 ha^{-1}) and WD5 (SD = 500 ha^{-1}). In WB5, the beech trees are still very small and do not yet affect stand precipitation considerably. In WD5, the Douglas fir trees are slightly higher than the beech trees in WB5 and very likely already reduce stand precipitation to some extent due to the increased interception storage capacity of their needles. Moreover, some pine trees are more dominant than in WREF and WB5 and thus further increase interception rates in WD5. Thus, current differences in stand precipitation between WREF, WB5 and WD5 are the result of pine stand density, pine social class and the height of the young trees in the stand. **After thinning**, measured interception losses are very similar in WREF, WB5 and WD5, even though the stand density in WD5 (SD = 300 ha^{-1}) is considerably lower than

in WB5 (SD = 460 ha^{-1}) and WREF (SD = 494 ha^{-1}). In WD5, the dominant trees and the growing Douglas fir cause similar stand precipitation rates as in WB5 and WREF, where stand densities are higher.

Measured interception in Wibbese partly agrees with measured PAI: Before thinning, WREF has the lowest PAI and the lowest interception rate. In WB5 and WD5, PAI and interception were higher than in WREF before thinning. After thinning, PAI is highest in WREF and lower in WB5 and WD5, which is to some extent reflected in lower interception values in WB5 and WD5.

In general, stand precipitation or interception measurements are in good agreement with literature values: Interception in pure coniferous forests is higher than in pure deciduous forests (EREF vs. EB25). The interception in mixed broadleaved and coniferous stands ranges between that of pure stands (EB15 vs. EREF and EB25). In mixed stands with very young trees (EB5, WB5, WD5), the young trees affect stand precipitation only slightly. Instead, the pine crown's structure and density governs interception. Young evergreen trees such as Douglas fir in WD5, however, are expected to have a greater influence on interception in the future because of their bigger leaf area and thus higher interception storage capacity. Moreover, the social class of tree individuals also affect the amount of stand precipitation (EB5, SB20). In multi-layered pine and beech forests, stand precipitation is thus linked to the canopy density of the pine layer, the mixing ratio of pine and beech trees, the stem number and distribution of beech trees and the presence or absence of ground vegetation.

Stem flow very likely still plays only a minor role in EB5 and WB5, as Müller (2012) do not report stem flow amounts for a mixed pine (33a) and beech (11 a) forest. However, he found stem flow increasing the infiltration rate by approximately 12 mm per year in a mixed pine (76 a) and beech (33 a) forest. In SB20 and EB15, the beech trees are still younger and stem flow very likely accumulates to less than 10 mm per year. In EB25, the beech trees are slightly younger and stem flow very likely accumulates to a similar amount as found by Müller (2012). This is still a very small amount compared to stand precipitation. Within the next years, however, stem flow will become more relevant for the amount of deep seepage: Stem flow will increase with growth of the beech trees and stem flow water will be distributed in the forest soil depending on the stand density of the beech trees. In dry periods, stem flow increases the soil moisture in the upper soil layers and thus supplies water to the tree and ground vegetation. Outside the growing season, stem flow water directly becomes deep seepage and increases the total deep seepage rate significantly (Müller 2012).

5.1.3 Discussion of soil moisture measurements

Measured soil moisture in 50 cm and 200 cm depth is an important state variable for calibrating the hydrological model. In order to capture the great **soil moisture variability** present in forest soils (Morgenstern et al. 2011), a large number of parallel soil moisture sensors (7 in Sandkrug, 8 in Elze and Wibbese) is used for every soil depth. The resulting soil moisture variability is thereby different among the forest plots: It is generally higher in 50 cm than in 200 cm depth. In 50 cm, the highest variability is found in EB5, SREF and SB20. In 200 cm, the highest variability is found in SB20, WD5 and EB25.

Measured **soil moisture levels** are mostly plausible: The measurements in 50 cm depth show soil moisture levels of 10 % to 12 % at field capacity and below 5 % during dry conditions in summer 2020 in SREF, SB20, EREF, EB5, EB15 and EB25. In Wibbese, soil moisture levels are slightly higher ranging between 5 % and 8 % in summer and between 9 % and 15 % in winter. In 200 cm depth, soil moisture levels in summer are slightly higher than in 50 cm depth and range between 6 % and 10 %. In winter, soil moisture levels in 200 cm show greater variations and range between 7 % and 13 %. Measured soil moisture levels at field capacity are in good agreement with field capacity values of 8 – 15 % given for sand by Sponagel (2005).

Soil moisture levels differ to some extent between the forest plots: In Sandkrug, soil moisture levels in SB20 are higher than in SREF both in summer and in winter, especially in 200 cm depth. This can be explained by a slightly higher silt content in SB20 in 200 cm depth, which causes an increased water holding capacity of the soil. Moreover, a single sensor registered soil moisture peaks resulting from high precipitation amounts caused by thunderstorms during summer 2019 in SB20. This implies preferential saturated water flow down to 200 cm depth. These preferential flow peaks do not occur in SREF. In Elze, EB25 shows a slightly higher and EB15 a slightly lower soil moisture level compared to EREF and EB5, which is very likely a result from slightly different grain size distributions of the soil. In Wibbese, winter soil moisture levels in 200 cm depth are higher in 2020 (9% - 11 %) than in 2019 (7 % - 8 %). These lower soil moisture levels in winter 2019 probably result from very dry previous soil conditions in 2018 and a relatively low winter precipitation sum. In general, the soil moisture measurements are generally plausible and reliable for all forest plots.

5.2 Discussion of modelled deep seepage and evapotranspiration

5.2.1 Calibration of model parameters

In order to reproduce measured stand precipitation and soil moisture, several model parameters are adjusted within given ranges. In a first step, the **model interception parameters** were calibrated manually. Resulting model LAI and SAI values correspond well with measured values, with only minor adjustments. The resulting interception storage capacities are in the same order as suggested by Federer (2019), Schmidt-Walter (2019), Zhao et al. (2019) for pine, beech and mixed pine and beech forests. However, interception storage capacities in Wibbese are lower than 1-2 mm as suggested for pine forests by Federer (2019) and the interception storage capacity in EB25 is also lower than suggested for example by Schmidt-Walter (2019). The so calibrated model reflects measured stand precipitation sums well. The resulting goodness-of-fit of modelled and observed stand precipitation is satisfactory for all observation plots, which is expressed in low MAE values (mostly < 1.0 mm) and NSE values being close to 1.

In a second step, model parameters affecting **modelled soil moisture** in 50 cm and 200 cm depth were calibrated automatically. Modelled and observed soil moisture first showed a significant offset. There are several possible reasons for this large offset: Measured soil moisture may be systematically underestimated by the soil moisture sensors due to a lacking site-specific sensor calibration (Bogena et al. 2017, Jackisch et al. 2020). On the other hand, the PTF by Wösten et al. (1999) used to derive the MvG parameters can only approximate the soil hydraulic properties. However, the PTF of Wösten et al. (1999) is found to be very robust to approximate the MvG parameters based on measured grain size distributions

(Weihermüller et al. 2021). The choice of PTF, however, can substantially affect simulated water fluxes and the soil water content that is stored in the soil matrix (Weihermüller et al. 2021). The calibration of the parameters *alpha*, *npar* and *ksat* improved the goodness-of-fit of modelled and observed soil moisture significantly. Thereby, parameter values of *alpha* and *npar* are hold within feasible ranges found for sandy soils (Ad-hoc-Arbeitsgruppe Boden 1999, Gupta et al. 2021, Wösten et al. 1999). Initially, *alpha* values as derived by the PTF (Wösten et al. 1999) were between 3.35 and 6.68. After model calibration, *alpha* ranges between 5.0 and 13.86. This range is above the range found for example in Wösten et al. (1999), but it is well within the range given for example in Ad-hoc-Arbeitsgruppe Boden (1999). The parameter ranges can thus be regarded as reliable. Initially, *npar* values as derived by the PTF (Wösten et al. 1999) range between 1.19 and 1.76, after model calibration *npar* ranges between 1.65 and 2.0. This is slightly higher than reported ranges in the literature (Ad-hoc-Arbeitsgruppe Boden 1999, Wösten et al. 1999). Initially, *ksat* values as derived by the PTF (Wösten et al. 1999) ranges between 561 and 1812, after model calibration *ksat* ranges between 1694 and 5472. This is higher than ranges found by Wösten et al. (1999), but it is well in the range for sand found by Gupta et al. (2021).

In a third step, the remaining sensitive **evapotranspiration and infiltration parameters** were calibrated and the fit of modelled and observed soil moisture was thus further improved. These parameters were calibrated for each plot individually. The **maximum plant conductance** (*mxkpl*) ranges between 2 and 5.6 mm d^{-1} MPa^{-1} in Sandkrug, between 2.0 and 2.6 mm d^{-1} MPa^{-1} in Elze and between 2.0 and 2.2 mm d^{-1} MPa^{-1} in Wibbese. *Mxkpl* values are thus lower than 8 mm d^{-1} MPa^{-1} as suggested for coniferous and deciduous forests by Federer (2019). Between the forest plots, mxkpl does not differ significantly. The **minimum plant leaf water potential** (*psicr*) has a wide range in SREF (between -1.5 and -3.0 MPa) and a narrow range in Wibbese, SB20, EREF and EB5 with ranges between -1.5 and -1.6 MPa. In EB15 and EB25, the range for *psicr* is medium (between -1.5 and -1.9 MPa). In the literature, *psicr* is found to range between -3.0 and -1.5 MPa and is species-dependent (Federer 2015b, Hinckley et al. 1978). Turgor loss points have been reported to be -1.5 MPa for pine (Irvine et al. 1998, Zweifel et al. 2007). However, under drought conditions, needle water potentials less than -2 MPa have been reported (Poyatos et al. 2013) and Kunert (2020) found a turgor loss point of -2.24 (+-0.054 MPa) during drought conditions in 2019. For beech, turgor loss points of -2.62 (+-0.02) MPa (Kunert 2020) and -2.6 MPa (Leuschner et al. 2019) have been found. Bartlett et al. (2012) indicate similar turgor loss points for temperate broadleaved and coniferous forests. The calibrated *psicr* values agree well with the values found in the literature and also the differences between the plots are only small. The **infiltration depth** (*ilayer*) ranges between 60 cm and 110 cm in Sandkrug, between 100 cm and 120 cm in Elze and between 120 cm and 150 cm in Wibbese. Thereby, water is predominantly directly routed to the lower soil layers in Sandkrug, EB25 and WREF, and uniformly distributed in the remaining forest plots. These infiltration depths indicate that a certain proportion of infiltrating water is directly routed to lower soil layers via macropore or preferential flow pathways, which are very common in forest soils (Guo & Lin 2018). However, infiltration seems to be overemphasized to some extent in all plots as modelled soil moisture in 50 cm depth reacts to every precipitation event, which is not shown by observed soil moisture in 50 cm depth.

The **maximum leaf vapour conductance** when stomata are fully open (*glmax*) was not included in model calibration and was set to 0.0053 m s^{-1} for all plots as suggested by

Federer (2019). This agrees well with Körner (1995), who reported that *glmax* does not differ among the major woody plants. Recently, Hoshika et al. (2018) found that short-lived leaves may have a higher glmax and photosynthetic capacity than long-lived leaves of forest tree species. *Glmax* for evergreen trees is thus found being 37 % lower than for deciduous trees. The assumption of similar *glmax* for all plots must therefore by questioned. Future modelling studies should take species-dependent *glmax* values into account and they should assess the effect of different *glmax* values on model results

5.2.2 Modelled transpiration and soil evaporation

Modelled **transpiration** can be compared to findings from Müller (2012), who reported transpiration of different forests in the vegetation period. Modelled transpiration rates in summer 2020 are higher than in summer 2019. Transpiration generally depends on meteorological conditions and relative transpiration rates in comparison to gross precipitation sums vary from year to year and are thus difficult to compare to literature values.

Müller (2012) found lower transpiration rates in pure pine forests than in pure beech and mixed pine and beech forests. In **Sandkrug**, modelled transpiration rates are higher in SREF than in SB20. This can be explained by the higher interception rate in SB20 compared to SREF, which reduces the infiltration rate. Thus, soil water available for transpiration is higher in SREF than in SB20. In addition, the turgor-loss point in SREF is lower than in SB20, which means that stomas close earlier in SB20 than in SREF under drought conditions and thus limit transpiration. Moreover, soil vegetation also transpires substantial amounts and therefore causes higher transpiration in SREF compared to SB20. In **Elze**, modelled transpiration is at the same level in EREF and EB5, which is plausible, as the young beech trees in EB5 do not have a significant influence yet. The transpiration rate in EB15 is higher than in EREF and EB5, which agrees well with the finding from Müller (2012). The transpiration rate in EB25, however, is below that of the other plots. This appears to be reasonable, as the beech forest is younger than comparable beech forests in the literature (Müller 2012). In **Wibbese**, modelled transpiration rates are comparable for all plots. This is plausible, as the pine tree layer is comparable for all plots and the young beech and Douglas fir trees do not contribute significantly to stand transpiration.

Modelled **soil evaporation** rates are very low in all stands. In LWF-Brook90R, soil evaporation occurs only when the soil is saturated. Moreover, ground evaporation extracts water only from the top soil layer, no matter how thick this layer is (Federer 2019).

5.2.3 Modelled deep seepage

Modelled **deep seepage** can be compared to findings from the literature (Klinck et al. 2012, Mohr 2001, Mohr et al. 2005, Müller 2011, 2012, Ringe et al. 2000, Schultze & Scherzer 2015). Annual deep seepage rates found in Sandkrug, Elze and Wibbese fit well to the range of annual deep seepage rates found by Klinck et al. (2012). Deep seepage rates vary significantly from year to year as they strongly depend on meteorological conditions. Deep seepage found in this study can therefore not directly be compared to literature values, but species-dependent differences can be compared to those found in the literature.

In **Sandkrug**, it was hypothesized that deep seepage increases from SREF to SB20. Modelled deep seepage in SREF and SB20 is at a similar level of 25 % of gross precipitation in 2019 and 2020. This is lower than deep seepage of 50 % of gross precipitation found by Mohr et al. (2005) in the pure pine forest (SREF), but it is higher than deep seepage between 12 %

and 18 % found by Müller (2011) for pine forests in Northeast Germany. There is no significant difference in deep seepage between SREF and SB20, where Müller (2011) found slightly higher deep seepage in a comparable mixed pine and beech forest compared to a pure pine forest. A smaller interception in SREF is counterbalanced by higher transpiration. This higher transpiration may be the result of the transpiration-relevant ground cover (blueberry shrubs, mosses), which is only present in SREF.

In **Elze**, it was hypothesized that deep seepage increases from EREF to EB5 to EB15 to EB25. Modelled deep seepage ranges between 32 % (EB5), 33 % (EREF, EB15) and 58 % (EB25) of gross precipitation. These deep seepage values are higher than those found by Müller (2011) in comparable forest stands in Northeast Germany. However, deep seepage of almost 400 mm in EREF, EB5 and EB15 in the period 01/2019 – 10/2020 correspond well with measured deep seepage of 350 mm to 400 mm within two years (1999, 2000) in a neighboring pure pine and mixed pine and beech forest (Ringe et al. 2000). The comparably small difference between EREF and EB5 results from similar interception and transpiration in these stands. In EB15, a slightly lower interception is counterbalanced by a higher transpiration, which results in a similar deep seepage as in EREF and EB5. In EB25, however, deep seepage is significantly higher. This great difference agrees well with the beneficial effect of broadleaved forests on the seepage rate as reported in the literature (Ellenberg et al. 1986, Harsch et al. 2009, Müller 2011, 2012, Prietzel & Bachmann 2011, Schmidt-Walter et al. 2020b, Schultze & Scherzer 2015).

In **Wibbese**, it was hypothesized that deep seepage decreases from WD5 to WB5 to WREF before thinning. Modelled deep seepage is 47 % of gross precipitation in WREF and approximately 30 % in WB5 and WD5 before thinning. Deep seepage in WREF is considerably higher than in the pine forests in Sandkrug and Elze. Modelled infiltration rates are probably overestimated in WREF, which causes this comparably high deep seepage. Deep seepage in WB5 and WD5 agrees well with deep seepage found for mixed pine stands in Sandkrug and Elze. However, it is higher than deep seepage found by Müller (2011) in comparable forest stands in Northeast Germany. Deep seepage in WB5 and WD5 do not differ significantly, which shows that the young Douglas fir and beech trees do not have a great effect on deep seepage rates yet. For the period after thinning it was hypothesized that deep seepage increases from WREF to WD5 to WB5. For WB5 and WD5 (04/2020 – 10/2020), deep seepage in WB5 (37 %) and WD5 (33 %) increases significantly and is at a comparable level as deep seepage in WREF (34 %). These seepage rates, however, are only limitedly comparable to literature values, as the seepage period only covered 7 months.

Overall, modelled deep seepage for the different forest plots agrees well with findings from the literature. Modelled deep seepage in the pure beech forest is considerably higher than in pure pine forests. Thereby, deep seepage is predominantly generated outside the growing season in winter, when evapotranspiration of the forest vegetation is low. However, as shown in Sandkrug and Elze, forest conversion does not necessarily increase deep seepage in the first conversion stages. Thereby, vegetation characteristics such as canopy density, stand density and tree species mixing ratio affect deep seepage rates the most: Reducing the stem number, the crown density and the mean social class of the pine increases deep seepage. A high share of beech trees compared to pine trees is beneficial for deep seepage amounts, as stem flow of the beech trees will moisten the forest soil in dry periods and directly becomes deep seepage in winter time (Müller 2012). 10 to 15 years after starting the

forest conversion, the competing ground vegetation will disappear and further increase deep seepage.

5.3 Suitability of the methods applied

5.3.1 Methods to measure LAI, stand precipitation and soil moisture

Meteorological variables are measured with professional sensors according to internationally valid standards set by the German Weather Service (DWD) and the World Meteorological Organization (WMO). Regular maintenance ensures the correct functioning of the sensors. Parallel measurement of precipitation sums with a tipping bucket collector and a manual collector (Hellmann) revealed measurement deviations of 6 % - 7 %, with particularly high deviations resulting from high precipitation intensities. These uncertainties are well within the common measurement uncertainty range of 10 % (Haberlandt 2016).

The measurement design to **measure stand precipitation** is inspired by different designs. The combination of several short gutters connected by tubes has to the current state of knowledge never been applied before. Compared to the reference bulk sampler (Hellmann), the precipitation sum measured by a gutter showed only small deviations between 2 % and 4 %, which is well within the common measurement uncertainty range of 10 % (Haberlandt 2016). Uncertainty sources in measured stand precipitation are clogged gutters and variable amount of leaves, needles and bark in the gutters that caused additional evaporation. However, the system worked reliably most of the time and the interception measurements are plausible and agree with measured stand parameters.

Systematically higher interception values measured by single rain collectors in Sandkrug than in Elze and Wibbese (measurements with gutters) indicate a systematic error in the measurement system. This difference might result from different evaporation losses from the single rain collectors and the gutters. The two stand precipitation measurement systems could be validated by parallel measuring with many single rain collectors as suggested by Zimmermann et al. (2016) and Zimmermann & Zimmermann (2014) and with rain gutters.

Due to the distance between the open space where the meteorological variables are measured and the forest plots (1 to 2 km), rainfall amounts can be different and lead to erroneous interception and stand precipitation values. Therefore, special care needs to be taken when convective, small-scaled precipitation events occur.

The **measurement of soil moisture** with TDR and FDR sensors is widely used. Due to the high number of soil moisture sensors, it is possible to account for high spatial soil moisture variability in forest soils. Preferential flow pathways can increase spatial soil moisture heterogeneity and are very common in forest soils. They can increase both infiltration and deep seepage and thus needs to be reflected by soil moisture measurements. Their detection and interpretation for quantitative estimation of water fluxes is still a major challenge in forest hydrology (Guo & Lin 2018).

Observed and modelled soil moisture show an offset in soil moisture level. This offset was reduced by calibrating the MvG parameters. However, it is reported in literature that soil moisture sensors are only to a certain extent able to reflect the absolute soil moisture level adequately (Jackisch et al. 2020). The accuracy of the soil moisture measurements can be improved by a sensor-specific calibration (Bogena et al. 2017).

The measurement depths of 50 cm and 200 cm depth can be considered as reasonable choice as soil moisture signals resulting from precipitation input and root water uptake are clear and pronounced in both depths. The measurements in 200 cm depth also reveal that root water uptake is very heterogeneous in the forest soil, as only some soil moisture sensors show water consumption in this depth. Some studies indicate that the maximum rooting depth in pine and beech forests on sandy soils is below 200 cm (Hertel 1999, Scherfose 1990, Steinmann 2015). Hence, further investigations are necessary to assess the maximum water extraction depth of the tree vegetation. Ideally, the lowest soil moisture sensor depth should correspond with the maximum depth, at which trees extract water in summer.

The **soil** plays an important role in this study. Thorough soil analyses are labor-intensive as many soil samples are needed to account for soil heterogeneity in depth and space. The soil analysis was designed to minimize disturbance to the soil by soil sampling while representing the entire range of soil conditions at a site. A larger number of soil samples would achieve a greater accuracy, however, the soil conditions of the three investigated soil cores from every forest plot were very similar. Hence, further investigations did not appear necessary. The methods used to estimate organic carbon content and bulk density (Blume et al. 2011) are standard methods of soil science and their reliability has been proven many times. The grain size distribution is measured by using particle size distribution based on laser diffraction technology. This is particularly attractive as measurement time is fast and the resulting continuous particle size distribution is reliable and can be classified manually (Eshel et al. 2004).

The **vegetation parameters** LAI, SAI and PAI are crucial in water balance modelling, however, their determination is time-consuming and to some extent error-prone (Yan et al. 2019). The 'true' PAI, LAI and SAI values could only be yielded by destructive methods, such as cutting the trees and directly measure the leaf or needle area in total. However, this was not possible and leaf area measurements were thus carried out indirectly. The DHP and litter fall sampling methods used to obtain PAI, LAI and SAI are widely applied and well documented in Fleck et al. (2016).

The successful derivation of LAI, SAI and PAI from the **DHP** method strongly depends on environmental factors such as light regime, exposure and technical equipment. Hence, comparable environmental and technical conditions are important for repetitive and comparative LAI measurements. To create environmental conditions as uniform as possible, hemispherical photos are only taken at dawn or during foggy and monotonously cloudy weather conditions. However, as light regimes differed slightly for the LAI assessment in the study period, resulting LAI values differed to a certain extent between the assessment dates. This hampered an accurate assessment of the seasonal LAI development within a year. Collecting needle litter could yield more confident leaf area measures that would also reflect seasonal growth patterns. Further uncertainties are associated with ground vegetation and mixed forest stands: The DHP method does not account for low growing vegetation: Digital hemispheric photographs are taken in 1 m height and thus does not account for vegetation below this height. Thus, soil vegetation as well as small trees and shrubs as they are present in EB5, WB5 and WD5 are not considered in the resulting leaf area measurements. In complex multi-species or uneven-aged forests, the plant area is underestimated because lower canopy elements mask upper parts of the canopy (Fleck et al. 2016). In mixed forests with deciduous and evergreen trees, the LAI can accurately be assessed separately for deciduous and evergreen trees. However, this is difficult for two-layered forests with evergreen trees,

as for example in WD5 (pine, Douglas fir). For WD5, the method of leaf area measurement needs to be adjusted in the future in order to assess Douglas fir and Scots pine LAI accurately. In order to overcome the limitations of the DHP method in mixed stands, the LAI has also been measured by means of laser scanning methods in a pilot study (Möhlmann 2021). In this pilot study, laser scanning methods have been used to estimate the leaf area in Elze and to assess, whether laser scanning methods can improve leaf area index estimations and differences between the forest plots. The results indicate, however, that laser scanning techniques are only to a limited extent applicable to multi-layered forest stands, such as EB15, as the lower layer (beech) shades the upper layer (pine).

For deciduous forests, direct **sampling of leaves** is frequently used in forest sciences and yields reliable leaf area measurements. Possible uncertainty sources are sampling errors due to wind influence and unrepresentatively selected sampling locations. Furthermore, the leaves may decompose slightly and thus lose their substance partly when they are not immediately measured after collection (Fleck et al. 2016). These errors are reduced to a great extent, by using many deep boxes and storing the leaves in a dry state at low temperatures.

In general, the leaf area measurements carried out in this study are reliable and resulting LAI, SAI and PAI values fit well to literature values for pine (Bealde et al. 1982, Bréda 2003, Lovynska et al. 2018, Soudani et al. 2002) and beech (Bréda 2003, Černý et al. 2018, Kram 1998, Leuschner et al. 2006, Meier & Leuschner 2008). For a long-term monitoring, the leaf area needs to be measured regularly. In order to overcome light regime-related uncertainties in the DHP method, digital hemispherical photographs could be taken multiple times per season and resulting leaf areas could be summarized as mean value. In mixed evergreen and deciduous forests, regular litter fall measurements are necessary to assess the leaf area.

Apart from leaf area measurements, **root depth distributions** of the respective trees are important vegetation input data. Their derivation according to Jackson et al. (1996) is appropriate, however, literature values indicate that maximum rooting depth and rooting depth distributions vary considerably even for trees of the same species (Steinmann 2015). Moreover, recent unpublished investigations of maximum rooting depths in Elze indicate that tree roots grow also in several meters depth and extract water from deep soil layers, especially under drought conditions. Therefore, the rooting depth distribution and maximum rooting depth should receive more attention in the future.

5.3.2 Methods to model the water balance

The **hydrological model LWF-Brook90R** is widely used in forest research. However, it represents real processes in nature, as any hydrological model, only simplified and incompletely. Therefore, the model has some limitations that need to be beard in mind when modelled data are analysed and interpreted.

Vegetation canopy is represented by one uniform layer (big leaf approach). In mixed forests, multiple canopy layers commonly occur but they cannot be explicitly considered in LWF-Brook90. Furthermore, the model does not take ground vegetation into account (Federer 2019, Hammel & Kennel 2001). Müller (2019) suggests to consider ground vegetation by species and coverage as well as to implement various parallel annual LAI courses to explicitly account for multiple canopy layers. During winter time, some deciduous trees do not get rid off dead leaves. These leaves do not transpire but still intercept precipitation and radiation, which cannot be simulated by LWF-Brook90. This also accounts for early leaf fall due

to prolonged water stress periods during the vegetation period. Early leaf fall can only be considered by manually constructing the seasonal LAI course based on field observations. Furthermore, stem flow, which is particularly important in older beech stands, remains to be implemented as explicit water flux in the model (Federer 2019, Müller 2019).

LWF-Brook90 simulates snow-related processes with some limitations, however, they are not important for this study as snow did not occur in the study period. The forest ground representation also suffers from some limitations. The influence of solar elevation, canopy structure and snow age on albedo is neglected. Shuttleworth & Wallace (1985) assume bare soil under the canopy layer for determination of soil evaporation. This neglects the litter layer as well as ground vegetation such as mosses, shrubs and herbs (Federer 2019).

Stand precipitation infiltrates into the soil as long as the net infiltration rate is lower than the maximum infiltration capacity. If the infiltration rate is higher than the maximum infiltration capacity, excess water is extracted from the system as surface runoff, even though it would infiltrate later when the infiltration capacity is restored. This effect overestimates surface runoff especially on horizontal surfaces, where surface runoff amounts are usually negligible. Therefore, surface runoff is entirely prevented in this study.

In the soil, LWF-Brook90 mainly focuses on vertical water movement and thus does not allow to incorporate horizontally heterogeneous physical soil characteristics, soil water content or matric potential values. In a natural soil, the soil pore geometry changes with time due to swelling and shrinking processes. However, LWF-Brook90 does not provide the possibility to change hydraulic and soil properties with time and thus ignores these pore geometry dynamics. Moreover, the model neglects water vapour transport through soil pores. Furthermore, the hysteresis of both the retention curve and the hydraulic conductivity are neglected, which primarily affects the modelled matric potential. In the model, the soil temperature never drops below 0°C and thus the effect of frost periods on soil water movement are ignored (Federer 2019, Hammel & Kennel 2001). According to Müller (2019), the MvG parameters should also be able to be determined by using pF-values, matric potential and hydraulic conductivity data from field and laboratory measurements. He also suggests to implement a separate matric flow path for infiltrating water from stem flow. Groundwater is represented in LWF-Brook90 by a first-order groundwater reservoir (Federer 2019) and thus greatly simplified.

These simplifications meet realistic conditions that are found in forested ecosystems only to a certain extent. Modelled processes therefore always diverge to some degree from field observations, even if the model is parameterized as sophisticated as possible. This must be kept in mind when modelled and measured data are compared and interpreted.

In order to **calibrate** LWF-Brook90R, many different methods exist. Manual calibration is to some extent subjective, therefore, automatic calibration techniques increasingly become popular in calibrating hydrological model parameters. Especially, Bayesian inference has widely been used to calibrate hydrological models towards measurements. For this purpose, many MCMC samplers exist (Hastings 1970, Laloy & Vrugt 2012, Vrugt et al. 2003, Vrugt et al. 2008a, Vrugt et al. 2008b). The DREAM algorithm, which has successfully been used for parameter fitting, has successfully been applied in various hydrological modelling studies before. The so calibrated models are able to represent observed stand precipitation and soil moisture. A limitation of the model was the overemphasis of modelled soil moisture

peaks in 50 cm depth. A profound verification of infiltration depths and corresponding infiltration distribution until this depth, however, would require detailed soil moisture measurements in many depths between 50 cm and 200 cm. In general, the calibration technique can be regarded as reliable for this purpose. However, upcoming improvements and developments in the field of automatic calibration techniques should be followed closely.

The model LWF-Brook90R was a reasonable choice to model the water balance at the forest plots, as measured stand precipitation and soil moisture could be reproduced reliably. However, the parameterization of multi-layered forests with several tree layers and ground vegetation was challenging, as LWF-Brook90R only provides one vegetation layer that can be specified. One option would be to use the hydrological model COUPMODEL (Jansson & Karlberg 2004), which allows the user to specify multiple vegetation layers with individual vegetation parameters. However, COUPMODEL is to date rarely used to model the water balance of forests in Germany and is not yet implemented in R.

5.4 Limitations of the study

5.4.1 Suitability of the tree species selected for forest conversion

Scots pine and European beech represent common tree species in the majority of forests in Northwest German lowlands. Currently, the share of pine in Northwest German forests decreases due to changing environmental conditions, emerging diseases and ecologically oriented forest management (Drenkhan et al. 2016, Mason & Alia 2000). Nevertheless, pine will very likely continue to play an important role in pure and mixed stands in the future due to its low demands on water and nutrient supply (Spellmann 2008). For beech, potential yield of beech on nutrient-poor and sandy sites is limited compared to pine and other coniferous species. However, converting evergreen forests into mixed and pure deciduous forests by planting beech as shade-tolerant species under the canopy of pine has great prospects of success (Bolte et al. 2016). The Douglas fir also grows on sandy and nutrient-poor sites and may become more important in the future due to its relatively high drought tolerance (Fischer 2008). The Douglas fir will presumably affect seepage rates negatively, especially when planted in mixed forests with other evergreen species.

Recently, drought conditions have led to damages in Northwest German forests. Norway spruce (*Picea abies*) was particularly affected by drought and secondary parasites. In contrast, significantly lower damage rates were observed for pine, beech and oak in Lower Saxony (Dammann & Paar 2021). The beech trees planted at the forest plots in Sandkrug, Elze and Wibbese also showed only low mortality rates. According to the current state of research, which underpins the adaptive capacity of European beech towards climate change (Bolte et al. 2016, Hajek et al. 2016, Thiel et al. 2014), reforestation with European beech is a reasonable choice as target species for forest conversion. However, the effect of unprecedented growth conditions such as excessive nitrogen input or soil acidification remains to be evaluated (Mergner et al. 2020).

5.4.2 Suitability of the study sites

The **soils** in Sandkrug, Elze and Wibbese are sandy and nutrient-poor and are representative for many pine forests in Northwest Germany. Detailed soil analyses revealed that soil texture varies slightly from site to site and even among the forest plots at one site. Differences in soil characteristics of the individual forest plots are compensated for in the study by using an artificial soil with mean soil properties. This allows a comparative investigation

of the water fluxes for every study site. The comparison of water fluxes between the study sites Sandkrug, Elze and Wibbese is limited, because different soils are used for water balance calculations in Sandkrug, Elze and Wibbese, respectively.

The **forest stands** in Sandkrug, Elze and Wibbese are largely comparable to comparable forests, for example in Northeast Germany (Müller 2019). However, the stand parameters have revealed some small differences between the forest plots in this study: The reference plots SREF, EREF and WREF differ to some extent with respect to stand density, diameter at breast height and tree status according to Kraft's classification. Stand density in SREF (~ 600 ha^{-1}) is slightly higher than in WREF (~ 500 ha^{-1}) and EREF (~ 400 ha^{-1}). At the same time, mean diameters at breast height are comparably small in SREF and the share of dominant trees is smaller. Additionally, the tree height of Scots pine in WREF is higher than in SREF and EREF. Stand parameters in mixed stands in Sandkrug, Elze and Wibbese also show some differences: In WB5 and WD5, stand densities of young beech and Douglas fir trees are lower than in EB5. In SB20, stand densities of both beech and pine are higher than in EB15. These different forest structures highlight the great natural variability of forests, which must be considered, when hydrological measurements are interpreted.

The study sites are also chosen to represent the range of **meteorological conditions** in the Northwest German lowlands. In the period 01/2019 – 10/2020, the precipitation sum in Sandkrug was higher than in Elze and Wibbese, which agrees with long-term climate data. However, the difference between Sandkrug and Elze / Wibbese is not as large as indicated by long-term climate data, as precipitation sums were below average in Sandkrug and Elze and slightly above average in Wibbese.

5.4.3 Representativeness and length of study period

The investigation period, characterized by **extremely warm and dry** years, must be critically questioned in terms of duration and representativeness. From a meteorological perspective, the investigation period was too warm and, especially in the beginning, too dry. The measurement plots were established in summer 2018, which has been one of the warmest, sunniest and driest summer in Germany ever since (Deutscher Wetterdienst 2018b). The entire year 2018 has been eventually the warmest and sunniest year in Germany since the beginning of regular records (Deutscher Wetterdienst 2018a). The meteorological drought ended in winter 2018/2019. Spring and summer 2019 were, again, relatively dry and warm and only rarely interrupted by local thunderstorms. Because of abundant rainfall in September and October 2019, rainfall amounts in 2019 were in accordance with long-term observations (Deutscher Wetterdienst 2019). After a relatively dry December 2019 and January 2020, excessive rainfalls occurred in February 2020 with monthly sums of more than 150 % compared to the long-term mean. Spring and summer 2020, however, were again dominated by high-pressure weather patterns and were thus very sunny and dry (Deutscher Wetterdienst 2020a). The entire study period was hence characterised by meteorological extremes with only a few periods of "average" weather conditions. With respect to precipitation, Sandkrug and Elze experienced greater negative deviations from mean precipitation than Wibbese. Due to above-average temperatures in winter, snow precipitation played only a negligible role in the observation period.

The meteorological drought in 2018 caused a considerable **soil drought** down to several meters depth. Dry soil conditions remained until 2019, affecting the soil water status and also the soil moisture measurements at the forest plots (Boergens et al. 2020, Sutmöller et

al. 2019). Hence, the soil moisture measurements in the study period largely reflect very dry soil moisture conditions, whereas moist soil conditions are underrepresented. This raises the question of how well the calibrated model will perform under wet conditions. It is very likely that the model needs to be further calibrated based on data from both dry and wet periods.

From a modelling perspective, the **study period** from 01/2019 to 10/2020 is too short. Federer (2015) recommends a fitting period length of preferably several years so differences between modelled and real water storages are negligible. Hence, one year for model calibration and 10 months for model validation may not be sufficiently long to yield stable model parameter sets. Schmidt-Walter et al. (2020) showed that using different time periods for model calibration yields different parameter sets when only one year is used for model calibration. Backes & Leuschner (2000) suggest to study tree water relations for at least three or four seasons to account for large inter-annual variabilities of these parameters in temperate humid environments. The study period is thus long enough to give first insights into the water balance of the forests, however, the period should be extended in order to capture representative environmental conditions and to account for inter-annual variabilities of water status parameters.

5.4.4 The role of ground vegetation

Ground vegetation is not explicitly considered in this study. In pure beech (EB25) and mixed forest with older beech trees (EB15 and SB20), ground vegetation is negligible. In pure pine forests (SREF, EREF, WREF) and mixed pine forests with young beech (EB5, WB5) and Douglas fir trees (WD5), however, ground vegetation is present formed by shrubs, herbs and grass. Ground vegetation additionally intercepts and transpires water and has thus a significant impact on the hydrological cycle (Lüttschwager et al. 1999, Müller 2011, Müller & Seyfarth 1999). In an experimental setup, the interception storage capacities of blueberry shrubs and wavy hair grass have been investigated (Schröter 2019). Resulting storage capacities for soil vegetation dominated by blueberry shrubs, grass and mosses are in an order of 1 to 2 mm. By not considering soil vegetation interception in water balance modelling, interception is very likely underestimated in forest plots with substantial ground vegetation (SREF, EREF, EB5, WREF, WB5, WD5). At the same time, deep seepage is very likely overestimated to some extent for these plots. Given this assumption, deep seepage rates in the mixed pine and beech forests SB20 and EB15 would be to some extent higher than deep seepage rates in the reference plots. This would fit well to the findings from Müller (2012), who found increasing deep seepage rates from pure pine to mixed pine and beech to pure beech stands.

Therefore, soil vegetation should be explicitly included in future investigations on the water cycle in forest ecosystems. In order to account for ground vegetation, it would be necessary to determine the interception of ground vegetation. Ground vegetation interception could be determined by measuring stand precipitation below the shrub and herb layer. These measurements, however, are difficult to establish and error-prone. Another option would be to use lysimeters (Coenders-Gerrits et al. 2010, Coenders-Gerrits et al. 2007, Müller 2011, Müller & Seyfarth 1999). However, these measurements are labor-intensive and costly. In addition, it would be necessary to quantify vegetation parameters of the ground vegetation needed for the hydrological model. It would be desirable to assess the ground cover LAI, for example by assessing the leaf area sum based on leaf thickness and digital

image analysis (Bolte 1996, Bolte & Anders 1995). If ground cover LAI and the corresponding interception were known, it would be possible to integrate ground cover LAI into tree LAI. Then, model interception parameters could be calibrated with measured interception rates from tree layer and ground cover. The resulting water fluxes would explicitly incorporate the effect of soil vegetation.

5.5 Implications for the temporal development of deep seepage during forest conversion

In this study, deep seepage rates in pure pine stands, in mixed pine and beech stands up to 20 years after the beginning of forest conversion, and in a pure beech stand 25 years after the beginning of forest conversion have been investigated. In addition, the effect of a mixed pine and Douglas fir forest as well as the thinning of the pine tree layer in Wibbese on deep seepage rates was investigated. Müller (2012) investigated deep seepage rates in comparable pure pine stands, in a sequence of comparable mixed pine and beech stands, and in a comparable pure beech stand. Schultze & Scherzer (2015) modelled deep seepage rates in a comparable mixed pine and Douglas fir stand and in a pure oak stand. Based on the results of this project and findings from Müller (2012) and Schultze & Scherzer (2015), it is possible to describe the development of deep seepage rates under pure pine, pure beech and mixed pine and beech forests at different forest conversion stages and over a long time period.

In the first 10 years after the beginning of forest conversion, Müller (2012) found a slight increase in deep seepage rates in a mixed beech and pine forest. Schultze & Scherzer (2015) found an increase in deep seepage rates of 50 mm in a mixed pine and oak forest 10 years after conversion compared to a pure pine forest. The measurements in mixed pine and beech stands 5 years after conversion (EB5, WB5) do not show an increase in deep seepage rates as clear as Müller (2012) and Schultze & Scherzer (2015): In EB5, deep seepage rates are at the same level as in EREF. In WB5, deep seepage rates are even lower than in WREF before thinning.

The thinning of the pine stand in WB5 showed the influence of the thinning on deep seepage rates in mixed pine forests at an early stage of forest conversion: The thinning caused a short-term increase of deep seepage rates by 10 to 25 %. This however, can only be regarded as first orientation, as the investigation time period of 7 months is very short. The thinning influenced not only deep seepage rates, but also evapotranspiration rates. Lagergren et al. (2008) found up to 40% lower transpiration rates in thinned pine-spruce stands directly after the intervention. However, the transpiration rate increased significantly in the following years (Lagergren et al. 2008). Similarly, Gebhardt et al. (2014) also found a decreased transpiration of up to 50% in a moderately and heavily thinned spruce stand during the first year after intervention. Later, transpiration rates increased but remained below the level as found before thinning. In WB5 and WD5, transpiration rates decreased by 5 to 10 %, which is considerably lower than literature values reported from Gebhardt et al. (2014) and Lagergren et al. (2008). In future investigations, a longer time period should be used in order to assess the effect of thinning on deep seepage rates and evapotranspiration. The growing conditions in Northwest Germany are generally favorable with abundant rainfall amounts and high atmospheric nitrogen inputs. The measurements in Elze and Sandkrug indicate that these conditions cause the thinned pine canopy to close rapidly after thinning, which may quickly reduce the deep seepage surplus. Liming of forests can further improve growth conditions and thus lead to accelerated canopy closure after

thinning. The future will show, if this effect will occur in the thinned pine stand in Wibbese as well.

30 years after the beginning of forest conversion, Müller (2012) found an increase in deep seepage rates from a pure pine forest (12 % of gross precipitation) to a mixed pine forest with 30 years old beech trees (18 % of gross precipitation), which is a relative increase in deep seepage rates of 50 %. Schultze & Scherzer (2015) found a deep seepage surplus in a mixed pine and oak forest compared to a pure pine forest of 50 mm after 10 years, 75 mm after 20 years and almost 100 mm after 30 years. In a pure oak forest, this surplus even exceeds 100 mm 30 years after the beginning of forest conversion. The measurements in EB15 and SB20 showed similar deep seepage rates as in the reference plots (EREF, SREF) and thus do not confirm the increasing deep seepage rates found for mixed forests at least 20 years after the forest conversion has started.

The measurements only showed a substantial increase in deep seepage rates in the pure beech stand (EB25). Here, deep seepage rates (58 % of gross precipitation) are 75 % higher than in the pure pine stand (EREF, 33 % of gross precipitation). This agrees well with findings from Müller (2012), who found an increase in deep seepage rates by 77 % from a 84 years old pine (12 % of gross precipitation) to a 28 years old beech forest (22 % of gross precipitation), but on a generally lower level. Schultze & Scherzer (2015) also report a clear increase in deep seepage rates in a 30 years old pure oak stand compared to a pure pine stand.

The development of deep seepage rates in a **mixed pine and Douglas fir** stand is presented by Schultze & Scherzer (2015). They found continuously lower deep seepage rates than in the pure pine stand, with 10 mm less seepage 10 years after the beginning of forest conversion and 50 mm less seepage 50 years after the beginning of forest conversion. In WD5, the Douglas fir trees are still small and their effect on the deep seepage rate could not be shown by our measurements yet. However, it is assumed that deep seepage rates in WD5 will decrease compared to the pure pine stand (WREF) (Prietzel & Bachmann 2011).

Based on these results, the effect of **forest conversion from pure pine to pure beech** stands on annual deep seepage rates for a **time period of 120 years** can be estimated. In the following, a forest conversion scenario with an early removal of the pine tree layer as discussed by Rumpf & Petersen (2008) is assumed. It is assumed that forest conversion is started by planting beech trees into a mature pine forest. For the next 30 years, the mixed pine and beech forest grows and is regularly thinned. In this period, deep seepage rates are in the order of 33 % of gross precipitation, as measured in EREF, EB5 and EB15. After 30 years, all pine trees are cut and a pure beech forest remains at the site until the forest is 120 years old. In this period, deep seepage rates have increased significantly to a level of 58 % of gross precipitation (as measured in EB25). Deep seepage is thus 75 % higher than in the first 30 years of forest conversion. Over the total time period of 120 years, the mean annual deep seepage rate is then 52 % of gross precipitation. As reference, a pure pine forest showing a deep seepage rate of 33 % of gross precipitation for the entire 120 years (as in EREF) is assumed. Gross precipitation is assumed to be 700 mm per year. As a result, the mean yearly deep seepage rate would be 230 mm a^{-1} in the reference pine forest and 360 mm a^{-1} in the converted forest. This indicates a difference of 130 mm a^{-1} for a time period of 120 years.

This scenario can only serve as a rough orientation, as deep seepage rates differ from year to year and the study period of almost 2 years is short. Therefore, absolute deep seepage amounts may change with further years included in the deep seepage investigation.

5.6 Recommendations to increase deep seepage during forest conversion

Deep seepage occurs predominantly outside the growing season in winter. Specific forest management measures in the conversion period can significantly affect deep seepage rates in different forest conversion stages. During forest conversion, the pine tree layer above the planted beech tree layer is usually managed with a stocking level of 0.7 (approximately 70% canopy cover) until maturity. Before the beech trees are planted underneath the pines, the pine layer is thinned. The best time for the next intensive thinning of the parent pine layer is between 5 and 15 years after plantation of the beech trees. The exact time is variable and needs to be determined carefully: The beech trees should already shade the ground to an extent that the ground vegetation is about to vanish. A too early thinning would lead to scrub encroachment of ground vegetation and dieback of the young beech trees. Both the reduction of the pine stocking level and the dieback of the ground vegetation will increase deep seepage. Naturally, the pine tree layer grows differently dense, which will lead to the development of areas with pine dominance and those with beech dominance. In order to increase deep seepage, it is useful to promote the dominance of beech in all areas in the course of further thinnings. As stem flow from beech trees directly increase deep seepage and moisten upper soil layers in dry periods, it is advantageous to maintain an even distribution of beech trees in the forest during thinnings. Deep seepage could be further increased by reducing the pine stocking level to below 0.6 more than 15 years before pine tree maturity. Another option is to entirely remove the pine tree layer already at an early conversion stage. This would increase deep seepage significantly, however, possible disadvantages are that the remaining unprotected beech trees could be damaged by wind, snow, late frost and sun. On the other hand, an early removal of the pine layer can accelerate the growth of dominant beech trees and it can reduce the risk of pine trees being threatened by age-related pests (Schröder et al. 2018).

The promotion of deep seepage is associated with felling of immature pine trees and thus with economic loss. Currently, forests are managed in a way to maximize economic gain through timber production. Forest owners who convert their forest to increase deep seepage, however, do not receive money for doing so. Therefore, for the forest owner, a forest conversion promoting deep seepage represents an ecological-economic trade-off in which the amount of water is increased but the revenue is reduced. In order to recognize the provision of water and timber as a comparably important ecosystem service, it is necessary to put a monetary value on water. If forest owners made money from both timber production and water provision, they could convert the forest to promote water provision without having to make economic trade-offs. In climatically dry regions with low groundwater recharge rates, the provision of water might even have a higher monetary value, making water-enhancing forest conversion more worthwhile than forests focused on timber production.

6. Conclusion & Outlook

Deep seepage was successfully modelled for 9 different forest plots representing different forest conversion stages by the hydrologic model *LWF-Brook90*. After calibrating relevant interception, evapotranspiration and soil parameters of the model, the plot-specific models accurately reproduced measured stand precipitation sums and soil moisture courses in different soil depths. These models were thus able to determine evapotranspiration and deep seepage plot-specifically. The resulting deep seepage rates are transferable to many forest sites in Lower Saxony that are comparable to the forest sites under study.

The hypothesis that seepage rates in pure pine stands are significantly lower than those in pure beech stands can be confirmed with the present results. Modelled deep seepage for different forest conversion stages indicate an overall increasing trend from pure pine to pure beech forests. In pure beech forests, the trees transpire only in summer and due to their leaf surface characteristics, interception is lower than in pine forests. Deep seepage thus almost doubled in the pure beech forest compared to the pure pine forest investigated in Elze.

The development of deep seepage in the intermediate conversion stages of pine forests being mixed with beech is less clear. It was hypothesized that deep seepage in mixed pine and beech forests would be higher than in pure pine forests and lower than in pure beech forests. According to the results of this study, deep seepage amounts in these mixed forests are lower than in pure beech forests but show no difference compared to pure pine forests. In an early forest conversion stage (5 years after conversion start), deep seepage is primarily affected by the dominant pine tree layer rather than by the newly planted trees. The comparison of two mixed pine forests with 5 years old beech and Douglas fir show no difference in deep seepage, which implies that evergreen (Douglas fir) and deciduous (beech) trees do not yet have a great effect on deep seepage at this conversion stage.

15 to 20 years after forest conversion start, the newly planted beech trees grow and increasingly affect the water cycle, which becomes evident in significant seasonal interception changes in mixed pine and beech forests. The interception in a mixed pine and beech forest in Elze revealed that an increased stand precipitation resulting from the thinned pine tree layer is outbalanced by the water consumption of the beech trees in summer. This led to deep seepage rates being at the same level as in the pure pine forest. This agrees well with findings from Sandkrug, where deep seepage in a pure pine and a mixed pine and beech forest were at the same level, too.

The effect of pine tree thinning on deep seepage was hypothesized to increase deep seepage. The results from the forest plots in Wibbese demonstrate that a reduction of the pine tree canopy by one third approximately increases seepage rates in the mixed forests by 10 to 25 %.

Even though deep seepage could be successfully modelled for the study plots, there is still potential for further improvements. With respect to in situ measurements, plot-specific maximum rooting depths and depth-specific root densities lack and are solely based on literature values so far. This information would be particularly valuable to estimate the actual root-accessible soil water storage, as literature values vary greatly and unpublished rooting depth investigations in Elze indicate a much greater rooting depth than assumed in this study. Maximum rooting depth and rooting depth distributions could be derived e. g. by soil

moisture measurements or soil core investigations. Moreover, stem flow of beech will play an increasingly important role in the future and should therefore be measured. Further adjustments can be made with respect to the modelling scheme. An extension of the study period that currently covers almost 2 years will improve model calibration and the representativeness of the model results. The current study period is characterized by mostly warm and dry periods. A longer period covering also wet and cool periods will improve the model as many different weather conditions in the calibration period will lead to a more robust model calibration. Furthermore, soil vegetation should be included into the model by for example including leaf area parameter and interception measurements of soil vegetation.

The findings highlight the positive effect of forest conversion towards deciduous forests on deep seepage compared to evergreen forests. However, it also becomes clear that deep seepage does not necessarily increase within the first 20 years of forest conversion. In order to yield a substantial water surplus, two management options can be recommended: First, regular thinning of the pine tree layer and promoting areas in the forest dominated by beech. This would correspond to a higher thinning degree than that of the mixed pine and beech tree forests under study in Sandkrug and Elze. Second, the pine tree layer could be removed entirely already after 30 years, as done in the pure beech forest in Elze, which would significantly increase deep seepage rates.

The forest directly benefits from this water surplus as an increased infiltration rate not only increase deep seepage but also fills the soil water storage. This increases soil water availability for the forest vegetation and thus counteracts water scarcity in drought periods. Surplus water recharges the groundwater on the one hand and is available to other water-dependent ecosystems on the other hand. Thus, forest conversion increases the adaptive capacity of forests towards climate change by simultaneously safeguarding timber production and water provision.

Today, the provision of water does not have the same economic value as the provision of timber in forestry. Since forest conversion promoting deep seepage involves the premature removal of trees and thus reduced profit from reduced timber production, this represents an economic loss to the forest owner. In order to promote forest conversion that increases deep seepage, the ecosystem service of water must be of equal economic value as timber production. Particularly in water-scarce areas, further increasing the economic value of water could promote forest conversion aimed at increasing water donation and thus ensure the regeneration of water reservoirs.

Climate change raises the question of how priorities can and will be set in future forestry: Currently, the main focus in forestry is set to timber production. The changing climate may mean that the most important task in the future will be to preserve the forest with its multifunctionality as an ecosystem in the first place. In this context, the focus is set on a site-appropriate choice of tree species, with tree species that have the necessary plasticity to changing climatic conditions. Although beech will not be suitable for all sites, other deciduous trees also fulfill many of their water-saving properties and can be considered for site-appropriate forest conversion while promoting deep seepage.

Literature

Abdul-Jabbar, A. S., Lugg, D. G., Sammis, T. W. & Gay, L. W. (1984): A Field Study of Plant Resistance to Water Flow in Alfalfa. Agronomy Journal, 76**,** 765-769.

Ad-Hoc-Arbeitsgruppe Boden (1999): Verknüpfungsregel 1.20. Bundesanstalt für Geowissenschaften und Rohstoffe, 1-3.

Ahrends, B. & Penne, C. (2010): Modeling the Impact of Canopy Structure on the Spatial Variability of Net Forest Precipitation and Interception Loss in Scots Pine Stands. The Open Geography Journal, 3**,** 115-124.

Ahrends, B., Sutmöller, J., Schmidt-Walter, P. & Meesenburg, H. (2018): Beitrag von Waldflächen zur Sickerwasserbildung in Niedersachsen. Hydrologie und Wasserbewirtschaftung, 39.18**,** 169-180.

Alaoui, A., Caduff, U., Gerke, H. & Weingartner, R. (2011): A Preferential Flow Effects on Infiltration and Runoff in Grassland and Forest Soils. Vadose Zone Journal, 10**,** 367-377.

Allison, G. B. & Hughes, M. W. (1978): The Use of Environmental Chloride and Tritium to Estimate Total Recharge to an Unconfined Aquifer. Australian Journal of Soil Research, 16**,** 181-195.

Alvera, B. (1976): Contribución al Estudio de la Intercepción de las Precipitaciones Atmosféricas en el Pinar de San Juan de la Pena. Publicaciones del Centro Pirenaico de Biología Experimental, 7**,** 95-100.

Amelung, W., Blume, H.-P., Fleige, H., Horn, R., Kandeler, E., Kögel-Knabner, I., Kretzschmar, R., Stahr, K. & Wilke, B.-M. (2018): Scheffer/Schachtschabel Lehrbuch der Bodenkunde. Berlin, Springer Spektrum.

Armbruster, M., Seegert, J. & Feger, K.-H. (2004): Effects of Changes in Tree Species Composition on Water Flow Dynamics – Model Applications and their Limitations. Plant and Soil, 264**,** 13-24.

Bartelink, H. H. (1997): Allometric Relationships for Biomass and Leaf Area of Beech (Fagus sylvatica L). Annals of Forest Science, 54**,** 39-50.

Bartlett, M. K., Scoffoni, C. & Sack, L. (2012): The Determinants of Leaf Turgor Loss Point and Prediction of Drought Tolerance of Species and Biomes: A Global Meta-Analysis. Ecology Letters, 15**,** 393-405.

Bartsch, N. & Röhrig, E. (2016): Wasserhaushalt von Bäumen und Ökosystemen. In: Bartsch, N. & Röhrig, E. (eds.): Waldökologie. Berlin, Heidelberg, Springer Spektrum.

Bates, B. & Campbell, E. (2001): A Markov Chain Monte Carlo Scheme for Parameter Estimation and Inference in Conceptual Rainfall-Runoff Modeling. Water Resources Research, 37, 937-947.

Bayerische Staatsforsten (2022): Waldumbau: Bäumchen wechsel dich! URL: https://www.baysf.de/de/wald-verstehen/waldumbau.html, accessed 28.11.2022.

Bazuhair, A. S. & Wood, W. W. (1996): Chloride Mass-Balance Method for Estimating Ground Water Recharge in Arid Areas: Examples from Western Saudi Arabia. Journal of Hydrology, 186, 153-159.

Bealde, C. L., Talbot, H. & Jarvis, P. G. (1982): Canopy Structure and Leaf Area Index in a Mature Scots Pine Forest. Forestry: An International Journal of Forest Research, 55, 105-123.

Beard, J. S. (1956): Results of the Mountain Home Rainfall Interception and Infiltration Project in Black Wattle, 1953/54. Journal of the South African Forestry Association, 27, 72-86.

Beven, K. & Kirkby, M. J. (1979): A Physically Based, Variable Contributing Area Model of Basin Hydrology. Hydrological Sciences Bulletin, 24, 43-69.

Bittelli, M. (2011): Measuring Soil Water Content: A Review. HortTechnology, 21, 293-300.

Blume, H.-P., Stahr, K. & Leinweber, P. (2011): Bodenkundliches Praktikum : Eine Einführung in pedologisches Arbeiten für Ökologen, insbesondere Land- und Forstwirte, und für Geowissenschaftler. Heidelberg, Spektrum Akademischer Verlag.

Bmelv (2011): Aufnahmeanweisung für die dritte Bundeswaldinventur (2011-2012). Bonn, Bundesministerium für Ernährung, Landwirtschaft und Verbraucherschutz (BMELV).

Böckmann, T., Hansen, J., Hauskeller-Bullerjahn, K., Jensen, T., Nagel, J., Nagel, R.-V., Overbeck, M., Pampe, A., Petereit-Bitter, A., Schmidt, M., Schröder, M., Schulz, C., Spellmann, H., Stüber, V., Sutmöller, J. & Wollborn, P. (2019): Klimaangepasste Baumartenwahl in den Niedersächsischen Landesforsten. Aus dem Walde - Schriftenreihe Waldentwicklung in Niedersachsen, 61, 1-86.

Boergens, E., Güntner, A., Dobslaw, H. & Dahle, C. (2020): Quantifying the Central European Droughts in 2018 and 2019 with GRACE Follow-On. Geophysical Research Letters, 47, 1-9.

Bogena, H. R., Huisman, J. A., Schilling, B., Weuthen, A. & Vereecken, H. (2017): Effective Calibration of Low-Cost Soil Water Content Sensors. Sensors, 17, 1-12.

Bolte, A. (1996): Die Bodenvegetation in Kiefernökosystemen - Eine Steuergröße für den Wasser- und Stoffhaushalt. Mitteilungen der Bundesforschungsanstalt für Forst- und Holzwirtschaft Hamburg, 185, 97-111.

Bolte, A. & Anders, S. (1995): Zur Rolle der Bodenvegetation bei der Destabilisierung stickstoffbelasteter Kiefernforstökosysteme. Beitrage fur Forstwirtschaft und Landschaftsokologie, 29, 151-155.

Bolte, A., Czajkowski, T., Cocozza, C., Tognetti, R., De Miguel, M., Pšidová, E., Ditmarová, Ľ., Dinca, L., Delzon, S., Cochard, H., Ræbild, A., De Luis, M., Cvjetkovic, B., Heiri, C. & Müller, J. (2016): Desiccation and Mortality Dynamics in Seedlings of Different European Beech (Fagus sylvatica L.) Populations under Extreme Drought Conditions. Frontiers in Plant Science, 7, 1-12.

Brechtel, H. M. (1969): Wald und Abfluss-Methoden zur Erforschung der Bedeutung des Waldes für das Wasserdargebot. Deutsche Gewässerkundliche Mitteilungen, 8, 24-31.

Bréda, N. & Granier, A. (1996): Intra- and Interannual Variations of Transpiration, Leaf Area Index and Radial Growth of a Sessile Oak Stand (Quercus petraea). Annals of Forest Science, 53, 521-536.

Bréda, N. J. J. (2003): Ground-based Measurements of Leaf Area Index: A Review of Methods, Instruments and Current Controversies. Journal of Experimental Botany, 54, 2403-2417.

Brocca, L., Morbidelli, R., Melone, F. & Moramarco, T. (2007): Soil Moisture Spatial Variability in Experimental Areas of Central Italy. Journal of Hydrology, 333, 356-373.

Brutsaert, W. (1982): Evaporation into the Atmosphere: Theory, History and Applications. Dordrecht, Springer Netherlands.

Bußkamp, J., Langer, G. J. & Langer, E. J. (2020): Sphaeropsis sapinea and Fungal Endophyte Diversity in Twigs of Scots pine (Pinus sylvestris) in Germany. Mycological Progress, 19, 985-999.

Bussotti, F., Pollastrini, M., Holland, V. & Brüggemann, W. (2014): Functional Traits and Adaptive Capacity of European Forests to Climate Change. Environmental and Experimental Botany, 111, 91-113.

Cape, J. N., Brown, A. H. F., Robertson, S. M. C., Howson, G. & Paterson, I. S. (1991): Interspecies Comparisons of Throughfall and Stemflow at Three Sites in Northern Britain. Forest Ecology and Management, 46, 165-177.

Carlyle-Moses, D. & Gash, J. H. C. (2011): Rainfall Interception Loss by Forest Canopies. In: Levia, D., Carlyle-Moses, D. & Tanaka, T. (eds.): Forest Hydrology and Biogeochemistry. Ecological Studies (Analysis and Synthesis). Dordrecht, Springer.

Černý, J., Haninec, P. & Pokorny, R. (2018): Leaf Area Index Estimated by Direct, Semi-Direct, and Indirect Methods in European Beech and Sycamore Maple Stands. Journal of Forestry Research, 31, 827-836.

Chen, J. M. & Black, T. A. (1991): Measuring Leaf Area Index of Plant Canopies with Branch Architecture. Agricultural and Forest Meteorology, 57, 1-12.

Chen, J. M. & Cihlar, J. (1995): Quantifying the Effect of Canopy Architecture on Optical Measurements of Leaf Area Index Using Two Gap Size Analysis Methods. IEEE Transactions on Geoscience and Remote Sensing, 33, 777-787.

Chianucci, F. & Cutini, A. (2012): Digital Hemispherical Photography for Estimating Forest Canopy Properties: Current Controversies and Opportunities. iForest - Biogeosciences and Forestry, 5, 290-295.

Chifflard, P., Gall, S. & Zepp, H. (2003): Untersuchungen zur Räumlichen Variabilität der Oberbodenfeuchte in Abhängigkeit von Relief und Boden. Innovative Feuchtemessung in Forschung und Praxis, 1, 283-306.

Clark, O. R. (1940): Interception of Rainfall by Prairie Grasses, Weeds, and Certain Crop Plants. Ecological Monographs, 10, 243-277.

Clarke, N., Zlindra, D., Ulrich, E., Mosello, R., Derome, J., Derome, K., König, N., Lövblad, G., Draaijers, G. P. J., Hansen, K., Thimonier, A. & Waldner, P. (2016): Part XIV: Sampling and Analysis of Deposition. In: Unece Icp Forests Programme Co-Ordinating Centre (eds.): Manual on Methods and Criteria for Harmonized Sampling, Assessment, Monitoring and Analysis of the Effects of Air Pollution on Forests. Eberswalde, Thünen Institute of Forest Ecosystems.

Clothier, B. E., Green, S. R. & Deurer, M. (2008): Preferential Flow and Transport in Soil: Progress and Prognosis. European Journal of Soil Science, 59, 2-13.

Coenders-Gerrits, M., Pfister, L. & Savenije, H. (2010): Spatial and Temporal Variability of Canopy and Forest Floor Interception in a Beech Forest. Hydrological Processes, 24, 3011-3025.

Coenders-Gerrits, M., Svenije, H. H. G., Hoffmann, L. & Pfister, L. (2007): New Technique to Measure Forest Floor Interception - An Application in a Beech Forest in Luxembourg. Hydrology and Earth System Sciences, 11, 695-701.

Czajkowski, T. & Bolte, A. (2006): Unterschiedliche Reaktion deutscher und polnischer Herkünfte der Buche (Fagus sylvaticaL.) auf Trockenheit. Allgemeine Forst- und Jagdzeitung, 177, 30-40.

Dammann, I. & Paar, U. (2021): WZE-Ergebnisse für alle Baumarten. In: Eichhorn, J., Paar, U., Dammann, I., Evers, J., Schulze, A., Weymar, J., Spielmann, M. & Westphal, B.

(eds.): Waldzustandsbericht 2020. Hannover, Niedersächsisches Ministerium für Ernährung, Landwirtschaft und Verbraucherschutz

De Boeck, H. J., Bloor, J. M. G., Kreyling, J., Ransijn, J. C. G., Nijs, I., Jentsch, A. & Zeiter, M. (2017): Patterns and Drivers of Biodiversity-stability Relationships under Climate Extremes. Journal of Ecology, 106**,** 890-902.

Delfs, J. (1955): Die Niederschlagszurückhaltung im Walde (Interception). Koblenz, Mitteilungen des Arbeitskreises "Wald und Wasser".

Deutscher Wetterdienst (2018a): Deutschlandwetter im Jahr 2018. URL: https://www.dwd.de/DE/presse/pressemitteilungen/DE/2018/20181228_deutschlandwetter_jahr2018_news.html, accessed 15.02.2021.

Deutscher Wetterdienst (2018b): Deutschlandwetter im Sommer 2018. URL: https://www.dwd.de/DE/presse/pressemitteilungen/DE/2018/20180830_deutschlandwetter_sommer_news.html, accessed 15.02.2021.

Deutscher Wetterdienst (2019): Deutschlandwetter im Jahr 2019. URL: https://www.dwd.de/DE/presse/pressemitteilungen/DE/2019/20191230_deutschlandwetter_jahr2019_news.html, accessed: 15.02.2021.

Deutscher Wetterdienst (2020a): Deutschlandwetter im Frühling 2020. URL: https://www.dwd.de/DE/presse/pressemitteilungen/DE/2020/20200529_deutschlandwetter_fruehjahr2020_news.html, accessed: 15.02.2021.

Deutscher Wetterdienst (2020b): DWD Climate Data Center (CDC): Vieljährige Stationsmittelwerte für Großenkneten für die Klimareferenzperiode 1981-2010. Accessed: 11.05.2020.

Deutscher Wetterdienst (2020c): DWD Climate Data Center (CDC): Vieljährige Stationsmittelwerte für Hannover-Langenhagen für die Klimareferenzperiode 1981-2010. Accessed: 11.05.2020.

Deutscher Wetterdienst (2020d): DWD Climate Data Center (CDC): Vieljährige Stationsmittelwerte für Lüchow für die Klimareferenzperiode 1981-2010. Accessed: 11.05.2020.

Deutscher Wetterdienst (2020e): DWD Climate Data Center (CDC): Vieljährige Stationsmittelwerte für Rosche-Stütensen für die Klimareferenzperiode 1981-2010. Accessed: 11.05.2020.

Devak, M. & Dhanya, C. T. (2017): Sensitivity Analysis of Hydrological Models: Review and Way Forward. Journal of Water and Climate Change, 8**,** 557-575.

Drenkhan, R., Tomešová-Haataja, V., Fraser, S., Bradshaw, R. E., Vahalík, P., Mullett, M. S., Martín-García, J., Bulman, L. S., Wingfield, M. J., Kirisits, T., Cech, T. L., Schmitz, S., Baden, R., Tubby, K., Brown, A., Georgieva, M., Woods, A., Ahumada, R., Jankovský, L., Thomsen, I. M., Adamson, K., Marçais, B., Vuorinen, M., Tsopelas, P., Koltay, A.,

Halasz, A., La Porta, N., Anselmi, N., Kiesnere, R., Markovskaja, S., Kačergius, A., Papazova-Anakieva, I., Risteski, M., Sotirovski, K., Lazarević, J., Solheim, H., Boroń, P., Bragança, H., Chira, D., Musolin, D. L., Selikhovkin, A. V., Bulgakov, T. S., Keča, N., Karadžić, D., Galovic, V., Pap, P., Markovic, M., Poljakovic Pajnik, L., Vasic, V., Ondrušková, E., Piškur, B., Sadiković, D., Diez, J. J., Solla, A., Millberg, H., Stenlid, J., Angst, A., Queloz, V., Lehtijärvi, A., Doğmuş-Lehtijärvi, H. T., Oskay, F., Davydenko, K., Meshkova, V., Craig, D., Woodward, S. & Barnes, I. (2016): Global Geographic Distribution and Host Range of Dothistroma Species: A Comprehensive Review. Forest Pathology, 46**,** 408-442.

Dvwk (1986): Ermittlung des Interzeptionsverlustes in Waldbeständen bei Regen. DVWK-Merkblätter zur Wasserwirtschaft, 211**,** 1-11.

Ellenberg, H., Schauermann, J. & Mayer, R. (1986): Ökosystemforschung : Ergebnisse des Sollingprojekts 1966 - 1986. Stuttgart, Ulmer.

Eriksson, E. & Khunakasem, V. (1969): Chloride Concentration in Groundwater, Recharge Rate and Rate of Deposition of Chloride in the Israel Coastal Plain. Journal of Hydrology, 7**,** 178-197.

Eshel, G., Levy, G. J., Mingelgrin, U. & Singer, M. J. (2004): Critical Evaluation of the Use of Laser Diffraction for Particle-Size Distribution Analysis. Soil Science Society of America Journal, 68**,** 736-743.

Federer, C. A. (1965): Sustained Winter Streamflow from Groundmelt. Research Note NE-41. Upper Darby, PA, U.S. Department of Agriculture, Forest Service, Northeastern Forest Experiment Station.

Federer, C. A. (2015a): BROOK90 - Parameters and Variables List. URL: http://www.ecoshift.net/brook/b90doc.html, accessed: 26.10.2020.

Federer, C. A. (2015b): BROOK90 - PET Potential Evapotranspiration. URL: http://www.ecoshift.net/brook/b90doc.html, accessed: 18.05.2020.

Federer, C. A. (2019): BROOK 90: A Simulation Model for Evaporation, Soil Water and Streamflow. URL: http://www.ecoshift.net/brook/brook90.htm, accessed: 17.08.2020.

Fischer, A. (2008): Die Eignung der Douglasie im Hinblick auf den Klimawandel. LWF-Wissen, 59**,** 63-66.

Fleck, S., Raspe, S., Cater, M., Schleppi, P., Ukonmaanaho, L., Greve, M., Hertel, C., Weis, W., Rumpf, S., Thimonier, A., Chianucci, F. & Beckschäfer, P. (2016): Part XVII: Leaf Area Measurements. In: Unece Icp Forests Programme Coordinating Centre (eds.): Manual on Methods and Criteria for Harmonized Sampling, Assessment, Monitoring and Analysis of the Effects of Air Pollution on Forests. Eberswalde, Thünen Institute of Forest Ecosystems.

Gale, M. & Grigal, D. (1987): Vertical Root Distribution of Northern Tree Species in Relation to Successional Status. Canadian Journal of Forest Research, 17**,** 829-834.

Gebhardt, T., Häberle, K.-H., Matyssek, R., Schulz, C. & Ammer, C. (2014): The More, the Better? Water Relations of Norway spruce Stands after Progressive Thinning. Agricultural and Forest Meteorology, 197**,** 235–243.

Gelman, A., Carlin, J. B., Stern, H. S. & Rubin, D. B. (1995): Bayesian Data Analysis. New York, Chapman and Hall/CRC.

Gelman, A. & Rubin, D. (1992): Inference from Iterative Simulation Using Multiple Sequences. Statistical Science, 7**,** 457-472.

Gerrits, A. M. J. & Savenije, H. H. G. (2011): Forest Floor Interception. In: Levia, D., Carlyle-Moses, D. & Tanaka, T. (eds.): Forest Hydrology and Biogeochemistry. Ecological Studies (Analysis and Synthesis). Dordrecht, Springer.

Glugla, G., Fischer, D., Höhne, U., Kortüm, F. & Helbig, A. (1982): Lysimeteruntersuchungen in der Letzlinger Heide - wichtiger Beitrag zur Bestimmung der Wasserressourcen bewaldeter Gebiete. Wasserwirtschaft/Wassertechnik, 9**,** 319-322.

Golden, H. E., Evenson, G. R., Tian, S., Amatya, D. & Sun, G. (2015): Hydrological Modeling in Forested Systems. In: Amatya, D., Williams, T. M., Bren, L. & De Jong, C. (eds.): Forest Hydrology: Processes, Management and Assessment. Wallingford, CABI Publishers.

Groh, J., Puhlmann, H. & Wilpert, K. (2013): Kalibrierung eines Bodenwasserhaushaltsmodells mit einer kombinierten Zielfunktion für die Optimierung der Wasserretentionskurve. Hydrologie und Wasserbewirtschaftung, 57**,** 152-163.

Guillaume, J. & Andrews, F. 2012. DREAM: DiffeRential Evolution Adaptive Metropolis. R Package Version 0.4-2.

Guo, L. & Lin, H. (2018): Chapter Two - Addressing Two Bottlenecks to Advance the Understanding of Preferential Flow in Soils. Advances in Agronomy, 147**,** 61-117.

Gupta, S., Hengl, T., Lehmann, P., Bonetti, S. & Or, D. (2021): SoilKsatDB: Global Database of Soil Saturated Hydraulic Conductivity Measurements for Geoscience Applications. Earth System Science Data, 13**,** 1593-1612.

Haberlandt, U. (2016): Niederschlag. In: Fohrer, N., Bormann, H., Miegel, K., Casper, M., Bronstert, A., Schumann, A. & Weiler, M. (eds.): Hydrologie. Bern, UTB Verlag.

Hajek, P., Kurjak, D., Wuehlisch, G., Delzon, S. & Schuldt, B. (2016): Intraspecific Variation in Wood Anatomical, Hydraulic, and Foliar Traits in Ten European Beech Provenances Differing in Growth Yield. Frontiers in Plant Science, 7**,** 1-14.

Hammel, K. & Kennel, M. (2001): Charakterisierung und Analyse der Wasserverfügbarkeit und des Wasserhaushalts von Waldstandorten in Bayern mit dem Simulationsmodell BROOK90. München, Forstliche Forschungsberichte 185.

Hanlon, V. C. T., Otto, S. P. & Aitken, S. N. (2019): Somatic Mutations Substantially Increase the Per-Generation Mutation Rate in the Conifer Picea sitchensis. Evolution Letters, 3, 348-358.

Harlin, J. & Kung, C.-S. (1992): Parameter Uncertainty and Simulation of Design Floods in Sweden. Journal of Hydrology, 137, 209-230.

Harsch, N., Brandenburg, M. & Klemm, O. (2009): Large-scale Lysimeter Site St. Arnold, Germany: Analysis of 40 years of Precipitation, Leachate and Evapotranspiration. Hydrology and Earth System Sciences, 5, 305-317.

Hartig, F., Dyke, J., Hickler, T., Higgins, S. I., O'hara, R. B., Scheiter, S. & Huth, A. (2012): Connecting Dynamic Vegetation Models to Data – An Inverse Perspective. Journal of Biogeography, 39, 2240-2252.

Hastings, W. K. (1970): Monte Carlo Sampling Methods Using Markov Chains and Their Applications. Biometrika, 57, 97-109.

Haynes, J. L. (1940): Ground Rainfall under Vegetative Canopy of Crops. Agronomy Journal, 32, 176-184.

Helvey, J. D. & Patric, J. H. (1965): Canopy and Litter Interception of Rainfall by Hardwoods of Eastern United States. Water Resources Research, 1, 193-206.

Hendriksson, N., Kulongoski, J., Massmann, G. & Newman, B. (2013): Using Isotopes for Design and Monitoring of Artificial Recharge Systems. Vienna, International Atomic Energy Agency.

Herrmann, M., Pust, J. & Pott, R. (2006): The Chemical Composition of Throughfall beneath Oak, Birch and Pine Canopies in Northwest Germany. Plant Ecology, 184, 273-285.

Hertel, D. (1999): Das Feinwurzelsystem von Rein- und Mischbeständen der Rotbuche: Struktur, Dynamik und interspezifische Konkurrenz. Berlin, Stuttgart, Gebrüder Borntraeger Verlagsbuchhandlung.

Hinckley, T., Lassoie, J. & Running, S. (1978): Temporal and Spatial Variations in the Water Status of Forest Trees. Forest Science, 20, 1-72.

Hogg, D. W. & Foreman-Mackey, D. (2018): Data Analysis Recipes: Using Markov Chain Monte Carlo. The Astrophysical Journal Supplement Series, 236, 1-18.

Höltermann, A. & Jessel, B. (2020): Wälder im Klimawandel: Steigerung von Anpassungsfähigkeit und Resilienz durch mehr Vielfalt und Heterogenität. Bundesamt für Naturschutz, Bonn.

Horiba Scientific (2020): LA-950 Laser Particle Size Analyzer. URL: https://www.horiba.com/de/scientific/products/particle-characterization/particle-size-analysis/details/la-950-laser-particle-size-analyzer-108/, accessed: 10.02.2020.

Hörmann, G., Branding, A., Clemen, T., Herbst, M., Hinrichs, A. & Thamm, F. (1996): Calculation and Simulation of Wind Controlled Canopy Interception of a Beech Forest in Northern Germany. Agricultural and Forest Meteorology, 79**,** 131-148.

Hörmann, G., Scherzer, J., Suckow, F., Müller, J., Wegehenkel, M., Lukes, M., Hammel, K., Knieß, A. & Meesenburg, H. (2003): Wasserhaushalt von Waldökosystemen: Methodenleitfaden zur Bestimmung der Wasserhaushaltskomponenten auf Level II-Flächen. 1-93.

Hoshika, Y., Osada, Y., De Marco, A., Peñuelas, J. & Paoletti, E. (2018): Global Diurnal and Nocturnal Parameters of Stomatal Conductance in Woody Plants and Major Crops. Global Ecology and Biogeography, 27**,** 257-275.

Hunt, E. R., Running, S. W. & Federer, C. A. (1991): Extrapolating Plant Water Flow Resistances and Capacitances to Regional Scales. Agricultural and Forest Meteorology, 54**,** 169-195.

Irvine, J., Perks, M., Magnani, F. & Grace, J. (1998): The Response of Pinus sylvestris to Drought: Stomatal Control of Transpiration and Hydraulic Conductance. Tree Physiology, 18**,** 393-402.

Jackisch, C., Germer, K., Graeff, T., Andrä, I., Schulz, K., Schiedung, M., Haller-Jans, J., Schneider, J., Jaquemotte, J., Helmer, P., Lotz, L., Bauer, A., Hahn, I., Šanda, M., Kumpan, M., Dorner, J., De Rooij, G., Wessel-Bothe, S., Kottmann, L., Schittenhelm, S. & Durner, W. (2020): Soil Moisture and Matric Potential – An Open Field Comparison of Sensor Systems. Earth System Science Data, 12**,** 683-697.

Jackson, R., Canadell, J., Ehleringer, J., Mooney, H., Sala, O. & Schulze, E. (1996): A Global Analysis of Root Distributions for Terrestrial Biomes. Oecologia, 108**,** 389-411.

Jansson, P.-E. & Karlberg, L. (2004): Coupled Heat and Mass Transfer Model for Soil-Plant-Atmosphere Systems. TRITA-LWR Report. Royal Institute of Technology, Department of Land and Water Resources Engineering, Stockholm, 1-427.

Jeremiah, E., Sisson, S., Marshall Price, L., Mehrotra, R. & Sharma, A. (2011): Bayesian Calibration and Uncertainty Analysis of Hydrological Models: A Comparison of Adaptive Metropolis and Sequential Monte Carlo Samplers. Water Resources Research, 47**,** 1-13.

Jochheim, H., Lüttschwager, D. & Wegehenkel, M. (2004): Simulation of the Water and Nitrogen Balances of Forests Within a Catchment in the Northeastern German Lowlands. European Journal of Forest Research, 123**,** 53-61.

Jonckheere, I., Fleck, S., Nackaerts, K., Muys, B., Coppin, P., Weiss, M. & Baret, F. (2004): Review of Methods for in situ Leaf Area Index Determination: Part I. Theories, Sensors and Hemispherical Photography. Agricultural and Forest Meteorology, 121**,** 19-35.

Kittredge, J. (1948): Forest Influences: The Effects of Woody Vegetation on Climate, Water, and Soil, with Applications to the Conservation of Water and the Control of Floods and Erosion. Minneapolis, McGraw-Hill Book Company.

Klein, M. (2000): Langjähriger Wasserhaushalt von Gras- und Waldbeständen - Entwicklung, Kalibrierung und Anwendung des Modells LYFE am Groß-Lysimeter St. Arnold. Osnabrück, Universität Osnabrück, Fachbereich Mathematik/Informatik.

Klinck, U., Rademacher, P., Wagner, M., Fleck, S., Ahrends, B., Meesenburg, H., Fier, A., Höper, H., Wallrabenstein, H. & Hassdenteufel, M. (2012): Stoffausträge mit dem Sickerwasser. GeoBerichte, 23**,** 152-162.

Knoben, W., Freer, J. & Woods, R. (2019): Technical Note: Inherent Benchmark or not? Comparing Nash–Sutcliffe and Kling–Gupta Efficiency Scores. Hydrology and Earth System Sciences, 23**,** 4323-4331.

Körner, C. (1995): Leaf Diffusive Conductances in the Major Vegetation Types of the Globe. In: Schulze, E. & Caldwell, M. (eds.): Ecophysiology of Photosynthesis. Berlin, Heidelberg, Springer.

Körner, C., Scheel, J. A. & Bauer, H. (1979): Maximum Leaf Diffusive Conductance in Vascular Plants. Photosynthetica, 13**,** 45-82.

Köstner, B. (2001): Evaporation and Transpiration from Forests in Central Europe - Relevance of Patch-level Studies for Spatial Scaling. Meteorology and Atmospheric Physics, 76**,** 69-82.

Köstner, B., Granier, A. & Cermák, J. (1998): Sapflow Measurements in Forest Stands: Methods and Uncertainties. Annals of Forest Science, 55**,** 13-27.

Köstner, B., Matyssek, R., Heilmeier, H., Clausnitzer, F., Nunn, A. & Wieser, G. (2008): Sap Flow Measurements as a Basis for Assessing Trace-Gas Exchange of Trees. Flora - Morphology, Distribution, Functional Ecology of Plants, 203**,** 14-33.

Kraft, G. (1884): Beiträge zur Lehre von den Durchforstungen, Schlagstellungen und Lichtungshieben. Hannover, Klindworth's Verlag.

Kram, K. J. (1998): Influence of Species Composition and Forest Age on Leaf Area Index. Polish Journal of Ecology, 46, 75-88.

Kriebitzsch, W. & Veste, M. (2012): Bedeutung trockener Sommer für die Photosynthese und Transpiration von verschiedenen Herkünften der Rot-Buche (Fagus sylvatica L.). Landbauforschung Volkenrode, 62, 193-210.

Kunert, N. (2020): Preliminary Indications for Diverging Heat and Drought Sensitivities in Norway spruce and Scots pine in Central Europe. iForest - Biogeosciences and Forestry, 13, 89-91.

Lagergren, F., Lankreijer, H., Kučera, J., Cienciala, E., Mölder, M. & Lindroth, A. (2008): Thinning Effects on Pine-Spruce Forest Transpiration in Central Sweden. Forest Ecology and Management, 255, 2312-2323.

Laloy, E. & Vrugt, J. A. (2012): High-dimensional Posterior Exploration of Hydrologic Models Using Multiple-try DREAM(ZS) and High-performance Computing. Water Resources Research, 48, 1-18.

Landesamt Für Bergbau, E. U. G. (2022): Grundwasser. URL: https://www.lbeg.niedersachsen.de/boden_grundwasser/grundwasser/grundwasser-536.html#:~:text=In%20Niedersachsen%20werden%20rund%2086%20%25%20des%20Trinkwassers,die%20restlichen%20Haushalte%20beziehen%20ihr%20Trinkwasser%20aus%20Privatbrunnen., accessed: 28.11.2022.

Landesamt Für Statistik Niedersachsen (2020): Ergebnisse der Landwirtschaftszählung Niedersachsen 2020. URL: https://www.statistik.niedersachsen.de/landwirtschaft_forstwirtschaft_fischerei/landwirtschaft_in_niedersachsen/landwirtschaftszaehlung_2020/ergebnisse-der-landwirtschaftszahlung-niedersachsen-2020-200649.html, accessed: 28.11.2022.

Larcher, W. (2001): Ökophysiologie der Pflanzen - Leben, Leistung und Stressbewältigung der Pflanzen in ihrer Umwelt. Stuttgart, Ulmer.

Leibundgut, C. & Seibert, J. (2011): Tracer Hydrology. In: Wilderer, P., Frimmel, F., Hanaki, K., Rogers, P., Uhlenbrook, S. & Vereijken, T. (eds.): Treatise on Water Science. Oxford, Academic Press.

Leuschner, C., Coners, H. & Icke, R. (2004): In situ Measurement of Water Absorption by Fine Roots of Three Temperate Forests: Species Differences and Differential Acitivty of Superficial and Deep Roots. Tree Physiology, 24, 1359-1367.

Leuschner, C. & Ellenberg, H. (2017): Ecology of Central European Forests: Vegetation Ecology of Central Europe, Volume I. Cham, Springer International Publishing AG.

Leuschner, C., Voß, S., Foetzki, A. & Clases, Y. (2006): Variation in Leaf Area Index and Stand Leaf Mass of European Beech across Gradients of Soil Acidity and Precipitation. Plant Ecology, 186, 247-258.

Leuschner, C., Wedde, P. & Lübbe, T. (2019): The Relation between Pressure–Volume Curve Traits and Stomatal Regulation of Water Potential in Five Temperate Broadleaf Tree Species. Annals of Forest Science, 76, 1-14.

Levia, D. F. & Germer, S. (2015): A Review of Stemflow Generation Dynamics and Stemflow-Environment Interactions in Forests and Shrublands. Reviews of Geophysics, 53, 673-714.

Levia, D. F., Michalzik, B., Näthe, K., Bischoff, S., Richter, S. & Legates, D. R. (2015): Differential Stemflow Yield from European beech Saplings: The Role of Individual Canopy Structure Metrics. Hydrological Processes, 29, 43-51.

Liu, C. L. C., Kuchma, O. & Krutovsky, K. V. (2018): Mixed-species Versus Monocultures in Plantation Forestry: Development, Benefits, Ecosystem Services and Perspectives for the Future. Global Ecology and Conservation, 15, 1-13.

Lovynska, V., Lakyda, P., Sytnyk, S., Kharytonov, M. & Piestova, I. (2018): LAI Estimation by Direct and Indirect Methods in Scots pine Stands in Northern Steppe of Ukraine. Journal of Forest Science, 64, 514-522.

Lüttschwager, D., Rust, S. & Forkert, J. (1999): Tree Canopy and Herb Layer Transpiration in Three Scots pine Stands with Different Stand Structures. Annals of Forest Science, 56, 265-274.

Lysimeter Research Group (2019): Lysimeter Data. URL: https://www.lysimeter.at/lysimeterplatform.html, accessed: 26.01.2021.

Marshall, L., Nott, D. & Sharma, A. (2004): A Comparative Study of Markov Chain Monte Carlo Methods for Conceptual Rainfall-Runoff Modeling. Water Resources Research, 40, 1-11.

Mason, W. L. & Alia, R. (2000): Current and future status of Scots pine (Pinus sylvestris L.) forest in Europe. Forest Systems, 9, 317-335.

Massey, F. J. (1951): The Kolmogorov-Smirnov Test for Goodness of Fit. Journal of the American Statistical Association, 46, 68-78.

Meesenburg, H., Ahrends, B., Kallweit, R., Scheler, B., Wagner, M. & Fleck, S. (2014): Interzeption in Wäldern: eine (zu) wenig beachtete Größe des Wasserkreislaufs. Forum für Hydrologie und Wasserbewirtschaftung, 34.14, 199-206.

Meier, I. C. & Leuschner, C. (2008): Leaf Size and Leaf Area Index in Fagus sylvatica Forests: Competing Effects of Precipitation, Temperature, and Nitrogen Availability. Ecosystems, 11**,** 655-669.

Mergner, U., Manthey, M., Scharnweber, T. & Kraus, D. (2020): Kronenverlichtung und Absterbevorgänge bei der Buche. AFZ Der Wald, 7/2020**,** 16-19.

Meschede, M. & Warr, L. N. (2019): The Geology of Germany - A Process-Oriented Approach. Cham, Springer International Publishing.

Metropolis, N., Rosenbluth, A. W., Rosenbluth, M. N., Teller, A. H. & Teller, E. (1953): Equation of State Calculations by Fast Computing Machines. Journal of Chemical Physics, 21**,** 1087-1092.

Micevski, T. & Kuczera, G. (2009): Combining Site and Regional Flood Information Using a Bayesian Monte Carlo Approach. Water Resources Research, 45**,** 1-11.

Mitscherlich, G. (1971): Wald, Wachstum und Umwelt: Waldklima und Wasserhaushalt. Frankfurt/Main, J. D. Sauerländers Verlag.

Möhlmann, M. (2021): Modeling The Leaf Area Index by Terrestrial Laser Scanning and its Influence on Rainfall Interception in Different Forests. Oldenburg, Carl-von-Ossietzky-Universität Oldenburg, Institut für Biologie und Umweltwissenschaften.

Mohr, K. (2001): Stickstoffimmissionen in Nordwestdeutschland - Untersuchungen zu den Ökologischen Auswirkungen auf Kiefernforsten und Möglichkeiten der Bioindikation. Oldenburg, Carl von Ossietzky Universität Oldenburg, Fachbereich Biologie, Geo- und Umweltwissenschaften.

Mohr, K., Meesenburg, H., Horváth, B., Meiwes, K. J., Schaaf, S. & Dämmgen, U. (2005): Bestimmung von Ammoniak-Einträgen aus der Luft und deren Wirkung auf Waldökosysteme (ANSWER-Projekt). Bundesministerium für Umwelt, Naturschutz und Reaktorsicherheit, Oldenburg, Göttingen, Braunschweig.

Morgenstern, Y., Puhlmann, H. & Von Wilpert, K. (2011): Erfassung und erste Analysen von Räumlichen Mustern der Bodenfeuchte auf Waldstandorten. Waldökologie, Landschaftsforschung und Naturschutz, 12**,** 47-59.

Moriasi, D., Arnold, J. G., Van Liew, M., Bingner, R., Harmel, R. D. & Veith, T. (2007): Model Evaluation Guidelines for Systematic Quantification of Accuracy in Watershed Simulations. Transactions of the American Society of Agricultural and Biological Engineers, 50**,** 885-900.

Mosello, R., Maria, C., Brizzio, D., Kotzias, D., Marchetto, A., Rembges, D. & Tartari, G. (2002): The Chemistry of Atmospheric Deposition in Italy in the Framework of the National Programme for Forest Ecosystems Control (CONECOFOR). Journal of Limnology, 61**,** 77-92.

Müller, H. (1967): Standortsökologische Wasserhaushaltsuntersuchungen an Vaccinium myrtillus L. Archiv für Forstwesen, 16**,** 587-590.

Müller, J. 2005. 30 Jahre forsthydrologische Forschung auf der Großlysimeteranlage in Britz - Zielstellung und Ergebnisse. *11. Gumpensteiner Lysimetertagung.* Höhere Bundeslehr- und Forschungsanstalt für Landwirtschaft, Irdning, Austria.

Müller, J. (2011): Die Anwendung von Lysimetern zur Ermittlung des Wasserhaushaltes in Wäldern des nordostdeutschen Tieflands. Waldökologie, Landschaftsforschung und Naturschutz, 12**,** 37-46.

Müller, J. (2012): Auswirkungen von Waldstrukturellen Veränderungen auf die Hydroökologischen Bedingungen in den Beständen im Zuge des Waldumbaus. In: Grünewald, U., Bens, O., Fischer, H., Hüttl, R. F. J., Kaiser, K. & Knierim, A. (eds.): Wasserbezogene Anpassungsmaßnahmen an den Landschafts- und Klimawandel. Stuttgart, Schweizerbart.

Müller, J. 2017. Die forstökologische Forschung mit Lysimetern: Möglichkeiten und Grenzen ihres Einsatzes. *17. Gumpensteiner Lysimetertagung.* Raumberg-Gumpenstein: Höhere Bundeslehr- und Forschungsanstalt für Landwirtschaft, Irdning, Austria.

Müller, J. (2019): Die forsthydrologische Forschung im Nordostdeutschen Tiefland: Veranlassung, Methoden, Ergebnisse und Perspektiven. Rostock, Universität Rostock.

Müller, J. (n. d.): Verdunstung der Bodenvegetation verbreiteter Bodenvegetationsformen der Kiefer des nordostdeutschen Tieflands in Abhängigkeit von der Art und ihrem Bedeckungsgrad. 1-12.

Müller, J. & Seyfarth, M. (1999): Methode zur Ermittlung des Wasserverbrauches Unterschiedlicher Waldbodenvegetationsdecken mit Hilfe von Wägbaren Lysimetern. Tagungsband der 8. Lysimetertagung der Bundesanstalt für Alpenländische Landwirtschaft in Gumpenstein am 13. und 14.04.1999, 177-178.

Müller, M. & Finkeldey, R. (2017): Genetic and Adaptive Trait Variation in Seedlings of European beech Provenances from Northern Germany. Silvae Genetica, 65**,** 65-73.

Nash, J. E. & Sutcliffe, J. V. (1970): River Flow Forecasting Through Conceptual Models Part I — A Discussion of Principles. Journal of Hydrology, 10**,** 282-290.

Natkhin, M. (2011): Modellgestützte Analyse der Einflüsse von Veränderungen der Waldwirtschaft und des Klimas auf den Wasserhaushalt grundwasserabhängiger Landschaftselemente. Potsdam, Mathematisch-Naturwissenschaftliche Fakultät der Universität Potsdam.

Neary, D. G., Ice, G. G. & Jackson, C. R. (2009): Linkages between Forest Soils and Water Quality and Quantity. Forest Ecology and Management, 258, 2269-2281.

Newman, E. I. (1974): Root-Soil Water Relations. In: Carson, E. W. (eds.): The Plant Root and its Environment. Charlottesville, University Press of Virginia.

Nguyen, Q., Polle, A. & Pena, R. (2017): Intraspecific Variations in Drought Response and Fitness Traits of Beech (Fagus sylvatica L.) Seedlings from three Provenances Differing in Annual Precipitation. Trees, 31, 1215-1225.

Nibis Kartenserver (2014a): Bodenkarte 1:50000 (BK50). Hannover, Landesamt für Bergbau, Energie und Geologie (LBEG).

Nibis Kartenserver (2014b): Historische Landnutzung in Niedersachsen 1 : 25000. Hannover, Landesamt für Bergbau, Energie und Geologie (LBEG).

Nibis Kartenserver (2014c): Lage der Grundwasseroberfläche 1:50000 (HK 50). Hannover, Landesamt für Bergbau, Energie und Geologie (LBEG).

Niedersächsische Landesforsten (2018): Das LÖWE-Programm. 25 Jahre langfristige ökologische Waldentwicklung. Braunschweig, Niedersächsische Landesforsten,.

Niedersächsisches Ministerium Für Ernährung Landwirtschaft Und Verbraucherschutz (2014): Der Wald in Niedersachsen. Ergebnisse der Bundeswaldinventur 3. Hannover, Niedersächsisches Ministerium für Ernährung, Landwirtschaft und Verbraucherschutz.

Niedersächsisches Ministerium Für Ernährung Landwirtschaft Und Verbraucherschutz (2022): Wald- und Forstwirtschaft. URL: https://www.ml.niedersachsen.de/startseite/themen/wald_holz_jagd/wald_und_forstwirtschaft/, accessed: 28.11.2022.

Nlwkn (2022): Öffentliche Trinkwasserversorgung und Wassergewinnungsanlagen für Industrie und Gewerbe. URL: https://www.nlwkn.niedersachsen.de/startseite/wasserwirtschaft/grundwasser/wasserversorgung/wassergewinnung/wassergewinnung-42573.html, accessed: 28.11.2022.

Norman, J. M. & Campbell, G. S. (1989): Canopy Structure. In: Pearcy, R. W., Ehleringer, J. R., Mooney, H. A. & Rundel, P. W. (eds.): Plant Physiological Ecology: Field Methods and Instrumentation. New York, Chapman and Hall.

Nossent, J., Elsen, P. & Bauwens, W. (2011): Sobol' Sensitivity Analysis of a Complex Environmental Model. Environmental Modelling & Software, 26, 1515-1525.

Ostermann, U. (2020): Neue Wasserquellen erschließen. Land & Forst, 22/2020, 18-20.

Otto, H.-J. (1986): Standörtliche Voraussetzungen, Ziele und Waldbautechnik in Fichten-Buchen-Mischbeständen des Harzes. Allgemeine Forst- und Jagdzeitung, 157, 214-222.

Paton, F., Maier, H. & Dandy, G. (2013): Relative Magnitudes of Sources of Uncertainty in Assessing Climate Change Impacts on Water Supply Security for the Southern Adelaide Water Supply System. Water Resources Research, 49, 1643-1667.

Paul, C., Brandl, S., Friedrich, S., Falk, W., Härtl, F. & Knoke, T. (2019): Climate Change and Mixed Forests: How do Altered Survival Probabilities impact Economically Desirable Species Proportions of Norway spruce and European beech? Annals of Forest Science, 76, 1-15.

Peck, A. (2004): Hydrometeorologische und mikroklimatische Kennzeichen von Buchenwäldern. Freiburg, Albert-Ludiwgs Universität Freiburg, Fakultät für Forst- und Umweltwissenschaften.

Peck, A. & Mayer, H. (1996): Einfluss von Bestandesparametern auf die Verdunstung von Wäldern. Forstwirtschaftliches Centralblatt, 115, 1-9.

Penne, C. (2009): Räumliche Variabilität der Humusspeicherung in Abhängigkeit von der Kronendachstruktur eines Kiefernbestandes. Horizonte Herrenhäuser Forschungsbeitträge zur Bodenkunde. Hannover, Gottfried Wilhelm Leibniz Universität Hannover, Institut für Bodenkunde.

Pianosi, F., Beven, K., Freer, J., Hall, J. W., Rougier, J., Stephenson, D. B. & Wagener, T. (2016): Sensitivity Analysis of Environmental Models: A systematic Review with practical Workflow. Environmental Modelling & Software, 79, 214-232.

Post, H., Vrugt, J. A., Fox, A., Vereecken, H. & Hendricks Franssen, H.-J. (2017): Estimation of Community Land Model Parameters for an improved Assessment of Net Carbon Fluxes at European Sites. Journal of Geophysical Research: Biogeosciences, 122, 661-689.

Poyatos, R., Aguadé, D., Galiano, L., Mencuccini, M. & Martinez Vilalta, J. (2013): Drought-induced Defoliation and long Periods of Near-Zero Gas Exchange play a Key Role in Accentuating Metabolic Decline of Scots pine. The New phytologist, 200, 388-401.

Poyatos, R., Granda, V., Flo, V., Adams, M. A., Adorján, B., Aguadé, D., Aidar, M. P. M., Allen, S., Alvarado-Barrientos, M. S., Anderson-Teixeira, K. J., Aparecido, L. M., Arain, M. A., Aranda, I., Asbjornsen, H., Baxter, R., Beamesderfer, E., Berry, Z. C., Berveiller, D., Blakely, B., Boggs, J., Bohrer, G., Bolstad, P. V., Bonal, D., Bracho, R., Brito, P., Brodeur, J., Casanoves, F., Chave, J., Chen, H., Cisneros, C., Clark, K., Cremonese, E., Dang, H., David, J. S., David, T. S., Delpierre, N., Desai, A. R., Do, F. C., Dohnal, M., Domec, J. C., Dzikiti, S., Edgar, C., Eichstaedt, R., El-Madany, T. S., Elbers, J., Eller, C. B., Euskirchen, E. S., Ewers, B., Fonti, P., Forner, A., Forrester, D. I., Freitas, H. C., Galvagno, M., Garcia-Tejera, O., Ghimire, C. P., Gimeno, T. E., Grace, J., Granier, A., Griebel, A., Guangyu, Y., Gush, M. B., Hanson, P. J., Hasselquist, N. J., Heinrich, I.,

Hernandez-Santana, V., Herrmann, V., Hölttä, T., Holwerda, F., Irvine, J., Isarangkool Na Ayutthaya, S., Jarvis, P. G., Jochheim, H., Joly, C. A., Kaplick, J., Kim, H. S., Klemedtsson, L., Kropp, H., Lagergren, F., Lane, P., Lang, P., Lapenas, A., Lechuga, V., Lee, M., Leuschner, C., Limousin, J. M., Linares, J. C., Linderson, M. L., Lindroth, A., Llorens, P., López-Bernal, Á., Loranty, M. M., Lüttschwager, D., Macinnis-Ng, C., Maréchaux, I., Martin, T. A., Matheny, A., Mcdowell, N., Mcmahon, S., Meir, P., Mészáros, I., et al. (2021): Global Transpiration Data from Sap Flow Measurements: The SAPFLUXNET Database. Earth System Science Data, 13**,** 2607-2649.

Prietzel, J. & Bachmann, S. (2011): Verändern Douglasien Wasser und Boden? LWF Aktuell, 84**,** 50-52.

Puhlmann, H. & Von Wilpert, K. (2011): Testing and Development of Pedotransfer Functions for Water Retention and Hydraulic Conductivity of Forest Soils. Waldokologie Online, 12**,** 61-71.

Putuhena, W. M. & Cordery, I. (1996): Estimation of Interception Capacity of the Forest Floor. Journal of Hydrology, 180**,** 283-299.

R Core Team (2017): R: A language and environment for statistical computing. R Foundation for Statistical Computing, Vienna, Austria.

Raj, R., Van Der Tol, C., Hamm, N. a. S. & Stein, A. (2018): Bayesian Integration of Flux Tower Data into a Process-based Simulator for Quantifying Uncertainty in Simulated Output. Geoscientific Model Development, 11**,** 83-101.

Reichelt, G. (1973): Vegetationsgeographie. Braunschweig, Westermann.

Rich, P. M. (1990): Characterizing Plant Canopies with Hemispherical Photographs. Remote Sensing Reviews, 5**,** 13-29.

Ridler, T. W. & Calvard, S. (1978): Picture Thresholding Using an Iterative Selection Method. IEEE Transactions on Systems, Man, and Cybernetics, 8**,** 630-632.

Ringe, H., Duijnisveld, W. & Böttcher, J. (2000): Qualität der Grundwasserneubildung in Abhängigkeit von Bestandsaufbau und Boden - Modelluntersuchungen im Fuhrberger Feld und angrenzenden Gebieten. Universität Hannover, Bundesanstalt für Geowissenschaften und Rohstoffe, Hannover.

Rohde, M., Hurling, R., Langer, G., Bußkamp, J., Plasil, P. & Graw, I. (2020): Insekten und Pilze. In: (eds.): Waldzustandsbericht 2020. Niedersächsisches Ministerium für Ernährung, Landwirtschaft und Verbraucherschutz.

Röper, T., Kröger, K. F., Meyer, H., Sültenfuß, J., Greskowiak, J. & Massmann, G. (2012): Groundwater Ages, Recharge Conditions and Hydrochemical Evolution of a Barrier Island Freshwater Lens (Spiekeroog, Northern Germany). Journal of Hydrology, 454-455**,** 173-186.

Rothe, A., Huber, C., Kreutzer, K. & Weis, W. (2002): Deposition and Soil Leaching in Stands of Norway spruce and European Beech: Results from the Höglwald Research in Comparison with other European Case Studies. Plant and Soil, 240**,** 33-45.

Ruhm, W., Englisch, M., Starlinger, F., Geburek, T., Perny, B. & Neumann, M. (2016): Buche (Rotbuche, Fagus Sylvatica L.). BFW-Praxisinformation, 41**,** 10-13.

Rumpf, H. & Petersen, R. (2008): Forest Conversion to Beech in Consideration of its Ecological Demands. Beiträge aus der NW-FVA, 3**,** 193-219.

Safford, L. & Bell, S. (1972): Biomass of Fine Roots in a White Spruce Plantation. Canadian Journal of Forest Research, 2**,** 169-172.

Safford, L. O. (1974): Effect of Fertilization on Biomass and Nutrient Content of Fine Roots in a Beech-Birch-Maple Stand. Plant and Soil, 40**,** 349-363.

Saltelli, A., Ratto, M., Andres, T., Campolongo, F., Cariboni, J., Gatelli, D., Saisana, M. & Tarantola, S. (2008): Global Sensitivity Analysis. The Primer. Chichester, John Wiley & Sons.

Schaefli, B. & Gupta, H. V. (2007): Do Nash Values have Value? Hydrological Processes, 21**,** 2075-2080.

Scharnweber, T., Manthey, M., Criegee, C., Bauwe, A., Schröder, C. & Wilmking, M. (2011): Drought matters - Declining Precipitation influences Growth of Fagus sylvatica L. and Quercus robur L. in North-Eastern Germany. Forest Ecology and Management, 262**,** 947-961.

Scherfose, V. (1990): Feinwurzelverteilung und Mykorrhizatypen von Pinus sylvestris in verschiedenen Bodentypen. Hannover, Fachbereich Landespflege der Universität Hannover.

Schleppi, P., Conedera, M., Sedivy, I. & Thimonier, A. (2007): Correcting Non-Linearity and Slope Effects in the Estimation of the Leaf Area Index of Forests from Hemispherical Photographs. Agricultural and Forest Meteorology, 144**,** 236-242.

Schmidt-Walter, P. (2019): Evaluation of Environmental Impacts of Short Rotation Coppice with Regard to the Amount and Quality of Groundwater Recharge. Göttingen, Georg-August-University Göttingen, Faculty of Forest Sciences and Forest Ecology.

Schmidt-Walter, P., Trotsiuk, V., Hammel, K., Kennel, M. & Federer, C. A. 2020a. LWFBrook90R: Run the LWF-Brook90 hydrological model in R. Zenodo.

Schmidt-Walter, P., Trotsiuk, V., Meusburger, K., Zacios, M. & Meesenburg, H. (2020b): Advancing Simulations of Water Fluxes, Soil Moisture and Drought Stress by Using

the LWF-Brook90 Hydrological Model in R. Agricultural and Forest Meteorology, 291, 108023.

Schneider, C. A., Rasband, W. S. & Eliceiri, K. W. (2012): NIH Image to ImageJ: 25 years of Image Analysis. Nature Methods, 9, 671-675.

Schröder, J., Degenhardt, A. & Guericke, M. (2018): Wie weiter mit der Buche nach dem Waldumbau? AFZ Der Wald, 15/2018,

Schröter, I. (2019): Quantifizierung der Interzeptionsverdunstung verschiedener Bodenvegetationstypen. Oldenburg, Carl von Ossietzky Universität Oldenburg, Institut für Biologie und Umweltwissenschaften.

Schulla, J. (2021): Model Description WaSiM (Water Balance Simulation Model). Technical Report, 397.

Schultze, B. & Scherzer, J. 2015. Wasserhaushaltssimulationen, Versickerungstabellen und Versickerungskarten. Projekt Wasserwald im Privatwald der östlichen Lüneburger Heide in Niedersachsen. Abschlussbericht.: UDATA, Landwirtschaftskammer Niedersachsen, Bundesministerum für Ernährung und Landwirtschaft, Bundesministerium für Umwelt, Naturschutz, Bau und Reaktorsicherheit.

Schwärzel, K. (2012): Stammabfluss bei Buchen als Auslöser für präferenzielle Fließvorgänge im Boden. Wasser ohne Grenzen. Forum für Hydrologie und Wasserbewirtschaftung, 31.12, 49-53.

Schwärzel, K., Menzer, A., Spank, U., Clausnitzer, F., Häntzschel, J., Köstner, B., Bernhofer, C. & Feger, K.-H. (2009): Soil Water Content Measurements deliver Reliable Estimates of Water Fluxes: A Comparative Study in a Beech and a Spruce Stand in the Tharandt Forest (Saxony, Germany). Agricultural and Forest Meteorology, 149, 1994-2006.

Shuttleworth, W. J. & Gurney, R. J. (1990): The Theoretical Relationship between Foliage Temperature and Canopy Resistance in Sparse Crops. Quarterly Journal of the Royal Meteorological Society, 116, 497-519.

Shuttleworth, W. J. & Wallace, J. S. (1985): Evaporation from Sparse Crops - An Energy Combination Theory. Quarterly Journal of the Royal Meteorological Society, 111, 839-855.

Song, X., Zhang, J., Zhan, C., Xuan, Y., Ye, M. & Xu, C. (2015): Global Sensitivity Analysis in Hydrological Modeling: Review of Concepts, Methods, Theoretical Framework, and Applications. Journal of Hydrology, 523, 739-757.

Sonntag, D. (1990): Important New Values of the Physical Constants of 1986, Vapor Pressure Formulations based on the ITS-90 and Psychrometer Formulae. Zeitschrift für Meteorologie, 70, 340-344.

Soudani, K., Trautmann, J. & Walter, J. M. N. (2002): Leaf Area Index and Canopy Stratification in Scots pine (Pinus sylvestris L.) Stands. International Journal of Remote Sensing, 23**,** 3605-3618.

Spathelf, P., Larsen, J. B., Bauhus, J., Boncina, A., Brang, P., Spathelf, P., Larsen, J. B., Bauhus, J., Bonc Ina, A., Chauvin, C., Drossler, L., Garcia-Guemes, C., Heiri, C., Kerr, G., Lexer, M. J., Mason, B., Mohren, F., Muhlethaler, U., Nocentini, S. & Svoboda, M. (2014): Suitability of close-to-nature Silviculture for Adapting Temperate European Forests to Climate Change. Forestry, 87**,** 492-503.

Speich, M. J. R., Zappa, M., Scherstjanoi, M. & Lischke, H. (2020): FORests and HYdrology under Climate Change in Switzerland v1.0: A spatially distributed Model combining Hydrology and Forest Dynamics. Geoscientific Model Development, 13**,** 537-564.

Spellmann, H. (2008): Die Kiefer - Ein Auslaufmodell? - Beiträge für eine zielgerichtete Entwicklung. Beiträge aus der NW-FVA, 2**,** 63-78.

Spellmann, H. (2020): Entscheidungshilfen zur Anpassung der Wälder an den Klimawandel. Ländlicher Raum, 20781**,** 20-23.

Spellmann, H., Ahrends, B., Albert, M., Andert, S., Barkmann, T., Böcher, M., Breckling, B., Christen, O., Dvorak, J., Eggers, M., Fleck, S., Fohrer, N., Gauly, M., Gerowitt, B., Gieseke, D., Grocholl, J., Hakes, W., Hammes, V., Hartje, V., Haunert, G., Hoffmann, M., Hufnagel, J., Isselstein, J., Kätzel, R., Kayser, M., Kehr, I., Knauer, H., Krott, M., Lambertz, C., Lange, A., Langer, G., Leefken, G., Löffler, S., Meesenburg, H., Meißner, R., Messal, H., Meyer, P., Möhring, B., Möller, K., Nagel, J., Nuske, R., Oetzmann, A., Ohrmann, S., Redwitz, C. V., Riediger, J., Schmidt, M., Schröder, J., Schröder, W., Siebert, R., Spindelndreher, D., Stahlmann, H., Stöck, L., Sutmöller, J., Svoboda, N., Tänzer, D., Tiedemann, A. V., Ulber, B., Wegner, K., Werner, P. C., M., W., Wüstemann, H., Zander, P. & Ziesche, T. (2017): Nachhaltiges Landmanagement im Norddeutschen Tiefland. Beiträge aus der NW-FVA, 18**,** 1-436.

Sponagel, H. (2005): Bodenkundliche Kartieranleitung : mit 103 Tabellen und 31 Listen. Stuttgart, E. Schweizerbart'sche Verlagsbuchhandlung Nägele und Obermiller.

Staelens, J., De Schrijver, A., Verheyen, K. & Verhoest, N. E. C. (2008): Rainfall Partitioning into Throughfall, Stemflow, and Interception within a single Beech (Fagus sylvatica L.) Canopy: Influence of Foliation, Rain event characteristics, and Meteorology. Hydrological Processes, 22**,** 33-45.

Steinmann, V. (2015): Tiefendurchwurzelung von Waldbäumen auf quartären Standorten im Norddeutschen Tiefland. Göttingen, Fakultät für Forstwissenschaften und Waldökologie der Georg-August-Universität Göttingen.

Sutmöller, J. (2014): Grundwasserneubildungsraten unter BZE-Punkten. In: Dammann, I., Paar, U., Weymar, J., Spielmann, M. & Eichhorn, J. (eds.): Waldzustandsbericht 2014 Niedersachsen. Göttingen, Nordwestdeutsche Forstliche Versuchsanstalt (NW-FVA).

Sutmöller, J., Dammann, I., Wagner, M. & Scheler, B. (2019): Die extreme Trockenheit 2018 in Nordwestdeutschland, Teil 1. AFZ Der Wald, 6/2019**,** 42-46.

Tagesson, T. (2006): Indirect Estimations and spatial Variation in Leaf Area Index of Coniferous, Deciduous and Mixed Forest Stands in Forsmark and Laxemar. Swedish Nuclear Fuel and Waste Management Co, Stockholm, Sweden.

Tapia-Arenas, C. A., Feger, K.-H. & Julich, S. (2020): Remote sensing data for calibrating hydrologic modeling: Hydrological impacts of land use change of the Reventado river sub-basin, Costa Rica. Revista Forestal Mesoamericana Kurú, 17**,** 16-28.

Thamm, F. & Widmoser, P. (1995): Zur hydrologischen Bedeutung der organischen Auflage im Wald: Untersuchungsmethoden und erste Ergebnisse. Zeitschrift für Pflanzenernährung und Bodenkunde, 158**,** 287-292.

Thiel, D., Kreyling, J., Backhaus, S., Beierkuhnlein, C., Buhk, C., Egen, K., Huber, G., Konnert, M., Nagy, L. & Jentsch, A. (2014): Different Reactions of Central and Marginal Provenances of Fagus sylvatica to Experimental Drought. European Journal of Forest Research, 133**,** 247-260.

Thimonier, A. (1998): Measurement of Atmospheric Deposition Under Forest Canopies: Some Recommendations for Equipment and Sampling Design. Environmental Monitoring and Assessment, 52**,** 353-387.

Thimonier, A., Sedivy, I. & Schleppi, P. (2010): Estimating Leaf Area Index in different Types of Mature Forest Stands in Switzerland: A Comparison of Methods. European Journal of Forest Research, 129**,** 543-562.

Thünen Institut (2021): Die Rolle der Baumarten im Landschaftswasserhaushalt. URL: https://www.thuenen.de/de/thema/wasser/wald-und-wasser/die-rolle-der-baumarten-im-landschaftswasserhaushalt/, accessed: 26.01.2021.

Topp, G. C., Davis, J. L. & Annan, A. P. (1980): Electromagnetic Determination of Soil Water Content: Measurements in coaxial Transmission Lines. Water Resources Research, 16**,** 574-582.

Ulrich, B. (1986): Die Rolle der Bodenversauerung beim Waldsterben: Langfristige Konsequenzen und forstliche Möglichkeiten. Forstwissenschaftliches Centralblatt, 105**,** 421-435.

Umwelt Geräte Technik Gmbh (2020a): About Soil Moisture Meters. URL: https://www.ugt-online.de/en/products/soil-science/soil-moisturetemperatureconductivity/about-soil-moisture-meters/, accessed: 12.10.2020.

Umwelt Geräte Technik Gmbh (2020b): SMT-100. URL: https://www.ugt-online.de/produkte/bodenkunde/bodenfeuchtetemperaturleitfaehigkeit/smt-100/, accessed, 12.10.2020.

Van Der Heijden, G., Legout, A., Pollier, B., Bréchet, C., Ranger, J. & Dambrine, E. (2013): Tracing and Modeling Preferential Flow in a Forest Soil - Potential Impact on Nutrient Leaching. Geoderma, 195-196**,** 12-22.

Van Genuchten, M. (1980): A Closed-form Equation for Predicting the Hydraulic Conductivity of Unsaturated Soils. Soil Science Society of America Journal, 44**,** 892-898.

Van Oijen, M. (2017): Bayesian Methods for Quantifying and Reducing Uncertainty and Error in Forest Models. Current Forestry Reports, 3**,** 269-280.

Von Willert, D., Matyssek, R. & Herppich, W. (1995): Experimentelle Pflanzenökologie - Grundlagen und Anwendungen. Stuttgart, New York, Thieme.

Vorobevskii, I., Kronenberg, R. & Bernhofer, C. (2020): Global BROOK90 R Package: An Automatic Framework to Simulate the Water Balance at Any Location. Water, 12**,** 2037.

Vrugt, J. A., Gupta, H. V., Bouten, W. & Sorooshian, S. (2003): A Shuffled Complex Evolution Metropolis Algorithm for Optimization and Uncertainty Assessment of Hydrologic Model Parameters. Water Resources Research, 39**,** 1201.

Vrugt, J. A. & Ter Braak, C. J. F. (2011): DREAM: An adaptive Markov Chain Monte Carlo Simulation Algorithm to solve Discrete, Noncontinuous, and Combinatorial Posterior Parameter Estimation Problems. Hydrology and Earth System Sciences, 15**,** 3701-3713.

Vrugt, J. A., Ter Braak, C. J. F., Clark, M. P., Hyman, J. M. & Robinson, B. A. (2008a): Treatment of Input Uncertainty in Hydrologic Modeling: Doing Hydrology backward with Markov Chain Monte Carlo Simulation. Water Resources Research, 44**,** W00B09.

Vrugt, J. A., Ter Braak, C. J. F., Diks, C. G. H., Robinson, B. A., Hyman, J. M. & Higdon, D. (2009): Accelerating Markov Chain Monte Carlo Simulation by Differential Evolution with Self-Adaptive Randomized Subspace Sampling. International Journal of Nonlinear Sciences and Numerical Simulation, 10**,** 273-290.

Vrugt, J. A., Ter Braak, C. J. F., Gupta, H. V. & Robinson, B. A. (2008b): Equifinality of Formal (DREAM) and Informal (GLUE) Bayesian Approaches in Hydrologic Modeling? Stochastic Environmental Research and Risk Assessment, 23**,** 1011-1026.

Watson, D. J. (1947): Comparative Physiological Studies on the Growth of Field Crops: I. Variation in Net Assimilation Rate and Leaf Area between Species and Varieties, and within and between Years. Annals of Botany, 11**,** 41-76.

Weihermüller, L., Lehmann, P., Herbst, M., Rahmati, M., Verhoef, A., Or, D., Jacques, D. & Vereecken, H. (2021): Choice of Pedotransfer Functions Matters when Simulating Soil Water Balance Fluxes. Journal of Advances in Modeling Earth Systems, 13**,** E2020MS002404.

Weis, W., Wellpot, A. & Falk, W. (2020): Standortfaktor Wasserhaushalt im Wald. LWF Aktuell, 03/2020**,** 14-17.

Wessolek, G., Kaupenjohann, M. & Renger, M. (2009): Bodenphysikalische Kennwerte und Berechnungsverfahren für die Praxis. Bodenökologie und Bodengenese, 40**,** 1-80.

West, P. W. (2015): Tree and Forest Measurement. Cham, Springer International Publishing.

Western, A. W., Blöschl, G. & Grayson, R. B. (1998): Geostatistical Characterisation of Soil Moisture Patterns in the Tarrawarra Catchment. Journal of Hydrology, 205**,** 20-37.

Wösten, J. H. M., Lilly, A., Nemes, A. & Le Bas, C. (1999): Development and Use of a Database of Hydraulic Properties of European Soils. Geoderma, 90**,** 169-185.

Wösten, J. H. M., Pachepsky, Y. A. & Rawls, W. J. (2001): Pedotransfer Functions: Bridging the Gap between available basic Soil Data and missing Soil Hydraulic Characteristics. Journal of Hydrology, 251**,** 123-150.

Yan, G., Hu, R., Luo, J., Weiss, M., Jiang, H., Mu, X., Xie, D. & Zhang, W. (2019): Review of Indirect Optical Measurements of Leaf Area Index: Recent Advances, Challenges, and Perspectives. Agricultural and Forest Meteorology, 265**,** 390-411.

Zhang, Y., Zhang, M., Niu, J. & Zheng, H. (2016): The Preferential Flow of Soil: A Widespread Phenomenon in Pedological Perspectives. Eurasian Soil Science, 49**,** 661-672.

Zhao, L., Hou, R. & Fang, Q. (2019): Differences in Interception Storage Capacities of Undecomposed Broad-leaf and Needle-leaf Litter under Simulated Rainfall Conditions. Forest Ecology and Management, 446**,** 135-142.

Zimmermann, A., Voss, S., Metzger, J., Hildebrandt, A. & Zimmermann, B. (2016): Capturing Heterogeneity: The Role of a Study Area's Extent for Estimating Mean Throughfall. Journal of Hydrology, 542**,** 781-789.

Zimmermann, A. & Zimmermann, B. (2014): Requirements for Throughfall Monitoring: The Roles of Temporal Scale and Canopy Complexity. Agricultural and Forest Meteorology, 189-190**,** 125-139.

Zöller, L. (2017): Die Physische Geographie Deutschlands. Darmstadt, Wissenschaftliche Buchgesellschaft.

Zweifel, R., Steppe, K. & Sterck, F. J. (2007): Stomatal Regulation by Microclimate and Tree Water Relations: Interpreting Ecophysiological Field Data with a Hydraulic Plant Model. Tree Physiology, 18**,** 2113-2131.

Appendix

Vegetation measurements

Table 52: ***Stand parameters assessed for Sandkrug, Elze and Wibbese****: Tree species, tree age, tree height, diameter at breast height, stand density and basal area. Stand parameters are separately assessed for the soil moisture measurement plot ($Plot_{SM}$), stand precipitation measurement plot ($Plot_{SP}$) and the forest plot including both measurement plots (Stand).*

Plot	Species	Subplot	Age *[a]*	Height *[m]*	DBH *[cm]*	SD *[ha^{-1}]*	BA *[m^2/ha]*
SREF	Pine	$Plot_{SM}$	70	23.0	26.0	625	33.7
		$Plot_{SP}$	70	23.0	25.2	556	28.1
		Stand	70	23.0	26.9	612	35.5
SB20	Pine	$Plot_{SM}$	70	23.0	34.3	417	39.3
		$Plot_{SP}$	70	23.0	34.1	454	44.1
		Stand	70	23.0	30.4	389	32.0
	Beech	$Plot_{SM}$	20	7.0	4.6	4792	8.9
		$Plot_{SP}$	20	7.0	4.6	5093	9.5
		Stand	20	7.0	4.5	4496	8.1
EREF	Pine	$Plot_{SM}$	70	22.0	31.0	417	32.3
		$Plot_{SP}$	70	22.0	29.7	417	29.9
		Stand	70	22.0	31.8	419	34.3
EB5	Pine	$Plot_{SM}$	70	21.6	30.7	417	31.3
		$Plot_{SP}$	70	21.6	34.5	278	26.4
		Stand	70	21.6	31.7	385	30.6
	Beech	$Plot_{SM}$	5	1.6	-	4167	-
		$Plot_{SP}$	5	1.5	-	4063	-
		Stand	5	1.6	-	4507	-
EB15	Pine	$Plot_{SM}$	70	20.2	35.7	347	34.9
		$Plot_{SP}$	70	20.2	37.9	347	39.9
		Stand	70	20.2	36.5	285	29.0
	Beech	$Plot_{SM}$	15	7.0	4.5	3681	6.7
		$Plot_{SP}$	15	7.0	4.4	2639	4.8
		Stand	15	7.0	4.5	3084	5.5
EB25	Beech	$Plot_{SM}$	25	7.5	6.9	1750	7.2
		$Plot_{SP}$	25	7.5	7.0	2100	9.1
		Stand	25	7.5	6.7	1908	7.3
W REF	Pine	$Plot_{SM}$	70	27.8	29.2	556	55.6
		$Plot_{SP}$	70	27.8	31.7	417	49.1
		Stand	70	27.8	31.2	494	45.1
W B5	Pine	$Plot_{SM}$	70	27.8	27.8 (27.8)	700 (500)	42.7 (30.5)
		$Plot_{SP}$	70	27.8	33.7 (33.7)	800 (700)	72.7 (63.6)
		Stand	70	27.8	32.1 (32.1)	640 (460)	53.1 (38.4)
	Beech	$Plot_{SM}$	5	1.5	-	3819	-
		$Plot_{SP}$	5	1.7	-	5208	-
		Stand	5	1.6	-	3847	-
W D5	Pine	$Plot_{SM}$	70	27.8	45.3 (45.3)	600 (400)	98.5 (65.6)
		$Plot_{SP}$	70	27.8	36.0 (36.0)	600 (400)	61.2 (40.8)
		Stand	70	27.8	39.4 (39.4)	500 (300)	62.4 (37.3)
	Douglas fir	$Plot_{SM}$	5	2.2	-	3750	-
		$Plot_{SP}$	5	2.3	-	3611	-
		Stand	5	2.3	-	3387	-

*Table 53: Dominating g**round vegetation species** and their degree of coverage at the forest plots.*

	S REF	S B20	E REF	E B5	E B15	E B25	W REF	W B5	W D5
Litter	15 %	95 %	20 %	20 %	75 %	95 %	15 %	20 %	15 %
Pleurozium schreberi (BRID.) MITT.	90 %	5 %	80 %	80 %	25 %	5 %	90 %	80 %	90 %
Vaccium myrtillus L.	88 %	-	10 %	15 %	<5 %	-	-	-	-
Polytrichastrum formosum (HEDW.) G.L.S.M.	10 %	-	-	-	-	-	-	-	-
Pinus sylvestris L.	38 %	-	<5 %	63 %	-	-	<5 %	<5 %	-
Quercus petraea (MATTUSCHKA) LIEBL.	<5 %	-	<5 %	38 %	-	-	<5 %	-	<5 %
Fagus sylvatica L.	<5 %	-	<5 %	-	-	-	<5 %	21 %	-
Sorbus aucuparia L.	<5 %	-	-	-	-	-	<5 %	<5 %	<5 %
Avenella flexuosa (L.) TRIN.	-	-	38 %	<5 %	-	-	38 %	38 %	63 %
Pseudotsuga menziesii (MIRBEL) FRANCO	-	-	-	-	-	-	-	-	10 %

*Table 54: The **classification of tree canopy** into the classes 'crown', 'gap' and 'intermediate' with their respective share of total canopy area based on classification of photographs. Based on the crown cover classification, the number of sensors per canopy category is estimated.*

	Crown (C)		Transition zone (T)		Gap (G)	
	Mean Area	Number of sensors/gutters	Mean Area	Number of sensors/gutters	Mean Area	Number of sensors/gutters
E REF	30 %	2	32 %	3	37 %	3
E B5	31 %	3	29 %	2	41 %	3
E B15	38 %	3	25 %	2	36 %	3
E B25	79 %	6	-	-	21 %	2
S REF	29 %	2	36 %	3	35 %	3
S B20	41 %	3	40 %	3	19 %	2
W REF	32 %	3	40 %	3	28 %	2
W B5	31 %	3	42 %	3	27 %	2
W D5	32 %	3	41 %	3	28 %	2

*Table 55: **LAI of European beech** in SB20, EB15 and EB25 estimated from **litter fall sampling** in 2020.*

SB20	Date	19.08.2020	01.09.2020	18.10.2020	28.10.2020	10.11.2020	26.11.2020	10.12.2020	21.12.2020
	DOY	232	245	292	302	315	331	345	356
	LAI	1.07	0.28	0.04	0.08	0.43	0.1	0.07	0.02
	LAI (cumulated)	1.07	1.35	1.39	1.47	1.90	2.0	2.07	2.09
EB15	Date	25.08.2020	08.10.2020	11.11.2020	18.12.2020	12.01.2021			
	DOY	237	281	315	352	12			
	LAI	1.35	0.02	1.79	0.17	0.02			
	LAI (cumulated)	1.35	1.37	3.16	3.33	3.35			
EB25	Date	25.08.2020	08.10.2020	11.11.2020	18.12.2020	12.01.2021			
	DOY	237	281	315	352	12			
	LAI	0.71	0.05	4.24	0.16	0.03			
	LAI (cumulated)	0.71	0.76	5.0	5.16	5.19			

*Table 56: **LAI of Scots pine and European beech** in Sandkrug, Elze and Wibbese based on DHP measurements and combined DHP and litter fall measurements (*). Litter fall measurements from 2020 are also used to derive summer LAI values for 2019.*

	Summer 2019		Winter 2019/2020		Summer 2020		Winter 2020/2021	
	LAI	SAI	LAI	SAI	LAI	SAI	LAI	SAI
SREF	3.2	0.5	2.8	0.5	3.4	0.6	2.6	0.4
SB20	4.9*	0.6	2.9	0.6	5.0*	0.6	3.0	0.6
EREF	2.2	0.4	3.1	0.5	4.2	0.7	3.4	0.6
EB5	2.4	0.4	2.9	0.5	3.6	0.6	3.1	0.5
EB15	5.8*	0.5	2.5	0.5	5.8*	0.5	2.5	0.5
EB25	5.2*	0.2	0	0.5	5.2*	0.5	0	0.7
WREF	2.6	0.4	3.0	0.5	3.5	0.6	2.6	0.4
WB5	2.8	0.5	2.6	0.3	3.4	0.6	2.4	0.4
WD5	3.1	0.5	2.8	0.5	3.3	0.5	2.1	0.3

Table 57: ***LAI construction based on DHP and litter fall sampling*** *before and after (*) model calibration in SB20, EB15 and EB25 in 2020.*

SB20		Maximum	19.08.2020 (232)	18.10.2020 (292)	10.11.2020 (315)	10.12.2020 (345)	21.12.2020 (356)
	Beech [m^2/m^2]	2.08	1.01	0.70	0.19	0.02	0
	Beech + Pine [m^2/m^2]	4.98	3.91	3.60	3.09	2.92	2.90
	Beech + Pine [% of maximum]	1	0.79	0.72	0.62	0.59	0.58
	Beech + Pine [m^2/m^2] *	4.98 *	4.48 *	4.28 *	4.03 *	3.98 *	3.98 *
	Beech + Pine [% of maximum] *	100 *	90 *	86 *	81 *	80 *	80 *
EB15		Maximum	25.08.2020 (238)	08.10.2020 (282)	11.11.2020 (316)	18.12.2020 (353)	12.01.2021 (12)
	Beech [m^2/m^2]	3.34	2.00	1.98	0.19	0.02	0
	Beech + Pine [m^2/m^2]	5.84	4.50	4.48	2.69	2.52	2.50
	Beech + Pine [% of maximum]	1	0.77	0.77	0.46	0.43	0.43
	Beech + Pine [m^2/m^2] *	5 *	4 *	4 *	2.65 *	2.5 *	2.5 *
	Beech + Pine [% of maximum] *	100 *	80 *	80 *	56 *	50 *	50 *
EB25		Maximum	25.08.2020 (238)	08.10.2020 (282)	11.11.2020 (316)	18.12.2020 (353)	12.01.2021 (12)
	Beech [m^2/m^2]	5.19	4.48	4.42	0.18	0.03	0
	Beech [% of maximum]	1	0.86	0.85	0.03	0.01	0
	Beech [m^2/m^2] *	4 *	3.4 *	3.4 *	0.12 *	0.04 *	0 *
	Beech [% of maximum] *	100 *	86 *	85 *	3 *	1 *	0 *

Precipitation measurements

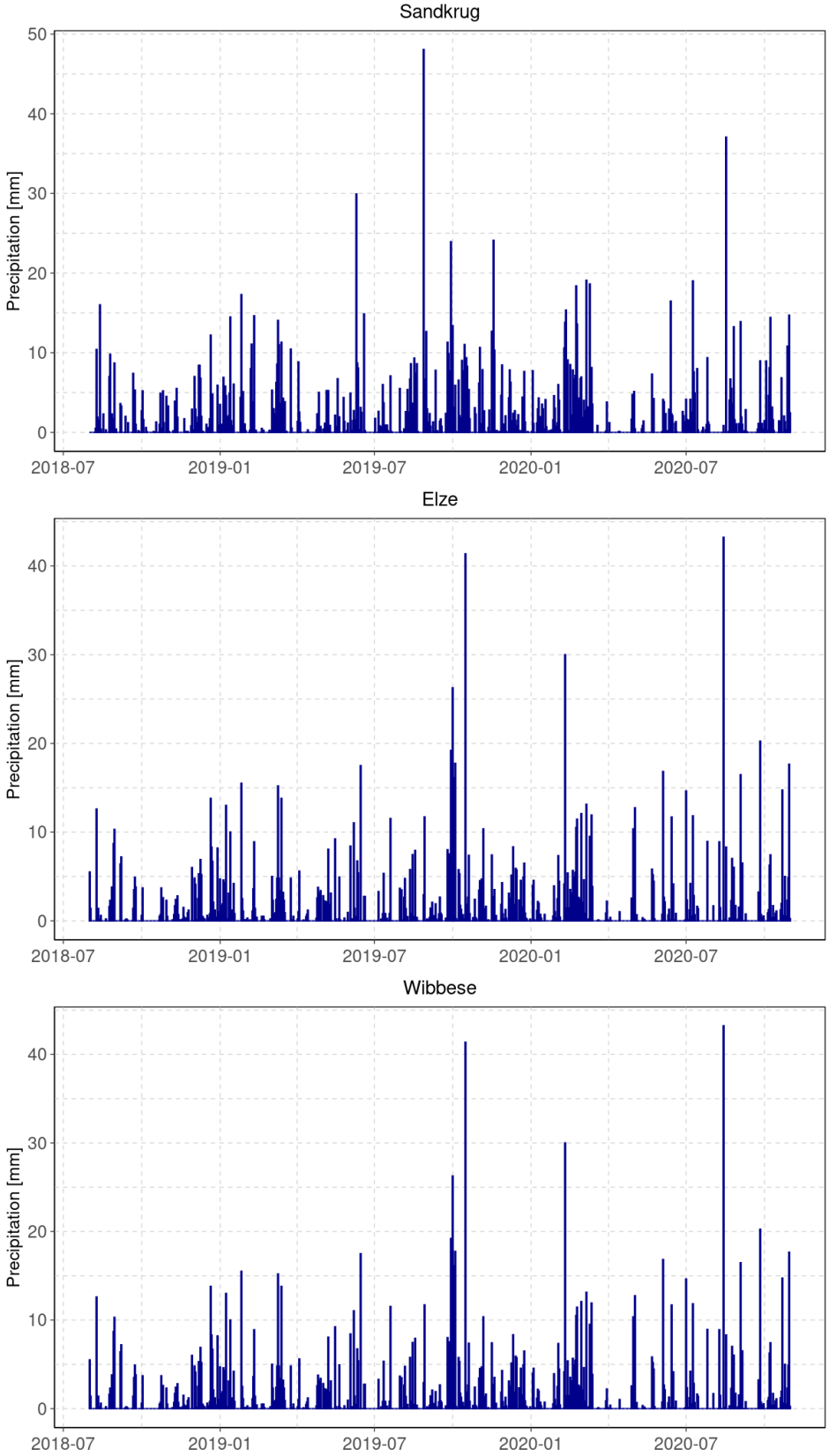

Figure 68: Measured daily precipitation sums in Sandkrug (top), Elze (middle) and Wibbese (bottom) in the period 08/2018 – 10/2020.

Soil measurements

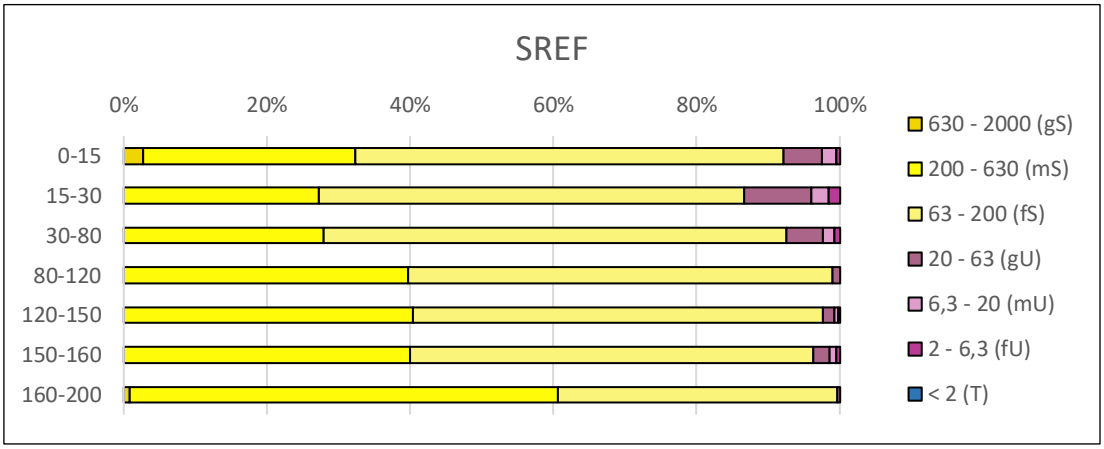

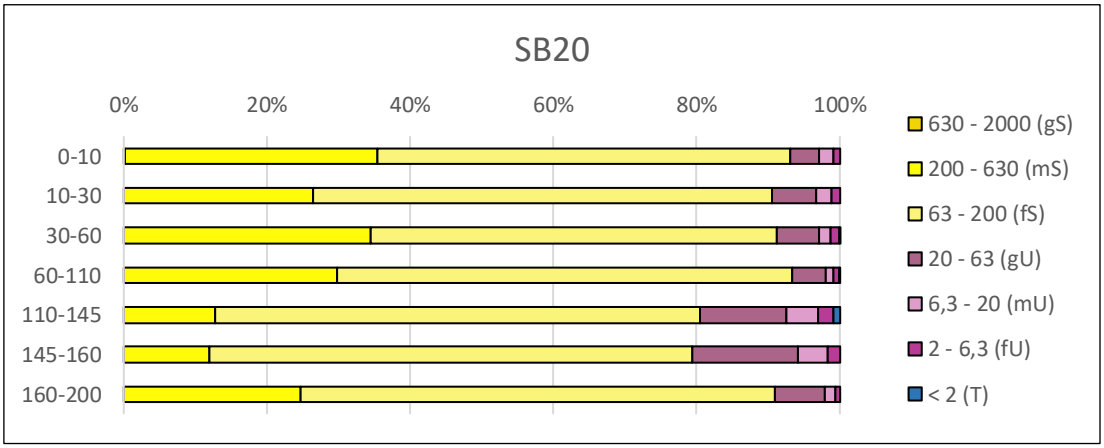

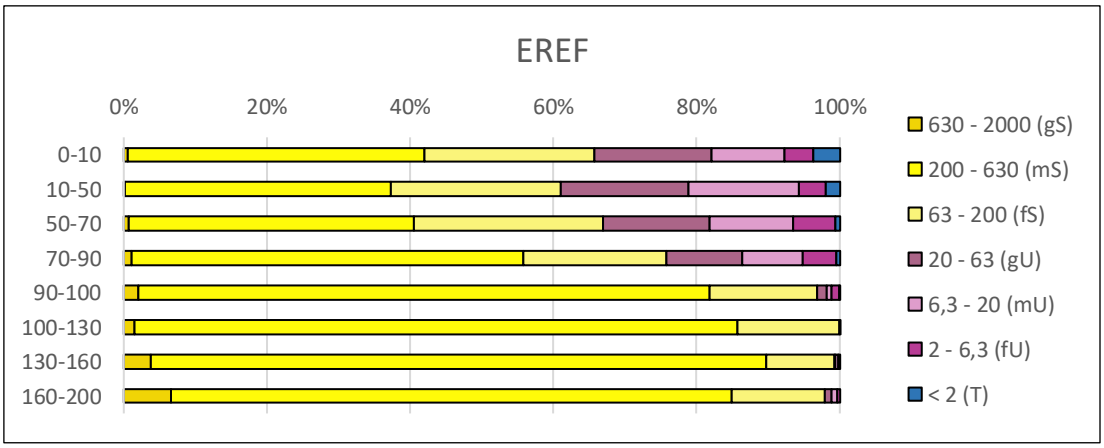

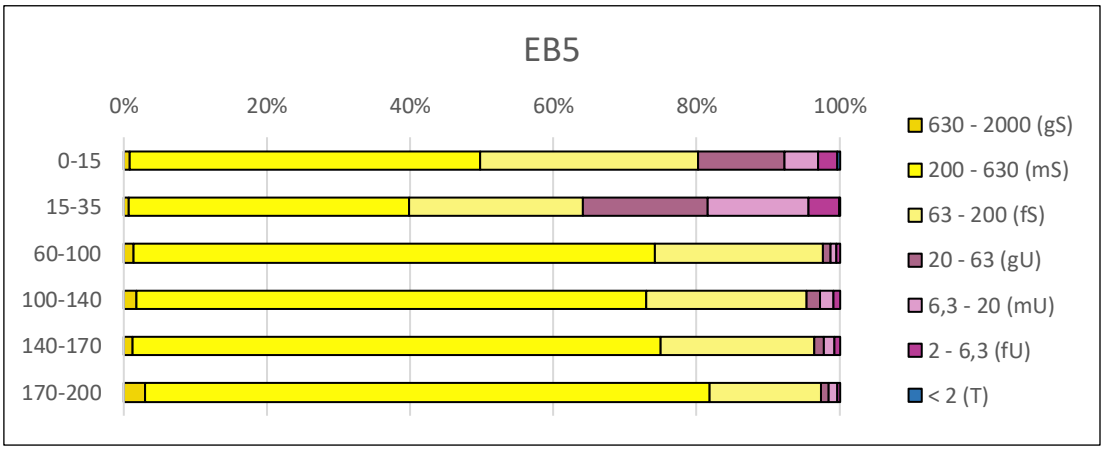
EB5
0%
20%
40%
60%
80%
100%
0-15
15-35
60-100
100-140
140-170
170-200
630 - 2000 (gS)
200 - 630 (mS)
63 - 200 (fS)
20 - 63 (gU)
6,3 - 20 (mU)
2 - 6,3 (fU)
< 2 (T)

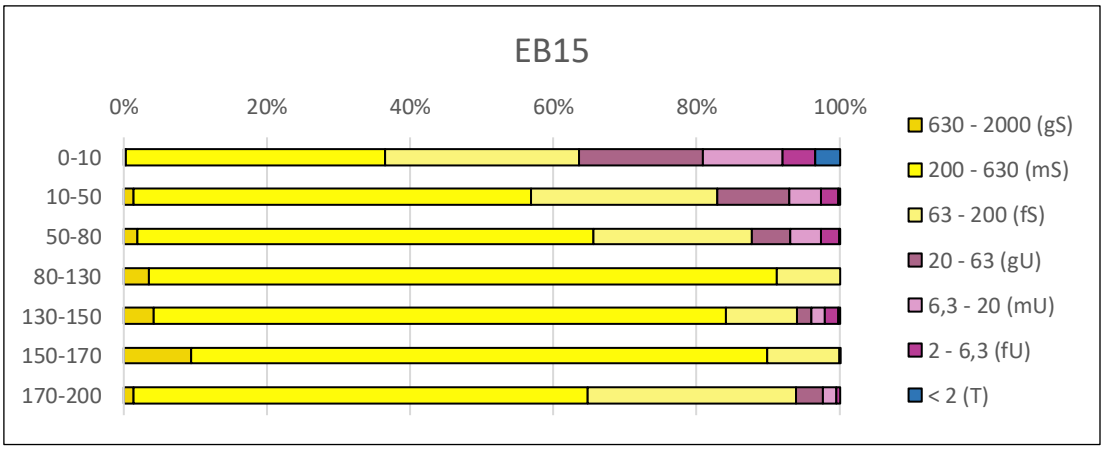
EB15
0%
20%
40%
60%
80%
100%
0-10
10-50
50-80
80-130
130-150
150-170
170-200
630 - 2000 (gS)
200 - 630 (mS)
63 - 200 (fS)
20 - 63 (gU)
6,3 - 20 (mU)
2 - 6,3 (fU)
< 2 (T)

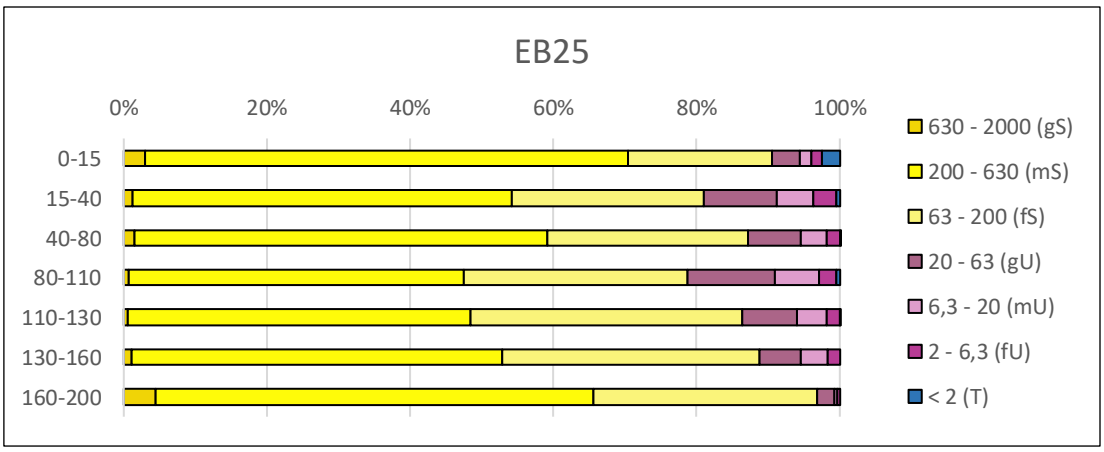
EB25
0%
20%
40%
60%
80%
100%
0-15
15-40
40-80
80-110
110-130
130-160
160-200
630 - 2000 (gS)
200 - 630 (mS)
63 - 200 (fS)
20 - 63 (gU)
6,3 - 20 (mU)
2 - 6,3 (fU)
< 2 (T)

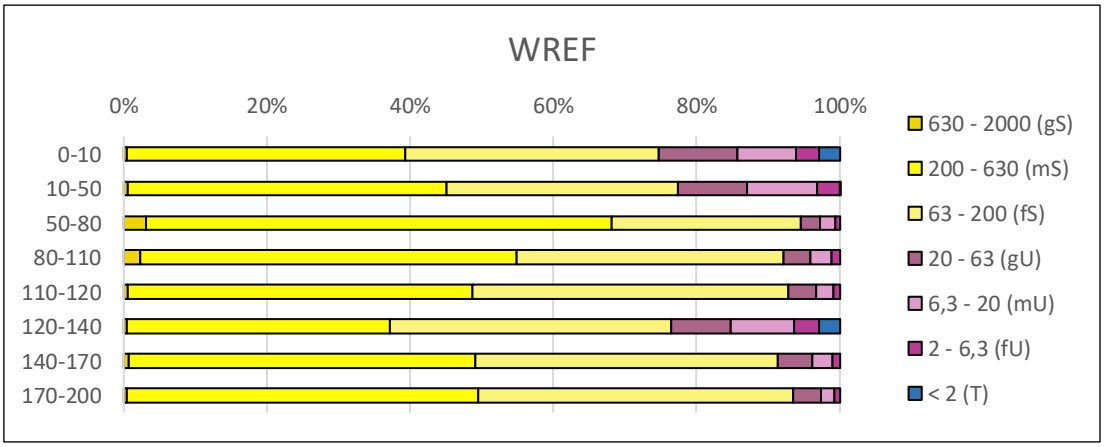
WREF
0%
20%
40%
60%
80%
100%
0-10
10-50
50-80
80-110
110-120
120-140
140-170
170-200
630 - 2000 (gS)
200 - 630 (mS)
63 - 200 (fS)
20 - 63 (gU)
6,3 - 20 (mU)
2 - 6,3 (fU)
< 2 (T)

Figure 69: Depth-specific grain size distribution measurements in Sandkrug, Elze and Wibbese (gS = coarse sand, mS = medium sand, fS = fine sand, gU = coarse silt, mU = medium silt, fU = fine silt, T = clay).

*Table 58: Measured depth-specific **gravel content** [%] at the forest plots.*

Depth	SREF	SB20	EREF	EB5	EB15	EB25	WREF	WB5	WD5
0-10	0	4.5	0.1	0	0.2	0.1	1.4	1.1	1.6
10-20	0	0.6	0.1	0	0.2	0.1	1.4	1.1	1.6
20-30	0.7	0.6	0.3	0	0.2	0.5	0.8	2.3	1.6
30-40	0.7	0.1	0.3	0	0.2	0.5	0.8	2.3	1.6
40-50	0	0.1	3.5	0	1.2	2.0	0.1	1.4	3.1
50-60	0	0.1	3.5	0	1.2	2.0	0.1	1.4	3.1
60-70	0	0.2	3.5	0	1.2	2.0	0.1	1.4	3.1
70-80	0	0.2	5.0	0.5	0.3	0.6	0	0.9	2.3
80-90	1.8	0.2	5.0	0.5	0.3	0.6	0	0.9	2.3
90-100	1.8	0.2	5.0	0.5	0.3	0.6	0	0.9	2.3
100-110	1.8	0.2	5.0	0.5	0.3	0.6	0	0.9	2.3
110-120	1.8	0.2	5.0	0.5	0.3	0.6	0	0.9	2.3
120-130	1.8	0.2	5.0	0.5	0.3	0.6	0	0.9	2.3
130-140	1.8	0.2	5.0	0.5	0.3	0.6	0	0.9	2.3
140-150	1.8	0.2	5.0	0.5	0.3	0.6	0	0.9	2.3
150-160	1.8	0.2	5.0	0.5	0.3	0.6	0	0.9	2.3
160-170	1.8	0.2	5.0	0.5	0.3	0.6	0	0.9	2.3
170-180	1.8	0.2	5.0	0.5	0.3	0.6	0	0.9	2.3
180-190	1.8	0.2	5.0	0.5	0.3	0.6	0	0.9	2.3
190-200	1.8	0.2	5.0	0.5	0.3	0.6	0	0.9	2.3

*Table 59: Measured **bulk density** [g/cm³] at the forest plots.*

Depth	S REF	S B20	E REF	E B5	E B15	E B25	W REF	W B5	W D5
0-20	1.52	1.51	1.32	1.46	1.32	1.42	1.48	1.41	1.41
20-40	1.52	1.51	1.47	1.47	1.32	1.45	1.44	1.44	1.41
40-70	1.57	1.67	1.58	1.30	1.51	1.39	1.52	1.49	1.53
70-100	1.58	1.64	1.58	1.57	1.58	1.56	1.41	1.50	1.53

*Table 60: Measured **organic carbon content** [%] at the forest plots.*

Depth	S REF	S B20	E REF	E B5	E B15	E B25	W REF	W B5	W D5
0-20	3.97	1.00	1.76	0.75	0.94	1.13	0.96	0.86	1.00
20-40	0.66	0.38	0.43	0.24	0.57	0.53	0.25	0.48	1.00
40-70	0.25	0.19	0.43	0.61	0.19	0.45	0.12	0.45	0.19
70-100	0.08	0.09	0.11	0.16	0.07	0.10	0.11	0.18	0.19

Table 61: ***Aggregated soil properties in Sandkrug****: Aggregated soil properties in* ***SREF*** *and* ***SB20*** *and* ***Sandkrug*** *(mean values from SREF and SB20) with weighed mean values for bulk density (bd), gravel, sand, silt, clay and organic carbon (corg) content.*

upper [cm]	lower [cm]	bd [g/cm³]	gravel [%]	sand [%]	silt [%]	clay [%]	c_{org} [%]
			SREF				
0	200	1.57	0	96.15	3.85	0	0.5
			SB20				
0	120	1.63	0	91.79	8.19	0.02	0.18
120	160	1.64	0	80.07	19.38	0.55	0.09
160	200	1.63	0	91.79	8.19	0.02	0.18
			Sandkrug				
0	120	1.6	0	93.97	6.02	0.01	0.34
120	160	1.61	0	88.11	11.62	0.27	0.3
160	200	1.6	0	93.97	6.02	0.01	0.34

*Table 62: **Aggregated soil properties in Elze**: Aggregated soil properties in **EREF**, **EB5**, **EB15** and **EB25** and **Elze** (mean values from EREF, EB5, EB15 and EB25) with weighed mean values for bulk density (bd), gravel, sand, silt, clay and organic carbon (corg) content.*

upper [cm]	lower [cm]	bd [g/cm³]	gravel [%]	sand [%]	silt [%]	clay [%]	c_{org} [%]
			EREF				
0	80	1.5	0.02	65.98	32.16	1.86	0.65
80	200	1.58	0.05	98.46	1.53	0.01	0.11
			EB5				
0	50	1.41	0	71.2	28.7	0.1	0.45
50	200	1.57	0	96.7	3.3	0	0.16
			EB15				
0	80	1.42	0.01	82.34	17.1	0.55	0.57
80	200	1.58	0	96.77	3.2	0.03	0.07
			EB25				
0	160	1.5	0.01	84.47	15.18	0.35	0.37
160	200	1.56	0.01	96.81	3.19	0	0.1
			Elze				
0	90	1.46	0.01	76.0	23.29	0.71	0.51
90	200	1.57	0.02	97.19	2.81	0	0.11

*Table 63: **Aggregated soil properties in Wibbese**: Aggregated soil properties in **WREF**, **WB5** and **WD5** and **Wibbese** (mean values from WREF, WB5 and WD5) with weighed mean values for bulk density (bd), gravel, sand, silt, clay and organic carbon (corg) content.*

upper [cm]	lower [cm]	bd [g/cm³]	gravel [%]	sand [%]	silt [%]	clay [%]	c_{org} [%]
			WREF				
0	50	1.48	0.01	76.91	22.61	0.48	0.44
50	200	1.42	0	91.04	8.64	0.32	0.11
			WB5				
0	50	1.46	0.01	78.36	21.51	0.13	0.6
50	200	1.5	0.01	90.97	9.0	0.03	0.18
			WD5				
0	50	1.45	0.02	62.62	35.8	1.6	0.73
50	200	1.53	0.02	78.95	18.87	2.18	0.19
			Wibbese				
0	50	1.46	0.01	72.63	26.64	0.73	0.59
50	200	1.48	0.01	86.99	12.17	0.84	0.16

Interception measurements

*Table 64: **Stand precipitation** [mm] and **interception** in % of bulk precipitation in **Sandkrug**.*

Date	Stand Precipitation [mm]		Interception [% of precipitation]	
	S REF	S B20	S REF	S B20
05.02.2019	46.92	43.78	27.0%	31.9%
04.03.2019	31.03	28.98	33.2%	37.6%
20.03.2019	47.71	40.16	37.2%	47.1%
03.04.2019	7.31	5.87	41.3%	52.8%
18.04.2019	9.74	8.99	24.6%	30.4%
02.05.2019	5.45	3.95	50.7%	64.3%
16.05.2019	9.92	7.10	31.5%	50.9%
27.05.2019	6.67	3.53	61.3%	79.5%
14.06.2019	43.98	35.51	26.0%	40.3%
28.06.2019	13.37	11.13	35.4%	46.2%
08.07.2019	1.33	0.53	71.9%	88.8%
25.07.2019	10.37	7.80	49.1%	61.7%
08.08.2019	4.60	2.81	46.6%	67.4%
22.08.2019	38.93	30.10	27.9%	44.2%
05.09.2019	58.94	50.91	21.4%	32.2%
18.09.2019	7.37	4.77	44.9%	64.3%
16.10.2019	105.42	85.46	25.5%	39.6%
14.11.2019	46.78	38.84	29.5%	41.5%
12.12.2019	62.04	53.36	31.1%	40.8%
07.01.2020	21.86	19.52	32.5%	39.8%
05.02.2020	20.32	17.52	54.5%	60.8%
03.03.2020	103.94	92.58	28.3%	36.2%
17.03.2020	34.80	34.00	37.8%	39.2%
30.04.2020	8.07	7.83	46.2%	47.8%
15.05.2020	2.93	1.87	64.5%	77.4%
28.05.2020	7.37	4.85	43.4%	62.7%
11.06.2020	9.18	5.65	27.6%	55.4%
23.06.2020	22.59	18.50	9.5%	25.8%
07.07.2020	5.01	3.28	73.1%	82.4%
21.07.2020	28.52	24.52	33.8%	43.0%
05.08.2020	8.81	6.39	31.8%	50.5%
19.08.2020	31.24	25.16	17.6%	33.7%
01.09.2020	21.08	15.99	45.4%	58.6%
15.09.2020	14.33	12.81	32.3%	39.4%
30.09.2020	8.61	6.48	37.7%	53.1%
13.10.2020	28.00	22.85	35.3%	47.2%
10.11.2020	35.57	30.65	34.5%	43.6%

Table 65: ***Stand precipitation*** *[mm] and* ***interception*** *in % of bulk precipitation in* ***Elze****.*

Date	Stand Precipitation [mm]				Interception [% of precipitation]			
	E REF	E B5	E B15	E B25	E REF	E B5	E B15	E B25
15.05.2019	14.59	14.48	14.64	17.25	28.8%	29.3%	28.6%	15.9%
12.06.2019	26.50	NA	27.54	NA	20.9%	NA	17.8%	NA
16.07.2019	7.76	7.99	8.25	8.86	31.3%	29.3%	27.0%	21.6%
01.08.2019	11.45	11.87	12.09	13.23	29.3%	26.7%	25.4%	18.3%
14.08.2019	12.19	12.35	NA	15.16	37.5%	36.6%	NA	22.2%
10.09.2019	23.87	23.35	23.70	26.87	33.1%	34.6%	33.6%	24.7%
26.09.2019	10.82	10.52	9.71	12.60	34.4%	36.2%	41.2%	23.6%
02.10.2019	63.05	NA	62.71	65.03	16.5%	NA	16.9%	13.9%
12.11.2019	25.75	NA	25.52	27.53	15.0%	NA	15.8%	9.2%
03.12.2019	15.80	15.68	16.49	20.40	34.7%	35.2%	31.9%	15.7%
09.01.2020	49.04	NA	49.97	63.96	28.7%	NA	27.4%	7.0%
19.02.2020	53.31	NA	56.18	72.77	31.8%	NA	28.2%	6.9%
12.03.2020	NA	NA	81.72	98.18	NA	NA	23.6%	8.2%
07.04.2020	4.24	4.62	5.27	7.32	43.5%	38.3%	29.8%	2.4%
14.05.2020	22.42	23.25	21.81	24.82	20.5%	17.6%	22.6%	12.0%
09.06.2020	27.82	25.74	NA	30.67	26.8%	32.3%	NA	19.3%
30.06.2020	13.92	14.62	12.96	17.37	25.9%	22.2%	31.1%	7.6%
30.07.2020	37.67	NA	36.32	40.94	25.4%	NA	28.1%	18.9%
25.08.2020	60.68	NA	58.89	64.19	17.4%	NA	19.9%	12.7%
17.09.2020	28.29	NA	28.29	32.16	26.7%	NA	26.7%	16.7%
08.10.2020	30.10	28.60	30.44	31.03	14.7%	19.0%	13.8%	12.1%
11.11.2020	50.43	NA	48.40	56.39	28.0%	NA	30.9%	19.4%

Table 66: ***Stand precipitation*** *[mm] and* ***interception*** *in % of bulk precipitation in* ***Wibbese****.*

Date	Stand Precipitation [mm]			Interception [% of precipitation]		
	W REF	W B5	W D5	W REF	W B5	W D5
14.05.2019	9.85	9.55	9.43	29.6%	31.8%	32.7%
28.05.2019	8.71	8.05	8.29	30.3%	35.6%	33.7%
04.07.2019	6.60	6.41	6.65	33.3%	35.3%	32.9%
01.08.2019	17.92	15.73	16.94	6.7%	18.0%	11.8%
14.08.2019	13.03	12.38	12.71	18.5%	22.6%	20.6%
02.10.2019	70.46	62.65	67.36	9.1%	19.2%	13.1%
22.10.2019	45.35	40.27	41.99	14.8%	24.3%	21.1%
13.11.2019	22.38	20.41	21.41	11.9%	19.7%	15.7%
04.12.2019	23.21	21.05	22.04	17.4%	25.1%	21.6%
09.01.2020	41.37	NA	37.91	18.9%	NA	25.7%
21.01.2020	4.42	4.08	4.10	35.9%	40.9%	40.6%
19.02.2020	56.57	51.61	49.45	22.2%	29.0%	32.0%
12.03.2020	82.85	75.99	76.77	9.0%	16.5%	15.6%
25.03.2020	5.81	5.61	4.77	28.3%	30.8%	41.1%
05.05.2020	22.46	23.49	23.69	13.6%	9.7%	8.9%
09.06.2020	23.50	23.42	22.84	16.1%	16.3%	18.4%
30.07.2020	51.74	50.63	50.15	18.5%	20.3%	21.0%
20.08.2020	6.53	7.64	8.12	44.2%	34.7%	30.6%
17.09.2020	29.58	29.18	28.15	22.2%	23.2%	25.9%
20.10.2020	48.51	47.28	47.38	19.8%	21.9%	21.7%
11.11.2020	35.65	35.00	35.24	20.6%	22.0%	21.5%

Soil moisture measurements

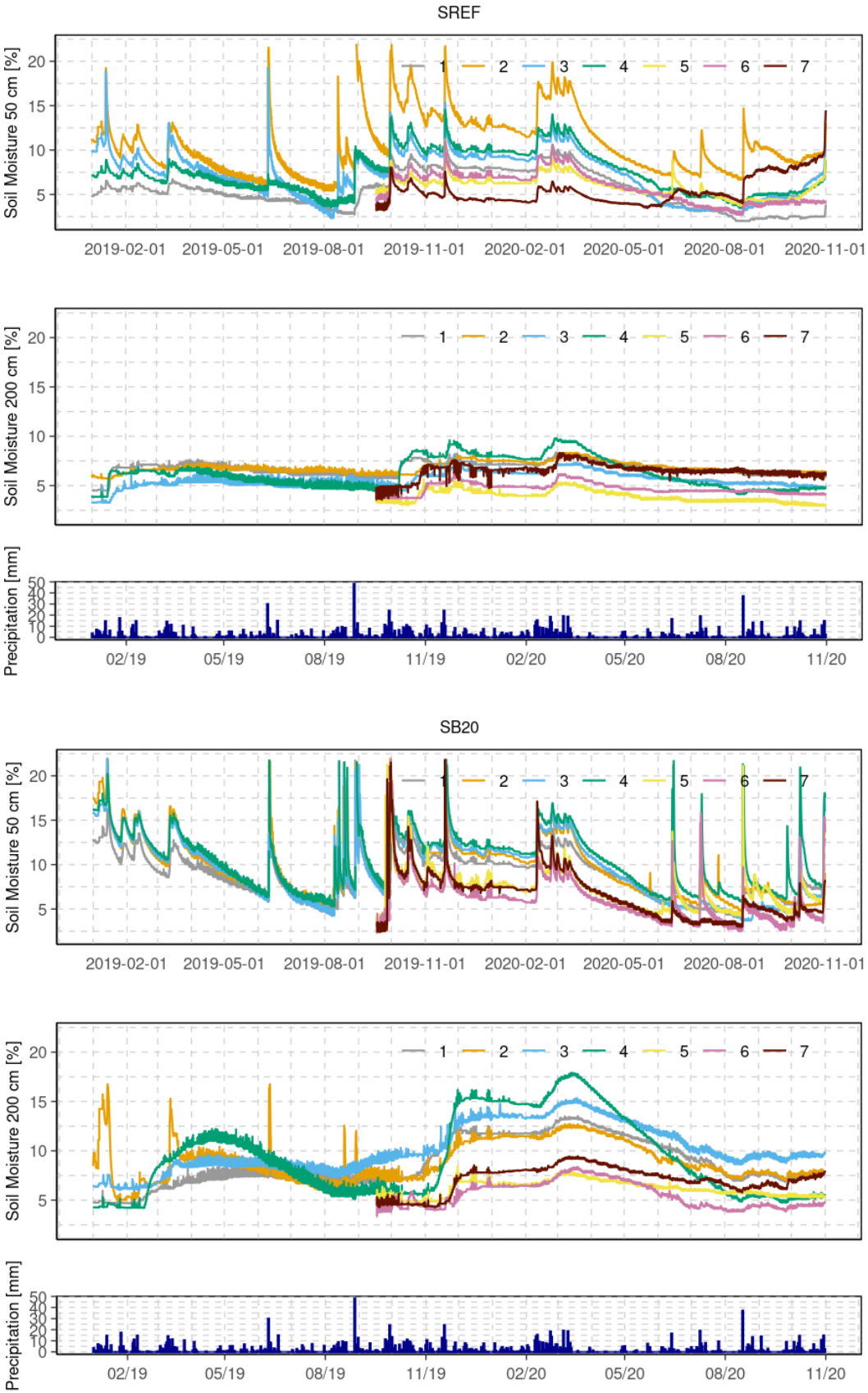

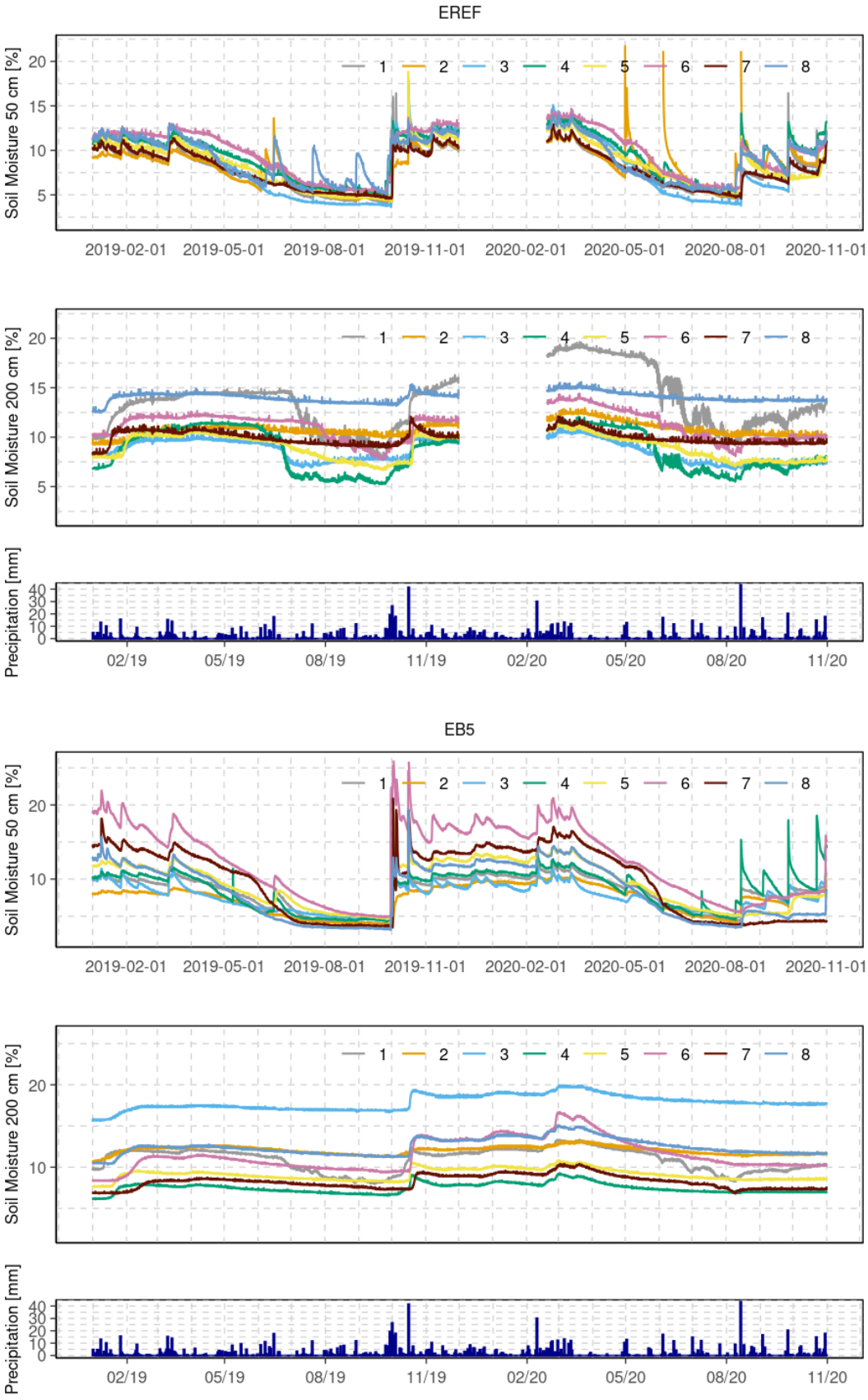
EREF
Soil Moisture 50 cm [%]
Soil Moisture 200 cm [%]
Precipitation [mm]
1 2 3 4 5 6 7 8
2019-02-01 2019-05-01 2019-08-01 2019-11-01 2020-02-01 2020-05-01 2020-08-01 2020-11-01
02/19 05/19 08/19 11/19 02/20 05/20 08/20 11/20
EB5

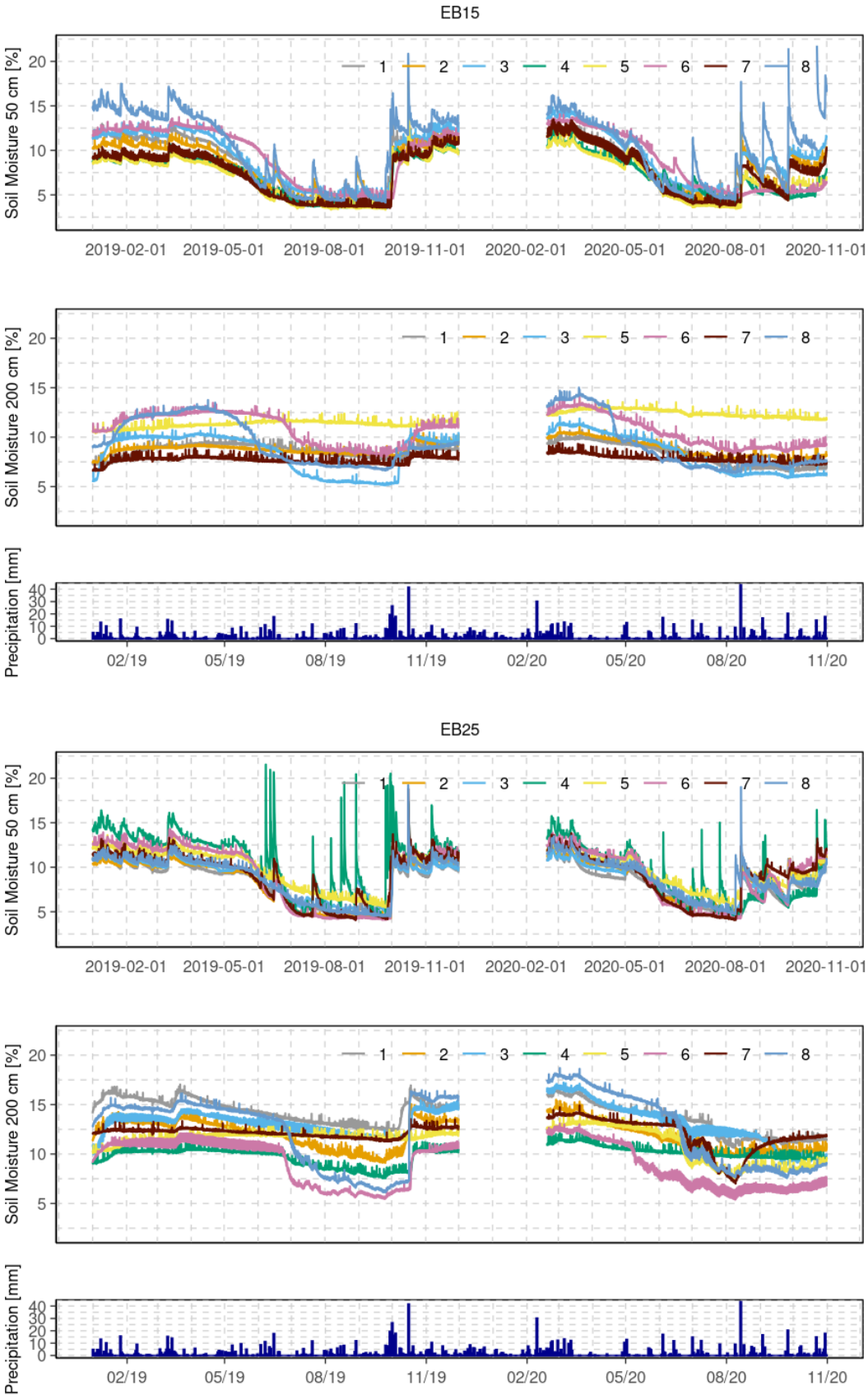
EB15
Soil Moisture 50 cm [%]
Soil Moisture 200 cm [%]
Precipitation [mm]
1 2 3 4 5 6 7 8
2019-02-01 2019-05-01 2019-08-01 2019-11-01 2020-02-01 2020-05-01 2020-08-01 2020-11-01
02/19 05/19 08/19 11/19 02/20 05/20 08/20 11/20
EB25

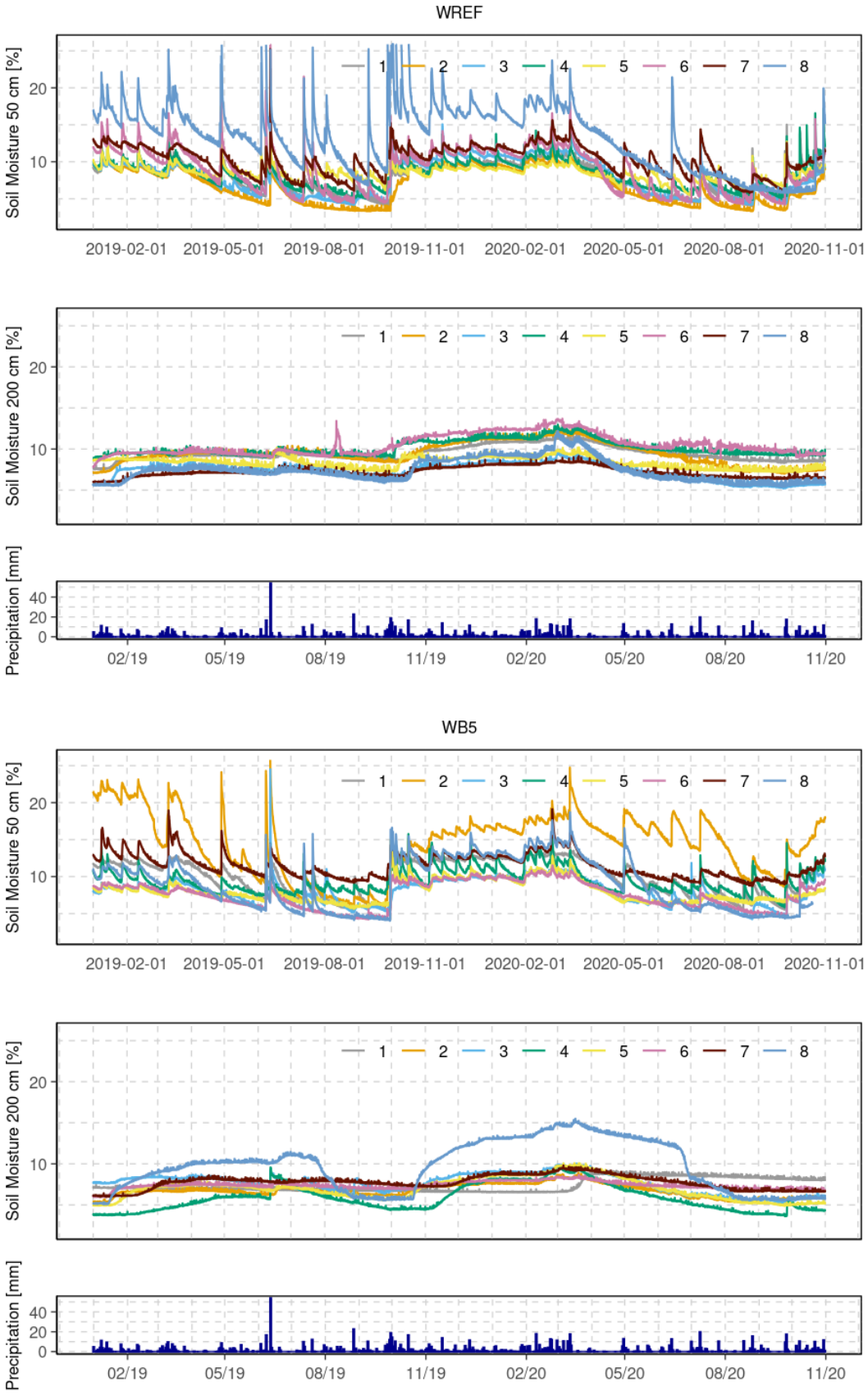
WREF
Soil Moisture 50 cm [%]
1 2 3 4 5 6 7 8
20
10
2019-02-01 2019-05-01 2019-08-01 2019-11-01 2020-02-01 2020-05-01 2020-08-01 2020-11-01
Soil Moisture 200 cm [%]
1 2 3 4 5 6 7 8
20
10
Precipitation [mm]
40
20
0
02/19 05/19 08/19 11/19 02/20 05/20 08/20 11/20
WB5
Soil Moisture 50 cm [%]
1 2 3 4 5 6 7 8
20
10
2019-02-01 2019-05-01 2019-08-01 2019-11-01 2020-02-01 2020-05-01 2020-08-01 2020-11-01
Soil Moisture 200 cm [%]
1 2 3 4 5 6 7 8
20
10
Precipitation [mm]
40
20
0
02/19 05/19 08/19 11/19 02/20 05/20 08/20 11/20

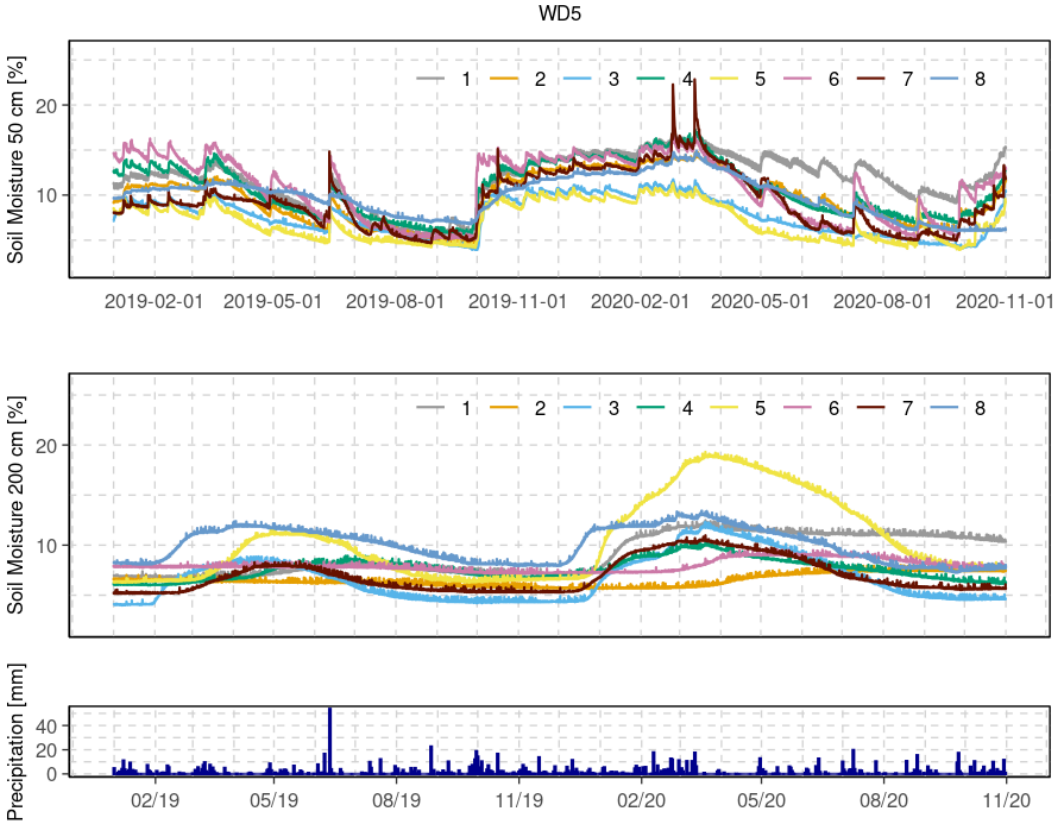

Figure 70: Soil moisture courses of the single soil moisture sensors in 50 cm (top) and 200 cm depth (middle) as well as daily precipitation sums (bottom) for every forest plot (From top to bottom: SREF, SB20, EREF, EB5, EB15, EB25, WREF, WB5, WD5).

LWF-Brook90

Table 67: Details about model parameters in LWF-Brook90R: Parameter abbreviation (Parameter), parameter description (Description), default value in the model (Default value), unit, model parameter group (Group) and parameter status with respect to model fitting (fixed = no parameter fitting, fitting parameter = fitting parameter).

Parameter	Description	Default value	Unit	Group	Fitting Parameter?
czr	Ratio of roughness length to mean height for smooth closed canopies for heights greater than HR when LAI>LPC	0.05 (Federer 2015a)	-	Canopy	fixed
czs	Ratio of roughness length to mean height for smooth closed canopies for heights less than HS when LAI>LPC	0.13 (Federer 2015a)	m	Canopy	fixed
hr	Smallest height to which CZR applies	10 (Federer 2015a)	m	Canopy	fixed
hs	Largest height to which CZS applies	1 (Federer 2015a)	m	Canopy	fixed
lpc	Minimum leaf area index defining a closed canopy	4 (Federer 2015a)	$m^2\ m^{-2}$	Canopy	fixed
lwidth	Average leaf width	0.1 (Schmidt-Walter et al. 2020b)	m	Canopy	fixed
nn	Eddy diffusivity extinction coefficient within canopy	2.5 (Shuttleworth & Gurney 1990)	-	Canopy	fixed
rhotp	Ratio of total leaf area to projected area	2 (Federer 2015a)	-	Canopy	fixed
zminh	Reference height for weather data above the canopy top height	2 (Federer 2015a)	m	Canopy	fixed
dslope	slope for downslope-flow	0 (Schmidt-Walter et al. 2020b)	deg	Flow	fixed
bypar	Switch to allow (1) or prevent (0) bypass flow in deeper layers	0 (Schmidt-Walter et al. 2020b)	-	Flow	fixed
drain	Switch for lower boundary condition to be free drainage (1) or no flow (0)	1 (Schmidt-Walter et al. 2020b)	-	Flow	fixed
slopelen	slope length for downslope-flow	200 (Schmidt-Walter et al. 2020b)	m	Flow	fixed
gsc	fraction of ground water storage that is transferred to groundwater flow and deep seepage each day	0 (Schmidt-Walter et al. 2020b) 0 – 0.1 (Federer 2015a)	d^{-1}	Flow	fitting parameter
gsp	Seepage fraction of groundwater discharge	0 (seepage = 0) 1 (streamflow = 0)	-	Flow	
ilayer	Number of layers from top to which infiltration is distributed	-	-	Flow	fitting parameter
imperv	Fraction of area which has an impermeable surface (like roads)	0 (Schmidt-Walter et al. 2020b)	-	Flow	fixed

infexp	Shape parameter for distribution of infiltration in first ILayer, for value 0 infiltration is in top layer only	0 (Schmidt-Walter et al. 2020b)	-	Flow	fitting parameter
qffc	Quickflow fraction of infiltrating water at field capacity, for value 0 there is no quickflow (bypass or surface) unless soil profile surface becomes saturated	-	-	Flow	fitting parameter
qfpar	Quickflow shape parameter	-	-	Flow	fitting parameter
qlayer	Number of layers which are considered for generation of surface or source area flow	-	-	Flow	fitting parameter
gwatini	Initial value of groundwater storage	0 (Federer 2015a)	mm	Initial	fixed
snowini	Initial value of water content of snow pack	0 (Federer 2015a)	mm	Initial	fixed
intrainini	Initial value of intercepted rain	0 (Federer 2015a)	mm	Initial	fixed
intsnowini	Initial value of intercepted snow	0 (Federer 2015a)	-	Initial	fixed
psiini	Initial pressure head of soil layers	-6.3 (Schmidt-Walter et al. 2020b)	kPa	Initial	fixed
cintrl	Maximum interception storage of rain per unit LAI	0.15 (Federer 2015a)	mm	Interception	fitting parameter
cintrs	Maximum interception storage of rain per unit SAI	0.15 (Federer 2015a)	mm	Interception	fitting parameter
cintsl	Maximum interception storage of snow per unit LAI	0.6 (Federer 2015a)	mm	Interception	fixed
cintss	Maximum interception storage of snow per unit SAI	0.6 (Federer 2015a)	mm	Interception	fixed
frintlai	Intercepted fraction of rain per unit LAI	0.06 (Federer 2015a)	-	Interception	fitting parameter
frintsai	Intercepted fraction of rain per unit SAI	0.04 (Federer 2015a)	-	Interception	fitting parameter
fsintlai	Intercepted fraction of snow per unit LAI	0.06 (Federer 2015a)	-	Interception	fixed
fsintsai	Intercepted fraction of snow per unit SAI	0.04 (Federer 2015a)	-	Interception	fixed
pdur	Average duration of precipitation events for each month of the year	4 (Federer 2015a)	hours	Interception	fixed
alb	Albedo of soil/vegetation surface without snow	0.2 (Schmidt-Walter et al. 2020b)	-	Meteo	fitting parameter
albsn	Albedo of soil/vegetation surface with snow	0.5 (Schmidt-Walter et al. 2020b)	-	Meteo	fixed
c1	Intercept of relation of solar radiation to sunshine duration	0.25 (Brutsaert 1982)	-	Meteo	fixed
c2	Intercept of relation of solar radiation to sunshine duration	0.5 (Brutsaert 1982)	-	Meteo	fixed
c3	Constant between 0 and 1 that determines the cloud correction to net	0.2 (Brutsaert 1982)	-	Meteo	fixed

	longwave radiation from sunshine duration				
fetch	Fetch upwind of the weather station at which wind speed was measured	5000 (Federer 2015a)	m	Meteo	fixed
ksnvp	Correction factor for snow evaporation	0.3 (Federer 2015a)	-	Meteo	fixed
wndrat	Average ratio of night time to day time wind speed	0.3 (Federer 2015a)	-	Meteo	fixed
z0s	Surface roughness of snow cover	0.001 (Federer 2015a)	m	Meteo	fixed
z0w	Roughness length at the weather station at which wind speed was measured	0.005 (Federer 2015a)	m	Meteo	fixed
coords_x	Longitude value of the simulation location	site-specific	decimal deg	Meteo	fixed
cords_y	Latitude value of the simulation location.	site-specific	decimal deg	Meteo	fixed
zw	Height at which wind speed was measured	10	m	Meteo	fixed
eslope	slope for evapotranspiration and snowmelt calculation	site-specific	deg	Meteo	fixed
aspect	Mean exposition of soil surface at soil profile (north: 0, west: 90, south: 180, east: 270)	site-specific	deg	Meteo	fixed
obsheight	Mean height of obstacles on soil surface (grass, furrows etc.), used to calculate soil surface roughness	0.025 (Schmidt-Walter et al. 2020b)	m	Meteo	fixed
dpsimax	maximum potential difference considered equal	0.0005 (Schmidt-Walter et al. 2020b)	kPa	Numerical	fixed
dswmax	maximum change allowed in SWATI	0.05 (Schmidt-Walter et al. 2020b)	% of SWATMX	Numerical	fixed
dtimax	maximum iteration time step	0.5 (Federer 2015a)	d	Numerical	fixed
budburst.species	Name of tree species for estimating budburst doy using Menzel-model	site-specific	-	Plant	fixed
budburstdoy	Budburst day of year	site-specific	doy	Plant	fitting parameter
emergedur	Leaf growth duration until maxlai is reached	site-specific	d	Plant	fitting parameter
height	plant height	site-specific	m	Plant	fixed
height.ini	initial plant height at the beginning of the simulaton	site-specific		Plant	fixed
leaffalldoy	start of leaffall	site-specific	doy	Plant	fitting parameter
leaffalldur	number of days until minimum lai is reached	site-specific	d	Plant	fitting parameter
sai	steam area index	site-specific	$m^2\ m^{-2}$	Plant	fitting parameter

sai.ini	steam area index at the end of the simulation	site-specific	$m^2\ m^{-2}$	Plant	
shape.leaffall	Shape parameter for leaf fall phase	site-specific	-	Plant	fitting parameter
shape.budburst	Shape parameter for leaf growth phase	site-specific	-	Plant	fitting parameter
shape.optdoy	day of year when optimum value is reached	site-specific	doy	Plant	fitting parameter
lai.doy	day of year values for lai-interpolation	site-specific	doy	Plant	fixed
lai.frac	fractional lai values for lai interpolation, corresponding to lai.doy	site-specific	-	Plant	fixed
winlaifrac	Minimum LAI as a fraction of maxlai	site-specific	-	Plant	fixed
cs	Ratio of projected stem area index to canopy height	0.035 (Federer 2015a)	m^{-1}	Plant	fixed
densef	Density factor for MaxLAI, CS, RtLen, RPlant	1 (Federer 2015a)	-	Plant	fixed
densef.ini	density factor (see densef) at the end of the simulation	1 (Federer 2015a)	-	Plant	fixed
maxlai	Maximum projected leaf area index	site-specific	$m^2\ m^{-2}$	Plant	fitting parameter
radex	Extinction coefficient for solar radiation and net radiation in the canopy	0.5 (Schmidt-Walter et al. 2020b)	-	Potential Transpiration	fitting parameter
cvpd	Vapour pressure deficit at which leaf conductance is halved	2 (Federer 2015a)	kPa	Potential Transpiration	fitting parameter
glmax	Maximum leaf vapour conductance when stomata are fully open	0.0053 (Schmidt-Walter et al. 2020b)	$m\ s^{-1}$	Potential Transpiration	fitting parameter
glmin	Minimum leaf vapour conductance when stomata are closed	0.0003 (Federer 2015a)	$m\ s^{-1}$	Potential Transpiration	fixed
r5	Solar radiation level at which leaf conductance is half of its value at RM	100 (Federer 2015a)	$W\ m^{-2}$	Potential Transpiration	fitting parameter
rm	Nominal maximum solar shortwave radiation possible on a leaf (to reach glmax)	1000 (Federer 2015a)	$W\ m^{-2}$	Potential Transpiration	fixed
t1	Lower suboptimal temperature threshold for stomata opening - temperature relation	10 (Federer 2015a)	°C	Potential Transpiration	fitting parameter
t2	Upper suboptimal temperature threshold for stomata opening - temperature relation	30 (Federer 2015a)	°C	Potential Transpiration	fitting parameter
th	Upper temperature threshold for stomata closure	40 (Federer 2015a)	°C	Potential Transpiration	fixed
tl	Lower temperature threshold for stomata closure	0 (Federer 2015a)	°C	Potential Transpiration	fixed

betaroot	Vertical root distribution β-coefficient	(Schmidt-Walter et al. 2020b)	-	Roots	fitting parameter
maxrootdepth	Maximum root depth	site-specific	m	Roots	fitting parameter
rootden.table	Data frame of relative root density depth distribution	-	-	Roots	-
rstemp	base temperature for snow-rain transition	-0.5 (Schmidt-Walter et al. 2020b)	°C	Snow	fixed
ccfac	cold content factor	0.3 (Federer 2015a)	MJ m^{-2} d^{-1} K^{-1}	Snow	fixed
grdmlt	rate of groundmelt of snowpack	0.35 (Federer 1965)	mm d^{-1}	Snow	fixed
laimlt	parameter for snowmelt dependence on LAI	0.2 (Federer 2015a)	-	Snow	fixed
maxlqf	maximum liquid water fraction of Snow	0.05 (Federer 2015a)	-	Snow	fixed
melfac	degree day melt factor for open	1.5 (Federer 2015a)	MJ m^{-2} d^{-1} K^{-1}	Snow	fixed
saimlt	parameter for snowmelt dependence on SAI	0.5 (Federer 2015a)	-	Snow	fixed
snoden	snow density	0.3 (Federer 2015a)	mm mm^{-1}	Snow	fixed
rssa	soil evaporation resistance at field capacity	500 (Shuttleworth & Gurney 1990)	s m^{-1}	Soil Evaporation	fitting parameter
rssb	exponent in relation of RSS to water potential	1 (Federer 2015a)	-	Soil Evaporation	fixed
soil_nodes	a data frame with soil nodes discretization	-	-	Soil	-
soil_materials	a data frame with soil materials (hydraulic parameters)	-	-	Soil	-
age.ini	Age of stand	site-specific	a	Water Supply	fixed
initrdep	Initial root depth	0.25 (Schmidt-Walter et al. 2020b)	m	Water Supply	fixed
initrlen	Initial water-absorbing root length per unit area	12 (Schmidt-Walter et al. 2020b)	m m^{-2}	Water Supply	fixed
rgroper	Period of net root growth	30 (Schmidt-Walter et al. 2020b)	a	Water Supply	fixed
rgrorate	Vertical root growth rate	0.03 (Schmidt-Walter et al. 2020b)	m a^{-1}	Water Supply	fixed
fxylem	Fraction of internal plant resistance to water flow that is in the Xylem	0.5 (Hunt et al. 1991)	-	Water Supply	fitting parameter
maxrlen	Total length of fine roots per unit ground area	species- and site-specific	m m^{-2}	Water Supply	fitting parameter
mxkpl	Maximum internal conductivity for water flow through the plants	8 (Hunt et al. 1991)	mm d^{-1} MPa^{-1}	Water Supply	fitting parameter

nooutf	Switch that prevents outflow from the root to the soil when the soil is dry	1 (Schmidt-Walter et al. 2020b)	-	Water Supply	fixed
psicr	Critical leaf water potential at which stomates close	species-specific	MPa	Water Supply	fitting parameter
rrad	Average radius of the fine or water-absorbing roots	0.35 (Schmidt-Walter et al. 2020b)	mm	Water Supply	fixed

Table 68: ***Model Soil File for Sandkrug*** *with weighed mean values for bulk density (bd), gravel, sand, silt, clay and organic carbon (corg) content from SREF and SB20 after calibration of the soil parameters alpha, npar and ksat.*

soil layer	upper [cm]	lower [cm]	bd [g/cm³]	gravel [%]	sand [%]	silt [%]	clay [%]	c_{org} [%]	ths	thr	alpha	npar	ksat	tort
1	10	0							0.85	0	98	1.19	98000	0.5
2	0	-5	1.6	0	93.97	6.02	0.01	0.34	0.39	0	5.09	1.84	3638	0.5
3	-5	-25	1.6	0	93.97	6.02	0.01	0.34	0.39	0	5.09	1.84	3638	0.5
4	-25	-35	1.6	0	93.97	6.02	0.01	0.34	0.39	0	5.09	1.84	3638	0.5
5	-35	-45	1.6	0	93.97	6.02	0.01	0.34	0.39	0	5.09	1.84	3638	0.5
6	-45	-55	1.6	0	93.97	6.02	0.01	0.34	0.39	0	5.09	1.84	3638	0.5
7	-55	-65	1.6	0	93.97	6.02	0.01	0.34	0.39	0	5.09	1.84	3638	0.5
8	-65	-75	1.6	0	93.97	6.02	0.01	0.34	0.39	0	5.09	1.84	3638	0.5
9	-75	-85	1.6	0	93.97	6.02	0.01	0.34	0.39	0	5.09	1.84	3638	0.5
10	-85	-95	1.6	0	93.97	6.02	0.01	0.34	0.39	0	5.09	1.84	3638	0.5
11	-95	-105	1.6	0	93.97	6.02	0.01	0.34	0.39	0	5.09	1.84	3638	0.5
12	-105	-115	1.6	0	93.97	6.02	0.01	0.34	0.39	0	5.09	1.84	3638	0.5
13	-115	-125	1.61	0	88.11	11.62	0.27	0.3	0.40	0	9.92	2.0	2328	0.5
14	-125	-135	1.61	0	88.11	11.62	0.27	0.3	0.40	0	9.92	2.0	2328	0.5
15	-135	-145	1.61	0	88.11	11.62	0.27	0.3	0.40	0	9.92	2.0	2328	0.5
16	-145	-155	1.61	0	88.11	11.62	0.27	0.3	0.40	0	9.92	2.0	2328	0.5
17	-155	-165	1.61	0	88.11	11.62	0.27	0.3	0.40	0	9.92	2.0	2328	0.5
18	-165	-175	1.6	0	93.97	6.02	0.01	0.34	0.39	0	5.09	1.84	3638	0.5
19	-175	-185	1.6	0	93.97	6.02	0.01	0.34	0.39	0	5.09	1.84	3638	0.5
20	-185	-195	1.6	0	93.97	6.02	0.01	0.34	0.39	0	5.09	1.84	3638	0.5
21	-195	-205	1.6	0	93.97	6.02	0.01	0.34	0.39	0	5.09	1.84	3638	0.5
22	-205	-210	1.6	0	93.97	6.02	0.01	0.34	0.39	0	5.09	1.84	3638	0.5
23	-210	-250	1.6	0	93.97	6.02	0.01	0.34	0.39	0	5.09	1.84	3638	0.5
24	-250	-300	1.6	0	93.97	6.02	0.01	0.34	0.39	0	5.09	1.84	3638	0.5

Table 69: ***Model Soil File for Elze*** *with weighed mean values for bulk density (bd), gravel, sand, silt, clay and organic carbon (corg) content from EREF, EB5, EB15 and EB25 after calibration of the soil parameters alpha, npar and ksat.*

soil layer	upper [cm]	lower [cm]	bd [g/cm³]	gravel [%]	sand [%]	silt [%]	clay [%]	c_{org} [%]	ths	thr	alpha	npar	ksat	tort
1	8	0							0.85	0	98	1.19	98000	0.5
2	0	-5	1.46	0.01	76.0	23.29	0.71	0.51	0.43	0	5.08	1.85	2047	0.5
3	-5	-25	1.46	0.01	76.0	23.29	0.71	0.51	0.43	0	5.08	1.85	2047	0.5
4	-25	-35	1.46	0.01	76.0	23.29	0.71	0.51	0.43	0	5.08	1.85	2047	0.5
5	-35	-45	1.46	0.01	76.0	23.29	0.71	0.51	0.43	0	5.08	1.85	2047	0.5
6	-45	-55	1.46	0.01	76.0	23.29	0.71	0.51	0.43	0	5.08	1.85	2047	0.5
7	-55	-65	1.46	0.01	76.0	23.29	0.71	0.51	0.43	0	5.08	1.85	2047	0.5
8	-65	-75	1.46	0.01	76.0	23.29	0.71	0.51	0.43	0	5.08	1.85	2047	0.5
9	-75	-85	1.46	0.01	76.0	23.29	0.71	0.51	0.43	0	5.08	1.85	2047	0.5
10	-85	-95	1.46	0.01	76.0	23.29	0.71	0.51	0.43	0	5.08	1.85	2047	0.5
11	-95	-105	1.57	0.02	97.19	2.81	0	0.11	0.39	0	7.17	1.66	5427	0.5
12	-105	-115	1.57	0.02	97.19	2.81	0	0.11	0.39	0	7.17	1.66	5427	0.5
13	-115	-125	1.57	0.02	97.19	2.81	0	0.11	0.39	0	7.17	1.66	5427	0.5
14	-125	-135	1.57	0.02	97.19	2.81	0	0.11	0.39	0	7.17	1.66	5427	0.5
15	-135	-145	1.57	0.02	97.19	2.81	0	0.11	0.39	0	7.17	1.66	5427	0.5
16	-145	-155	1.57	0.02	97.19	2.81	0	0.11	0.39	0	7.17	1.66	5427	0.5
17	-155	-165	1.57	0.02	97.19	2.81	0	0.11	0.39	0	7.17	1.66	5427	0.5
18	-165	-175	1.57	0.02	97.19	2.81	0	0.11	0.39	0	7.17	1.66	5427	0.5
19	-175	-185	1.57	0.02	97.19	2.81	0	0.11	0.39	0	7.17	1.66	5427	0.5
20	-185	-195	1.57	0.02	97.19	2.81	0	0.11	0.39	0	7.17	1.66	5427	0.5
21	-195	-205	1.57	0.02	97.19	2.81	0	0.11	0.39	0	7.17	1.66	5427	0.5
22	-205	-210	1.57	0.02	97.19	2.81	0	0.11	0.39	0	7.17	1.66	5427	0.5
23	-210	-250	1.57	0.02	97.19	2.81	0	0.11	0.39	0	7.17	1.66	5427	0.5
24	-250	-300	1.57	0.02	97.19	2.81	0	0.11	0.39	0	7.17	1.66	5427	0.5

Table 70: ***Model Soil File for Wibbese*** *with weighed mean values for bulk density (bd), gravel, sand, silt, clay and organic carbon (corg) content from WREF, WB5 and WD5 after calibration of the soil parameters alpha, npar and ksat.*

soil layer	upper [cm]	lower [cm]	bd [g/cm³]	gravel [%]	sand [%]	silt [%]	clay [%]	c_{org} [%]	ths	thr	alpha	npar	ksat	tort
1	4	0							0.85	0	98	1.19	98000	0.5
2	0	-5	1.46	0.01	72.63	26.64	0.73	0.59	0.43	0	6.83	1.71	1676	0.5
3	-5	-25	1.46	0.01	72.63	26.64	0.73	0.59	0.43	0	6.83	1.71	1676	0.5
4	-25	-35	1.46	0.01	72.63	26.64	0.73	0.59	0.43	0	6.83	1.71	1676	0.5
5	-35	-45	1.46	0.01	72.63	26.64	0.73	0.59	0.43	0	6.83	1.71	1676	0.5
6	-45	-55	1.46	0.01	72.63	26.64	0.73	0.59	0.43	0	6.83	1.71	1676	0.5
7	-55	-65	1.48	0.01	86.99	12.17	0.84	0.16	0.42	0	5.03	2.0	3152	0.5
8	-65	-75	1.48	0.01	86.99	12.17	0.84	0.16	0.42	0	5.03	2.0	3152	0.5
9	-75	-85	1.48	0.01	86.99	12.17	0.84	0.16	0.42	0	5.03	2.0	3152	0.5
10	-85	-95	1.48	0.01	86.99	12.17	0.84	0.16	0.42	0	5.03	2.0	3152	0.5
11	-95	-105	1.48	0.01	86.99	12.17	0.84	0.16	0.42	0	5.03	2.0	3152	0.5
12	-105	-115	1.48	0.01	86.99	12.17	0.84	0.16	0.42	0	5.03	2.0	3152	0.5
13	-115	-125	1.48	0.01	86.99	12.17	0.84	0.16	0.42	0	5.03	2.0	3152	0.5
14	-125	-135	1.48	0.01	86.99	12.17	0.84	0.16	0.42	0	5.03	2.0	3152	0.5
15	-135	-145	1.48	0.01	86.99	12.17	0.84	0.16	0.42	0	5.03	2.0	3152	0.5
16	-145	-155	1.48	0.01	86.99	12.17	0.84	0.16	0.42	0	5.03	2.0	3152	0.5
17	-155	-165	1.48	0.01	86.99	12.17	0.84	0.16	0.42	0	5.03	2.0	3152	0.5
18	-165	-175	1.48	0.01	86.99	12.17	0.84	0.16	0.42	0	5.03	2.0	3152	0.5
19	-175	-185	1.48	0.01	86.99	12.17	0.84	0.16	0.42	0	5.03	2.0	3152	0.5
20	-185	-195	1.48	0.01	86.99	12.17	0.84	0.16	0.42	0	5.03	2.0	3152	0.5
21	-195	-205	1.48	0.01	86.99	12.17	0.84	0.16	0.42	0	5.03	2.0	3152	0.5
22	-205	-210	1.48	0.01	86.99	12.17	0.84	0.16	0.42	0	5.03	2.0	3152	0.5
23	-210	-250	1.48	0.01	86.99	12.17	0.84	0.16	0.42	0	5.03	2.0	3152	0.5
24	-250	-300	1.48	0.01	86.99	12.17	0.84	0.16	0.42	0	5.03	2.0	3152	0.5

Declaration of originality and confirmation of conformance

I, Kilian Loesch, hereby declare that I am the sole author of this dissertation entitled 'The effect of forest conversion from coniferous to broadleaved forests on deep seepage rates in Northwest Germany'. All references and data sources that were used in the dissertation have been appropriately acknowledged.

I furthermore declare that this work has not been submitted elsewhere in any form as part of another dissertation procedure.

Oldenburg, 11.01.2023

Kilian Loesch

Acknowledgements

First of all, I want to thank Dr. Karsten Mohr from the Chamber of Agriculture Lower Saxony in Oldenburg: As project coordinator, he gave me the opportunity to write my dissertation in an exciting, varied and practice-oriented research project. As my supervisor and an empathetic person, he has always supported me with advice and action and encouraged me even in challenging times. I am very grateful to have had such an inspiring person as you during my PhD years.

Secondly, I thank Prof. Dr. Gudrun Massmann for her willingness to take over the supervision of my dissertation and to integrate me as an external doctoral student into the social and academic community of the Institute for Biology and Environmental Sciences of the University of Oldenburg. In addition, I am very grateful for the support of Prof. Dr. Jürgen Müller and Dr. Henning Meesenburg, whose excellent expertise and great willingness to help me contributed greatly to the success of the research project and my dissertation. I would also like to thank Prof. Dr. Karl-Heinz Feger and Prof. Dr. Luise Giani for reviewing my dissertation.

A very special thank you goes to Dr. Paul Schmidt-Walter and Dr. Janek Greskowiak, who supported me in all technical matters related to water balance modelling. A big thank you also goes to my good friend Kilian R., who helped me to raise the performance of my computer to a level that could cope with the demanding computing tasks.

A number of other people enthusiastically supported me in a wide variety of tasks, to whom I would like to express my gratitude: Ulrike Kücks, Elke Ahrensfeld and Solveig Nachtigall, who were a great help to me in the laboratory; the conscientious students Ina Schröter, Michael Geisler and Mike Möhlmann, whose Bachelor and Master theses made it possible to shed even more light on certain aspects of the project; Olaf Zander, who was my reliable contact person on any occasion I could think of; and my dear colleagues from the Chamber of Agriculture for their support.

My family and friends deserve a very special thank you for always being there for me both in happy and hard times. Thank you also to my friends and flatmates in Oldenburg, who made Oldenburg feel like home in no time.

And to you, Tim, thank you for being always by my side.

Curriculum Vitae

Personal Data

Name:	Kilian Loesch
Date of Birth:	10.07.1991
Place of Birth:	Braunschweig, Germany
Nationality:	German

Education

Since 03/2018	Doctoral Thesis, Carl von Ossietzky University, Oldenburg
10/2014 – 05/2017	M. Sc. Environmental Systems and Sustainability, Ludwig-Maximilians-University, Munich
10/2011 – 09/2014	B. Sc. Geography (Major), Meteorology (Minor), Ludwig-Maximilians-University, Munich
06/2010	Abitur, Gymnasium 'Eichenschule', Scheeßel